Neural adaptation in the auditory pathway of crickets and grasshoppers

D I S S E R T A T I O N

zur Erlangung des akademischen Grades

doctor rerum naturalium (Dr. rer. nat.)
im Fach Biologie

eingereicht an der
Mathematisch-Naturwissenschaftlichen Fakultät I
Humboldt-Universität zu Berlin

von
Dipl.-Biol. Kai Jannis Hildebrandt
30.8.1976 in Göttingen

Präsident der Humboldt-Universität zu Berlin:
Prof. Dr. Dr. h.c. Christoph Markschies

Dekan der Mathematisch-Naturwissenschaftlichen Fakultät I:
Prof. Dr. Lutz-Helmut Schön

Gutachter:
1. PD Dr. Matthias Hennig
2. Dr. Jan Benda
3. Prof. Dr. Jutta Kretzberg

eingereicht am: 23.2.2010
Tag der mündlichen Prüfung: 1.6.2010

Abstract

Neural adaptation serves to adjust the sensory pathway to the current environment of an animal. While the effect and time course of adaptation can be observed directly within single cells, its underlying cause is a combination of many different mechanisms spread out along the sensory pathway. The present work has the objective to unite these different levels of understanding of the term adaptation. In order to do so, several experimental and theoretical studies were carried out. In two of these studies, a combination of current injection and auditory stimulation was used, in order to disentangle intrinsic adaptation from network effects. In one of the studies, carried out in the auditory system of locusts, it was revealed that the mechanisms behind adaptation that are activated within different parts of the auditory system depend critically on identity and function of the cell under study. Similar methods enabled the identification of presynaptic inhibition as a possible mechanisms behind the important mathematical operation of division in the auditory system of crickets. Additionally, a modeling study pursued the question, where adaption should work in the auditory system from the perspective of two different tasks of sensory processing: identification of a signal and localization of its source. The results obtained from the model suggest conflicting demands for these two tasks and also present a solution of this conflict. In a fourth study, it was asked wether adaptation in the auditory system of crickets serves to guarantee optimal representation of the entire sensory environment or if it helps to separate one most important signal from the background. In summary, not only which mechanisms of adaptation are at work is of crucial importance for sensory processing, but also the exact placement of these along the pathway.

Keywords: sensory adaptation, auditory system, computational neuroscience, insects

Zusammenfassung

Neuronale Adaptation dient dazu, eine Sinnesbahn kurzfristig an die aktuelle Umgebung des Tieres anzupassen. Ihr Effekt und zeitlicher Verlauf lässt sich in der Antwort einzelner Nervenzellen direkt beobachten. Der Adaptation unterliegen eine Vielzahl verschiedener Mechanismen, die über die gesamte Sinnesbahn verteilt sein können. In der vorliegenden Arbeit wurde der Versuch unternommen, diese unterschiedlichen Betrachtungsebenen zusammenzuführen. Dazu wurden mehrere experimentelle und theoretische Studien durchgeführt. In zwei der vorgestellten Studien wurden Kombinationen aus Strominjektionen und akustischen Reizen verwendet, um intrinsische Adaptation von Netzwerkeffekten zu trennen. Dabei ergab sich in einer experimentellen Studie am auditorischen System der Heuschrecke, dass die Adaptationsmechanismen, die in verschiedenen Teilen der Hörbahn rekrutiert werden, sehr stark von Identität und Funktion der jeweils untersuchten Nervenzelle abhängen. Ähnlich Methoden ermöglichten es, im auditorischen System der Grille präsynaptische Hemmung als Substrat für die wichtige mathematische Operation der Division zu identizifieren. Zusätzlich wurden Modellierungen durchgeführt, bei denen die Frage bearbeitet wurde, wo Adaptation in der Hörbahn wirken sollte, bezogen auf zwei verschieden Aufgaben: die Lokalisation eines Signals und die neuronal Abbildung dessen zeitlicher Struktur. Die Ergebnisse dieser Studie deuten darauf hin, dass die Anforderungen für diese beiden Aufgaben sehr unterschiedliche sind. In einer vierten Studie wurde untersucht, ob die Adaptation in einem auditorischen Interneuron der Grille dazu dient, die gesamte sensorische Umgebung gut abzubilden, oder ob durch die Adaptation eine Abtrennung des jeweils lautesten Signals erreicht werden kann. Zusammenfassend lässt sich sagen, dass sowohl die Adaptationsmechanismen, als auch deren genaue Platzierung innerhalb der sensorischen Bahn wesentlich für Sinnesleistungen sind.

Schlagworte: senosorische Adaptation, auditorisches System, Computational Neuroscience, Insekten

Contents

List of figures ix
List of tables xi
List of abbreviations xiii

1 Introduction **1**

2 General methods **9**
2.1 Animal Preparation 9
2.1.1 Preparation of *Locusta migratoria* (Chapter 3) 9
2.1.2 Preparation of crickets (Chapters 5 & 6) 9
2.2 Pharmacological interventions (Chapter 5) 10
2.3 Electrophysiology 10
2.3.1 Intracellular recordings (Chapters 3 & 5) 10
2.3.2 Extracellular recording (Chapters 5 & 6) 10
2.4 Stimulation 11
2.4.1 Acoustic stimuli (Chapters 3, 5 & 6) 11
2.4.2 Current stimuli (Chapters 3, 5) 11
2.5 Data analysis 12
2.5.1 Spike frequency estimation (Chapters 3, 4 & 5) 12

I Where does adaptation act? **13**

3 The origin of adaptation in the auditory pathway of the locust **15**
3.1 Introduction 15
3.2 Methods 16
3.2.1 Stimulus design 16
3.2.2 Data analysis 16
3.3 Results 18
3.3.1 Characterization of spike frequency adaptation 18
3.3.2 Response curves 18
3.3.3 Magnitude of spike frequency adaptation 20
3.3.4 Time course of spike frequency adaptation 22
3.3.5 Hyperpolarization after stimulus offset 24
3.3.6 Hyperpolarization after individual spikes 28
3.3.7 Response characteristics under acoustic stimulation 30
3.4 Discussion 32
3.4.1 Different origins of SFA in the three cell types 33
3.4.2 Impact of the stimulation site 33
3.4.3 SFA and signal transmission properties 35
3.4.4 Functional role of the distribution 35

4 Functional implications of the distribution of adaptation **37**
4.1 Introduction . . . 37
4.2 Optimal response curves and adaptation . . . 39
4.2.1 The optimal response curve . . . 39
4.2.2 The role of noise . . . 40
4.2.3 $\oplus$-neuron: coding of temporal pattern . . . 41
4.2.4 $\ominus$-neuron: coding of stimulus direction . . . 43
4.3 Simulation of adaptation dynamics . . . 46
4.3.1 Simulation of local neurons . . . 47
4.3.2 Ascending $\ominus$-neuron . . . 50
4.3.3 Summary of the modelling of adpatation dynamics . . . 61
4.4 Discussion . . . 61
4.4.1 Validity of model assumptions . . . 62
4.4.2 Different time scales for localization and pattern processing . . . 64
4.4.3 Comparison to mammalian auditory system . . . 65

II How does adaptation act ? **67**

5 Presynaptic inhibition in the auditory pathway of crickets **69**
5.1 Introduction . . . 69
5.2 Methods . . . 71
5.2.1 Stimulus protocols . . . 71
5.2.2 Data analysis . . . 71
5.3 Results . . . 72
5.3.1 Changes of the response curves in the two carrier channels . . . 72
5.3.2 Cross-adaptation with current . . . 74
5.3.3 Cross-adaptation with other carrier frequency . . . 76
5.3.4 Blocking of presynaptic inhibition . . . 80
5.4 Discussion . . . 82
5.4.1 Summary . . . 82
5.4.2 Presynaptic inhibition and gain control . . . 82
5.4.3 Input gain-control vs. output gain-control . . . 83
5.4.4 What is the source of presynaptic inhibition? . . . 84
5.4.5 Biological relevance of gain control by presynaptic inhibition . . . 84

III Why does adaptation act? **87**

6 Selective coding in the auditory pathway of crickets **89**
6.1 Introduction . . . 89
6.2 Methods . . . 92
6.2.1 Stimulus protocols . . . 92
6.2.2 Data analysis . . . 94
6.3 Results . . . 97
6.3.1 Time course of adaptation . . . 97
6.3.2 Adaptation to the statistics of the acoustic environment . . . 101

6.4 Discussion . . . 112
6.4.1 Several time scales of adaptation . . . 112
6.4.2 Infomax vs. background suppression . . . 112
6.4.3 Optimality vs. improvement . . . 114
6.4.4 Stream segregations . . . 114

7 Conclusion **117**
7.1 Time scales . . . 117
7.2 Competing demands . . . 119
7.3 Design principles for the placement of adaptation . . . 121
7.3.1 Divergence and convergence . . . 121
7.3.2 The role of nonlinearities . . . 122

Appendix A **127**

Appendix B **133**

Deutschsprachige Zusammenfassung **137**
D1 Einleitung . . . 137
D2 Der Ursprung von Adaptation in der Hörbahn der Heuschrecke . . . 137
D3 Funktionelle Erwägungen zur Verteilung von Adaptation . . . 138
D4 Präsynaptische Hemmung in der Hörbahn der Grille . . . 138
D5 Selektive Informationskodierung in der Hörbahn der Grille . . . 139
D6 Schlussbetrachtung . . . 140

Bibliography **141**

Selbständigkeitserklärung **153**

Publikationen **155**

Danksagung/Acknowledgments **157**

List of Figures

1.1 Examples of adaptation mechanisms 2
1.2 Investigation of adaptation 4
1.3 Auditory system of crickets and locusts at the thoracic level 6

2.1 Typical recording trace from a cricket AN2 neuron 11

3.1 Input response curves for acoustic and current stimulation. 19
3.2 Magnitude of spike frequency adaptation. 20
3.3 Time course of spike frequency adaptation 22
3.4 Hyperpolarization after stimulus offset 24
3.5 Comparison of the reponses to acoustic and current stimulation 26
3.6 Spontaneous activity after stimulus offset 27
3.7 Spike shapes of the different cell types 29
3.8 Adaptation and coding properties under acoustic stimulation 30
3.9 Distribution pattern of adaptation mechanisms 34

4.1 Layered network in the metathoracic ganglion of grasshoppers 38
4.2 Network used for numerical simulation 47
4.3 Example of responses of simulated local neuron 48
4.4 Characterization of adaptation in local neurons 49
4.5 Responses of simulated local neurons to RAM stimuli 51
4.6 Frequency responses of the $\ominus$-neuron to periodic stimuli 54
4.7 Change of mutual information about IID over time 55
4.8 Dependency of directionality information on mean level 56
4.9 Ambiguity of responses to interaural level differences 58
4.10 Confusion matrices with and without adaptation in $\ominus$-neuron 59

5.1 Subtractive and divisive adaptation effects on response curves 69
5.2 Stimulus protocol for adapted response curves 71
5.3 Effect of adaptation on the onset response curves 72
5.4 Changes of response curves for all recorded cells 75
5.5 Cross-adaptation with current 76
5.6 Cross-adaptation with respective other frequency 78
5.7 Blocking presynaptic inhibition 81
5.8 Emergence of divisive inhibition at presynaptic terminals 83

6.1 Optimal response curves for different stimulus distributions 90
6.2 Summary of the experimental protocols 93
6.3 Examples of responses after adaptation to noise stimuli 98
6.4 Example of response curves for different adaptation times 99

6.5 Time course of adaptation and recovery 100
6.6 Optimal response curves for multimodal distributions 102
6.7 Responses of an AN2 cell to amplitude-modulated noise 103
6.8 Typical examples of stimulus response curves after adaptation 104
6.9 Summary of changes of the shift of the response curves 107
6.10 Summary of changes of the slope of the response curves 108
6.11 Adaptation induced changes of mutual information 110

7.1 Sensory pathway as a combination of serial nonlinearities 123
7.2 Effect of adaptation in a pathway with two serial nonlinearities 124

A1 Examples of $\ominus$-neuron model performance 130

List of Tables

6.1 Summary of the adaptation and recovery time constants. 100
6.2 Summary of predictions for the two coding hypothesis 102

A1 Parameters used for the model of local neurons in Chapter 4. 128
A2 Parameters used for the model of $\ominus$-neuron in Chapter 4. 129

List of abbreviations

$\oplus$-neuron	Interneuron that sums information from both ears
$\ominus$-neuron	Interneuron that subtracts information from both ears
AN1	Ascending interneuron 1 (crickets)
AN2	Ascending interneuron 2 (locusts and crickets)
BSN1	Bisegmental interneuron 1 (locusts)
CDI	Corollary discharge interneuron (crickets)
EIF	Exponential integrate-and-fire neuron
EPSP	Excitatory post-synaptic potential
GABA	γ-Aminobutyric acid
IID	Interaural intensity difference
IPSP	Inhibitory post-synaptic potential
PDF	Probability density function
RAM	Randomly amplitude-modulated
SFA	Spike frequency adaptation
TN1	T-shaped interneuron 1 (locusts)

1 Introduction

Neurons provide the machinery that allows animals to sense their environment, process information and behave appropriately. Although animals are adapted to virtually all imaginable environments and there is a vast diversity of neuronal layouts, there are some basic features that the majority of these nervous systems rely on. These features constitute building blocks for *evolutionary* adaptation of the nervous system of a species. *Neural* adaptation is one of these basic features found in virtually all sensory systems.

Neural adaptation can be studied on different levels, and the definition of it varies with the perspective: it can be seen from a functional point of view, from a phenomenological perspective, or the mechanisms that cause adaptation can be at the centre of interest. Often, neural adaptation is studied only on one of these levels, at the risk to miss demands and constraints imposed by the respective other levels. The goal of this work is to assist in uniting these perspectives by relating them to each other in exemplary studies, and thereby ask whether general principles for the organization of neural adaptation within sensory pathways can be formulated.

Functional level The functional level is what the term 'adaptation' originally refers too, meaning an adjustment. If evolutionary adaptation means a change, by which an organism or species becomes better suited to its environment, neural adaptation (from here on: simply *adaptation*) means a change to become better suited to the *sensory* environment. In contrast to evolutionary adaptation, neural adaptation works within the nervous system of individual animals, has a much faster time course and is generally reversible. Of course, neural adaptation itself is subject to evolutionary adaptation and whenever 'design principles' are mentioned within this work, it is in the context of the nervous system being shaped by evolutionary processes just as any other organ. Neural adaptation is a change to become better suited to the current environment an individual animal is confronted with and it is often necessary, because the range of sensitivity is restricted or because efficient coding depends on the sensory context. There are numerous studies that show how neurons in sensory pathways change their coding scheme in order to match features of the sensory environment (Laughlin, 1981; Brenner et al., 2000; Dean et al., 2005; Maravall et al., 2007).

Phenomenological level On the phenomenological level, adaptation is the change of the strength of the neuronal response during prolonged stimulation (typically a decrease). This is commonly observed in experiments, in which a sensory or current stimulus is transiently turned on, usually preceded by a situation, in which the neuron is not excited. Then, the neurons starts to respond strongly, and this response will decay and eventually reach a steady state value. Other terms used instead of adaptation on the phenomenological level are 'response decrement' or the classification of neural response types into phasic, tonic or phasic-tonic. There is a connection between

the phenomenological and the functional perspective on adaptation: a 'phenomenologically' adapting neuron will react differently to novel stimuli after the response to a prolonged stimulus has decayed. Thus, it codes differently for the novel stimulus than before presentation of the adapting, prolonged stimulus. However, this does not automatically imply that this change provides means for the sensory system to be adjusted to the current environment. The phenomenological perspective rather looks on the *process* of adaptation, while the functional view focuses on the result.

The purely phenomenological view has the advantage that it can be studied without knowing the exact function beforehand and that its description covers a broader range of adaptation. Therefore, adaptation that serves other functions than the pure adjustment of the coding scheme can be included, e.g. optimizing energy consumption (Heitwerth et al., 2005; Niven et al., 2007) and dynamic processing of time varying signals (Torkkeli et al., 2001; Benda et al., 2005). Because it describes the process rather than the result of adaptation, the phenomenological view can also be linked more easily to the mechanisms behind adaptation.

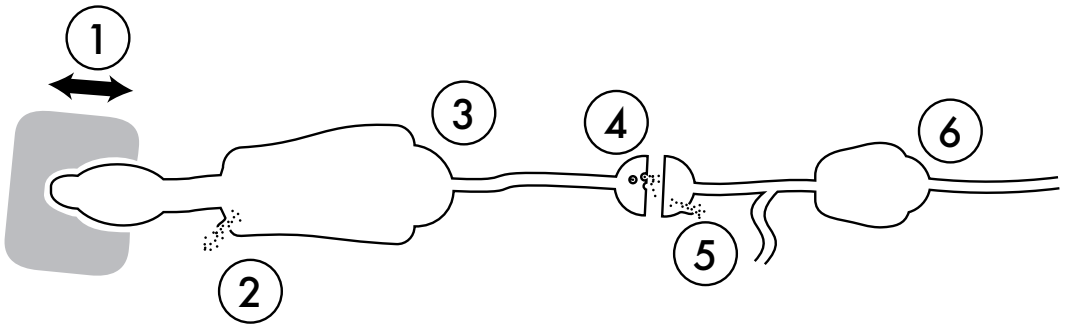

Figure 1.1: **Examples of mechanisms that enable adaptation along an auditory pathway.** An auditory receptor cell and a sensory interneuron are displayed. Mechanisms that give means to adaptation can act directly at the mechanics of transduction (1), they can affect the transduction currents (2), and the spike generator of either cell (3&6). In addition, pre- and postsynaptic changes at the synapses (4&5), like presynaptic inhibition and synaptic depression can result in adaptation.

Mechanistic level The third level, on which adaptation can be studied, are the mechanisms that enable it. Adaptation can result from many different mechanisms along a sensory pathway. Fig. 1.1 refers to examples of these mechanisms in the first stage of an insect auditory pathway. These mechanisms include the transduction process in receptors cells (Hudspeth et al., 2000; Gollisch and Herz, 2004; Albert et al., 2007; Fig. 1.1, no. 1&2), spike dependent adaptation currents (Brown and Adams, 1980; Madison and Nicoll, 1984; Fleidervish et al., 1996) in all cells of the sensory pathway (Fig.1.1, no. 3&6), synaptic depression (Chance et al., 1998; Abbott et al., 1997; Rothman et al., 2009; Fig.1.1, no. 4&5), and inhibitory inputs (Finlayson and Adam, 1997; Ingham and McAlpine, 2005).

The definition of adaptation used throughout the present work is a combination of the functional and the phenomenological perspective and includes many potential

mechanisms. Here, it is assumed that the process of adaptation, which serves a functional adjustment, will take the form described for the phenomenological definition, whenever the dynamics of this adaptation are considered. The combined definition is reflected in the way adaptation is examined and quantified throughout this thesis (Fig. 1.2).

Dynamics of adaptation In the different studies contained in the present work, the dynamics of adaptation are studied by presenting pulses with constant intensity as stimuli. If the response of a neuron to the stimuli is measured in a time-resolved manner, the decrease of the response during prolonged stimulation can be quantified and characterized by one or several time constants of exponential decays (Fig. 1.2B). In most sensory systems, several of these time constants can be found, often spanning large ranges (Ulanovsky et al., 2004; Drew and Abbott, 2006). The time course of adaptation has important implications for the coding of dynamical stimuli (Benda et al., 2005). A second feature that can be examined with the help of long duration pulses is the adaptation strength, describing how much a neuron adapts by comparing the response at the beginning of the stimulus to the response when adaptation has reached a steady state (Fig. 1.2B). The quantification of adaptation strength corresponds to the discrete classification of neurons into tonic, phasic and phasic-tonic response types on a continuous scale.

Changes of the onset response curves Adaptation is quantified throughout the present work by measuring the change of response curves due to adaptation. In order to achieve this, an adapting stimulus is presented until adaptation results in a steady state response and then test pulses of varying intensity are presented (Fig. 1.2A). In this way, the *onset* response curve can be measured, which is altered by adaptation depending on the adapting stimulus (Fig. 1.2C). The change of the onset response curve reflects how the neuron will respond to a novel stimulus after adaptation to the prevailing sensory environment. For the neural representation of stimuli that change on a time scale faster than the dynamics of adaptation, the adapted onset response represents the relevant input-output transformation. With regard to the time scale of such fast changing stimuli, adaptation can be seen as resulting in a static change of the coding scheme. Depending on how adaptation changes the onset response curve, it influences the coding of novel stimuli. In this way, it provides means for operations between the adapting background and new signals and for an adjustment of the coding scheme to the sensory environment.

The definition of adaptation used here and the way adaptation is quantified means that any coding 'changes' that are inherent in the neural transformation itself are excluded (see Hong et al., 2008, for examples of such 'purely input driven adaptation'). A second class of adjustments that is not covered here are those that are irreversible or act on much longer time scales including all phenomena that are subsumed as learning.

In order to combine the functional, phenomenological and mechanistic levels, three questions are used as guidelines for the different studies presented here: *where* does adaptation take place, *how* is it implemented and *why* is it acting? The different studies include more than one of the above perspectives on adaptation, and for the complete

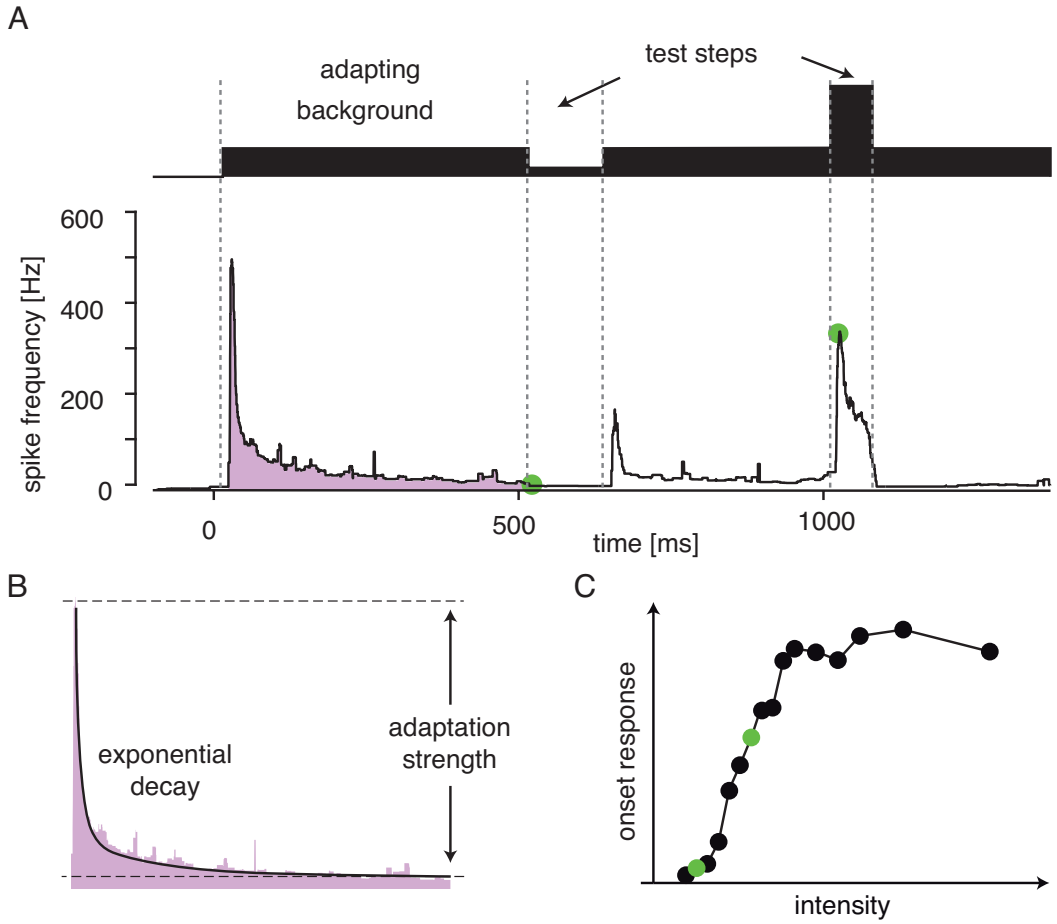

Figure 1.2: **Investigation of adaptation.** Throughout the present work, adaptation is examined and quantified either by studying how a neuron responds to an ongoing and constant stimulus (pink), or the change of the responses to novel stimuli as a result of adaptation is examined (green dots). Panel (A) shows an exemplary stimulus design to illustrate both aspects. The graph depicts the spike frequency response of a neuron to the stimulus shown above. During the process of adaptation (pink), dynamics can be studied, but also the adaptation strength can be quantified (B). The black line in (B) represents a double exponential fit to the response to the adapting background in (A). After the response of the neuron has reached a steady state, test steps can be applied, and the onset response (green dots in A) can be measured. With the help of these test steps, an onset response curve can be constructed (C) that depends on the adapting background. For the study of the change of onset response curves, the background can be any type of stimulus. The data depicted in the figures stems from the AN2 of crickets (cf. Chapter 5).

picture, the three questions cannot be answered separately. Later, these studies are integrated to search for general design principles governing adaptation.

Adaptation was approached in three exemplary studies in the auditory system of crickets and grasshoppers (Fig 1.3). Both systems are well suited for three reasons: First (1), their auditory system is relatively simple, but nonetheless performs complex computations, such as recognition of temporal patterns of acoustic signals and localization of their source (von Helversen and von Helversen, 1995; Pollack, 2000; Wendler, 1990). The auditory pathway is organized mainly in a feed-forward manner (Fig 1.3), which simplifies the identification of the origin of adaptation, because feed-back from higher centres can largely be omitted (Hennig et al., 2004). Second (2), the relevant stimulus space is well known, because these systems evolved primarily for very defined tasks such as predator detection and conspecific mate recognition. The behavioural relevance of different aspects of signals, as for instance the directionality information, has been tested in behavioural studies (von Helversen and Rheinlaender, 1988; Hennig and Weber, 1997). This simplifies the formulation of the potential functionality of adaptation, because the tasks that have to be performed are well known. In addition, the behavioural relevance of adaptation in the auditory system of grasshoppers has been shown directly (Ronacher and Hennig, 2004). Third (3), the auditory system of crickets and grasshoppers is constituted by few identified neurons (Fig 1.3) that can be recorded *in-vivo*, both intra- and extracellularly. *In-vivo* intracellular recordings make it possible to use acoustic and current stimuli in the same experimental setting, in the same cell, providing a tool to disentangle different sources of adaptation. Extracellular recordings allow for long duration recordings with large stimulus arrays and for pharmacological intervention during recording *in-vivo*.

This thesis is organized along the three questions *where*, *how* and *why* adaptation acts in sensory pathways, which is reflected by the structuring into three parts. The first part covers the question of *where* adaptation acts and how the different sources of it are distributed. It is composed of two chapters, one that reports experimental work (Chapter 3) and a second theoretical part that is motivated by the experimental results and sets these into a functional framework (Chapter 4).

In Chapter 3, it is studied *where* adaptation acts in the auditory pathway of locusts. The arrangement of different mechanisms in different neurons of the sensory pathway (Fig. 1.1) indicates that adaptation does not occur at one single specific location in a sensory pathway. If one records the response of any neuron in the pathway, the observed adaptation is likely the combination of several mechanisms peripheral to the neuron under study (Fig.1.1) and to feedback from higher centres. If one wants to understand adaptation on the different levels discussed above, the exact pattern of how adaptation mechanisms are laid out and interact in the sensory pathway must be considered. In Chapter 3, three functional distinct neuron types in the auditory system of locusts are examined. By using current and auditory stimuli in the same cell, the distribution of adaptation mechanisms along the pathway is explored. The influence of adaptation in the periphery of the cells, intrinsic adaptation and direct inhibition on the cells are disentangled and the specific layout for each cell is discussed with respect to its function. Additionally, the time course of adaptation is examined and related to

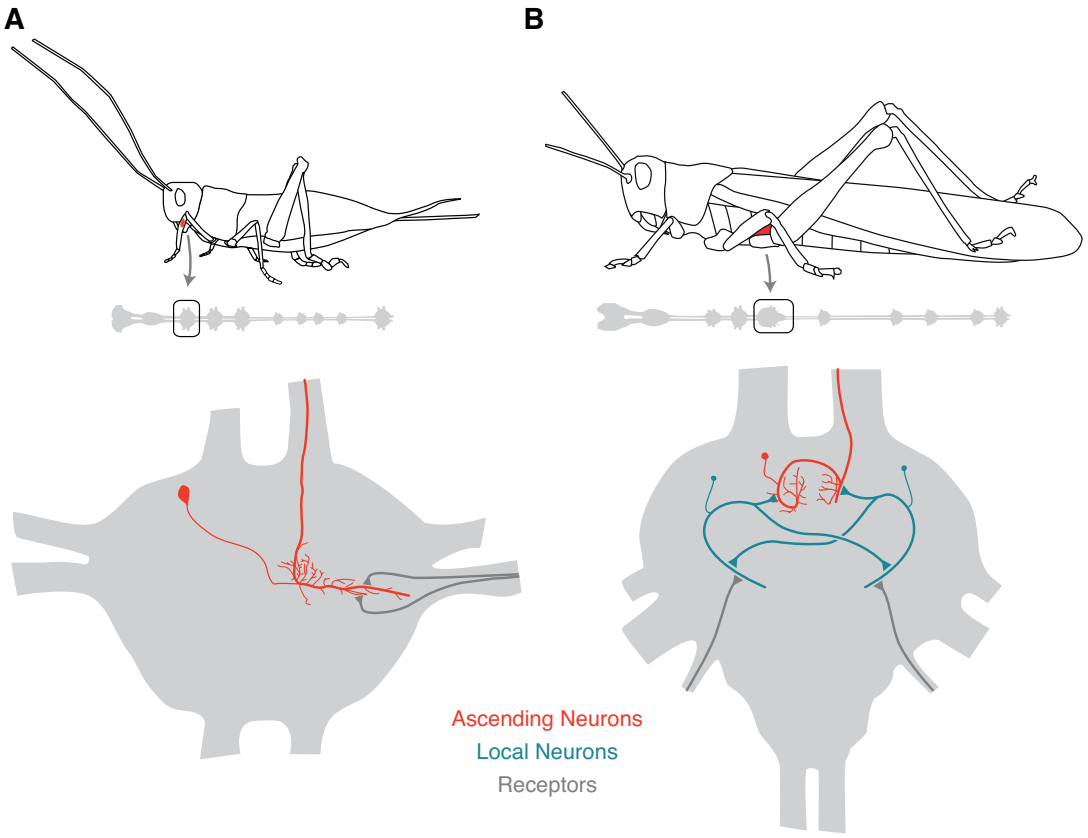

Figure 1.3: **Auditory system of crickets and locusts at the thoracic level.** In crickets, sound is received via the tympana in the forelegs (red spot, A), where it is transduced by receptors neurons. Receptors project to the ventral nerve chord (shown below the cricket) into the prothoracic ganglion that constitutes the first processing station for auditory information in crickets. From here, ascending neurons directly transfer the information up to the brain. The red neuron depicts an AN2 (ascending interneuron 2) type neuron that is examined in Chapters 5 & 6. Local auditory interneurons in the cricket were omitted for clearness, as they are not studied in this work. In the locust (B), the ears are located in the first abdominal segment (red area), where auditory stimuli are transduced and information about the stimuli is transferred to the metathoracic ganglion by receptor neurons. In locusts, the auditory receptors project onto local neurons that in turn have direct connection to ascending neurons, transferring information to the brain. The bisegmental interneuron 1 (BSN1) and the T-shaped interneuron 1 (TN1), examined in Chapter 3 are of the local neuron type. The blue neurons in (B) are schematic representatives of this class. The red neuron in (B) depicts an ascending neuron (AN2) in the locust. The AN2s in crickets and locusts are not homologue or functionally equivalent, the identical nomenclature being pure coincidence.

signal-processing properties of the cells.

The differences in the layout of the origin of adaptation in the three cell types in Chapter 3 is the basis for a theoretical analysis and numerical simulations reported in Chapter 4. In Chapter 4, the distribution patterns of adaptation mechanisms observed are put to test with respect to the function of the different cell types. Specifically, it is explored, whether adaptation should be placed centrally or peripherally, in a situation where information from both ears is combined. Two examples from the auditory pathway of grasshoppers are considered: processing of directionality of a signal and reliable coding of the temporal pattern. These considerations link the functional and the mechanistic levels of adaptation.

In the second part of the present work the question about *how* adaptation acts is raised: Chapter 5 explores the role of presynaptic inhibition in an interneuron of the auditory system of crickets. Divisive and subtractive changes of the response curve due to adaptation are described. The mechanisms driving them are identified by a combination of intra- and extracellular recordings and pharmacological interventions. In this study, differences in how adaptation acts on low frequency sound as found in conspecific signals and high frequency sound resembling predator signals emphasize the connection between the mechanistic and the functional level.

The last part of this thesis is dedicated to the question *why* adaptation acts in a sensory pathway. In Chapter 6, two alternative hypotheses for the function of slow adaptation in the auditory system of crickets are tested. Two competing coding principles, the maximization of information about the entire sensory environment and selective coding of only one specific signal out of several were assessed by evaluating which of these is favoured by adaptation when stimuli with distinct statistical properties are presented.

The overall goals of this work are to (1) integrate specific systems and pathways into a more universal picture of adaptation and (2) to search for general design principles for adaptation in sensory pathways. Along the three parts containing different examples from the auditory pathway of crickets and grasshoppers, three general themes for such design principles emerge: the importance of the time course of adaptation (1), the competing demands for different processing streams in the sensory pathway (2) and principles for the distribution pattern of adaptation (3). In the conclusion, these three themes are discussed and results from the different parts of this work are integrated into a more general framework for the design of adaptation in sensory pathways.

2 General methods

Since the experimental methods used in the different studies of this thesis overlap largely, their descriptions are pooled here. The relevant chapter for each method is given in parenthesis in the respective section titles. The same is true for the estimation of spike frequency that is also used Chapters 3, 4 & 5. The description of stimulus design and data analysis are specific to the different studies and are placed in the respective chapters.

2.1 Animal Preparation

2.1.1 Preparation of *Locusta migratoria* (Chapter 3)

Experiments were performed on adult locusts (*Locusta migratoria*), obtained from a commercial supplier. Legs, wings, head, the anterior part of the abdomen and the gut were removed. The animals were fixated by wax on a platform, dorsal side up. The thorax was opened dorsally in order to expose the metathoracic ganglion. The ganglion was put on a small NiCr 'spoon' to minimize movements and the torso was filled with locust Ringer solution (Pearson and Robertson, 1981). All experiments were performed at room temperature ($22 \pm 2°$C). Recordings of *L. migratoria* were obtained from 18 cells of three distinct cell types (TN1, $n = 9$; BSN1, $n = 5$; AN2, $n = 4$).

2.1.2 Preparation of crickets (Chapters 5 & 6)

Laboratory reared crickets of the species *Teleogryllus oceanicus* and *Teleogryllus leo* were used. For preparation, both pairs of wings and the meso- and metathoracic legs were removed. The animal was fixed ventral side up to a small platform and the prothoracic legs with the ears were waxed to pins at the coxae and the tarsi in a normal walking position. All experiments were performed at room temperature ($22 \pm 2°$C). For extracellular recordings, ascending and descending connectives from the prothoracic ganglion were cut in order to reduce neuronal background activity (see Hennig, 1988 for a more detailed description).

Data for the experiments of Chapter 5 stemmed from 30 females of the species *T. leo*. For intracellular recordings and pharmacological interventions in these experiments, the prothoracic ganglion was exposed and stabilized by a small metal platform.

For the characterization of the time course of adaptation in Chapter 6, individuals of *T. oceanicus* and *T. leo* were used. For the experiments with the multimodal stimuli, mainly *T. leo* individuals were used.

2.2 Pharmacological interventions (Chapter 5)

For the study of divisive gain control in the AN2 (Chapter 5), picrotoxin was used to block presynaptic inhibitory channels sensitive to $GABA_A$.

In order to do this, the prothoracic ganglion was exposed and a glass electrode with a broken tip was used to perforate the membrane of the ganglion 5-7 times. This was done in preparations with extracellular recordings only. Following the control stimulus protocol, ringer was taken off and picrotoxin dissolved in ringer was applied. For the next 15 minutes, ringer with picrotoxin was replaced every minute and afterwards, the stimulus protocol was tested again. For the wash condition, the picrotoxin ringer was replaced and during a 15-minute period the ganglion was rinsed every minute with fresh ringer. For another 20 minutes, ringer was replaced every 5 minutes. After this procedure, the stimulus ensemble was presented again. Only preparations, in which the recordings lasted for the long time of this procedure (about 100 minutes), were used for the analysis ($n = 6$).

2.3 Electrophysiology

2.3.1 Intracellular recordings (Chapters 3 & 5)

Intracellular recordings were obtained with sharp electrodes pulled on a horizontal puller (P-2000 or P87, Sutter Instruments, Novato, CA) using borosilicate glass (GCF 100F-10, Harvard Apparatus, Edenbridge, UK). Electrode tips were filled with a 3-5% solution of Lucifer yellow (Sigma-Aldrich, Taufkirchen, Germany) in 0.5 M *LiCl*. Electrodes had resistances of 40-60 M, allowing for the large currents necessary in the experiments to pass through. The voltage was amplified (SEC05LX, npi electronic, Tamm, Germany). Recordings were sampled to the hard disk of a personal computer via a 20 kHz A/D-converter (PCI-6014, National Instruments, Austin, TX). From the digitized recordings, the spike times were extracted by a peak detection algorithm (Todd, 1999).

After completion of experiments, the ganglia recorded from (metathoracic for *L. migratoria*, prothoracic for *T. leo*) were removed, fixed in 4% paraformaldehyde, dehydrated and cleared in methylsalicylate. The stained cells were identified under a fluorescent microscope (Olympus) according to their characteristic morphology (*L. migratoria*: Römer and Marquart, 1984; Stumpner and Ronacher, 1991, *T. leo*: Hennig, 1988).

2.3.2 Extracellular recording (Chapters 5 & 6)

Two extra-cellular hook-electrodes were made from tungsten wire and placed in parallel around one of the two connectives ascending from the prothoracic ganglion. These connectives contain the axon of the ascending interneuron AN2. Vaseline was placed around connectives and hooks in order to isolate the electrodes electrically and keep the connective from drying out. The voltage trace was amplified differentially (npi, EXT-10C, Tamm, Germany) and bandpass-filtered with cut-off frequencies of 300 Hz and 3 kHz (npi, DPA 2F). The trace was then digitized at 20 kHz sampling rate (National Instruments, PCI-6014, Austin, TX) and stored to the hard disk of a personal computer. Spikes of the AN2 were detected on the basis of the amplitude peaks of

the voltage trace using custom software (MATLAB 7, The MathWorks, Natick, MA). Fig. 2.1 shows an example recording and the spike detection window.

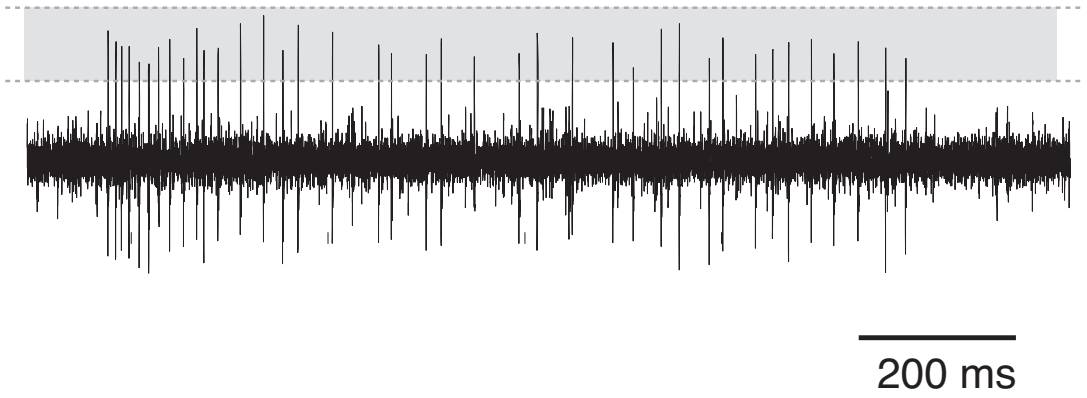

Figure 2.1: **Typical recording trace from a cricket AN2 neuron** (*T. oceanicus*). The figure shows the voltage trace during constant stimulation (duration 1 s) with a sinusoidal tone of 16 kHz frequency. The shaded area depicts the spike detection window, bounded by the lower and upper threshold.

2.4 Stimulation

2.4.1 Acoustic stimuli (Chapters 3, 5 & 6)

Acoustic stimuli were delivered in a cage lined with sound absorbing foam via one of two speakers (D-28/2, Dynaudio, Skanderborg, Denmark) located at $\pm 90^\circ$ and 35 cm away from the preparation.

For the experiments described in Chapters 3 and 6, signal envelopes were digitally stored and delivered by custom-made software (LabView, National Instruments, Austin, TX) via a 10 kHz D/A-converter (PCI-6014, National Instruments, Austin, TX). Subsequently, the envelopes were multiplied (multiplier: Heinecke, Seewiesen, Germany) with a sine wave (FG-506, Voltcraft, Hirschau, Germany). For the experiments in Chapter 5, real-time signals were delivered at a sampling rate of 100 kHz (PCI-6014, National Instruments, Austin, TX). Real-time and multiplied signal were attenuated under digital control (PA5, Tucker-Davis Technologies, Gainesville, FL), and amplified (GTA 2100B, Blaupunkt, Hildesheim, Germany). Sound intensities were calibrated with a 1/2″ microphone (type 2209, Brüel & Kjær, Bremen, Germany).

2.4.2 Current stimuli (Chapters 3, 5)

Current stimuli were digitally stored and delivered by custom-made software (LabView) via the recording electrode. The amplifier (SEC-05LX, npi electronic, Tamm, Germany) was set to either bridge or discontinuous current clamp modus. Discontinuous switching rates were adjusted on a cell-to-cell basis to values of 15-20 kHz. In several cells both recording modes were applied in order to verify that the outcome of the analysis did not depend on the recording procedure.

2.5 Data analysis

2.5.1 Spike frequency estimation (Chapters 3, 4 & 5)

Spike frequency $f(t)$ at each time t was estimated by taking the inverse of the interspike intervals (ISIs) between the preceding and the following spike for every trial separately. At the time of a spike, the value of the preceding ISI was taken. For all times before the first and after the last spike in the recording $f(t)$ was set to zero. The mean spike frequency $\bar{f}(t)$ and standard deviation was obtained by averaging across trials. The onset response $\bar{f}_{on}(x)$ was obtained by taking the maximum of $\bar{f}(t)$ in the first 30 ms after stimulus onset. The steady state response $\bar{f}_{ss}(x)$ (Chapter 3) was calculated as the mean of the 30 ms interval starting at 420 ms after stimulus onset.

Part I. Where does adaptation act?

Experimental approaches and theoretical considerations

3 The origin of adaptation in the auditory pathway of the locust

3.1 Introduction

In this chapter, the main goal of the work was to describe adaptation at different levels of the auditory pathway (Fig. 1.3) and to determine the location of adaptation within the sensory pathway, or *where* adaptation originates. Adaptation is quantified by means of the decrease of spike frequency, the inverse of the interspike intervals, and is referred to as spike frequency adaptation (SFA).

The net SFA observed in the intact sensory pathway will typically result from the sum of many processes occurring between the stimulus and the recording site (Fig. 1.1). All cells involved in the transformation of the physical stimulus to neural information, all cells that transform the neural signal and pass it on and all connections between these sensory cells are potential sites of adaptation. Each of these steps along the pathway transforms the representation of sensory information, and the distribution of adaptation mechanisms among these steps has been proposed to reflect a general design principle (Laughlin, 1989; Baccus and Meister, 2004).

Disentangling the respective contributions to SFA within a pathway is a difficult task. Most attempts to examine SFA have been done either by using sensory stimulation *in-vivo* or current stimuli *in-vitro*. In the latter case, intrinsic properties of isolated cells or small circuits are isolated, while sensory stimulation invokes adaptation mechanisms within the entire pathway. Here, the auditory pathway of locusts (*Locusta migratoria*) serves as model for the functional relevance of the distribution of mechanisms of SFA. In order to do so, SFA is investigated *in-vivo* in response to both acoustic stimuli and injected currents in the same cell. Specific identified auditory interneurons in the metathoracic ganglion of the locust were surveyed and different characteristic patterns of adaptation mechanisms were identified for different cell types.

The auditory pathway of locusts at the level of the metathoracic ganglion is a hierarchical network with three layers: receptors and receptor-like interneurons, local neurons, and ascending neurons. Three exemplary interneurons from each processing level were selected: TN1 receives monosynaptic input from receptor cells and exhibits spiking responses that are similar to those of the receptors, BSN1 is a local interneuron that represents an intermediate processing level, and AN2 is an ascending interneuron that transmits information directly to the insect's brain (Stumpner and Ronacher, 1991). On present evidence there is no direct connection between the three cell types presented here. Overall connectivity in the network appears to be low (Vogel and Ronacher, 2007), consisting of feed-forward connections between the layers but no connections between neurons of the same layer (Marquart, 1985; Boyan, 1992, 1999; Vogel and Ronacher, 2007).

During the experiments presented here, the magnitude and time course of SFA were

systematically quantified for the three cell types in response to the two stimulation modes. Subsequently, the distribution of adaptation mechanisms along the auditory pathway is explored and its possible consequences for sensory processing are discussed. Finally, it is discussed whether SFA predicts differences in coding of temporal aspects of signals for those cell types. All results presented in this chapter have been published in Hildebrandt et al. (2009).

3.2 Methods

3.2.1 Stimulus design

Each recorded cell was stimulated both acoustically and intracellularly by current injection. For both stimulation modes the range and resolution of intensity values for all experiments was chosen such that the entire response curve was appropriately covered. This was achieved by online-spike detection and calculation of response curves.

For the input-response curves pulses of 500 ms duration were used. The pulses included a 2 ms ramp at beginning and end. For acoustic stimulation, the carrier frequency for each cell was set to either 5 or 12 kHz, chosen on a cell-to-cell basis, depending on which frequency the cell was most sensitive to. For both stimulation modes, stimulation at each intensity level was repeated ten times.

To characterize coding properties of the cells under acoustic stimulation, a randomly amplitude-modulated (RAM) stimulus was used that had a duration of 5 s and was repeated 15 times. The amplitude modulation was obtained by low-pass filtering Gaussian noise at 100 Hz and multiplication with a constant carrier of the same frequency as the pulse stimuli used for characterization of SFA. The standard deviation of the RAM stimulus was in all cases 6 dB, independent of the mean level, and the highest peak in the amplitude distribution was 18 dB (three times the standard deviation) above mean.

3.2.2 Data analysis

Characterization of spike frequency adaptation

For the study of the cell-specific origin of spike frequency adaptation (SFA), adaptation to current and acoustic stimuli was compared. The comparison of SFA under the two stimulation modi is complicated by the fact that SFA depends on signal intensity. For this reason, the onset and steady state input response curves were interpolated linearly in order to obtain values for $\bar{f}_{ss}$ at a given reference onset response f_{on}^{ref} of 70 and 140 Hz, respectively.

For this purpose, the first value of $\bar{f}_{on}(x)$ that exceeded f_{on}^{ref} and the value at the next lower intensity were considered. Then, x_{ref} is obtained by linear interpolation, for which $f_{ss}(x_{ref})$ can be calculated. The adaptation ratio r_a is then given by $r_a(x) = \bar{f}_{ss}(x)/\bar{f}_{on}(x)$. Propagated errors were calculated by partial differentiation for all four spike frequencies contributing to the interpolation equation.

If adaptation mechanisms intrinsic to receptors and interneurons added up linearly, the ratio for acoustic stimuli r_a^{ac} in an interneuron that is mono-synaptically connected to receptors should be the product of the adaptation ratio of the interneuron r_a^{cu} and

that of the receptors cells. Spike frequency in receptors adapts to $\approx 50\%$ of their onset response (Benda, 2002). Thus, in the simplest case: $r_a^{ac} = 0.5 r_a^{cu}$. The data was compared to this relation.

The time constant of SFA was obtained by fitting an exponentially decaying function with three free parameters (onset spike frequency $\bar{f}_{on}$, adaptation time constant $\tau_{adapt}(x)$, and steady-state spike frequency $\bar{f}_{ss}$ to $\bar{f}(t)$ by least squares. It was verified that double exponential fits did not significantly improve the fit quality. The time course of SFA proved to be strongly dependent on input intensity. For this reason $\tau_{adapt}(x)$ was pooled and displayed as histograms. For the comparison of the time course of SFA under current and acoustic stimulation (see Fig. 3.3), only values of $\tau_{adapt}(x)$ were taken, at which the regression coefficient between fitted and real data was > 0.8.

Quantification of adaptation effects after stimulus offset

The decrease in spontaneous activity due to SFA was quantified by a rate coefficient $c^r(x)$:

$$c_i^r(x) = \left\langle \frac{n_i^{after} - n_i^{before}}{n_i^{after} + n_i^{before}} \right\rangle, \tag{3.1}$$

where n_i^{before} and n_i^{after} indicate the number of action potentials in a 200 ms-segment before and after the stimulus in the ith trial at a given intensity x. Only those trials, for which $n_i^{after} + n_i^{after} > 0$ were taken for further analysis. Angle brackets indicate averaging over all such trials. For TN1, the window had to be extended to 300 ms in order to collect a significant number of spikes for evaluation.

Hyperpolarization was quantified as the minimum of the membrane potential within 200 ms after stimulus offset averaged over trials. The minimum was evaluated for single trials separately and the mean of the respective trials 200 ms before the stimulus was subtracted before averaging.

Afterhyperpolarizations

Spike shapes were obtained by taking the median of each data point within time windows 50 ms before and 250 ms after each occurrences of a spontaneous spike. Time constants of the decay of afterhyperpolarizations were acquired by fitting a single exponential function to the time course of the median spike shape from the minimum on. The minimum of the hyperpolarization was measured relative to the peak amplitude of the spikes in order to compensate for variations in recording site and quality.

Characterization of coding properties

In order to describe coding properties, RAM stimuli were presented with an intensity that elicited an onset response of $\approx 250 \pm 5\,Hz$. RAM stimuli were filled with the same carrier frequency as the test pulses presented for the characterization of SFA. To obtain an estimate of the frequency transmission properties of the cell types, the gain functions were calculated. Spike frequency responses to RAM stimuli 500 ms after stimulus onset were sampled in 1-ms-bins. Subsequently, hamming windows of 1024 ms duration

and overlapping 50% were transformed to the frequency domain and compared to the respective window in the stimulus:

$$g(f) = \left| \frac{\langle R_r s(f) \rangle}{\langle R_{ss}(f) \rangle} \right|, \tag{3.2}$$

where $R_{rs}(f)$ is the cross-spectral density between response and stimulus, $R_{ss}(f)$ is the autospectral density of the stimulus, $\langle * \rangle$ indicates averaging across the 1024 ms–windows and $| * |$ is the magnitude of the complex argument.

3.3 Results

3.3.1 Characterization and comparison of spike frequency adaptation

In a first step, spike frequency adaptation (SFA) was characterized in three auditory interneurons at different processing levels by determining the input-response relations. To do this, the onset and steady state responses to both current and acoustic pulse stimuli were obtained at different intensity levels.

3.3.2 Response curves

Stimulated acoustically, TN1 showed a steep sigmoid, receptor-like response curve, saturating at higher intensity levels. This was observed for both the onset and the steady state response. Spike frequency adaptation was moderate, reducing the steady state response to about 30-40 % of the onset response (Fig. 3.1A, left panel). Under current stimulation, TN1 showed a linear input-response relation throughout the entire range of currents from 0 to 5 nA (Fig. 3.1B, left panel). The steady state response was also linear and about half that of the onset response. For the respective stimulation modes, the general shape of onset and steady state response function was the same.

BSN1 showed pronounced SFA under acoustic stimulation, had a considerably lower threshold than TN1, and the onset response saturated quickly. At higher intensities, the steady state response was reduced to zero, while the onset response remained unchanged (Fig. 3.1A, middle panel). The spike raster plot at the bottom of the middle panel of Fig. 3.1A displays how spiking is suppressed entirely after a short onset response at intermediate intensity levels. Under current stimulation, BSN1 generally resembled the response patterns of TN1, and exhibited a linear input-response relationship for onset and steady state response up to relatively large currents (Fig. 3.1B, middle panel). BSN1 saturated at higher intensities. It was possible to elicit much larger responses in BSN1 than in TN1, a fact that might be attributed to the actual site of recording and may account for these differences between the two cells.

In AN2, the slope of the onset response curve during acoustic stimulation was shallower than in either BSN1 or TN1 (Fig. 3.1A, right panel). It fired phasically in both stimulation modes; spikes at the end of the 500 ms stimulus occurred only at intermediate intensities. At high intensities firing ceased entirely after the onset response (Fig. 3.1A, right panel, bottom). This pattern of AN2 was similar to BSN1 under acoustic stimulation. AN2, however, showed the same response pattern under current stimulation: for larger injected currents, spikes occurred only at the beginning of the stim-

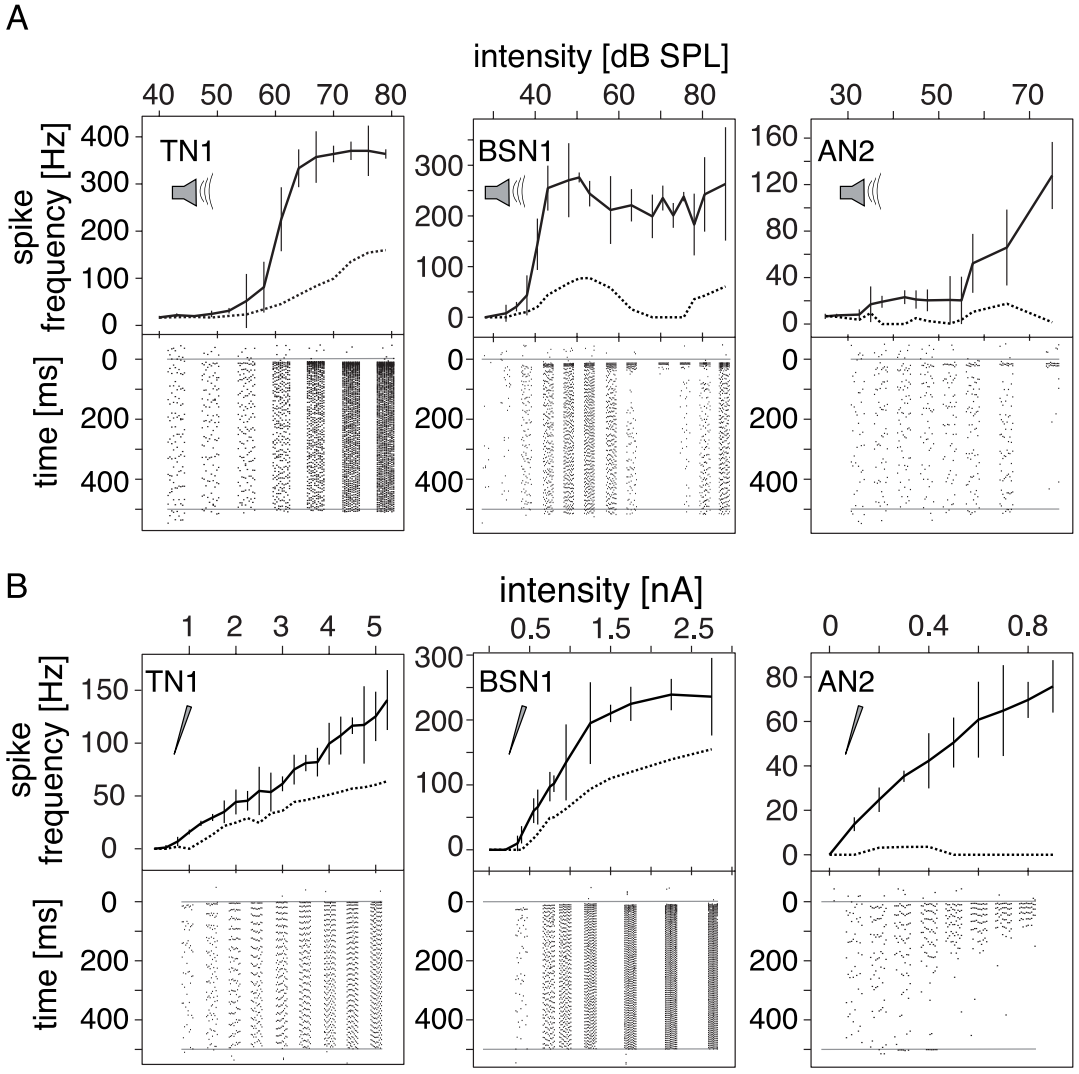

Figure 3.1: **Input response curves for acoustic and current stimulation.** Responses to constant stimuli at different intensities for three different cell types. The thick line in the upper part of each graph describes the onset response curve, measured as the maximum firing rate during the first 30 ms of a 500 ms rectangular stimulus. The dashed line represents the mean response to a 30 ms interval starting 420 ms after stimulus onset. Mean values and standard deviations for ten repetitions are shown. The lower parts of the graphs show exemplary spike raster plots for the same stimuli at the intensity indicated by the respective axis, time running from top to bottom. Grey lines indicate the onset and end of the stimulus. (A): acoustic stimulation. (B): current stimulation (identical cells as in A).

ulus (Fig. 3.1B, right panel).

3.3.3 Magnitude of spike frequency adaptation

In order to quantify and compare the magnitude of SFA, the ratio between steady state and onset response was computed at both stimulation modes. In most cases, this ratio was not constant over different intensity levels that elicited different onset responses (Fig. 3.3.3A). Starting with two onset ratios for two different frequencies, the input-response relation to estimate the ratios at 70 and 140 Hz onset spike frequency were interpolated linearly. This makes it possible to compare the magnitude of SFA under acoustic and current stimulation directly and to relate the ratios to SFA in receptor neurons, as studied by Benda (2002).

In TN1, the adaptation ratio for current stimulation was between 0.5 and 0.8 at almost all intensity levels (Fig. 3.3.3A, lower left panel). During acoustic stimulation, SFA was much stronger and ratios were usually below 0.5 (Fig. 3.3.3A, upper left panel). Direct comparison of the adaptation ratios at 70 and 140 Hz (Fig. 3.3.3B&C) showed that the magnitude of SFA to acoustic stimuli is qualitatively in agreement with a linear combination of SFA in receptors and adaptation mechanisms within TN1, leading to a multiplication of adaptation ratios. Cells exhibiting stronger SFA under current stimulation should also adapt more strongly to acoustic stimuli, yet no positive correlation between the ratios for acoustic and current stimuli was found for TN1 ($r = 0.09$, $p = 0.81$; Fig. 3.3.3B and C). The putative correlation may have been masked by the large errors in the input-response curves that propagated to the adaptation ratios.

Figure 3.2 *(following page):* **Magnitude of spike frequency adaptation.** (A): Comparison between onset and steady state spike frequency at different stimulus intensities. Different cells areof represented by different symbols. In the upper (acoustic stimulation) and lower (current stimulation) graphs data from the same cells are shown. The dotted line marks a ratio f_{ss}/f_{max} of 1, corresponding to no SFA while the solid line depicts a decrease of the spike frequency by 50%. The black arrows indicate those onset spike frequencies, for which adaptation ratios are plotted in (B) and (C) (70 and 140 Hz). (B) and (C): Comparison of adaptation ratios (f_{ss}/f_{max}) for current and acoustic stimulation at a single onset spike frequency. Onset and steady state spike frequencies were derived from linear interpolations; error bars depict standard deviation as calculated by propagation of error (see methods). The solid line marks equal SFA under current and acoustic stimulation, the dashed line depicts the expectation from a simple linear multiplication of adaptation mechanisms in the receptors and spiking-triggered adaptation currents in the interneuron. (B): Onset frequency 70 Hz, C - 140 Hz, only those cells are shown, for which in both stimulation modes a spike frequency of at least 140 Hz were reached. (Filled circles: AN2; open triangles: BSN1; filled squares: TN1).

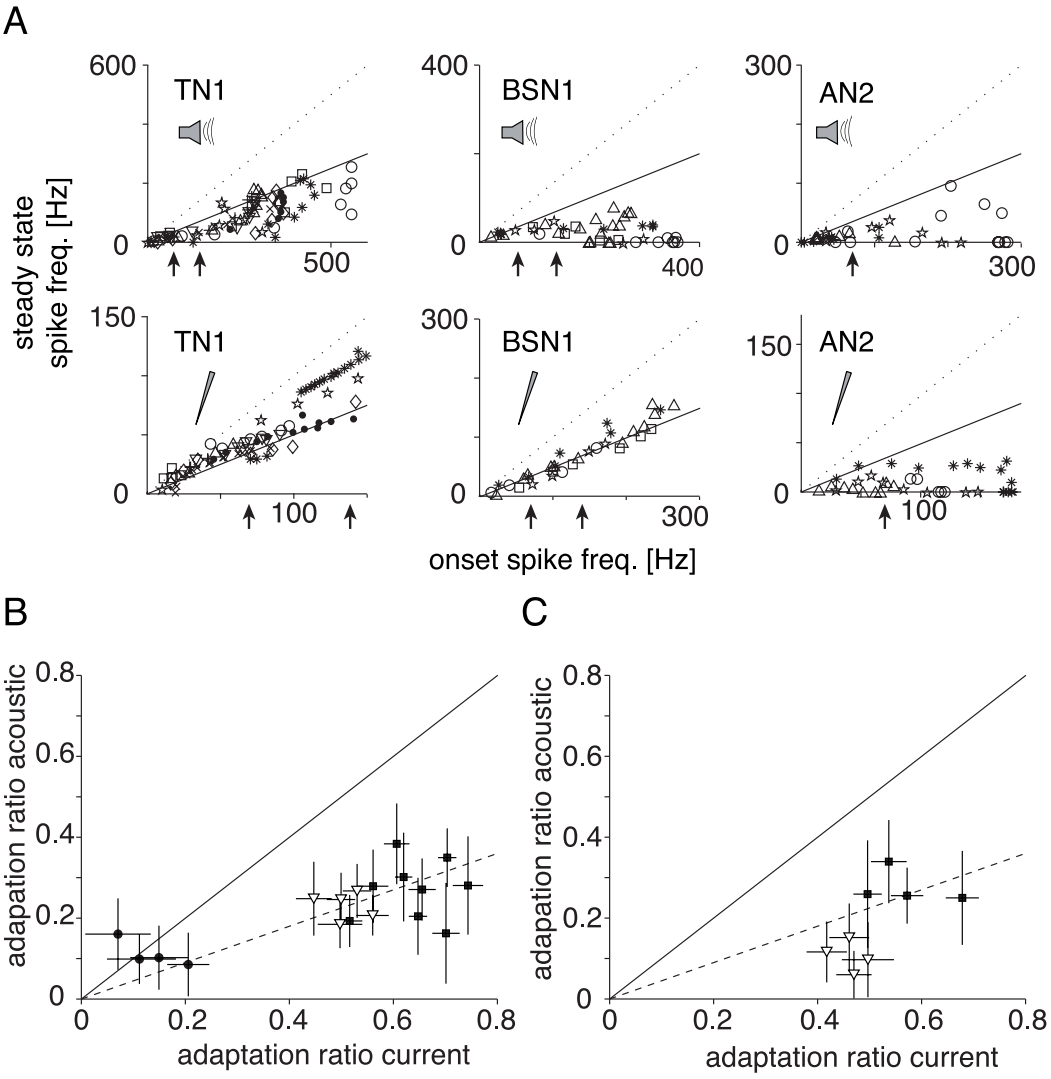
A
600
TN1
0
500
400
BSN1
0
400
300
AN2
0
300
steady state
spike freq. [Hz]
150
TN1
0
100
300
BSN1
0
300
150
AN2
0
100
onset spike freq. [Hz]
B
adapation ratio acoustic
0.8
0.6
0.4
0.2
0
0
0.2
0.4
0.6
0.8
adaptation ratio current
C
adapation ratio acoustic
0.8
0.6
0.4
0.2
0
0
0.2
0.4
0.6
0.8
adaptation ratio current

In BSN1, SFA to current stimulation showed a constant ratio around 0.5 (Figs. 3.1A, 3.3.3A). Under acoustic stimulation, the magnitude of SFA depended on stimulus intensity, but was always lower than 0.5 (Figs. 3.1A, 3.3.3A). At 70 Hz onset response, the ratio under acoustic stimulation was about half of that under current stimulation, similar to what was observed in TN1 (Fig. 3.3.3B). At 140 Hz onset response, SFA during acoustic stimulation was much stronger than expected from adaptation mechanisms within receptors and BSN1 alone, suggesting additional processes underlying the SFA at higher acoustic stimulus levels.

In AN2, the magnitude of SFA was nonlinear with respect to intensity, both under current and acoustic stimulation (Figs. 3.1A&B, 3.3.3A). The adaptation ratio was in both cases around 0.2 for the 70 Hz response. At these levels the large errors rule out an interpretation of the relation between these two. AN2 was not analysed at the higher onset response, because only one of the cells under study responded with more than 140 Hz at both stimulation modes.

3.3.4 Time course of spike frequency adaptation

The second important characteristic of spike frequency adaptation is its time course. During acoustic stimulation, the time course of SFA elicited by current stimulation is convolved with the kinetics of all adaptation processes peripheral to the cell, whereas in the current injection it is not. Thus, only if SFA under acoustic stimulation is dominated by intrinsic mechanisms of the cell, the time course and its intensity-dependence should be similar under acoustic and current stimulation.

In TN1, the decrease of spike frequency was approximately exponential over all intensity levels (Fig. 3.3A&B), while in BSN1 this was only the case for current stimulation (Fig. 3.3B). In BSN1 the time course of responses to current stimuli was essentially intensity invariant (Fig. 3.3B), while higher intensity levels under acoustic stimulation led to a discontinuous, phasic firing behaviour (Fig. 3.3A). This phasic firing pattern at certain intensity levels was observed in the AN2 for both acoustic and current stimulation (Fig. 3.3A&B). The time course was quantified by single exponential fits, where possible. For the following analysis only data was included, for which a single exponential fit yielded a regression coefficient > 0.8. In TN1 the time courses for acoustic

Figure 3.3 *(following page):* **Time course of spike frequency adaptation** during 500 ms constant stimulation at different intensity levels for current and acoustic stimulation. (A) and (B): the black bar at the bottom of each graph indicates the presentation of the stimulus. The solid black line represent the lowest, the grey line an intermediate and the dashed line the highest intensity level. (C): Comparison of time constants of SFA. Time constants for all available stimulus presentations (data were rejected if a single exponential fit did not yield a regression coefficient > 0.8). Above the histograms, means $\pm$ standard deviations are indicated, asterisks mark significance at the 1% level. All data from the cells shown in (A) and (B) are coloured in grey. Open bars represent acoustic stimulation, filled bars depict current stimulation.

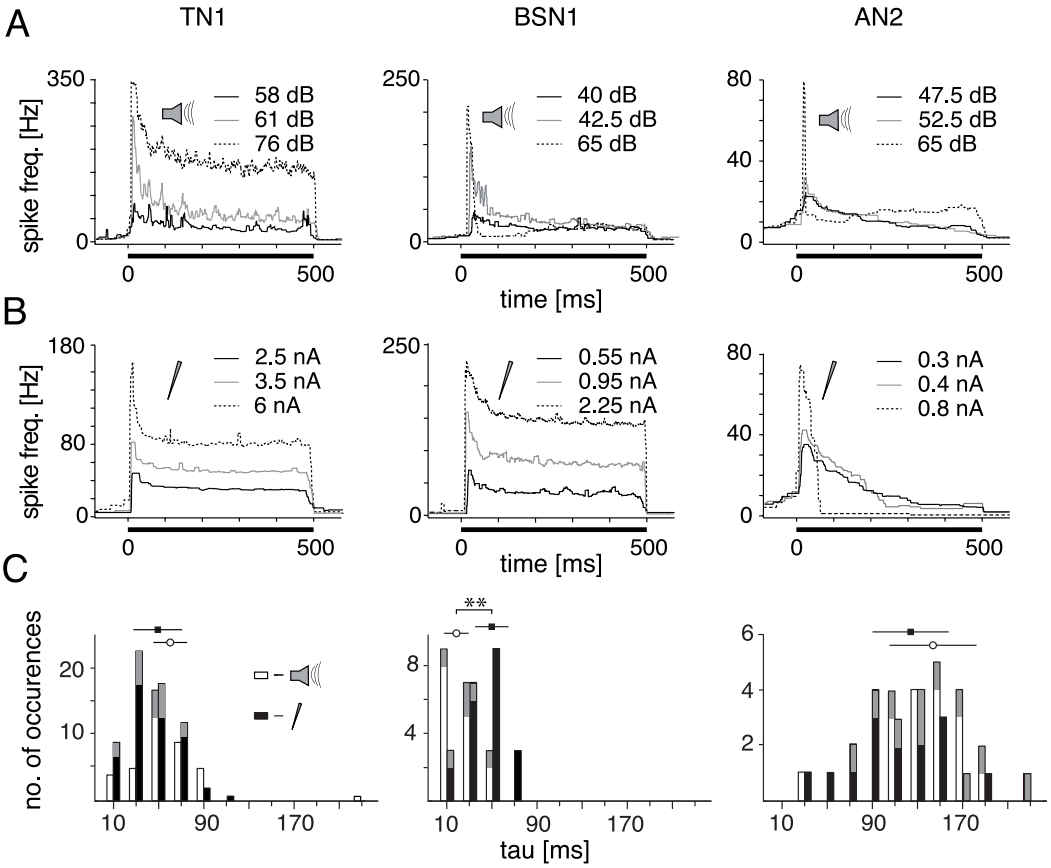
A
TN1
BSN1
AN2
spike freq. [Hz]
350
0
58 dB
61 dB
76 dB
250
40 dB
42.5 dB
65 dB
80
40
47.5 dB
52.5 dB
65 dB
0
500
time [ms]
B
180
80
2.5 nA
3.5 nA
6 nA
0.55 nA
0.95 nA
2.25 nA
0.3 nA
0.4 nA
0.8 nA
C
no. of occurences
20
10
8
4
6
2
10
90
170
**
tau [ms]

and current stimuli were rather similar (Fig. 3.3A&B) and did not differ significantly ($p = 0.37$, Wilcoxon ranks sum test; acoustic stimulation: 60.0 ± 14.9 ms; current stimuli: 49.3 ± 21.6 ms, Fig. 3.3C). In BSN1 time constants differed between current and acoustic stimulation ($p < 0.01$): current stimuli reduced spike frequency with a time constant of 49.8 ± 14.8 ms, similar to TN1, while acoustic stimuli led to shorter time constants of 18.7 ± 10.9 ms (Fig. 3.3C). In AN2, SFA acted on longer time scales than in TN1 and BSN1. Both current and acoustic stimulation revealed time constants longer than 100 ms and were not significantly different from each other (acoustic: 143.6 ± 38.2 ms, current: 123.8 ± 35.0 ms, $p = 0.68$, Fig. 3.3C).

In summary, TN1 and BSN1 showed very similar adaptation characteristics when stimulated with current and revealed a moderate and linear SFA with time constants around 50 ms. When stimulated acoustically, this pattern changed dramatically in BSN1 and became much more similar to the pattern observed for the AN2 that exhibited strong SFA with a high dependence on the stimulus level. In AN2, current and acoustic stimuli led to very similar results with respect to time course and magnitude of SFA. These findings provide evidence for strong network effects on SFA under acoustic stimulation in BSN1, while in AN2 SFA can be understood mainly by intrinsic properties. In TN1, SFA observed under acoustic stimulation is in good agreement with a linear combination of adaptation mechanisms within receptors and in the interneuron itself.

3.3.5 Hyperpolarization after stimulus offset

Having analysed the magnitude and time course of SFA, the next step is to reveal the mechanisms behind SFA in the cell under study, specifically hyperpolarizing currents and inhibition. If SFA affects a cell directly, the reduction in spike frequency should be observed as a decrease in excitability of a cell and should be maintained after stimulus offset. Therefore spontaneous activity and hyperpolarizations directly after the stimulus were evaluated as measures of excitability. A post-stimulus hyperpolarization due

Figure 3.4 *(following page):* **Hyperpolarization after stimulus offset** (A): Time course of the membrane potential for the first 100 ms after stimulus offset for different stimulus intensities. The dotted line depicts the mean potential before stimulus presentation. Darker shading represents a higher intensity of the stimulus. TN1: current – 0.5, 1.0, 1.5 and 2.5 nA, acoustic – 60, 66, 72 and 78 dB. BSN1: current – 0.55, 0.95, 1.5 and 2.25 nA, acoustic – 40, 47.5, 55 and 65 dB. AN2: current - 0.5, 0.6, 0.7 and 0.8 nA, acoustic 45, 55, 65 and 75 dB. (B-D): Hyperpolarization after stimulus offset as a function of the maximal spike frequency response during stimulation. Each data point depicts the mean and standard deviation of the minimum of the membrane potential for ten repetitions in a window 200 ms after stimulation relative to the mean potential before stimulus onset. Open symbols: acoustic stimulation, filled symbols: current stimulation. Lines show linear fits to the data. (B-D) data from the same cells as in Fig. 3.6A-C). (E): Regression coefficients for linear fits to rate hyperpolarization vs. max. spike frequency for all recorded cells for current and acoustic stimulation.

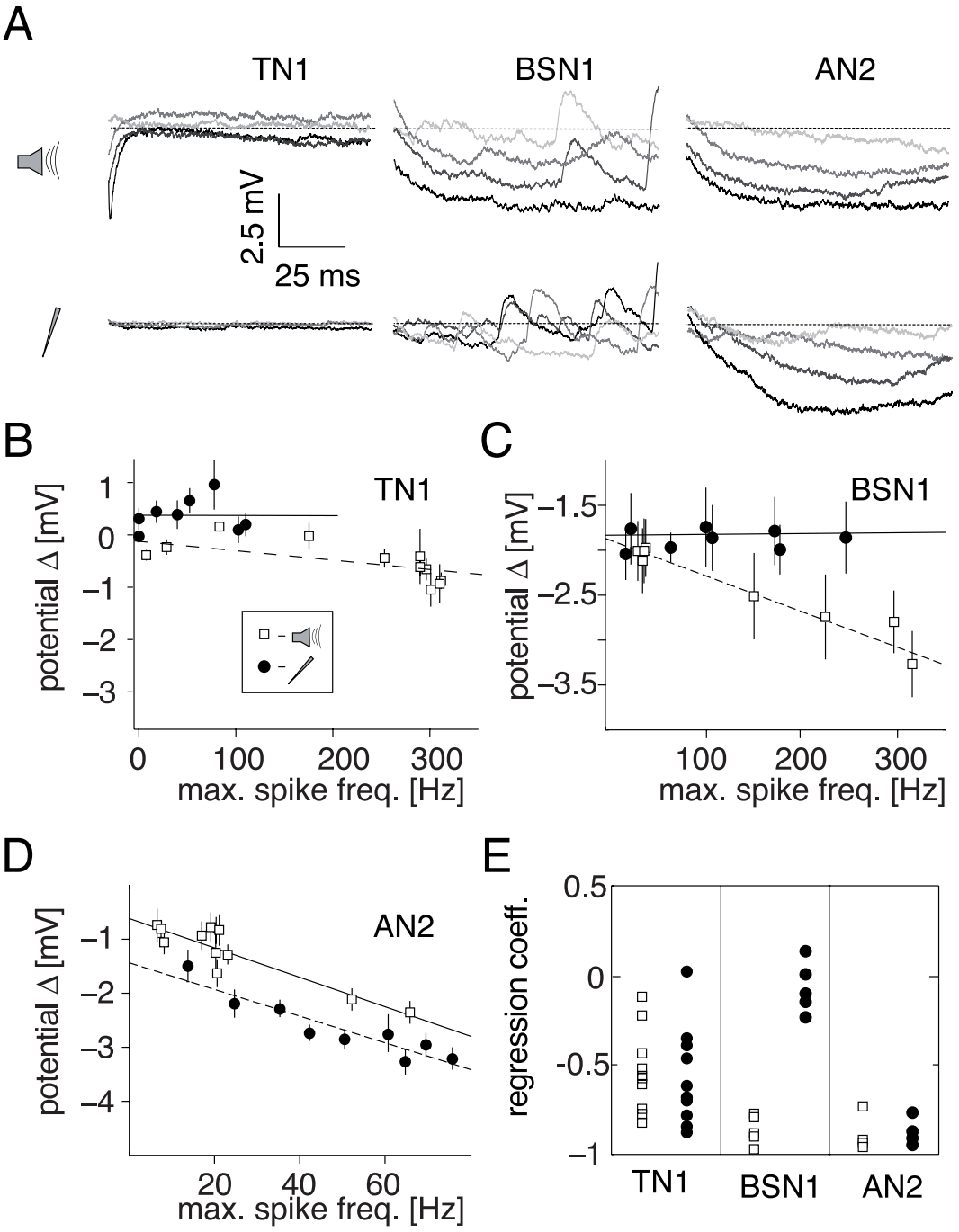
A
TN1
BSN1
AN2
2.5 mV
25 ms
B
TN1
potential Δ [mV]
max. spike freq. [Hz]
C
BSN1
potential Δ [mV]
max. spike freq. [Hz]
D
AN2
potential Δ [mV]
max. spike freq. [Hz]
E
regression coeff.
TN1
BSN1
AN2

to SFA can have two sources: if it is the result of intrinsic adaptation currents, then it should occur after both current and acoustic stimulation; on the other hand, only acoustic stimulation will cause another neuron to inhibit the observed cell, but not current injection.

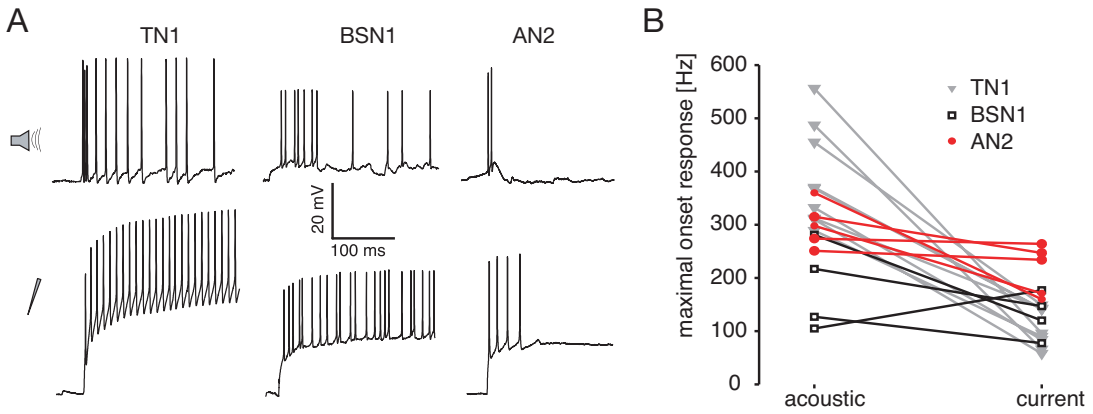

Figure 3.5: **Comparison of the reponses to acoustic and current stimulation.** (A): Example voltage traces as responses to acoustic and current traces for the three cell types. For each cell type, upper and lower traces originate from the same cell, respectively. (B): Maximal onset responses elicited by current and acoustic stimulation. Data from single cells are connected.

The relationship between activity during stimulation and reduced excitability after stimulation as revealed by spontaneous activity was quantified by analysing the voltage traces after stimulus offset. In TN1 the membrane potential returned to its initial value already 10 ms after stimulus offset for both current and acoustic stimulation (Fig. 3.4A). The membrane potential after acoustic stimulation displayed a very brief hyperpolarization directly after stimulus offset, which was not observed after current injection (Fig. 3.4A). Further inspection of the voltage traces revealed the consistent appearance of a hyperpolarization for spikes at the end of the stimulation period. These hyperpolarizations were always of the same amplitude and resembled the hyperpolarization after single spikes (Fig. 3.7). These fast hyperpolarizations were not observed after current stimulation, probably because spikes seldom occurred just at the end of a stimulus due to lower firing rates in TN1 under these conditions. As a result, only a very weak or no correlation between response strength during stimulation and after stimulus hyperpolarization was observed in TN1 (Fig. 3.4B&E).

Higher levels of acoustic stimulation led to larger hyperpolarizations in BSN1 (Fig. 3.4A), while current stimulation in BSN1 had almost no effect on the membrane potential after stimulation (Fig. 3.4B). This is reflected in the correlations between the response strength during and the level of the membrane potential after stimulation (Fig. 3.4A&C, current: $r = 0.04$, $p = 0.92$, acoustic: $r = -0.93$, $p = 0.0001$). All five BSN1 cells showed this pattern (Fig. 3.4E). In AN2, hyperpolarization under current and acoustic stimulation increased clearly with stimulus amplitude (Fig. 3.4A) and correlated with response strength during stimulation (Fig. 3.4D, current: $r = -0.92$, $p = 0.00001$, acoustic: $r = -0.93$, $p = 0.0003$). Highly significant relations for all tested AN2-type cells were observed (Fig. 3.4E).

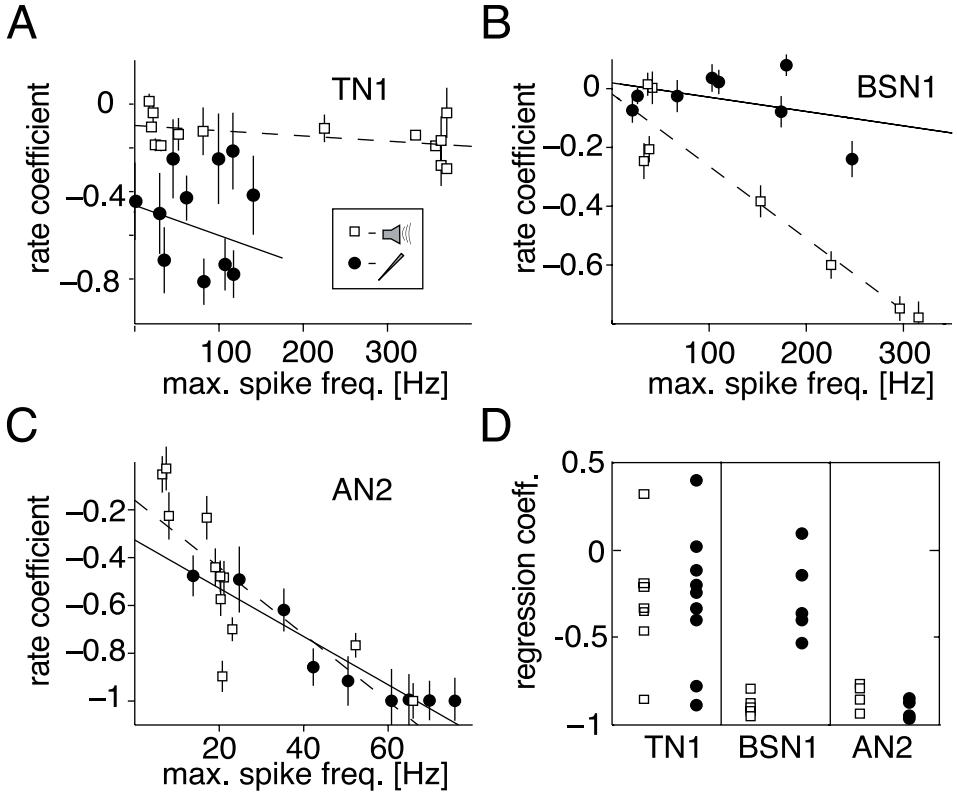

Figure 3.6: **Spontaneous activity after stimulus offset** as a function of the maximal spike frequency response during stimulation. Activity is expressed as the difference in the number of spikes in a window of 200 ms (300 ms for TN1, see text) before and after stimulation relative to the sum of spike numbers in both windows (= rate coefficient). Each data point depicts the mean and standard error mean of ten repetitions. Open squares: acoustic stimulation, filled circles: current stimulation. Lines show linear fits to the data. (A)-(C): exemplary data from single cells. (A): TN1, (B): BSN1, (C): AN2. (D): Regression coefficients for linear fits to the rate coefficient vs. the maximal spike frequency for all recorded cells for current and acoustic stimulation.

While the pronounced afterhyperpolarizations observed in AN2 provide strong evidence for spike activated adaptation currents within AN2 for both stimulation modes, the absence of long-lasting hyperpolarizations in TN1 and BSN1 after current stimulation could also be due to a site of recording distant from the spike initiating zone. TN1, for example was possibly recorded much more axonally than BSN1 and AN2 (for examples of voltage traces see Fig. 3.5A) and thus lasting hyperpolarizations in the dendritic part of the neuron may not have propagated into the axon. As a control, the spontaneous activity in the three cells was analysed before and after current or acoustic stimulation. In this case, only spike numbers are evaluated, on which the actual recording site should not have an effect.

In order to quantify spontaneous activity, spikes were counted in 300-ms-windows before and after each stimulus and compared by a rate coefficient. Negative values of this coefficient indicate a reduction of spontaneous activity due to stimulation. For the TN1 shown in Fig. 3.6A no correlation between the response strength and the spontaneous activity after stimulus end was observed during acoustic or current stimulation (acoustic: $r = -0.45$, $p = 0.11$; current: $r = -0.20$, $p = 0.38$). Although there was a small overall decrease in spontaneous activity after current stimulation, this decrease did not depend on spiking activity. All but one out of nine cells of the type TN1 failed to exhibit a significant correlation between stimulated spiking activity and the number of spikes directly after acoustic stimulation. In seven recordings no correlation between current stimulation and subsequent spontaneous activity was observed (Fig. 3.6D). The time window for the TN1 was extended to 300 ms in order to collect a sufficient number of spontaneous spikes.

BSN1, on the other hand, remained less excitable and showed less spontaneous activity after the end of acoustic stimulation (Fig. 3.6B, $r = -0.95$, $p = 0.0003$). Under current stimulation, there was no observable effect ($r = -0.39$, $p = 0.34$) in any of the 5 cells tested (Fig. 3.6D). This implied that BSN1, even though it adapted slightly under current stimulation, did not change its excitability on longer time scales; the strong effects under acoustic stimulation must have their origin earlier in the sensory pathway. AN2 remained less excitable after the end of both current and acoustic stimulation (Fig. 3.6D). This effect correlated strongly with the response strength during stimulation for current and acoustic stimuli (Fig. 3.6C, current: $r = -0.794$, $p = 0.002$, acoustic: $r = -0.95$, $p = 0.0001$) and was observed in all four cells of this type (Fig. 3.6D). Thus, the analysis of spontaneous activity after stimulation confirmed the results obtained by quantifying afterhyperpolarizations (Fig. 3.4). The conclusion from these results is that in both BSN1 and AN2, strong SFA is accompanied by a distinct hyperpolarization and reduction of excitability. For BSN1 hyperpolarization was not observed during current stimulation and is likely mediated by presynaptic sites. For AN2 hyperpolarizing currents were spike dependent and played an important role for SFA as well as the overall spiking pattern. In TN1, however, no long lasting effect of SFA was observed.

3.3.6 Hyperpolarization after individual spikes

The analysis of hyperpolarization after current stimuli revealed that only the AN2 exhibits long lasting hyperpolarizations as a result of its own spiking activity, while the TN1 displayed only very brief effects and the BSN1 showed almost no effect at all (Figs. 3.4, 3.6). As afterhyperpolarization currents at the end of single spikes are

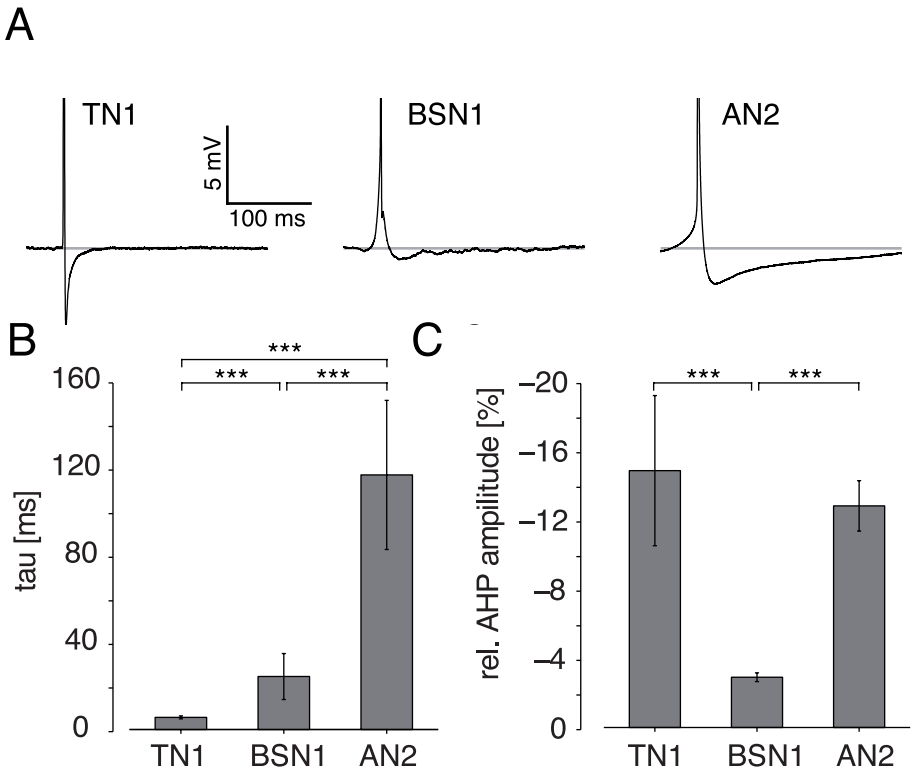

Figure 3.7: **Spike shapes of the different cell types.** (A): Median spike form from three exemplary cells, spikes are truncated in order to display afterhyperpolarization. (B): Mean and standard deviation of the time constants of decay of afterhyperpolarization for all tested cells. (C): Mean and standard deviation of the minimum of afterhyperpolarization, relative to peak spike amplitude. Asterisks mark significance at the 0.1% level.

thought to be one major source of intrinsic spike frequency adaptation, a close look at the spike forms can partly reveal the contribution of intrinsic adaptation currents in the tested cells. Only spontaneous spikes were investigated in order to minimize any extrinsic impact. The spike forms turned out to be very specific for each cell type (Fig. 3.7A). The TN1 exhibited a strong, but very fast decaying hyperpolarization, while in BSN1 only very weak hyperpolarizations were observed. In AN2, strong hyperpolarization was found, which also lasted much longer than in both TN1 and BSN1. The high specificity of the spike forms became apparent when population data was quantified. A fit by a single exponential function to the decay of afterhyperpolarizations showed that all three cell types differed from each other significantly at the 0.0001% significance level: 5.6 ± 0.7 ms in TN1, 24.6 ± 10.7 ms in BSN1 and 118.3 ± 34.7 ms in AN2 (Fig. 3.7B). Notably for the AN2, the time constant of the decay of afterhyperpolarizations resembled that of SFA in this cell type (123.8 ± 35.0 ms, Fig. 3.3C). The relative magnitude of afterhyperpolarizations was significantly smaller in BSN1 ($2.9 \pm 4.3\%$) than in both TN1 ($14.8 \pm 4.3\%$) and AN2 ($12.8 \pm 1.5\%$), while no significant difference between AN2 and TN1 was observed (Fig. 3.7). The spike forms help to understand the result of the analysis of hyperpolarization at stimulus offset: in TN1 afterhyperpolarization decays so rapidly that no effect lasting for more than 10 ms can be observed. BSN1 displayed almost no after-hyperpolarization and thus only an extrinsic, inhibitory influence can be responsible for hyperpolarizations observed after acoustic stimulation. In AN2 slowly decaying after-hyperpolarizations during stimulation accumulate over time and lead to an activity-dependent decrease in excitability.

3.3.7 Response characteristics under acoustic stimulation

For this study, three different cell types with different response properties were chosen, namely TN1, BSN1 and AN2. Following the analysis of SFA in these neurons, their coding properties were compared in order to determine the effect of spike frequency adaptation on signal processing. For this comparison, the gain function was used as an estimation of the frequency transmission properties of the cells (Fig. 3.8).

Figure 3.8 *(following page):* **Coding properties of TN1, BSN1 and AN2 under acoustic stimulation.** (A): Spike responses of TN1, BSN1 and AN2 under acoustic stimulation by randomly amplitude-modulated stimuli. The first 50 ms, first 500 ms and last 500 ms of a 5 s RAM stimulus are shown. The stimuli had a standard deviation of 6 dB and were filled with a constant carrier at the best frequency of the respective cell. The intensity was chosen to elicit an onset spike frequency response of about 250 Hz in each of the three cells. At the bottom the envelope of the stimulus is shown. (B): Gain functions for a TN1 neuron at two different intensity levels, for a BSN1 and an AN2. In the legend, the mean spike frequency responses in a 4500 ms time window starting 500 ms after stimulus onset are noted. Squares mark the high-pass cut-off for the cells as predicted by their adaptation time constant. Circles mark the mean spike frequency, which predicts the low-pass cut-off.

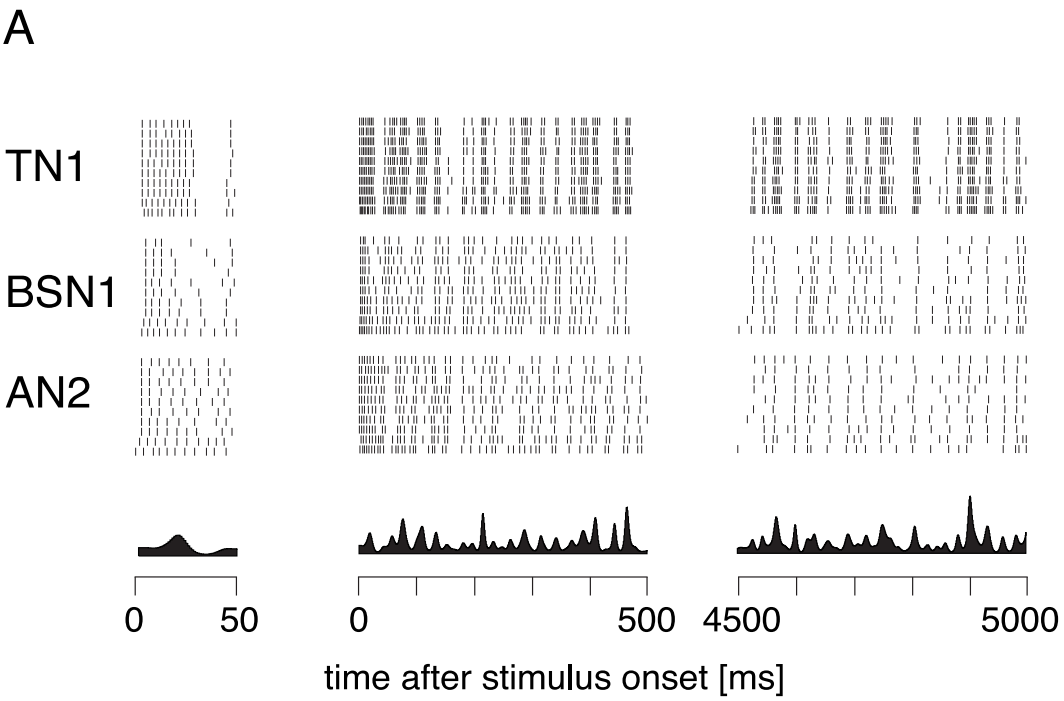
A
TN1
BSN1
AN2
0
50
0
500
4500
5000
time after stimulus onset [ms]

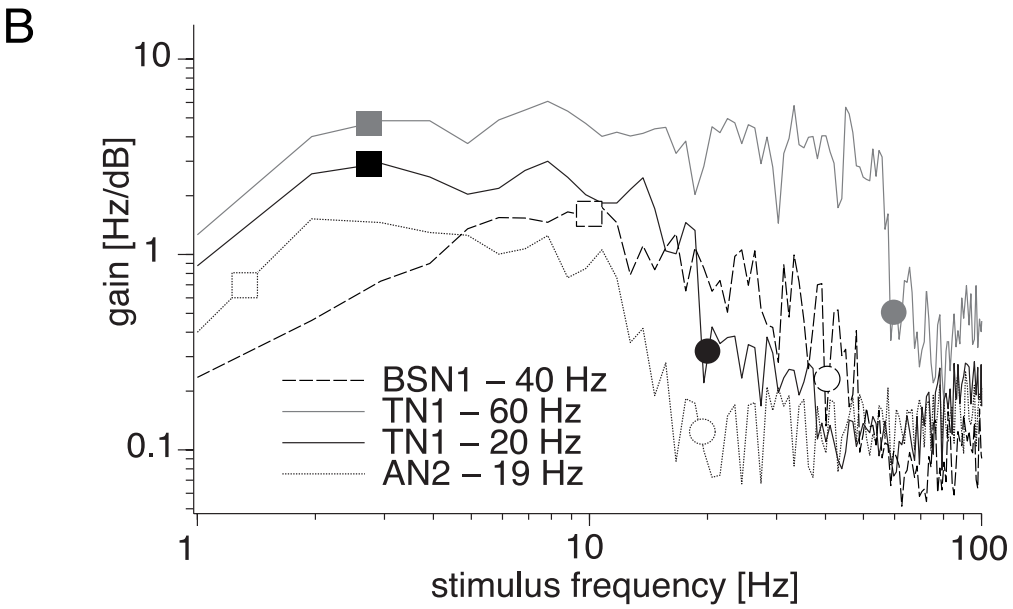
B
10
1
0.1
gain [Hz/dB]
BSN1 – 40 Hz
TN1 – 60 Hz
TN1 – 20 Hz
AN2 – 19 Hz
1
10
100
stimulus frequency [Hz]

For this set of experiments the intensity of a randomly amplitude-modulated stimulus (standard deviation 6 dB, carrier: best frequency for the respective neuron) was chosen such that the initial spike frequency was 250 Hz. All three cells in Fig. 3.8A responded with the same onset spike frequency of about 200 Hz. The pattern of the spike response of the TN1 approximately followed the time course of the amplitude modulations of the stimulus even after several seconds of continuous stimulation (Fig. 3.8A). Over such a long time spike responses of 200 Hz were regularly reached in response to larger stimulus deviations (Fig. 3.8A, left panels). In BSN1 and AN2 spike frequency decreased strongly over time and after continuous stimulation for several seconds the spiking patterns failed to follow smaller amplitude deviations (Fig. 3.8A, right panels). Thus, BSN1 and AN2 showed a similar reduction in spike frequency over time and — in comparison to the mainly tonically responding TN1 — they eventually exhibited a similar locking to temporal features of the stimulus. Note that the similarity between BSN1 and AN2 developed over time only and was not observed during the first 100 ms (Fig. 3.8A, left panel). As a measure of the frequency transmission properties, the gain function of the neurons was determined. All three neurons displayed band-pass characteristics (Fig. 3.8B). The mean spike frequency response of the neurons predicted the low-pass cut-off, as indicated by the circles in Fig. 3.8B. This dependence was apparent for the two different functions depicted for a TN1 (grey circles in Fig. 3.8B), which differed in the mean amplitude of the stimulus and consequently in the mean response. While the high-pass filter characteristic and the general course of the function below 15 Hz were very similar for both intensity levels, the cut-off frequency of the low-pass differed between the two recordings and depended on the mean spiking response of the cell. The high-pass characteristic on the other hand, can be predicted by time constants of SFA. If onset and steady state response curves were approximated by linear functions, the cut-off frequency f^{hi} for transmission of AM stimuli depended only on the time constant of SFA and can be predicted by $f^{hi}(\tau) = (2\pi\tau)^{-1}$ (Benda and Herz, 2003). In TN1, the gain decreased for frequencies below 3 Hz, while the prediction by a mean adaptation time constant of 60.0 ms lied at 2.6 Hz (Fig. 3.8B). For the BSN1, which adapted much more rapidly under acoustic stimulation (mean $\tau = 18.7\,ms$) a higher high-pass cut-off at 10 Hz was observed (predicted: 8.5 Hz). The gain function of the AN2, which adapted slowly with a mean time constant of 143.6 ms, revealed a high-pass characteristic with a cut-off between 1 and 2 Hz (prediction: 1.1 Hz). In summary, BSN1 and AN2 showed similar response characteristics under acoustic stimulation, shaped by a strong decrease of response strength over time. The TN1 on the other hand responded tonically and showed stronger, but less selective locking to the time course of the stimulus.

3.4 Discussion

In the present chapter, the origin of spike frequency adaptation was examined in different identified neurons along the auditory pathway of locusts. Between the three cell types, SFA differed significantly in strength and time course when stimulated acoustically. It was possible to discern the locations of adaptation mechanisms in the sensory pathway underlying SFA by an analysis of SFA under current injection and an evaluation of changes of the membrane potential after stimulation. Thereby, three distinct

patterns were found: a balanced influence of adaptation mechanisms in the afferents and intrinsic to the cells (TN1), predominantly network effects via inhibition (BSN1), and primarily intrinsic, spike-triggered adaptation currents (AN2).

3.4.1 Different origins of SFA in the three cell types

The results of the present chapter reveal three different patterns of how SFA is based on mechanisms resulting from intrinsic properties or the respective peripheral pathway in auditory interneurons of the locust (Fig. 3.9). First, both network and intrinsic cell properties can have a balanced impact on SFA as observed in TN1. In this cell, adaptation strength under acoustic stimulation was only moderately larger than under current stimulation (Figs. 3.3.3B, C). Adaptation time constants for both stimulation modes (Fig. 3.3C) were similar to those found in receptor cells (10-80 ms, Benda, 2002), in which SFA arises mainly from encoder adaptation (Fig. 3.9, no. 2; Benda and Herz, 2003; Gollisch and Herz, 2004. Thus, there is no evidence for an additional adaptation process other than in the afferent receptor cells and the intrinsic mechanisms of TN1 (Fig. 3.9, no. 2 and 4, cf. Ocker and Hedwig, 1996).

Second, SFA can arise from network effects acting either peripherally or on the cell itself. This pattern was apparent in BSN1, which adapted quickly with time constants below 20 ms (Fig. 3.3C). The strong SFA was accompanied by long lasting hyperpolarizations (Fig. 3.4A). Since these were not the result of spiking activity of the BSN1 (Fig. 3.4C), they probably are imposed by inhibitory inputs leading to slow hyperpolarizing currents (Fig. 3.9, no. 3, see also Weschke and Ronacher, 2008).

Third, SFA can be dominated by intrinsic properties, as observed in AN2. This cell revealed long lasting spike-triggered after-hyperpolarizations that accumulate over time and lead to a long lasting reduction in excitability (Figs. 4, 6). This finding makes a spike-triggered, hyperpolarizing AHP- or M-type current the most likely mechanism behind SFA in AN2 (Fig. 3.9, no. 4, Baldissera et al., 1973; Baldissera and Gustafsson, 1974). Notably, in AN2 SFA was stronger but slower than SFA seen in receptor neurons (Fig. 3.3C, Benda, 2002). Thus, intrinsic adaptation mechanisms may overwrite the time course of SFA in the upstream pathway, provided sufficient adaptation strength.

3.4.2 Impact of the stimulation site on the comparability between acoustic and current stimulation

All three cells are large and show an extended dendritic tree (Römer and Marquart, 1984; Stumpner and Ronacher, 1991) and the site of current injection may have an impact on the results and their interpretation. Therefore, the onset responses was compared as an indicator for the effective amount of current delivered in the two stimulation modes. In BSN1 and AN2, the maximal onset response to current and acoustic stimuli were similar, (Fig. 3.5B), and pronounced excitatory postsynaptic potentials suggest a more dendritic position of the electrode (Fig. 3.4A and Fig. 3.5A).

In TN1, large sound intensities elicit very strong responses not reached by current stimulation, probably due to a more axonal position of the electrode in TN1 recordings (Fig. 3.5A). Thus, the conclusions for TN1 are strictly valid only for onset responses up to 150 Hz. However, in TN1 both adaptation strength and dynamics were largely independent of intensity (Fig. 3.3.3, 3.3 and 3.5B) and there is no evidence for a more

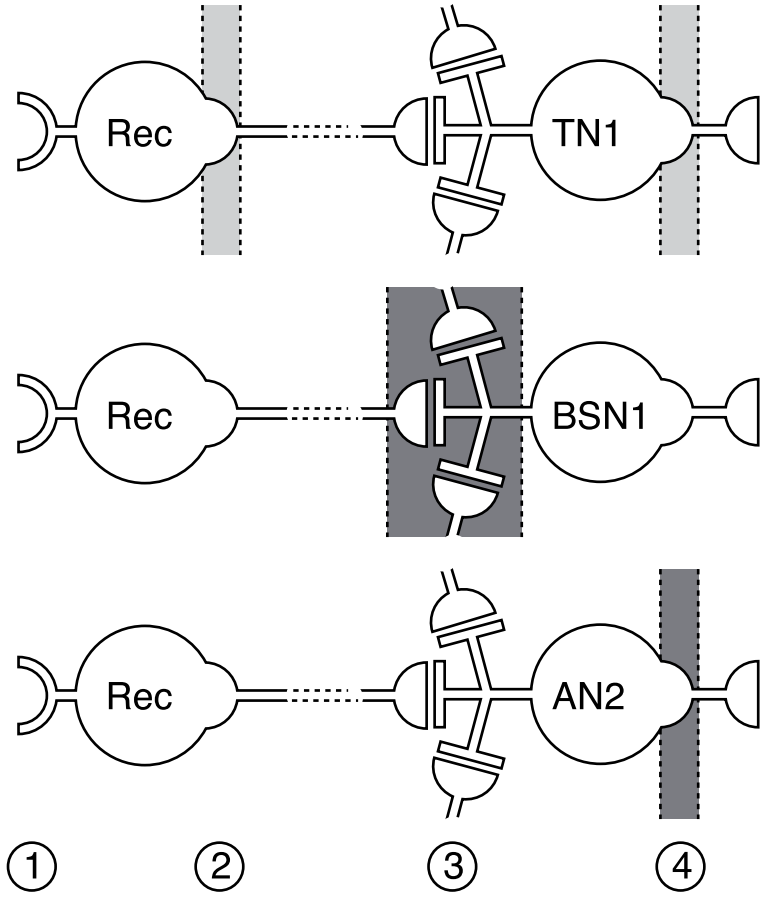

Figure 3.9: **Distribution pattern of adaptation mechanisms within the auditory pathway.** Schematic drawing of the dominating source and location of adaptation for the three cell types under study. The connection between interneurons and receptors cells can be monosynaptic but also indirect, indicated by the broken lines at their connection. The light grey areas in the sketch for TN1 represent balanced influence of two sources; dark grey areas depict one main source of adaptation. Numbers indicate mechanisms of adaptation discussed here: transducer adaptation (1), encoder adaptation in receptor neurons (2), synaptic effects (3) and encoder adaptation in the interneuron (4).

complicated scheme at higher intensities (see Gabbiani and Krapp, 2006 for similar results in a large visual interneuron).

3.4.3 SFA and signal transmission properties

Identified auditory interneurons in locusts have different temporal transmission properties (Stumpner and Ronacher, 1991; Prinz and Ronacher, 2002; Vogel and Ronacher, 2007). Can SFA, which is known to be of relevance for signal recognition in grasshoppers (Ronacher and Hennig, 2004), be linked to known transfer characteristics of neurons?

SFA acts mainly as a high-pass filter at low frequencies Benda et al. (2005) and the time constants of SFA predicted the observed differences in the cut-off frequency (Fig. 3.8C). Weschke and Ronacher (2008) also found a high-pass characteristic in BSN1 with a cut-off between 10 and 20 Hz, which matches the findings presented here (Fig. 3.8C). Notably, in AN2, the high-pass is shifted to lower frequencies than at earlier processing stages by strong but slower adaptation dynamics. This is possible, because the overall gain is lower than in more peripheral neurons (e.g. TN1). While the high-pass characteristics reported here are difficult to compare with previous studies due to the different methods of quantification, the low-pass characteristics predicted by mean frequency confirm known cut-off frequencies (Prinz and Ronacher, 2002; Weschke and Ronacher, 2008). However, in order to further link cell type specific SFA to temporal processing in the respective neurons, experiments with long-duration natural stimuli would be required.

3.4.4 Functional role of the distribution of adaptation mechanisms

The main finding of the present study is that spike frequency adaptation acts at all levels of a sensory pathway. Similar results were reported for the locust's visual pathway (Gabbiani and Krapp, 2006) as well as for vertebrate visual (Sanchez-Vives et al., 2000a,b; Solomon et al., 2004), somatosensory Derdikman et al. (2006); Katz et al. (2006) and auditory systems (McAlpine et al., 2000; Ingham and McAlpine, 2005, 2004; Avissar et al., 2007).

Different computational tasks may call for distinct distributions of adaptation mechanisms: e.g. (1) summation over many inputs to achieve high fidelity might require distributed mechanisms at several levels Baccus (2006); Baccus and Meister (2004), whereas (2) converging inputs from different processing channels might require channel specific adaptation mechanisms mostly at presynaptic stations (Abbott et al., 1997; Luksch et al., 2004).

In grasshoppers, the auditory pathway extracts the 'what' and 'where' information by processing of temporal and directional cues in parallel pathways (Hennig et al., 2004; von Helversen and von Helversen, 1995), and most auditory interneurons can be classified accordingly (Stumpner and Ronacher, 1994). Can the different distributions of adaptation mechanisms as present here be related to these functional aspects of auditory processing?

TN1 summates over many excitatory inputs from both sides (Stumpner and Ronacher, 1994) – a process, by which directional information is lost and the representation of temporal aspects enhanced. Mechanisms behind SFA for TN1 are distributed over

several levels of processing (Fig. 3.9), thus matching the expectations for summation over many inputs (1) as also observed in the visual pathway of vertebrates (Solomon et al., 2004; Dunn et al., 2007).

BSN1 appears to serve both localization and pattern processing. SFA as observed in BSN1 is distinctly input dependent, as expected for the integration of several information streams in a single neuron (2). However, accumulated hyperpolarizations, probably due to inhibitory inputs, have a lasting effect. Then, SFA to a stimulus via one input affects the response to subsequent stimulation via another input and will lead to a cross-interaction of temporal and directional information.

In AN2 the intrinsic adaptation state depends mainly on the excitation of the AN2 itself and is thus largely invariant to which input triggered excitation. AN2 exhibits a strict directionality that is achieved by a balance between ipsilateral excitation and contralateral inhibition. When an adapting stimulus is presented laterally, mainly the contralateral AN2 but not the afferents to AN2 will reduce excitability - and possibly preserve the functionally important balance between inhibition and excitation. Thus, the AN2 may represent a third functional principle for the distribution of adaptation mechanisms: if the computation performed by a sensory neuron relies on the ratio of incoming inhibition and excitation, the neuron itself should adapt and not the presynaptic input.

The analysis presented here on the effect of SFA on coding properties revealed similar results for AN2 and BSN1 (Fig. 3.8); however, if directional coding is taken into account, BSN1 and AN2 display different responses (Stumpner and Ronacher, 1994) and SFA would be expected to act differently on these two neurons. Since only stimuli from the side that elicited a larger response for each neuron were tested, the present investigation of SFA was restricted to temporal processing. Nevertheless, for BSN1 a lateralized adaptor could mainly decrease excitability of either contralateral inhibition or ipsilateral excitation, thereby changing the balance of these two. In AN2, excitability is mainly controlled in the postsynaptic neuron but not in its inputs and therefore directional information should be unbiased by localization of a previous stimulus.

The results presented here raise questions of the functional significance of the main source of adaptation, specifically in the context of central summation of information from both sides and directionality coding. One way to peruse these questions is to manipulate the distribution of adaptation mechanisms experimentally and observe the consequences for pattern processing and localization. However, this is difficult to do in an experimental setting. For this reason, theoretical and numerical modelling was done, which is presented in Chapter 4.

4 Functional implications of the distribution of adaptation

4.1 Introduction

The specific pattern of adaptation mechanisms in the auditory pathway of the locust (Chapter 3) raised questions about the functional consequences of the distribution of these mechanisms between central ascending neurons and the periphery. Is there a reason for the very strong intrinsic adaptation observed in AN2 (Chapter 3, Hildebrandt et al., 2009)? The pronounced intrinsic adaptation in AN2 even overrides peripheral adaptation with its longer time constant and dominates the low-pass characteristic of AN2's transfer function. AN2 is one of two neurons believed to carry directional information to the locust's brain, while most other ascending neurons code for the temporal pattern of the amplitude modulations of the sound (Stumpner and Ronacher, 1994). Here, I want to explore whether coding of directionality and pattern of a sound pose different demands on where and how adaptation should act within a sensory pathway.

After processing in the metathoracic ganglion, information within the auditory pathway of grasshoppers is separated into two channels, represented by different neurons that code the temporal pattern and the directionality of the sound (Stumpner and Ronacher, 1994; von Helversen and von Helversen, 1995). For both channels, the input to both ears is combined (Fig. 4.1A). In the case of temporal pattern coding, summation over the receptor responses form both ears increases the signal-to-noise ratio but leads to a loss of the directionality information. For directionality, the interaural intensity difference (IID) is evaluated by the system, because interaural time differences are much to small to be assessed in grasshoppers (differences of 5-6 μs at most; Krahe and Ronacher, 1993). In order to evaluate IIDs, the receptor input from the contralateral ear is subtracted from the ipsilateral input by contralateral inhibition, enhancing the directional tuning. The AN2 in locusts is thought to code for the direction of the stimulus (Stumpner and Ronacher, 1994). In both channels, the receptor responses are integrated by local neurons before information from the two ears is combined, and subsequently projected onto the ascending neurons (Fig. 4.1A).

Here, it is explored *where* adaptation should mainly act in these two pathways for optimal information processing. The strong intrinsic adaptation in AN2 in the directionality pathway is placed centrally (Chapter 3), *after* combining information from both sides. The question raised here is whether this central placement is due to specific demands of the directionality pathway in contrast to adaptation in the pattern processing pathway. In this context, the question where adaptation should take place can be narrowed down to whether it should act peripherally, in receptors and local neurons, or centrally, in ascending neurons. Although in principle, all three layers in Fig. 4.1A represent possible sites for adaptation, the network shown in Fig. 4.1A can be simplified in the present theoretical analysis: both pathways will be represented by few 'lo-

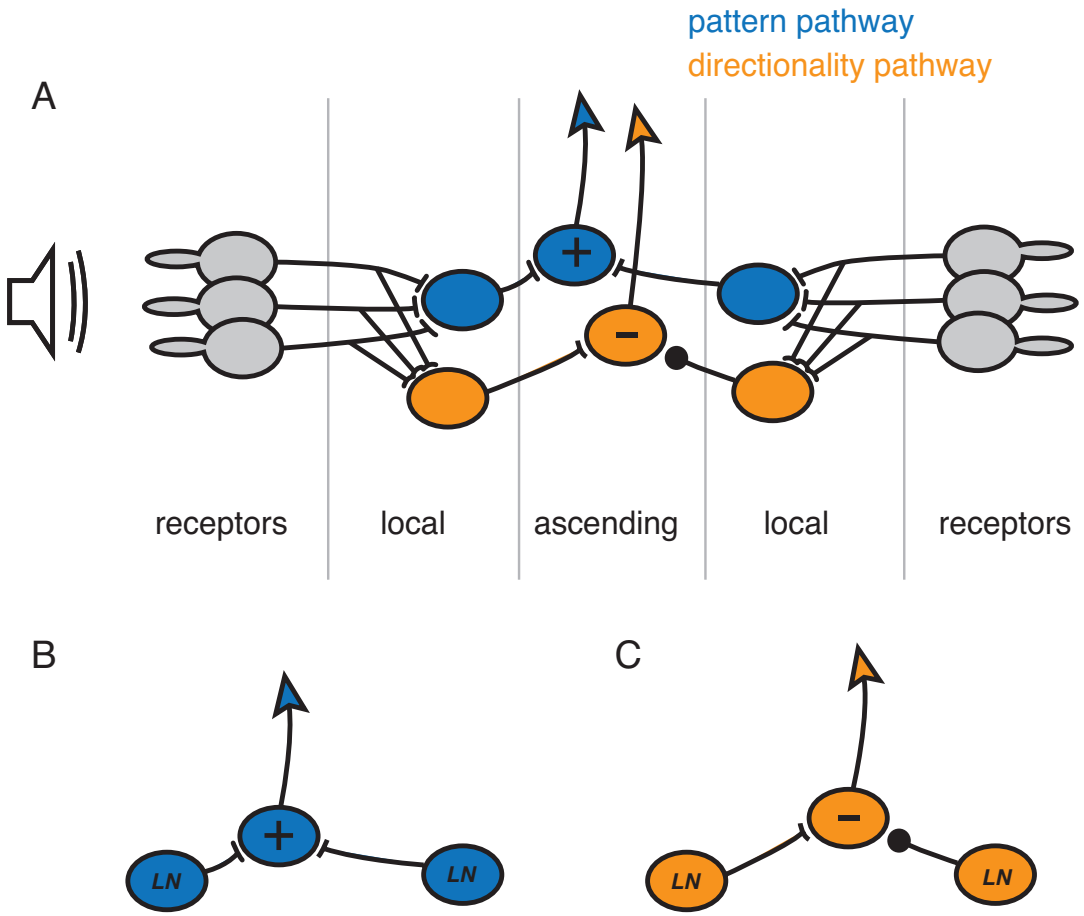

Figure 4.1: **Layered network in the metathoracic ganglion of grasshoppers and model abstraction.** Sound is received by receptors on both sides with different levels, depending on signal direction (A). Local neurons sum over the receptor population and project onto ascending neurons that send auditory information to the brain. At the level of the metathoracic ganglion, information about sound direction (orange) and temporal pattern (blue) is separated and processed in two parallel pathways. For the analytical treatment, the network was reduced to local and central neurons. (B) depicts the neurons that sums over local neurons from both sides ($\oplus$-neuron), (C) the central neuron that subtracts both sides for localization ($\ominus$-neuron).

cal neurons' (periphery) and the respective ascending (central) neuron (Fig. 4.1B&C). Therefore, the response curves of the local neuron (LN) refer to the output of the entire network composed of receptors and local neurons on one side. Similarly, 'adaptation in the LN' includes the combined effective adaptation at several places within the local network.

In order to examine the optimal placement of adaptation mechanisms within the pathways, adaptation is separated into static and dynamic components (Ly and Doiron, 2009; Sutherland et al., 2009). In the static point of view, adaptation is seen as an operation on the onset response curve of a neuron, adjusting it to a new environment or a novel stimulus distribution (see Chapter 5 for a more detailed discussion). An adjustment of the response curve can be seen as static, if adaptation is slow relative to the time course of the stimulus variations (Sutherland et al., 2009). For the dynamic component, the *process* of adaptation is modelled in order to test the performance of the model to amplitude-modulated stimuli with a time course faster than adaptation.

In the first section, adaptation is examined from the static perspective, and all neurons in the network are described analytically by their onset response curves. Adaptation is described by the change of the onset response curves as an adjustment to different stimulus distributions. In the analysis, adaptation is allowed to act peripherally, changing the response curves of the LNs or centrally, on the ascending neurons. Whether adaptation is desirable in either local or ascending neurons is indicated by the strength of the dependency of the optimal response curve on the stimulus distribution. Additionally, the effects of noise and integration time on the optimal response curves are discussed, since both represent important parameters for optimal information transfer and thus interact with adaptation.

In the second section, the dynamic aspect of adaptation is studied, and for this purpose, numeric simulations of the network are used. Local and ascending neurons are simulated by spiking neurons that incorporate adaptation mechanisms and reflect peripheral and central adaptation. The parameters for the dynamics of both peripheral and central adaptation are chosen to match experimental results. The simulations permit to test for the functional consequences of central adaptation as observed in AN2 (Chapter 3) by comparing model versions with and without adaptation. Since the dynamics of adaptation are important for the representation of amplitude modulations, the consequences of peripheral and central adaptation will be studied with regards to the coding of amplitude-modulated stimuli.

4.2 Optimal response curves and adaptation

4.2.1 The optimal response curve

In order to describe in which way a response curve $r(x)$ should ideally be changed by adaptation to match a stimulus x described by its probability density function (PDF) $p_x(x)$, we first need to know the optimal response curve $r^0(x)$ given $p_x(x)$. Then, it can be explored which parameters need to be changed by adaptation if the distribution changes. This problem has already been addressed for constant variance by Nadal and Parga (1994) and with a more general response solution by McDonnell and Stocks (2008). The solution depends on how the variance of the response σ_r^2 depends on r. The simplest case, which I will consider here, is constant σ_r^2 over the entire range of

the response curve. In this case, the ideal response curve is the same as the cumulative probability function of the stimulus (Nadal and Parga, 1994):

$$r^0(x) = \int_{-\infty}^{x} p_x(\Phi) d\Phi. \tag{4.1}$$

4.2.2 The role of noise

If there is no noise in the response curve, the output of the network can transmit information about stimulus intensity up to arbitrarily high precision, the response curve could be shallow and its dynamic range could encompass all possible values of stimulus intensity, stretching over all stimulus PDFs the animal encounters. In this case, p_x in eq. 4.1 would be the distribution of all possible stimulus values and not the PDF of one signal in a specific behavioural context and adaptation would not be necessary. However, there is considerable noise in the receptor responses already, and also in the local neurons (Vogel et al., 2005), reducing the capacity to code for variations in the stimulus. This variability of responses introduces uncertainty about the input from the perspective of an observer of the output of the neuron. The Fisher Information of the response curves J takes this into account. It is a measure of how much information about the stimulus can be transmitted at each point of the response curve. The Fisher Information depends on the derivative of the response curve and the (constant) variance of the rate σ_r^2 at each stimulus value x:

$$J(x) = \frac{\left(\frac{\delta r}{\delta x}\right)^2}{\sigma_r^2}. \tag{4.2}$$

From the fisher information, the mutual information between a stimulus PDF and $r(x)$ can be calculated:

$$I = H_x - \frac{1}{2}\int_{-\infty}^{\infty} p_x(x) log_2\left(\frac{2\pi e}{J(x)}\right) dx, \tag{4.3}$$

$$\text{with the stimulus entropy} \qquad H_x = -\int_{-\infty}^{\infty} p_x(x) ln\left(p_x(x)\right) dx.$$

Combining eqs. 4.2 and 4.3, one gets

$$I = H_x - \frac{1}{2} log_2\left(2\pi e \sigma_r^2\right) + \int_{-\infty}^{\infty} p_x log_2\left(\frac{\delta r}{\Delta x}\right) dx. \tag{4.4}$$

The mutual information increases by $log_2(\sigma_r)$ with the standard deviation of the stimulus. This raises the question whether there is a way to reduce the variance in order to increase mutual information? If the spiking of a neuron can be described as a general renewal process, the variance of the spike count σ_N^2 is linked to the counting time window T (Nawrot et al., 2008) by a multiplicative constant: $\sigma_N = DT$. If $r(x)$ is the spike count N with variance σ_N^2 divided by the duration of counting window T:

$$\sigma_r^2 = \frac{\sigma_N^2}{T^2} = \frac{D}{T}\,, \tag{4.5}$$

where constant factor D depends on global spike train statistics only. Thus, to increase the mutual information between a given response curve and a stimulus PDF, integration over larger time windows increases the mutual information. The contribution of the time window is $0.5log_2(T)$, so a doubling of the integration time would increase the mutual information by 0.5 bit. This means that there is a trade-off between the temporal resolution of a neural code and the precision of amplitude coding as quantified by the Fisher Information of the response curve. As the fisher information scales inversely with the variance but directly with the square of the slope of the response curve (eq. 4.2), a decrease in slope can be directly compensated by an equal decrease of variance. Since the standard deviation scales inversely with the square root of the evaluation time window (eq. 4.5), a decrease of the slope by a factor c can be compensated dividing the integration time T by c^2. If, for example, the slope of a curve is halved ($c = 0.5$), the equivalent compensation would be to multiply T by a factor of 4 (divide by 0.25). Stretching a given response function $r(x)$ by multiplying its input by a constant factor d gives $r(dx)$ with a slope altered by the factor d^{-1}. The dynamic range of $r(dx)$ will also scale with d. This depends on the definition of dynamic range, but this characteristic is desirable, because otherwise, it would depend on the units used for the input. This means, consequently, that an enlargement of the dynamic range can be compensated by prolonging the duration of the integration by the square of the enlargement factor.

4.2.3 $\oplus$-neuron: coding of temporal pattern

First, I will consider the ascending neuron that sums up information from both sides in order to represent the temporal pattern of an acoustic signal (Fig. 4.1B). The relevant stimulus PDF for the $\oplus$-neuron is the distribution of amplitude modulations of a given signal x around its mean μ_x. For a Gaussian stimulus PDF, the optimal response curve from eq. 4.1 for the $\oplus$-neuron is described by the error function:

$$r^0_{\oplus}(x) = \frac{1}{2}\left(1 + erf\left(\frac{x-\mu_x}{\sigma_x}\right)\right). \tag{4.6}$$

This also means that the information about the mean level of the stimulus is not represented in the response of the $\oplus$-neuron. This is probably beneficial, because the important information of the signal is usually contained in the changes *relative* to the mean. The same acoustic signal, located at different distances from the receiver will have different means, although the temporal pattern is the same. Thus, the response curve in eq. 4.6 enables a representation of the temporal structure *invariant* of the mean intensity (Benda and Hennig, 2007).

Adaptation in local neurons

In order to understand how adaptation should act in the LNs that provide input to the $\oplus$-neuron, one needs to find those response curves in the LNs that give rise to the optimal response curve in eq. 4.6. The response curve of the $\oplus$-neuron is the result of

the sum of the response curves from the ipsi- and contralateral side:

$$r_{\oplus}(x) = \frac{1}{2}\left(r_{ipsi}(x) + r_{contra}(x)\right). \tag{4.7}$$

As the signal moves around the animal, the stimulus distributions at both LNs are shifted by the interaural intensity difference (IID) Δx and $-\Delta x$, respectively ($\Delta x \in [-\Delta x_{max}; \Delta x_{max}]$). One solution for the combination of eqs. 4.6 and 4.7 is

$$\begin{aligned} r_{ipsi}(x) =& \frac{1}{2}\left(1 + erf\left(\frac{x - (\mu_x + \Delta x)}{\sigma_x}\right)\right) \text{ and} \\ r_{contra}(x) =& \frac{1}{2}\left(1 + erf\left(\frac{x - (\mu_x - \Delta x)}{\sigma_x}\right)\right). \end{aligned}$$

The most obvious solution is that the response curves of the LNs equal the optimal curve for the $\oplus$-neuron, but shifted by $\mu_x + \Delta x$ instead of only by μ. The general solution for optimal response curve of the LN are $r^0_{ipsi}(x) = r^{0\oplus}(x - \Delta x)$ and $r^0_{contra}(x) = r^{0\oplus}(x + \Delta x)$. This does not tell us whether there are other solutions for the response curves, but they will never be better than the one pointed out here. From the perspective of adaptation, this is the most probable solution. Every other setting would have to involve an asymmetry. For example, one LN could code for the lower part of the PDF and the other LN for the upper half. Each LN itself does not have information about the direction of the stimulus, a soft sound from the ipsilateral side will have the same PDF as a loud sound from the contralateral side. Thus, the role of each neuron for an asymmetric shift could not be decided by the lateralization of the stimulus, but would have to be hard-wired. As a consequence, one side would always be less sensitive than the other. This seems very unlikely and no evidence for such an asymmetry in the grasshopper auditory system has been found.

Why sum up information from both sides? Averaging over the two LNs (eq. 4.7), the variance of the $\oplus$-neuron is half the variance of the LNs, because the noise in the local neurons of both sides is independent. The only reason to sum information from the two sides in the pattern processing pathway is to reduce the signal-to-noise ratio. Looking at the term for the mutual information (eq. 4.4), we can see that this equals a gain of information of 0.5 bit. This gain of information can also be seen in terms of the integration time window: due to the benefit from the central summing, the system would be able to shorten the integration time by the factor $\sqrt{2}^{-1}$ (≈ 0.71).

Adaptation intrinsic to the $\oplus$-neuron

The above statements about optimal response curves in the LNs and adaptation only hold for the linear summing as given by eq. 4.7. Under these circumstances, there is no benefit for intrinsic adaptation in the $\oplus$-neuron from the perspective of optimal information transfer. However, the transfer function from postsynaptic voltage to the output could be characterized by an additional nonlinearity and only if the voltage is approximately linear within the range of the input currents elicited by the LNs eq. 4.7 and the derivations above hold.

Are there other reasons to adapt centrally in the pattern pathway? A possible con-

straint that could provide reasons for adaptation within the ⊕-neuron could be energy preservation (Niven et al., 2007; Heitwerth et al., 2005). However, what is referred to as 'local neuron' here is in reality not a single cell but a convergent network (Fig. 4.1A). If energy expenditure plays a role in coding in the auditory system at all, one would expect it to influence the response curves of earlier stages first.

From the perspective of the ⊕-neuron discussed here, the ideal response curves of its inputs are as stated above. Thus, from the static view of changes of response curves as discussed in this section there is no obvious reason to adapt centrally in the pattern coding pathway, if invariance to mean intensity can be established more peripherally.

Summary ⊕-neuron

Te ascending ⊕-neuron increases the information capacity of its response curve by averaging over the two sides. The optimal response curves of the LNs that provide input to the ⊕-neuron are optimal with respect to the shifted PDF they receive themselves. In order to allow for steep response curves in the periphery, adaptation in the temporal pattern pathway should act before summation to avoid saturation in the LNs. Steep response curves, in turn, enable high temporal resolution, because less integration over time is required for reliable coding of signal amplitudes. Central adaptation within the ⊕-neuron was not found to be required.

4.2.4 ⊖-neuron: coding of stimulus direction

Next, I will consider the ascending neuron (⊖-neuron) that is excited by the local neuron ipsilateral to itself and inhibited by the contralateral neuron (Fig. 4.1C). The ⊖-neuron evaluates the interaural intensity difference (IID). The contralateral inhibition effectively increases the directional tuning of the neuron. With the combined information ofthe ⊖-neurons from both sides, the brain is thought to be able to detect the direction of a sound. It should be noted that although the modelling in this and the following section is based is on data from experiments on the AN2 (Chapter 3; Hildebrandt et al., 2009), there is at least one more ascending neuron in grasshoppers thought to carry directional information (Stumpner and Ronacher, 1994). However, the examinations carried out here hold for any neuron with the described wiring and characteristics, including auditory pathways in many animal systems.

Optimal response curve for ⊖-neuron

The rate of the ⊖-neuron is given by the difference between the rates of the ipsi- and contralateral LN, similar to eq. 4.7:

$$r_{\ominus}(x, \Delta x) = \frac{1}{2}\left(r_{ipsi}(x + \Delta x) - r_{contra}(x - \Delta x) + 1\right), \tag{4.8}$$

where x is the intensity of a sound at both ears if the animal is directed towards the sound source and will be referred to as the 'mean level' from now on. The addition of 1 is introduced to avoid negative values of $r_{\ominus}$ and thereby restrict the range of its response to values between 0 and 1. If the animal turns away from the source, intensity at one ear is increased by Δx and attenuated by the same amount at the other ear. Δx is independent of x due to the logarithmic scaling of the perceived dB scale.

I will now proceed with the same ansatz as for the $\oplus$-neuron. First, I will find the optimal response curve for the $\ominus$-neuron and then show how to construct this from the response curves of the LNs. In the case of the $\ominus$-neuron, the relevant parameter that needs to be coded for by the response curve is Δx not x. Δx only varies in the boundaries of the maximal intensity difference between the two ears. In this interval, it is uniformly distributed:

$$p_{\Delta x}(\Delta x) = \frac{1}{2\Delta x_{max}}, \quad \Delta x \in [-\Delta x_{max}, \Delta x_{max}] \tag{4.9}$$

The optimal response curve is given by the cumulative probability function of $p_{\Delta x}$:

$$r^0_{\ominus}(\Delta x) = \frac{\Delta x}{2\Delta x_{max}} + \frac{1}{2}, \quad \Delta x \in [-\Delta x_{max}, \Delta x_{max}]\,. \tag{4.10}$$

For any function $f(z)$ that is symmetric with respect to the point $f(0) = 0.5$ and thus obeys $f(-z) = 1 - f(z)$,

$$f(z) - f(-z) = 2f(z) - 1. \tag{4.11}$$

This is just the same as eq. 4.8 with $f(z) = r_{ipsi}(\Delta x) = r_{contra}(\Delta x) = r_{\ominus}$. So the optimal response curves of the LNs are again the same with respect to Δx. However, this holds only true if the mean stimulus level between the two ears x is 0. Similar to what we have described for the $\oplus$-neuron, from the perspective of adaptation, we would like it to shift response curves according to the stimulus level. There is a difference, however. For the $\oplus$-neuron, we wanted each LN to centre its response curve at $\mu_x + \Delta x$, because this is the mean intensity of the distribution of the amplitude modulations at each side. If we applied the same shift to the LNs that provide input to the $\ominus$-neuron, $r_{\ominus}$ would be 0 for all values of Δx. In the $\ominus$-LNs, the perfect shift would be just x. However the value of x itself is not available to the LNs. A contralateral stimulus that has the value $x - \Delta x$ for an LN is indistinguishable from a softer sound x' from ipsilateral side if it is softer by exactly $2\Delta x$ (the IID). Without feedback from central neurons, the LNs cannot adapt to the actual stimulus level, but without their input, central neurons have no information about Δx that is necessary for the shift. Thus, adaptation in LNs it is not possible to adjust the response curves with respect to the mean level of the stimulus.

Invariance to the absolute level

If the stimulus value varies between x_{min} and x_{max}, the range of IIDs between the ears encountered is between $x_{min} - \Delta x_{max}$ to $x_{min} + \Delta x_{max}$ and $x_{max} - \Delta x_{max}$ to $x_{max} + \Delta x_{max}$, respectively. In order to accomplish the linear response curve in eq. 4.10 for all possible values of x and Δx, the response curves of both local neurons need to be linear over the whole range:

$$\begin{aligned} r_{LN}(x_{eff}) =& \frac{x_{eff}}{(2\Delta x_{max} + x_{max} - x_{min})} - \frac{x_{min} - \Delta x_{max}}{2\Delta x_{max} + x_{max} - x_{min}}, \\ & x_{eff} \in [(x_{min} - \Delta x_{max}), (x_{max} + \Delta x_{max})] \end{aligned} \tag{4.12}$$

where x_{eff} is the effective stimulus reaching each ear, $(x + \Delta x)$ for the ipsilateral LN and $(x - \Delta x)$ for the contralateral LN. The zero-point of the x_{eff}-axis can be chosen

arbitrarily and we can simply set the lower bound of the entire range of x_{eff} to zero: $x_{min} - \Delta x_{max} = 0$. Eq. 4.12 then becomes:

$$r_{LN}(x_{eff}) = \frac{x_{eff}}{(\Delta x_{max} + x_{max})}, \quad x_{eff} \in [0, (x_{max} + \Delta x_{max})]\,. \tag{4.13}$$

By inserting this into eq. 4.8, we receive a linear function $r_{\ominus}(\Delta x)$ with a slope of $(x_{max} + \Delta x_{max})^{-1}$. In order to restore the optimal slope of eq. 4.10, a gain factor needs to be introduced into to eq. 4.8:

$$r_{\ominus}(x, \Delta x) = \frac{(\Delta x_{max} + x_{max})}{2\Delta x_{max}} \left(r_{ipsi}(x + \Delta x) - r_{contra}(x - \Delta x)\right) + \frac{1}{2}. \tag{4.14}$$

While this gain factor restores the slope, it also increases the variance of the response of the $\ominus$-neuron by the square of the factor:

$$\sigma^2_{\ominus} = \left(\frac{\Delta x + x_{max}}{2\Delta x_{max}}\right)^2 \sigma^2_{LN} = \frac{1}{4}\left(1 + \frac{x_{max}}{\Delta x_{max}}\right)^2 \sigma^2_{LN}. \tag{4.15}$$

The variance can be substituted by DT^{-1} (eq. 4.5), it scales with the inverse of the integration time window T. In order to compensate for the loss of mutual information (eq. 4.4) following the increase in variance due to the larger dynamical range of the LN, the $\ominus$-neuron needs to enlarge its integration time proportional to the square of the maximal stimulus relative to the maximal Δx. If $x_{max} = 0$, the stimulus level is static at the midpoint between $-\Delta x$ and Δx. If the mean stimulus level itself already varies between $-\Delta x$ and Δx ($x_{max} = \Delta x_{max}$), the integration time has to be multiplied by a factor of four already. Such longer integration time is accompanied by the cost of lower temporal resolution.

While the $\oplus$-neuron needs to follow fast amplitude modulations and cannot afford the long integration times, the locality of a signal source usually changes on a much slower time scale. For example, a conspecific mate constitutes a temporally static sound source and it may be perfectly suitable to integrate over longer stretches of the song for localization. In the parallel pattern pathway, adaptation should act quickly and then code for fast amplitude modulation with high accuracy and high temporal resolution independent of the distance of the potential mate.

Summary $\ominus$-neuron

Due the uniform PDF of the IIDs, the ideal response curve for localization in the $\ominus$-neuron is a linear function of Δx. Subtracting linear response curves from LNs from each side results in this optimal response curve in the $\ominus$-neuron, if the absolute stimulus value is at the midpoint of the response curves. Thus, adaptation in the LNs would ideally act in response to the absolute stimulus value, which is not available in the periphery. If the response curves of local neurons in the directionality pathway cannot be adapted, they need to be shallower in order for their dynamic range to encompass all possible absolute stimulus values. Finally, loss of information transfer due to shallower slopes could be counteracted by larger integration times because the time course of the change of directional cues should be much slower than that of amplitude modulations.

4.3 Simulation of adaptation dynamics

The results of the analytical treatment showed that for the representation of the temporal pattern, peripheral adaptation is desirable. For the directional pathway (Fig. 4.1A&C), however, the analysis revealed no need for adaptation, and no explanation for the strong intrinsic adaptation that was encountered in the directional sensitive AN2 (Chapter 3; Stumpner and Ronacher, 1994) was found.

Pattern and directional pathways should diverge as early as possible, because they pose different demands on peripheral adaptation. Receptor neurons are shared by both pathways and should not adapt. Once the pathways diverge, the specific local neurons of the pattern pathways should shift their steep response curves according to the stimulus mean, while LNs in the directionality pathway should not adapt. However, experimental results revealed adaptation in the receptors and response curves are shifted during the presentation of a stimulus (Römer, 1976; Benda, 2002). In addition, there is evidence from both experiments and modelling studies that show that it is difficult to achieve the large shifts needed for invariant pattern coding within a single layer (Benda and Hennig, 2007; Ziehm et al., 2009). It seems that for complete intensity invariance over a large range of values, at least two subsequent layers are needed – a combination of adaptation in local neurons and receptors. As a result, the directionality pathway probably shares more peripheral adaptation with the pattern pathway than desirable.

Therefore, intrinsic adaptation in AN2 could be a response to peripheral adaptation, which degrades the directional information contained in the difference of its inputs. Here, the following hypothesis is tested: due to the shared periphery of pattern and directionality pathways, peripheral adaptation eventually degrades directional information in the inputs of the $\ominus$-neuron; strong intrinsic adaptation in the $\ominus$-neuron (AN2) serves to restrict its response to the onset of a novel stimulus, when directional information has not yet been deteriorated. This hypothesis is evaluated by dynamic simulations of the directional pathway, which incorporate adaptation in the periphery and within the $\ominus$-neuron itself.

Layout of the network used for the simulations

Similar as in the analytical treatment, in the numerical simulation receptor and local neuron levels (Fig. 4.1A) are combined into the response of the local neurons. For the numerical model three local neurons were used on each side as inputs to the central neurons (Fig. 4.2) to better match the experimentally observed voltage traces spiking behaviour of the central neurons. In order to model the response of the LNs, the sound amplitude is transformed by a sigmoidal nonlinearity to the input current of an exponential integrate-and-fire neuron (EIF, for a detailed description see appendix A). After the transformation, a noise current is added to the input to the EIF. A pair of directionally sensitive ascending neurons ($\ominus$-neurons) was simulated. The input to each of these is provided by three local neurons from each side (Fig. 4.2) and these connections are either excitatory, if the stem from the ipsilateral LNs or inhibitory, if their origin is contralateral. All LNs were simulated separately and independent noise was added to their inputs. Inhibitory and excitatory neurons were simulated using the same set of parameters; the only difference between them constitutes their postsynaptic effect.

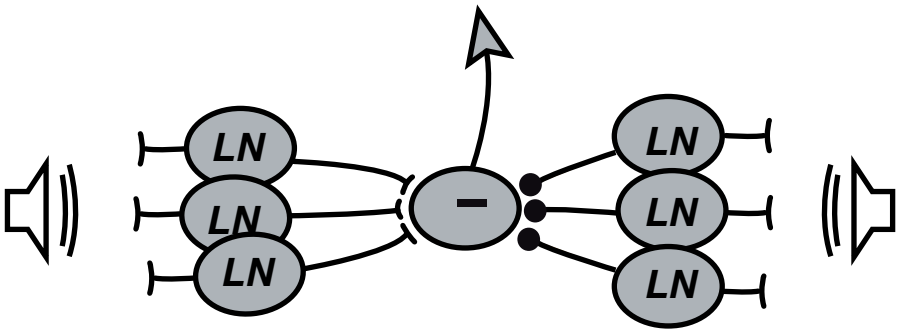

Figure 4.2: **Network used for numerical simulation.** For the numerical simulation, the layered auditory pathway of the locust (Fig. 4.1A) was reduced to three 'local neurons' (LN) that transduce the sound on both sides and directly project onto the central $\ominus$-neuron. The $\ominus$-neuron receives excitatory input from one side and inhibitory from the other. All local neurons (inhibitory and excitatory) are simulated with the same parameters, the only difference between contra- and ipsilateral LNs is the postsynaptic effect in the $\ominus$-neuron.

4.3.1 Simulation of local neurons

Adaptation in the LNs is implemented by dynamically moving the centre of their input-nonlinearity according to the stimulus history . Details of the implementation can be found in appendix A. In short, the position of the nonlinearity is changed according to the stimulus history weighted exponentially over time.

Response to constant stimuli

Fig. 4.3 shows the result of the stimulation of a LN with a constant sound pulse played at an intensity above the midpoint of the input-nonlinearity. The LN reacts with a fast onset response that gradually decays as the stimulus presentation persists. This decay is present in all trials. If the mean spike frequency for all trials is plotted over time (Fig. 4.3, lower panel), an approximately exponential time course with a time constant of the same magnitude as the weighting exponential of the input-adaptation (40 ms in the example of Fig. 4.3) can be observed.

The time course of adaptation in the LNs approximately matches experimental results (Chapter 3; Hildebrandt et al., 2009; Benda, 2002). In Fig. 4.4A the spike frequency of an LN in response to the onset of a stimulus pulse played at different sound levels is shown. All values fall well into the range observed in different receptors and candidate LNs (i.e. TN1; Hildebrandt et al., 2009; Fig. 3.3).

The shift of the response curves that result from the adaptation in the simulation are shown in Fig. 4.4B. The overall shape of the curves is dominated by the input-nonlinearity. If the neuron was adapted to a certain background intensity (dotted lines in Fig. 4.4)B before testing, the response curves are shifted accordingly. For all following simulations, LNs with the properties described here were used.

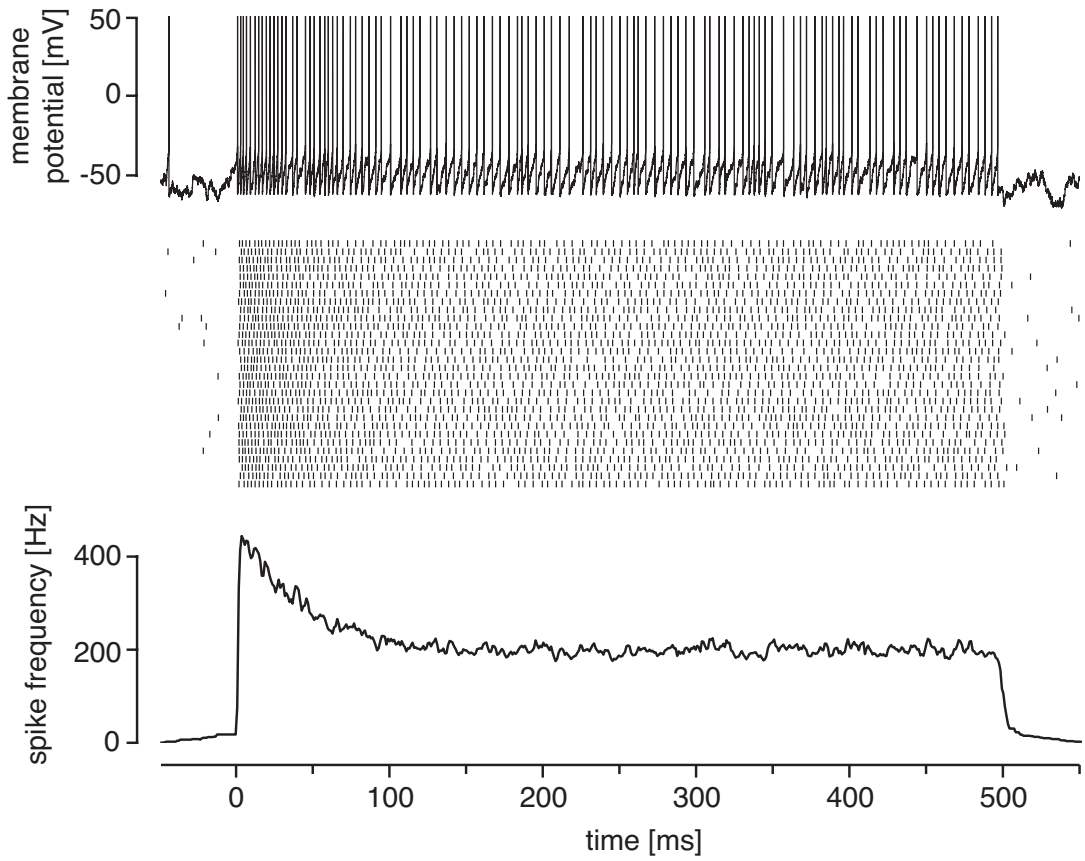

Figure 4.3: **Example of responses of simulated local neuron.** The stimulus used in the simulation is a square pulse of 500 ms duration. The time axis is scaled relative to stimulus onset (0 ms). The uppermost panel shows an example voltage trace of the EIF used for the LN with a shifting nonlinearity. The middle panel depitcts dot plots of 30 trials of the same stimulus with the same parameters but different noise currents. The lower panel shows the time course of spike frequency, calculated from the 30 trials shown above. Spike frequency was calculated as described in the methods section. The time constant of weighting the stimulus history that controls the position of the nonlinearity is 40 ms.

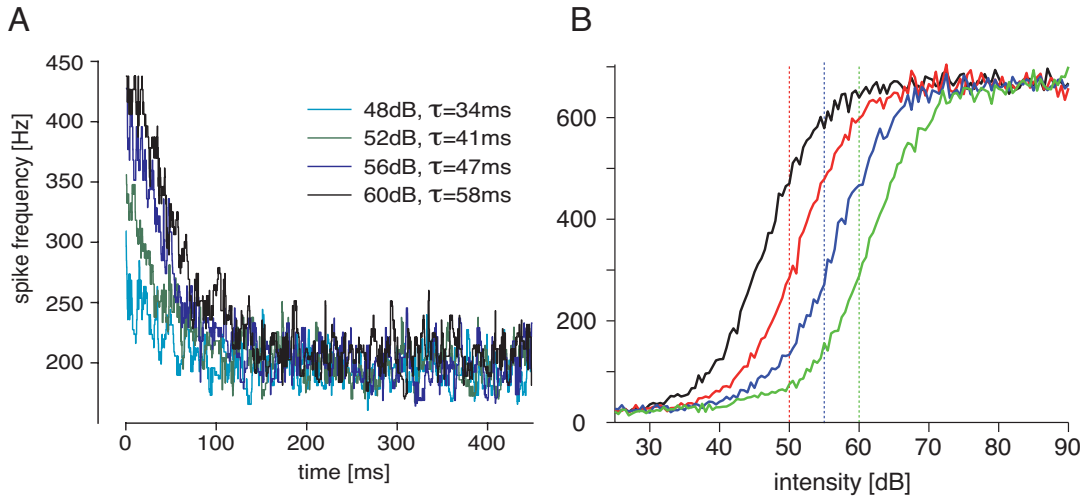

Figure 4.4: **Characterization of adptation in local neurons.** (A): Time course of spike frequency adaptation in simulated local neurons. The responses of a simulated LN to the onset of a pulse stimulus at different intensities are shown. Different colours depict different sound intensities as indicated by the legend. All simulations were run with the same time constant of the leaky integrator driving adaptation (40 ms). The values of τ given in the legend are the results of exponential fits to the time course of the spike frequency for each stimulus level. (B): shifting of onset response curves as a result of adaptation. The black line marks the unadapted onset response curve of a LN, when silence preceded the test pulse. The coloured lines depict the onset response when before presentation of the test pulse, the LN was adapted to the background intensity indicated by the dotted lines of the respective colour. The spike frequency is calculated as the inverse of the first spike latency.

Response to dynamic stimuli

So far, only constant sounds and step-like onsets were considered. In reality, the temporal structure of a sound carries most information and auditory objects in the animal's environment can be identified by the shape of the amplitude modulations. In a natural situation, the animal will be confronted with a signal (e.g. a conspecific song) that starts at some point in time and carries on revealing its specific temporal structure. Usually, such a signal will not change its location before it stops and starts over again, so within one presentation, distance (mean level) and direction (interaural intensity difference) do not change. How the adapting LNs react to a randomly amplitude-modulated (RAM) stimulus is displayed in Fig. 4.5 that shows mean spike frequency responses to the same RAM stimulus played back at different sound levels. At the onset of the stimulus, responses diverge strongly, but after about 100 ms, the responses are invariant to the mean stimulus level, because adaptation shifts the input-nonlinearity of the LN accordingly. At the highest intensity (72 dB, blue line in Fig. 4.5), there is not much modulation of the response at the beginning, because it is largely saturated. Later it is strongly modulated by the stimulus variations. At the lowest intensity, the response does not capture small stimulus deviations in the beginning of the stimulus. Once adaptation has adjusted the input-nonlinearity to the mean level of the stimulus, the amplitude modulations can be represented reliably at all mean sound levels.

For the $\oplus$-neuron, the response of the LNs in Fig. 4.5 after about 100 ms are optimal, because, they reliably represent the temporal structure of the signal, invariant of the mean level that is not important for recognition. Since the mean is already removed at the LN-level, processing in the $\oplus$-neuron can focus on reducing noise by summing over both sides and on detecting more abstract signal features. These results are in good agreement with the analytical findings. In the following, I will concentrate on the $\ominus$-neuron.

Instead of the same signal played from different distances, the simulations in Fig. 4.5 can also be interpreted as the same, but lateralized signal presentation. In this case, pairwise intensity differences (e.g. 54 and 60 dB, red and green lines in Fig. 4.5) can be seen as the responses of LNs from the two ears at the same time. These would then constitute the input to the $\ominus$-neuron and the difference between the two LN responses. It can easily be seen that contrary to what has been discussed regarding the $\oplus$-neuron, most information about intensity difference and thus direction is in the beginning of the stimulus, when the LNs have not yet adapted to the mean sound level. At the beginning, the green and the red line rise and fall in parallel and the difference between them will be approximately constant. Over time, they merge and no difference can be detected any more.

4.3.2 Ascending $\ominus$-neuron

The hypothesis behind the next steps of the numerical simulations for the $\ominus$-neuron is the following: because information in the periphery about direction of the signal vanishes over time, strong intrinsic adaptation in the central neuron helps to focus its response on the informative part of the signal and effectively 'tune out', when reliable information about direction fades.

The ascending $\ominus$-neuron is simulated by an EIF type model similar to that of the

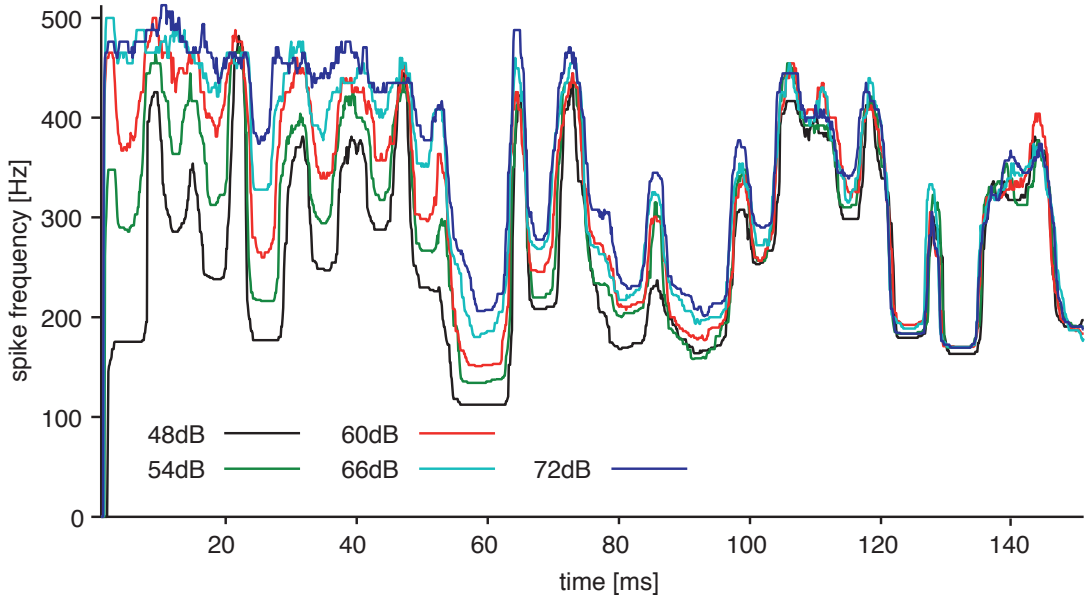

Figure 4.5: **Responses of simulated local neurons to RAM stimuli.** Displayed are responses to the same randomly amplitude-modulated stimulus at different mean levels indicated by the colours of the lines. Spike frequency was quantified by averaging over 30 trials each. The parameters used are the same as in the previous figures. The intensity differences can either be interpreted as the same 'object' at different distances or pairwise as interaural level differences, stemming from a lateralized sound source.

LNs, but without an additional nonlinearity. For a detailed description, see appendix. It receives excitatory input from three local neurons from one side and from three inhibitory neurons from the other (Fig. 4.2). Synaptic processes are simulated by transforming input spikes to exponentially decaying positive or negative currents. In addition, an output-driven adaptation current is either added to the $\ominus$-neuron or not, defining different testing conditions. Each time a spike is elicited in the $\ominus$-neuron, an exponentially decaying, inhibitory current is added to the neuron. From here on, the model without additional adaptation in the $\ominus$-neurons and the one incorporating it will be referred to as the 'two model versions'. If any other parameter is changed, this will explicitly be stated. The amplitude of these steps and their decay rate were chosen in order to match the experimental results presented in Chapter 3. For model details and a comparison between experimental and modelling data see appendix A.

Time course of responses of the $\ominus$-neuron

Typically, biologically relevant signals have a periodic temporal structure (Gerhardt and Huber, 2002). Here, an artificial grasshopper song produced by females of the species *Chortippus biguttulus* is used for the simulations (for details see appendix A). This is done for two reasons: (1) behavioural experiments show that males are able to locate these songs with good accuracy (von Helversen and Rheinlaender, 1988; von Helversen and von Helversen, 1995; Schul et al., 1999), providing us with experimental data to compare the model to and (2) the auditory network of locusts that were used

in the experiments in Chapter 3 is very similar to that of *Ch. biguttulus*. We can assume that adaptation characteristics like other physiological parameters are similar in most grasshopper species at this level (Neuhofer et al., 2008), and that all signals that have a similar periodic structure should in principle be localized by such a model network. Simulations were also done with pulsed and sinusoidally modulated sounds, but results of these are not shown here. The outcome from these was indistinguishable from the data presented here.

In the simulations, the signal was changed in two ways independently: when a signal is moved around the animal, the intensity difference between the two ears changes, referred to as change of interaural intensity differences (IIDs). When, on the other hand, the signal at both ears becomes louder or softer, this will effect what is defined here as 'mean level' – mean referring to mean between the two ears, not over time. The mean level is independent on the direction of the sound. It should be noted that both parameters mean level and IID are not properly defined by observing the sound intensity at one ear, without knowing that at the respective other.

Fig. 4.6 shows the responses of the $\ominus$-neuron pair to the first three syllables, each composed of six individual pulses that are depicted in the figure backgrounds. The simulation ran for six syllables, but after three a steady state was reached already and responses to subsequent syllables did not differ from the last one in Fig. 4.6. In Fig. 4.6A, the response of the $\ominus$-neuron pair to an artificial song presented with five IIDs are shown. The $\ominus$-neuron model version without intrinsic adaptation was used for the tests in Fig. 4.6A. For the simulation in Fig. 4.6A, long integration times in the $\ominus$-neuron were implemented by large time constant of inhibitory (38.4 ms) and excitatory (12 ms) synaptic decay. With these large time constants, individual pulses are not well copied by the spike frequency and only during the first syllable, the responses strongly depended on the IID. This can best be seen in the bottom trace, where the difference between the ipsi- and the contralateral $\ominus$-neuron is depicted. Up to about 100 ms into the stimulus, the responses of the two $\ominus$-neurons differ and larger IIDs lead to larger response differences between both, indicated by the good separation of the different lines in the bottom trace of Fig. 4.6A. This separation vanishes after about 100 ms and the directionality information fades. At later times, both $\ominus$-neurons are still actively responding. A non-zero and equal response of both $\ominus$-neurons is exactly what would be expected for a stimulus that is located directly in front of the animal. Thus, without intrinsic adaptation in the $\ominus$-neuron (Fig. 4.6A), information about directionality would not only decay after about 100 ms, but the brain would receive misleading information, indicating a false direction.

Fig. 4.6B shows the same simulation of the same model version (without intrinsic adaptation) but with much faster synaptic integration (1.5 ms for excitation, 4.8 ms for inhibition). With these parameters, the single pulse structure can be copied with higher accuracy. On the other hand, with faster integration, directionality information decays faster (Fig. 4.6B, lower trace) and responses to the different IIDs are not constantly well separated, even in the first 50 ms. The large variation introduced by the fine structure of the stimulus and fast temporal integration deteriorates directional information.

In Fig. 4.6C&D the same simulations are run, but this time with the model version incorporating intrinsic, output-driven adaptation within the $\ominus$-neurons. For both temporal integration parameter sets (Fig. 4.6C&D), this limits the response mainly to the first stimulus syllable, keeping the informative part of the stimulus, but almost shut-

ting off the ⊖-neurons, when information from the LNs becomes unreliable. Notably, the response difference in the slowly integrating ⊖-neurons (Fig. 4.6C) is a more reliable indicator of IIDs than in the fast integration ⊖-neurons (Fig. 4.6D).

Mutual information between interaural level differences and ⊖-neuron responses

In order to quantify the qualitative effects that were observed in Fig. 4.6, the mutual information between spike counts in 50 ms time windows and the IIDs was calculated. The model was run at 10 different mean levels with 10 different IIDs each. 1000 repetitions for each combination were used. Fig. 4.7 shows how the mutual information develops over time. If one compares the absolute values for the model version with adaptation to that without adaptation (Fig. 4.7A), both versions start off at about the same level, while the model version without adaptatio in ⊖-neuron contains slightly more information. Information decays somewhat faster with adaptation than without adaptation, reaching a similar level at steady state. The model without ⊖-neuron adaptation is always just above the one with adaptation, but the difference is small. The calculation of mutual information also confirms the impression from Fig. 4.6 that information about directionality is less reliable at fast integration times (dashed lines in Fig. 4.7A). This is true although in Fig. 4.7A, mutual information for slow and fast integration was calculation in the same time windows (50 ms), if the information is computed in time window corresponding to the integration times, the difference would be much more pronounced.

This changes considerably if information is calculated per spike (Fig. 4.7B). In this case, the model with adaptation is always far more informative about the IIDs than the one without. Thus, one advantage of strong intrinsic adaptation in the ⊖-neurons is efficiency. Spike numbers are greatly reduced, and especially at those points in time, where overall information is low anyway. The adapting ⊖-neuron model version reaches very similar absolute information rates by using considerably less spikes.

Invariance of directionality coding on mean stimulus level

The direction of a sound source needs to be decoded independently of stimulus mean level. If, for example, the sender is in the same direction but further away, this should not influence localization. In order to test for this, the model was simulated for a range of IIDs at a large range of mean levels. As already discussed in the first section of this chapter, the LNs providing input to the ⊖-neuron should have a shallow input response curve, so their dynamic range covers a large interval of mean levels. The input-nonlinearity results from the modelling of the 'transduction' in the LNs (Fig. 4.4B). Here, a nonlinearity was used that yields a threshold at 34 dB. (intensity, at which 10% of maximal response is reached); the response saturates at 64.5 dB (90% of maximal response).

Fig. 4.8 gives an overview on the level dependency of the coding of interaural intensity differences in the two versions of the ⊖-neuron model. Each line in the graphs shows the response difference between the two ⊖-neurons for a wide range of mean stimulus levels. In contrast to Fig. 4.6, where the response difference is plotted for a fixed mean level over time, the panels A-F of Fig. 4.8 show the mean frequency difference over different time windows for many mean stimulus levels. Ideally, one IID,

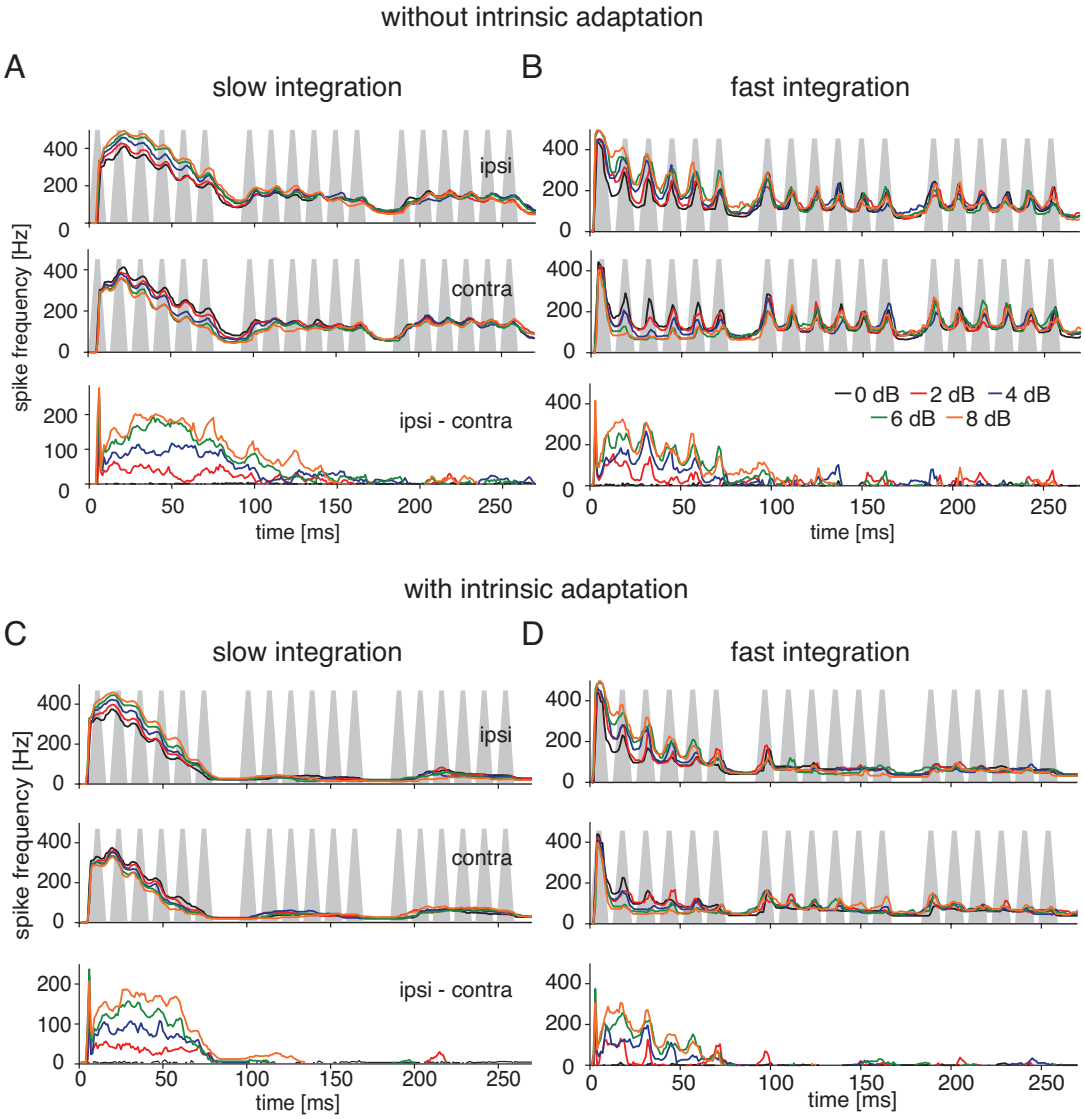

Figure 4.6: **Frequency responses of the ⊖-neuron to periodic stimuli.** The upper two rows of each panel show the responses of the two ⊖-neurons ipsi and contralateral to differently lateralized sounds with the interaural intensity difference indicated by the legend in panel (B). The stimulus is shown in the background. The bottom row depicts the difference between the two ⊖-neurons. (A) and (B) show the responses of ⊖-neurons without intrinsic adaptation, (C) and (D) with intrinsic adaptation. In (A) and (C) the integration time of the ⊖-neurons is eightfold that of (B) and (D). All responses are quantified as mean values over 30 trials.

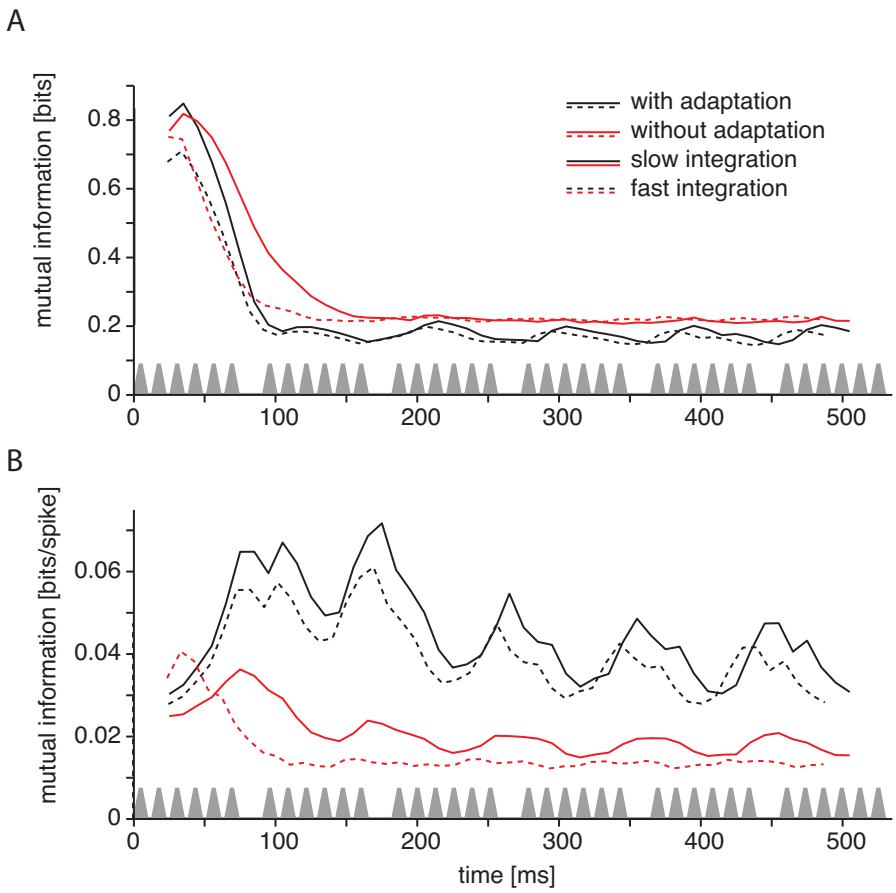

Figure 4.7: **Change of mutual information about IID over time.** The mutual information was calculated over 50 ms time windows for spike counts in these windows. The time windows were moved over the entire stimulus in 10 ms steps. (A) shows absolute mutual information between 10 interaural intensity differences at 10 different mean sound levels and the spike count. Mean level was treated as noise. Each combination of mean level and IID was repeated 1000 times. In (B) the same data is normalized by the mean spike count for all simulations in the specific time window. The black lines depicts the case where adapting $\ominus$-neurons were used, the red line represents the model version with non-adapting $\ominus$-neurons. Solid lines show the model with slow integration, corresponding to Fig. 4.6A& C. Dashed lines depict simulations with fast integration time (Fig. 4.6B& D). The grey area at the bottom of both (A) and (B) represents the amplitude modulation of the artificial grasshopper song used for the simulation.

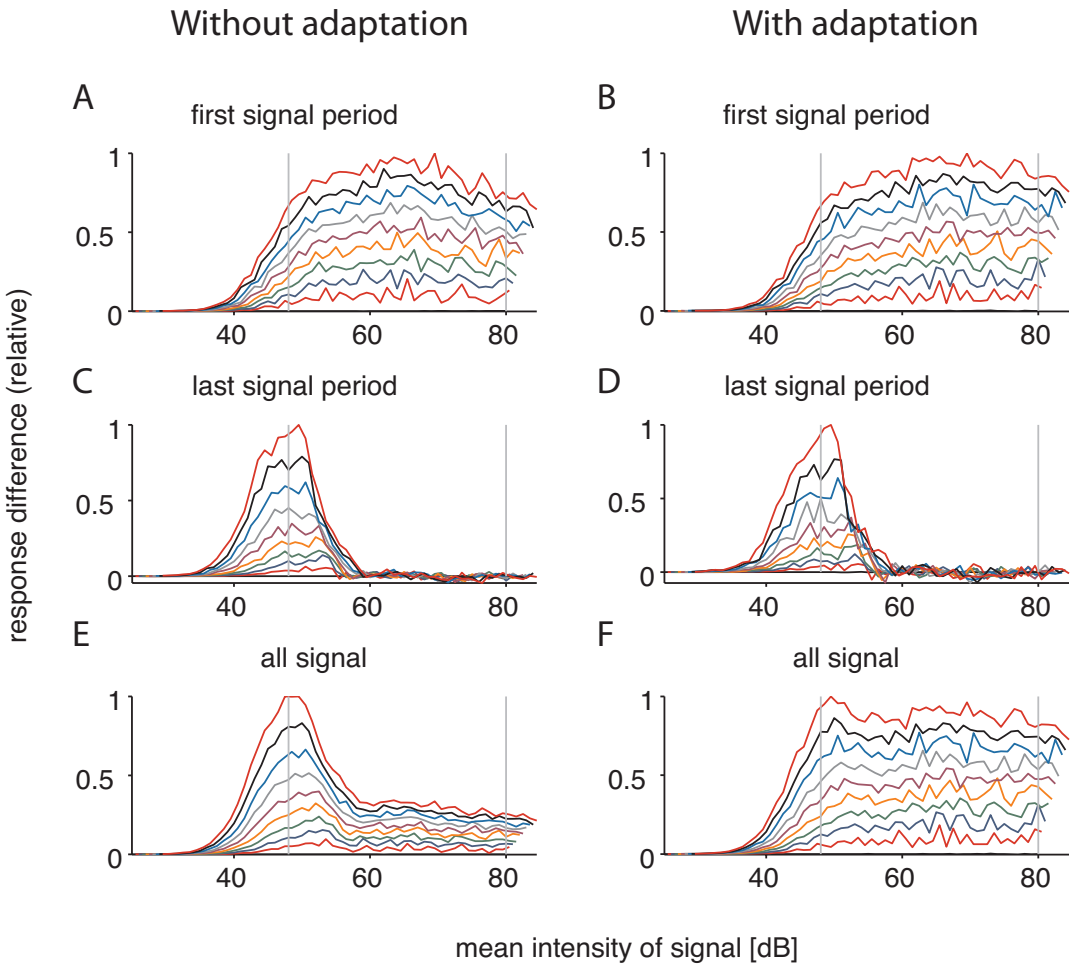

Figure 4.8: **Dependency of directionality information on mean level.** The graphs show the response differences between the two $\ominus$-neurons depending on interaural level difference and the mean level of the sound. Different colours depict different level differences. The level differences range between 1dB (lower red line) and 9dB (upper red line). Responses were averaged over the time window indicated above each plot (A, B, C&D: 70 ms, E&F: 520 ms), after passing through a cubic nonlinearity. Grey lines indicate the 'dynamic range' used in subsequent analysis. (A), (C) and (E) are simulated without adaptation in the $\ominus$-neurons, (B), (D) and (F) show the results of a model with adaptation in the $\ominus$-neuron.

represented by the different colours in Fig. 4.8, would elicit the same response difference for all mean levels and different IIDs would elicit well separated, specific response differences.

One way to interpret the response difference in Fig. 4.8 is direct or indirect motor output to left and right leg muscles, which drive movement toward (or away) from a sound source. While the direction an animal walks should depend on the difference of the responses of the two $\ominus$-neurons, how much it actually walks in that direction should depend on the spike frequencies, with which the two $\ominus$-neurons react. Weighting the responses with the response amplitude results in a nonlinearity. Here, frequencies from the two $\ominus$-neurons are passed through an cubic nonlinearity before the difference is plotted, with the consequence that larger spike frequencies are given more weight. This is done to take the motor output into account. The cubic nonlinearity yields better classification results for both model versions than simple squaring. It was thus used to illustrate how well classification can be done with the models. Quadratic (simple weighting) yields the same results with overall worse classification results, but does not change how the two versions of the model compare to each other.

If only the first period of the artificial grasshopper song is taken into account (Fig. 4.8 A&B), both model versions show good separation of the response differences over a large mean level range. For the first pulse, no difference between the model versions regarding the invariance to mean intensity can be observed. Fig. 4.9 demonstrates how IIDs map onto response differences independent of mean level. Any overlap between the response differences at different IIDs can lead to classification errors, because the mapping is ambiguous. The black symbols in Fig. 4.9A&B symbolize those data points, for which the mean level ranged between the grey lines in Fig. 4.8. For the first signal period (Fig. 4.9), there is not a large difference for the situation with and without adaptation in the $\ominus$-neurons. Classification results for the first signal period are plotted in the confusion matrices in Fig. 4.10A&B. Mean correct classification success is 31.0% for the model without $\ominus$-neuron adaptation and 31.3% for the model with adaptation in the $\ominus$-neurons. Thus, classification results during the first signal period do not provide a direct explanation for the need of adaptation in the $\ominus$-neurons. However, mean spike rates are considerably smaller in the model version with $\ominus$-neuron adaptation without degrading classification success. Thus, the model version with adaptation is more efficient.

So far, only the first signal part has been considered. If we follow the idea that the $\ominus$-neurons provide direct or indirect input to a motor pathway driving phonotaxis, we will have to take into account the rest of the signal because the phonotaxis will not be limited to any single part of the stimulus. At this point, it should be made clear that 'motor output' or 'phonotaxis' does not automatically mean real-time movement during stimulus presentation. Movement during perception may actually degrade the signal for the recognition process and movement before recognition would not be efficient in most cases. The output of the $\ominus$-neuron system looked at here could well be stored in an internal memory, thereby also integrated over time and than used later, when the signal is recognized. The animals need at least three signal periods for recognition (Ronacher and Krahe, 1998), so all (or at least three) periods matter. If we only look at the last signal period (in this case, period no. 6, Fig. 4.8C&D), it can be seen that only in a very small range of mean levels, just above the threshold of the LNs, the IID can be detected reliably. Any stimulus played at higher mean levels will yield

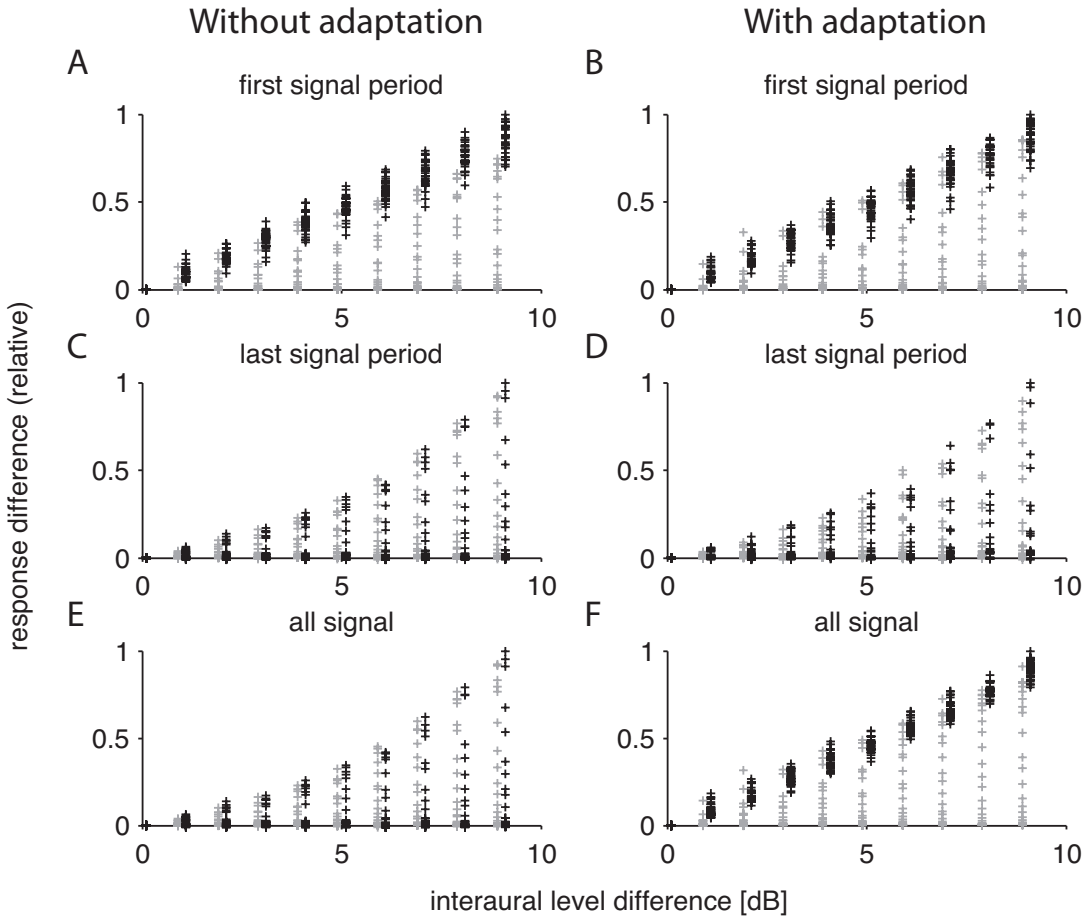

Figure 4.9: **Ambiguity of responses to interaural level differences at different mean stimulus levels.** Scatter plots show how the mean spike frequencies plotted in the respective panels in Fig. 4.8 map onto the interaural level differences, irrespective of mean level. Grey symbols depict the entire intensity range in Fig. 4.8, black symbols results of simulation carried out at mean levels between the grey lines in Fig. 4.8. All panels (A-F) correspond to the time windows and model versions of the respective panels in Fig. 4.8A-F and contain the same data plotted in a different way.

almost no information about the IIDs. This can easily be understood if looking back to Fig. 4.6, where the stimulus played was well above threshold and the intensity difference is removed by LN adaptation. Close to the threshold this does not occur, because in the models, the nonlinearity only shifts down to an absolute threshold, to prevent the neuron to become infinitely sensitive. The degraded detectability of the IID is reflected in Fig. 4.9C&D: most points in the scatter plots are close to zero difference between the $\ominus$-neuron responses, irrespective of the real IID. Close inspection of the two model versions in Figs. 4.8C&D and 4.9C&D reveal that adaptation in the $\ominus$-neuron actually degrades the directionality information at later signal periodsevenslightly-more, which has already been shown by the absolute values of mutual information (Fig. 4.7A). Fig. 4.10C&D shows that if classification is carried out by the responses to the last signal period only, success is reduced to just above change level (16.8% in both cases: without and with adaptation).

As already stated above, most relevant to the localization task is how the detection of direction performs for the entire signal and not for single periods. Figs. 4.8E&F and 4.9E&F show the mean over the entire signal. Due to the cubic nonlinearity, high frequency are weighted higher than low ones, and there is a focus of IID detection on those times, when the $\ominus$-neurons respond with high spike frequencies. For the model version without adaptation this lets the model perform better for the entire stimulus than for the last period only, but worse than for the first period (Figs.. Figs. 4.8A&E, 4.9A&E and 4.10A&E, 26.5% correct classification). This is different in the model version that incorporates $\ominus$-neuron adaptation, inspired by experimental evidence (Figs. 4.8A&E, 4.9A&E and 4.10A&E). Classification success raises to 35.1%, which is even higher than for the first signal period alone.

The explanation for the different performance of the two model versions is probably as follows: adaptation in the $\ominus$-neurons reduces spike frequency for the later periods, during which the LN inputs do not provide useful information. This yields a weighted sum over the response to the entire signal in such a way that the more informative part (the beginning) contributes stronger to the mean than the less informative part (the rest of the signal). This is not true for the model version without $\ominus$-neuron adaptation. It is important to note that this does not depend on the cubic nonlinearity chosen.

Figure 4.10 *(following page):* **Confusion matrices with and without adaptation in $\ominus$-neuron.** Colour plots show the percentage of response differences elicited by an interaural level difference (x-axis) that are classified by finding the closest mean response to the interaural level differences on the y-axis. This analysis was carried out separately for the different time windows (A&B: first signal period, C&D: last signal period, E&F: entire signal). Panels (A-F) correspond to the respective panels in Figs. 4.8 and 4.9 and are based on the same data as in those.

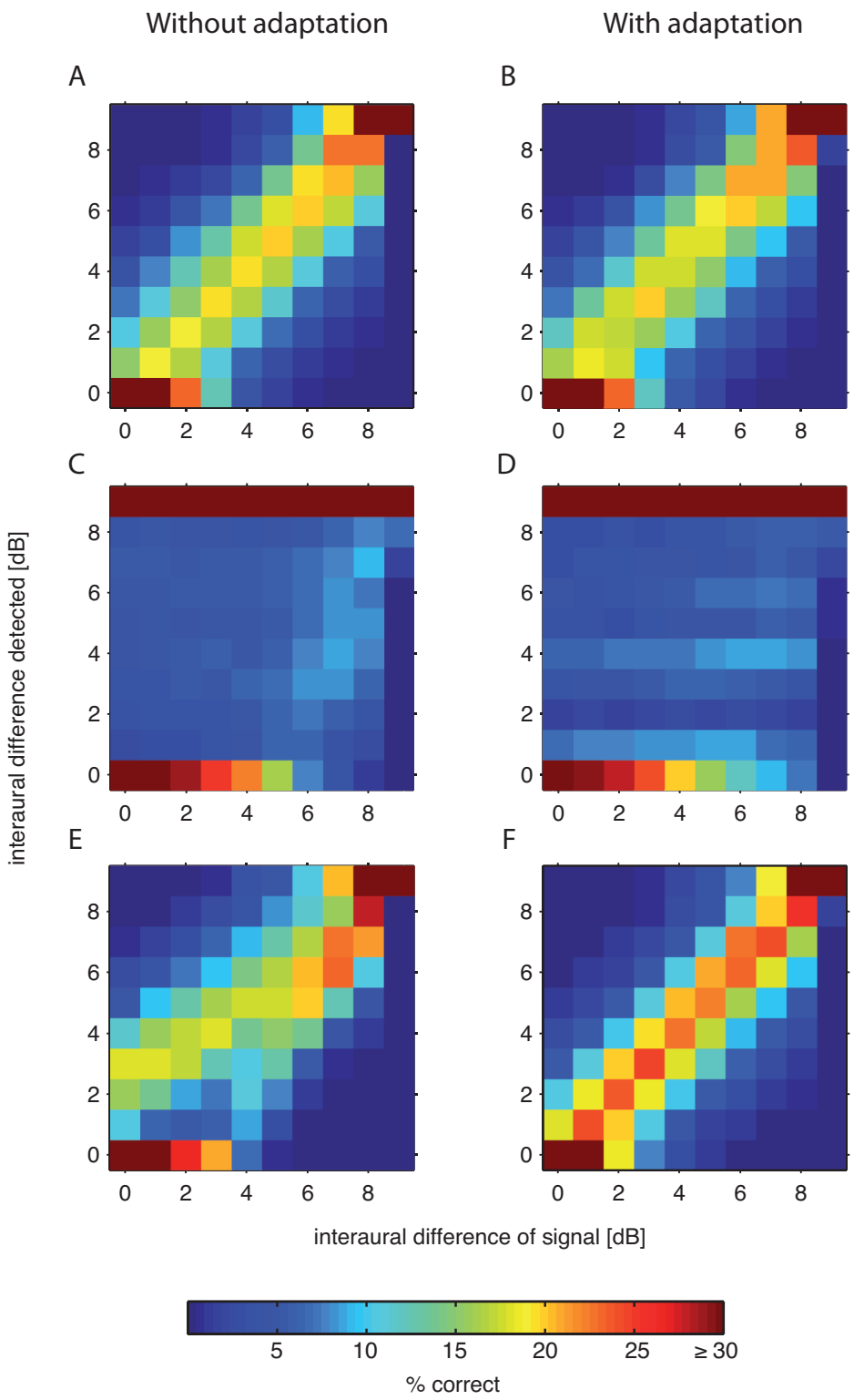
Without adaptation
With adaptation
A
B
C
D
E
F
interaural difference detected [dB]
interaural difference of signal [dB]
0
2
4
6
8
5
10
15
20
25
≥ 30
% correct

The reason is that in the none-adaptation model version the distribution of response differences during the first signal period and subsequent period overlap so much that just by means of the absolute values of the $\ominus$-neuron response there is no way to attenuate the contribution of the responses to the first period relative to the rest. This explains the difference in classification success for the entire signal between the two model versions (Figs. 4.8E&F, 4.9E&F and 4.10E&F), but cannot account for the better classification successs of the adaptation version of the model when the entire signal is included (4.10B&F). To understand this, we need to look at the low intensity range, where peripheral adaptation does not degrade the signal (Fig. 4.8D). At these intensities, the responses to the latter signal period are informative about interaural level difference because of the absolute threshold. These low intensities just above threshold will evoke least adaptation in the $\ominus$-neurons, because they are driven at low spike frequencies. Less adaptation means a stronger contribution of the latter periods.

Thus, the analysis of classification revealed that central adaptation intrinsic to the $\ominus$-neurons does not only 'tune out' over time when the important information degrades: this tuning is present depending on whether the information degrades in the course of the signal or not.

4.3.3 Summary of the modelling of adpatation dynamics

In agreement with the analytic results, the simulations presented hear reveal that peripheral adaptation is beneficial for pattern coding but degrades directional information over time. Therefore, the peripheral response to the onset of a signal contains most information about the direction of its source from. Additional central adaptation in the directionality pathway allows for more efficient coding without losing information, by focusing on the more informative beginning of the signal. Adaptation in the $\ominus$-neuron enables weighting of local neuron responses according to their informativeness: strong central responses at the beginning of the signal, and very weak responses when directional information fades. Finally, this weighting greatly enhances the ability to classify directionality of a sound at a large range of mean levels if the entire signal is taken into account.

4.4 Discussion

In this chapter, the demands of localization and temporal pattern recognition on the placement of adaptation mechanisms were explored. Analytical evaluations showed that these two essetntial goals of auditory processing have very different requirements on both response curve shape and adaptation in the periphery. For pattern recognition, high temporal precision is important. Small integration times impede averaging over time. Thus, steep responses curves are needed to compensate for the loss information due to noise (sec. 4.2.3). Intensity invariance should be accomplished by peripheral adaptation mechanisms already before combining information from both sides (Fig. 4.5). For localization on the other hand, adaptation in the periphery is counterproductive. Ideally, intensity invariance in the directionality pathway should be achieved by shallow response curves in the periphery with large dynamic ranges (sec. 4.2.4). The loss in reliability due to the shallow response curves and noise could be compensated for by larger integration times, because there is less need for high temporal resolution.

Analytical treatment did not propose the need for adaptation in the central neurons of either pathway. The numerical model showed that *if* there is peripheral adaptation that deteriorates directional information, intrinsic adaptation in the directional sensitive central neuron ($\ominus$-neuron) provides means for temporal weighting of its input (Fig. 4.6). This weighting allowed for better and more efficient classification of signal direction (Fig. 4.10).

4.4.1 Validity of model assumptions

For the analytical treatment, noise in the LNs was assumed to be independent of output rate. If this was true, the relation between Fano-factor and the coefficient of variation and the mean rate should be a hyperbolic function. A previous study on the variability of the responses of auditory neurons in locusts shows that this is indeed the case for receptors and to some extend also for local neurons (Vogel et al., 2005). In the study by Vogel et al., several different local neurons are combined in a single plot, making an assessment of single cells difficult. It seems that the assumption of constant noise is valid for the system under study. Moreover, in the present study, the focus lies on the *change* of response curves as an effect of adaptation. The above deviations can easily by transferred to more general noise dependencies with the help of the relation between a PDF and the optimal response curve derived by McDonnell and Stocks (2008).

The input-adaptation implemented in the LNs of the numerical model did not yield the same dynamics (Fig. 4.4A) as the real receptors (Benda, 2002). Especially at intensities much larger than the initial saturation level, a step pulse did not elicit a decrease of the spike frequency right from the start in the model, but spike frequency levelled out at the maximal response for some time. To avoid this problem, all other simulations were carried out at intensity levels up to just above saturation, where model dynamics are still within the variability between different cells as revealed by experiments (Benda, 2002).

In general, parameters for the numerical simulation of LNs and central neurons were chosen to match experimental data (Benda, 2002; Vogel et al., 2005; Hildebrandt et al., 2009) best. For example, the $\ominus$-neuron was first tested with current input only, and adaptation time constant, adaptation strength and noise parameters were adjusted in order to match the results of Chapter 3. In a second step, the model was used for simulations with acoustic input via the LNs (Fig. 4.5). However, parameters were not fit for best performance of the model for classification (Fig. 4.10) or information transfer (Fig. 4.7). Consequently, the conclusions drawn are only valid for the parameter combination tested here. It is not claimed that either intrinsic adaptation in the $\ominus$-neuron *in general* is preferable or that the chosen set of parameter provides the optimal weighting. These were the ones found in experiments and the goal of the present study was to find out whether strong adaptation within the $\ominus$-neuron with long time constants was beneficial for the task of localization and it was shown that this is indeed the case.

Would other models of intrinsic adaptation show a better performance? Strong adaptation is needed in order to suppress firing entirely after the informative part of the input is over, so less pronounced adaptation leads to worse performance. The time constant (190 ms in the model) seems to match the decrease of information due to the faster adaptation in the periphery (Fig. 4.5) well, although it would be interesting to test different combinations of time scales. Other versions of the adaptive exponen-

tial integrate-and-fire neuron include a sub-threshold adaptation that does not depend on output spikes, but resembles rather a form of input adaptation with regard to the spike generator (e.g.Brette and Gerstner 2005). Such a form of adaptation would most probably lead to better performance at the tests applied here, because the $\ominus$-neuron could really be shut off after a certain time. In the model version presented here, the $\ominus$-neuron will recover from adaptation when it is not spiking itself, eventually start spiking again, activating adaptation currents. This leads to some form of oscillation that does not contain information about the input. Sub-threshold adaptation was not implemented here, because so far, there had not been any experimental evidence for it. The AN2 showed pronounced, long-lasting afterhyperpolarizations (Chapter 3, Fig. 3.4) and it was concluded that these are the main cause for adaptation intrinsic to AN2. Results from the analysis presents here suggests the presence of some form of sub-threshold adaptation in AN2, which in future experiments could easily be tested by intracellular current stimulation below spiking-threshold.

4.4.2 Different time scales for localization and pattern processing

How adaptation changes the representation of signal depends critically on the relation between the time scale of adaptation and relevant signal modulations (Benda and Herz, 2003). Here, theses modulations were classified into two categories. Modulations of the overall signal quality (1) include the relative position of the sound source and the mean intensity perceived (which depends also on the distance), but could also include more general features of the acoustic space, like the level of background noise. The second relevant time scale is that of modulation of the signal itself (2), which carries much information about signal identity. These can include both amplitude and frequency modulations. Usually, the overall signal changes on a much slower time scale than the fast signal modulations.

This has some major consequences for coding and adaptation in the two pathways discussed here. Regarding the integration times, slow features like the direction of a sound source allow for longer integration times beneficial for shallow response curves, possibly enabling a reduction of noise. There are good theoretical arguments that longer integration times will reduce response variance (Nawrot et al., 2008) and experimental evidence from other systems has shown this to be the case (Kara et al., 2000). However, a study on variability of spike counts and interspike intervals in the auditory pathway of the locusts could not find this relation (Vogel et al., 2005), so grasshoppers may not be able to take advantage of this possibility to reduce noise. In the study by Vogel et al. constant sound signals were used, perhaps results are different with more relevant, amplitude-modulated stimuli, although there is no indication from a theoretical point of view that this should be the case.

Coding of fast stimulus features needs fast integration times. Most of the slow features of the sound are noise from the perspective of pattern coding. Adaptation provides means to high-pass filter the signal (Benda and Herz, 2003) and thereby enables invariant coding of the fast signal features (Fig. 4.5, Benda and Hennig, 2007).

Usually, divergent pathways for slow and fast signal features share at least some of their peripheral inputs. Achieving invariance in one pathway means removing the important information in the other, inevitably. This problem is not new in the discussion of adaptation. One solution that has been proposed is that different statistical properties of spike trains carry information about distinct features changing on different time scales (Fairhall et al., 2001). It is not clear, however, how different statistic moments, like the form of the exact interspike interval distribution can be read out. Here, a different solution is proposed: central adaptation in the slow feature pathway (localization) focuses on the beginning of the signal, while the coding of fast stimulus variations gets more invariant and reliable during the course of the stimulus. This model is supported by evidence from behavioural experiments in grasshoppers that the modulations of the later parts of a song are indeed more informative. Males of the species *Chortippus biguttulus* where able to recognize conspecific songs that were otherwise not recognized, if the songs were preceded by an adapting sound pulse of the same intensity as the song (Ronacher and Hennig, 2004).

It should be noted that 'slow features' here does not mean continuously slowly varying signal characteristics, but that a signal is turned on at some point in time and does not change these features during its presence until the next occurrence. This means, the signal has a clear beginning, starting with a transient. For many biological rele-

vant acoustic signals, this is a realistic assumption. Most communication signal are not continuous, including human speech, sounds made by predators will often occur suddenly and the same is true for the sound a potential prey elicits.

However, the requirement of a suddenly appearing but lasting signal also limits the application of the mechanism for localization proposed here. It is only valid if locality is a slow signal feature in the sense defined above. If either sound source or receiver are moving, the change of locality is a quality of the signal itself and becomes a fast feature. An example of this would be the case for hunting bats, for which sound source and receiver are in motion, but also for ambush-predators like the barn owl, for which the *change* of the position of a piece of prey itself is a central information.

4.4.3 Comparison to mammalian auditory system

In general, the model discussed here is applicable whenever the relevant signals have the temporal structure described above. More specifically, the mammalian auditory system shares some of the central features of what has been described here. Peripheral adaptation at similar time scales as in the receptor neurons of the locust has been revealed in auditory nerve of guinea pigs (Westerman and Smith, 1984; Yates et al., 1985), probably also removing some of interaural intensity differences over time. At later stages of the pathway neurons have been shown to respond invariant to mean intensity after a short adaptation period (Dean et al., 2005). Although, mammals can also rely on interaural time differences, they use IIDs for sound localization and information from both ears is combined centrally, in neurons of the lateral superior olive (LSO). Similar to the system presented her, this is done subtractively via inhibition and excitation (Moore and Caspary, 1983; Finlayson and Caspary, 1989; Park et al., 2004). The inputs to these central neurons display shallow response curve with large dynamic ranges (Finlayson and Caspary, 1989) and neurons in the LSO and higher brain centres have been shown to code IIDs invariant of mean level (Park et al., 2004).

Strikingly, central LSO neurons project back to their inputs via recurrent, presynaptic inhibition (Magnusson et al., 2008), which would have a similar effect as intrinsic, output-driven adaptation described here — both are implementation of negative feedback loop. Thus, the similarity of the task to process intensity differences between the two ears, while accomplishing intensity variance for pattern recognition at the same time, could have lead to different implementations of the same algorithm in such distant animal groups as insects and mammals.

Part II. How does adaptation act ?

A mechanism for divisive gain control

5 Presynaptic inhibition in the auditory pathway of crickets

5.1 Introduction

So far, the pattern of distribution of mechanisms and the functional consequences of that pattern was discussed. It was shown that adaptation acts at different places (Chapter 4) and that the pattern of distribution of the mechanisms can be explained by the function a neuron serves in the processing of sensory signals (Chapter 4). Thus, *where* adaptation occurs is of central functional relevance, but what about *how* adaptation is realized, by which actual mechanism?

The modelling of adaptation in Chapter 4 provides examples for the consequences of adaptation on the coding of subsequent stimuli. Generally, how a neuron transforms its inputs into the output spike frequency is not fixed but changes in response to sensory environment, performed task and context. These adaptations to a specific behavioural or sensory background will change the input-response curve of a sensory neuron. These changes can be seen as modulatory operations between background and acute signal parameters. In this context, adaptational changes of response curves can be classified into two types: subtractive and divisive modulations (Fig. 5.1): by subtraction, the threshold of the curve shifts, but the slope of the curve remains unchanged. Divisive alterations, also referred to as gain control, change the slope of the curve. Both operations are known to be of central importance to the nervous system (Barlow and Levick, 1965; Carandini and Heeger, 1994; Peña and Konishi, 2001; Gabbiani et al., 2002), since they provide basic building blocks of computation: subtraction and division.

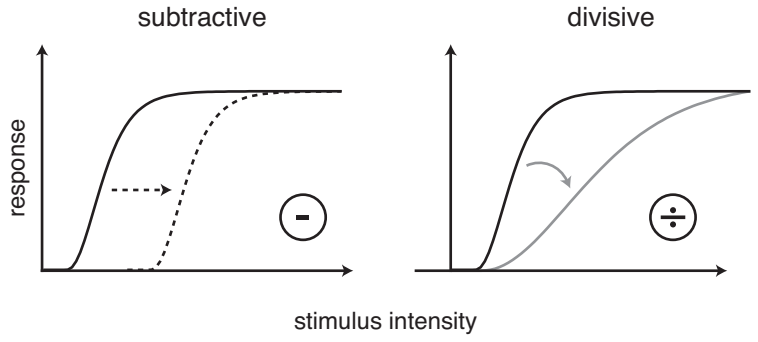

Figure 5.1: **Subtractive and divisive adaptation effects on response curves.**

The biophysical machinery behind subtractive changes is well documented, including both hyperpolarizing and shunting inhibition (Holt and Koch, 1997; Chance et al., 2002) as well as spike driven adaptation currents (Benda and Herz, 2003). However

proposed mechanisms of divisive gain control have shown to be elusive and often only the interplay of several mechanisms was observed to act divisively. These include conductance changes controlled by large populations of balanced inhibitory and excitatory inputs (Chance et al., 2002; Baca et al., 2008), shunting inhibition in combination with synaptic noise (Prescott and Koninck, 2003; Ly and Doiron, 2009) and combinations of pre- and postsynaptic nonlinearities (Gabbiani et al., 2002). Recently, short-term synaptic plasticity also has been shown to provide means for gain control (Abbott et al., 1997; Rothman et al., 2009).

With the exception of synaptic plasticity, these mechanisms demand large number of inputs that provide a synaptic background, which may not be available in the sensory periphery in both invertebrates and vertebrates. A candidate for gain modulation in peripheral sensory and motor circuits is presynaptic inhibition, a mechanism that is widely termed 'gain control' (Burrows and Matheson, 1994; Root et al., 2008), but its divisive nature has not been thoroughly tested. Presynaptic inhibition results from an axo-axonal connection, in which the target neurons terminal is inhibited by GABAergic ionotropic Cl^--channels, which have a shunting effect on the membrane potential of the target cell and reduce the amplitude of incoming spikes (Clarac and Cattaert, 1996; Rudomin, 2009).

Here, I want to test the effect of different mechanisms that alter the response curve of an auditory interneuron in crickets (AN2). The AN2 receives direct input from two populations of receptor neurons (Hennig, 1988) that are sensitive in two different frequency ranges (Imaizumi and Pollack, 1999). These carrier frequencies are relevant in different behavioural contexts: the low frequency channel (3 kHz) is mainly devoted to processing of conspecific songs, while at frequencies higher than 15 kHz, receptors mainly detect echolocation sounds of predating bats (Moiseff et al., 1978). In addition to the excitatory inputs to AN2 by afferents, it is also the target of direct postsynaptic inhibition (Nolen and Hoy, 1987; Pollack, 2005), but presynaptic GABAergic connections at the afferent terminals are also reported (Hardt and Watson, 1999). At the level of the receptors, the two frequency channels are well separated, but they converge centrally, where processing has to comply with different computational demands for the two frequencies (Marsat and Pollack, 2004). It is thus likely that the input-response curves for the two frequencies in AN2 have different shapes, reflecting these demands. Possibly, the modulatory effect of adaptation on the response curve is also different for low and high frequency sound.

The first goal of the experiments described below was to test if (1) subtractive and divisive effects of a modulatory background will be different in the two carrier frequency domains. In a second step (2), cross-adaptation paradigms with current or the respective other frequency revealed where in the pathway different components of divisive and subtractive modulation of the response curves take place. Finally (3), selective pharmacological blocking of presynaptic inhibition uncovered its specific modulatory effect.

5.2 Methods

5.2.1 Stimulus protocols

In all experiments, response curves were obtained by presenting 100 ms square pulses with 2 ms ramps. For the adapted response curves, these pulses were preceded by at least 500 ms of the adapting background intensity (Fig. 5.2). When adaptor and test pulse were both acoustic and of the same frequency, 2 ms ramps lead from the adapting background to the test amplitude. For current and cross-frequency adaptation experiments, the latency for each stimulation modus was obtained separately and the onset corrected in such a way that switching off the adaptor and switching on of the test pulse coincided. Latency for current stimuli was shortest (2.4 ± 0.7ms), followed by the high frequency stimuli (9.7 ± 2.7ms) and low frequency (12.4 ± 3.1ms). All stimuli were repeated at least 15 times.

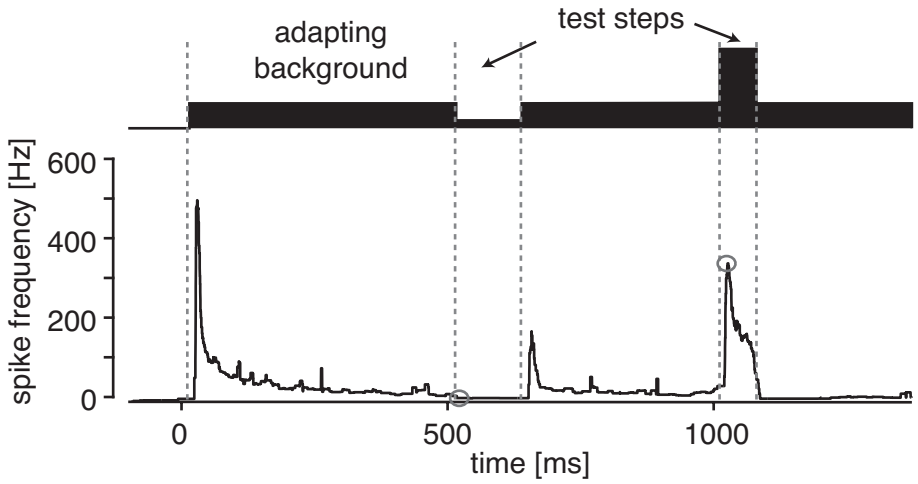

Figure 5.2: **Stimulus protocol for adapted response curves.** In order to construct onset response curves at different adaptation levels, a background stimulus was played and interrupted for short test pulses (upper trace). The neural response for each test intensity was quantified as the spike frequency response at the beginning of the test pulses, indicated by the grey circles.

5.2.2 Data analysis

For the parameterization of the unadapted response curves, a squared hyperbolic tangent of the form

$$f_{on}(x) = \begin{cases} f_{max} tanh^2(k(x_{thr} - x)) & ; \text{if } x > x_{thr} \\ 0 & ; \text{else} \end{cases} ,$$

was used. Squaring was introduced to match the asymmetric shape of the response curves. x is the input intensity in dB, x_{thr} is the threshold of the neuron, f_{max} is the maximal spike frequency of the response curve and k is a slope factor and can be used

to calculate the slope at the turning point of the curves s_{on}:

$$s_{on} = \frac{4}{3\sqrt{3}} f_{max} k.$$

For the quantifications of shift and slope change, the adapted onset response curves were parameterized using the same f_{max} as for the unadapted curve and only k and x_{thr} were fit to the data.

5.3 Results

5.3.1 Changes of the response curves in the two carrier channels

The AN2 of crickets is sensitive in two frequency ranges that correspond to two different behavioural contexts, mate selection and predation risk (Moiseff et al., 1978). Since the demands on coding and processing in these two contexts are different (Marsat and Pollack, 2004) , it was first tested whether adaptation changes the response curve of the AN2 in a frequency-specific way. To test for this, stimuli of different intensities were presented with either no adapting background (unadapted response curve) or preceded by a defined adaptation level of the same carrier frequency (Fig. 5.2). Both carrier frequencies were tested separately in this way and the onset response to each test step was quantified by the spike frequency.

Examples of a single cell are shown in Fig. 5.3. For the low frequency the response curves retained their overall shape, but thresholds shifted considerably depending on the adaptation level. This shift was observed over a wide range of intensities, in some cases up to 20 dB (Fig. 5.3A). When the adapting background was subtracted from the absolute stimulation level, all adapted curves matched the unadapted curve, demonstrating a strictly subtractive effect of the adapting background intensity at the low carrier frequency (Fig. 5.3B). At the high carrier frequency, response curves were shifted as at low frequencies, but also showed a clear decrease of the slope in response two different adapting backgrounds (Fig. 5.3C). Plotting relative rather than absolute intensities (Fig. 5.3D), a subtractive change was observed, but this did not account for the entire effect of adaptation. In a second step, the input intensities of the adapted

Figure 5.3 *(following page):* **Effect of adaptation on the onset response curves.** Displayed are onset responses curves at two different carrier frequencies, 3 kHz (A and B) and 16 kHz (C, D and E) for a single recorded neuron. Black symbols and lines represent unadapted response curves. Coloured symbols and lines represent response curves after adaptation to the background level indicated by the dashed lines in (A) and (C), respectively. In order to illustrate a shift of the response curves, in panels (B) and (D) the data in (A) and (C) was re-plotted with the adaptation background subtracted from input intensity for each curve. In (E), input intensity was additionally divided by the adaptation background to show the divisive effect of adaptation at 16 kHz. Error bars indicate standard deviation, solid lines in panels (A) and (C) stem from hyperbolic tangent fits to the data.

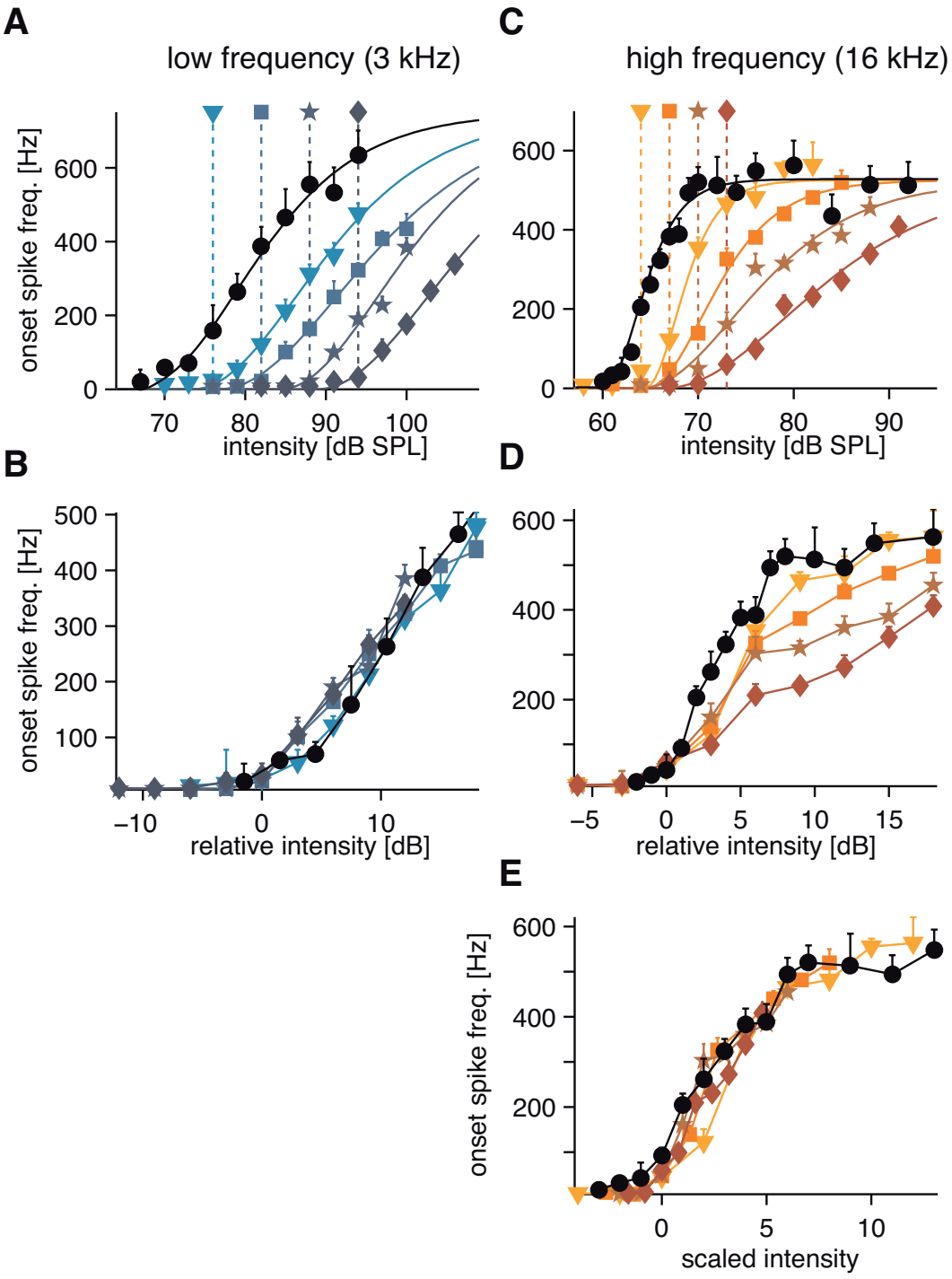
A
low frequency (3 kHz)
onset spike freq. [Hz]
600
400
200
0
70
80
90
100
intensity [dB SPL]
C
high frequency (16 kHz)
600
400
200
0
60
70
80
90
intensity [dB SPL]
B
onset spike freq. [Hz]
500
400
300
200
100
−10
0
10
relative intensity [dB]
D
600
400
200
−5
0
5
10
15
relative intensity [dB]
E
onset spike freq. [Hz]
600
400
200
0
5
10
scaled intensity

response curves were divided by the respective relative background intensities (corrected by a single constant scaling factor, Fig. 5.3D). These input-divided curves all matched the original, unadapted curve very well, showing that adaptation at high carrier frequencies has a subtractive and a divisive effect on the input dimension of the response curves.

In order to fully quantify this effect, the change of two parameters of the fits to the adapted response curves were analysed for all recordings: threshold shift and slope. If the effect was purely subtractive, a linear relation between background and threshold shift is expected and the slope should remain constant. The prediction for a divisive gain control is a monotonic decrease of the relation between background intensity and slope of the respective curve. For both carrier frequencies, a positive linear relation between background and threshold shift could be observed (Fig. 5.4A). At the low carrier, in the range between 0 and 2 dB relative background, the slope of the linear relation was one, indicating that the threshold shifted exactly to the background intensity. At the high carrier, the shift was frequently below the relative background intensity (Fig. 5.4C), which indicates a smaller subtractive contribution due to adaptation. At the low carrier, no change in slope could be observed for all cells tested, as predicted for strictly subtractive adaptation (Fig. 5.4B). At the high carrier, there was a linear relation between relative background and response curve slope up to about 10dB (Fig. 5.4D). Thus, within the observed range, adaptation had a reliable divisive effect and provides means to divide background and a novel signal.

5.3.2 Cross-adaptation with current

After observing the significant difference in the effect of adaptation in the two carriers frequency channels, the next question was where in the auditory pathway the two different effects – subtractive and divisive – arise from. Since AN2 receives direct input from the receptor neurons, there are four potential locations: (1) the two different populations of receptor neurons for the two different carriers (Fig. 5.5A, no. 1), (2) the synapses between receptor neurons (Fig. 5.5A, no. 2) or the AN2 itself, either (3) because of inhibitory inputs or (4) by adaptation currents activated by its own spiking (Fig. 5.5A, no. 3&4).

First adaptation currents within AN2 itself were tested. In order to do so, cross-adaptation experiments with injected current were performed. The protocol resembled that of the first experiment (Fig. 5.3), but the background adaptation was introduced by current injection that elicited spiking only in the AN2, while test stimuli were again acoustic stimuli of the two carrier frequencies. The adaptation mechanism activated in this experiments is shared by both frequency channels (Fig. 5.5A). Thus, the effect of adaptation to current stimuli should be the same for the two frequencies (Fig. 5.5A).

Intrinsic adaptation in AN2 to current injections had an effect in both frequency channels (Fig. 5.5B). The effect was subtractive on the response curves at both carriers (Fig. 5.5B&C), as predicted from modelling studies (Benda and Herz, 2003). As expected, the effect of adaptation to current injections was indistinguishable for both carriers (Fig. 5.5C&D). However, this effect was smaller than expected from acoustic adaptation at sound levels that elicited the same onset response as the current injection ('equivalent dB', Fig. 5.5C). This result provided evidence that the subtractive effect is a combination of the intrinsic adaptation in AN2 and adaptation mechanisms located

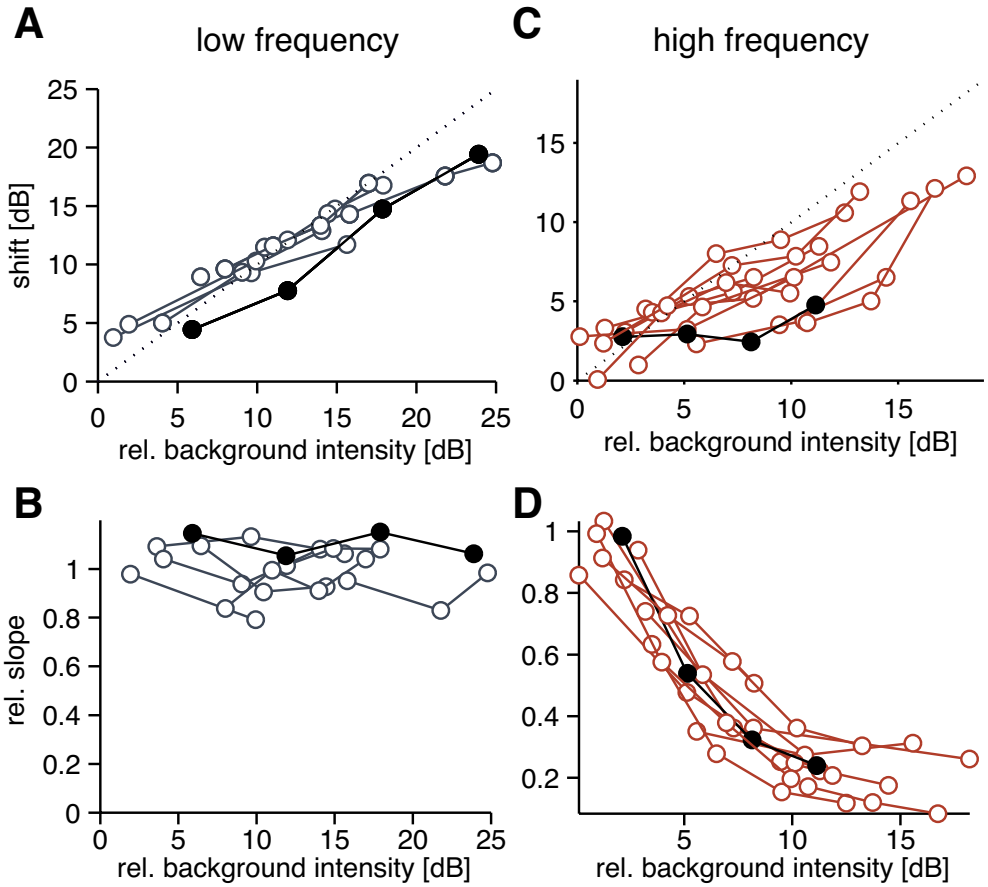

Figure 5.4: **Changes of response curves for all recorded cells.** Displayed are the values for the shift of the threshold (A&C) and change of slope (B&D) of hyperbolic tangent fits to the adapted response curves. Each data point represents one tested background intensity, points connected by lines stem from the same cell. The filled black symbols represent the cell that is displayed in Fig. 5.3. Background intensities are plotted relative to the unadapted threshold for each cell. The slope is given relative to the respective unadapted curve and values below one indicate shallower response curves than the unadapted curve (A&C). The shift is quantified by the difference in threshold between the adapted and the unadapted response curve (B&D), the dashed line has a slope of one, representing a shift of the threshold exactly according to the background level. Curves below the diagonal in (B) stem form cells that exhibited only a small shift of threshold.

more peripheral, either in the receptor neurons or at the synapses. This may also explain the difference between the two carriers observed in the first experiment: at the high carrier the subtractive effect appears to be less pronounced than in the low carrier (Fig. 5.4B, right). Thus, there may be stronger subtractive adaptation in the low frequency receptor population. There was no indication of any change of the slope of the response curves due to intrinsic adaptation (Fig. 5.5D). In summary, intrinsic adaptation within the AN2 at least contributed to the subtractive effect observed in both carrier frequencies (Fig. 5.4A&C), but cannot account for the divisive operation observed with acoustic stimulation at the high carrier frequency.

5.3.3 Cross-adaptation with other carrier frequency

Since divisive adaptation is not due to adaptation within AN2 itself (Fig. 5.5), its origin must be located more peripherally. There are three possible locations (Fig. 5.5A): (1) within each single receptor, second, (2) it could be located at the synapses either via presynaptic inhibition or synaptic depression, or (3) it is elicited by postsynaptic inhibition to AN2. If either of the two receptor populations are the source of divisive adaptation or the divisive effect is mediated by synaptic inhibition, adaptation to one frequency should not affect responses to the other. In order to elucidate the contribution of receptors, cross-adaptation experiments with the respective other frequency were carried out: the pathway was adapted by playing a constant background stimulus of one carrier frequency directly followed by test pulses of the other. Onset-response curves at different background levels were constructed as before (Fig. 5.1B). If the divisive effect is due to mechanisms within the high frequency receptor population or due to synaptic depression, one does not expect a divisive effect of adaptation to high frequencies on the low frequency response, but only a shift similar to what was observed in the current adaptation paradigm.

Figure 5.5 *(following page)*: **Cross-adaptation with current.** In (A), inputs to AN2 and possible locations of adaptation are shown. AN2 receives direct input from two receptor populations (low and high frequency). Additionally, there are inhibitory inputs on the presynaptic terminals whose origin is unknown (grey, no. 2). AN2 also receives direct postsynaptic inhibition via another auditory interneuron, the omega neuron (no. 3). Potential locations of mechanisms of adaptation as observed in AN2 during acoustic stimulation include intrinsic adaptation in the receptor neurons (1), presynaptic inhibition (2), postsynaptic inhibition (3), and spiking-activated adaptation currents within AN2 itself (4). The grey box in the top of panel (B) shows the only adaptation mechanisms that are activated by the 'background' current injection. Filled neurons indicate which part of the pathway is subsequently excited by the acoustic test pulses used to construct the response curves in the lower panel. Response curves in (B) stem from two different cells. Since background intensity has not the same units as the response curves, the elicited onset response to the adapting current injections are used to indicate the background level by horizontal dashed lines (B). The vertical lines represent the 'equivalent dB' value, constructed by the intersection of the fit to the unadapted response curve with the horizontal line (B). Panels (B&C) show response curve parameters for all recorded cells (n=5 for each frequency), for details see Fig. 5.4.

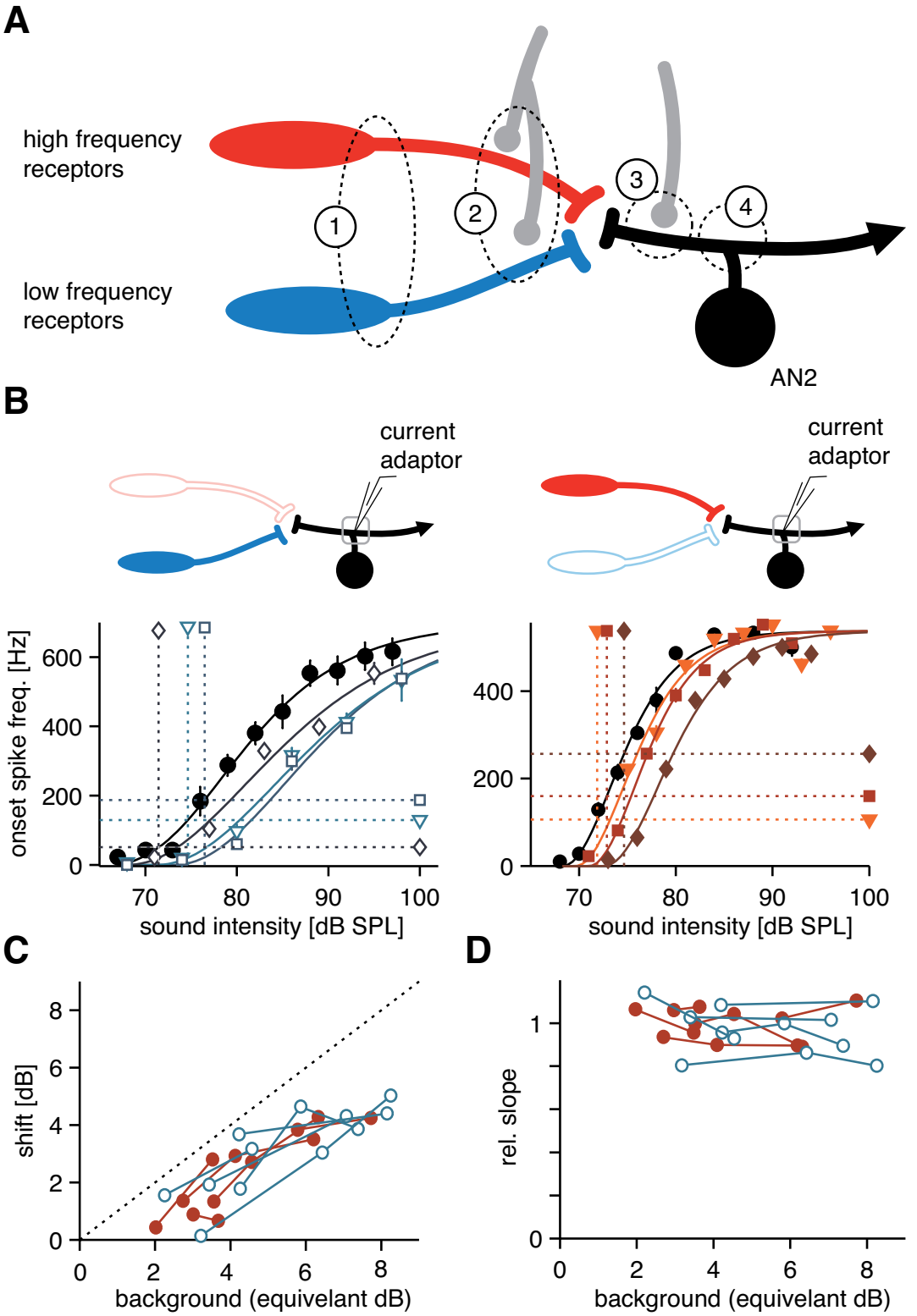
A
high frequency receptors
low frequency receptors
1
2
3
4
AN2
B
current adaptor
current adaptor
onset spike freq. [Hz]
0
200
400
600
70
80
90
100
sound intensity [dB SPL]
0
200
400
70
80
90
100
sound intensity [dB SPL]
C
shift [dB]
0
2
4
6
8
background (equivelant dB)
D
rel. slope
0
1
0
2
4
6
8
background (equivelant dB)

When the pathway was adapted to the low carrier frequency, the response curve to subsequent stimuli of the high carrier shifted, but did not change its slope (Fig. 5.6, left panels). Very low intensities near the threshold of the example AN2 in Fig. 5.6A already resulted in a shift of more than 3 dB. However, turning the low frequency background further up did not result in a more pronounced shift. Both effects can also be observed when looking at all 7 AN2 recorded using this stimulus paradigm: although the low frequency background was able to elicit onset spike frequencies over the whole range of the response curves of AN2 (Figs. 5.3, 5.6B&C), the resulting shift never exceeded 5 dB (Fig. 5.6C) and only in one case the shift was below 2 dB. Both bounds are in good agreement with previously shown results: as can be seen in Fig. 5.4 B (left), the low frequency background shifted the low frequency response curves never less than 3 dB, even at background intensities close to the threshold. Current injections on the other hand, which share the adaptation intrinsic to AN2 with the paradigm present here (upper panels in Figs. 5.5A and 5.6A), never shifted the response curves more than 5 dB. The lower bound may well be attributed to postsynaptic inhibition onto AN2 directly (Fig. 5.5A, no. 3) with a lower threshold than can be observed in AN2. Part of the receptor population sensitive to lower frequencies has lower thresholds than AN2 (Imaizumi and Pollack, 1999), which can also be observed in the second ascending neuron, AN1 (Benda and Hennig, 2007). Such inhibition from the lower frequency range onto AN2 has been reported before (Nolen and Hoy, 1987). Thus, the large subtractive shifts for

the low frequencies (Fig. 5.4C) are probably mediated by a combination of (1) adaptation in the low frequency receptor population, (2) postsynaptic inhibitory input to AN2 and (3) intrinsic adaptation in AN2.

It was also tested how adaptation in the high frequency channel changes response curves for low frequency sounds (Fig. 5.6A, upper right). Surprisingly, a clearly divisive effect of the high on the low frequency response curves was observed (Fig. 5.6A&B, right). This effect was of similar magnitude as on response curves for the high frequency (Fig. 5.4C) and could be seen in all tested cells (Fig. 5.6B, right). The divisive effect can neither be attributed to the receptors or synaptic depression, because the population excited during adaptation and testing do not overlap (Fig. 5.6A), nor can it be activated by intrinsic adaptation in AN2, because it is not seen during current injection (Fig. 5.5). Notably, this effect provides means to accomplish a divisive operation of signals in the lower and higher frequency channels.

Figure 5.6 *(following page):* **Cross-adaptation with respective other frequency.** The grey box in the top of panel (A) shows the adaptation mechanisms that are activated by the background stimulus. Dotted lines indicate locations of possible inhibitory input elicited by the background. Filled neurons indicate which part of the pathway is subsequently excited by the acoustic test pulses used to construct the response curves in the lower panel. Colours are the same as in previous figures (low frequency–blue; high frequency–orange/red). Response curves in (A) stem from different cells. Since background intensity has not the same units as the response curves, the elicited onset response to the adapting stimuli are used to indicate the background level by horizontal dashed lines (A). Panels (B&C) show response curve parameters for all recorded cells (n=7 for each frequency), for details see Fig. 5.4.

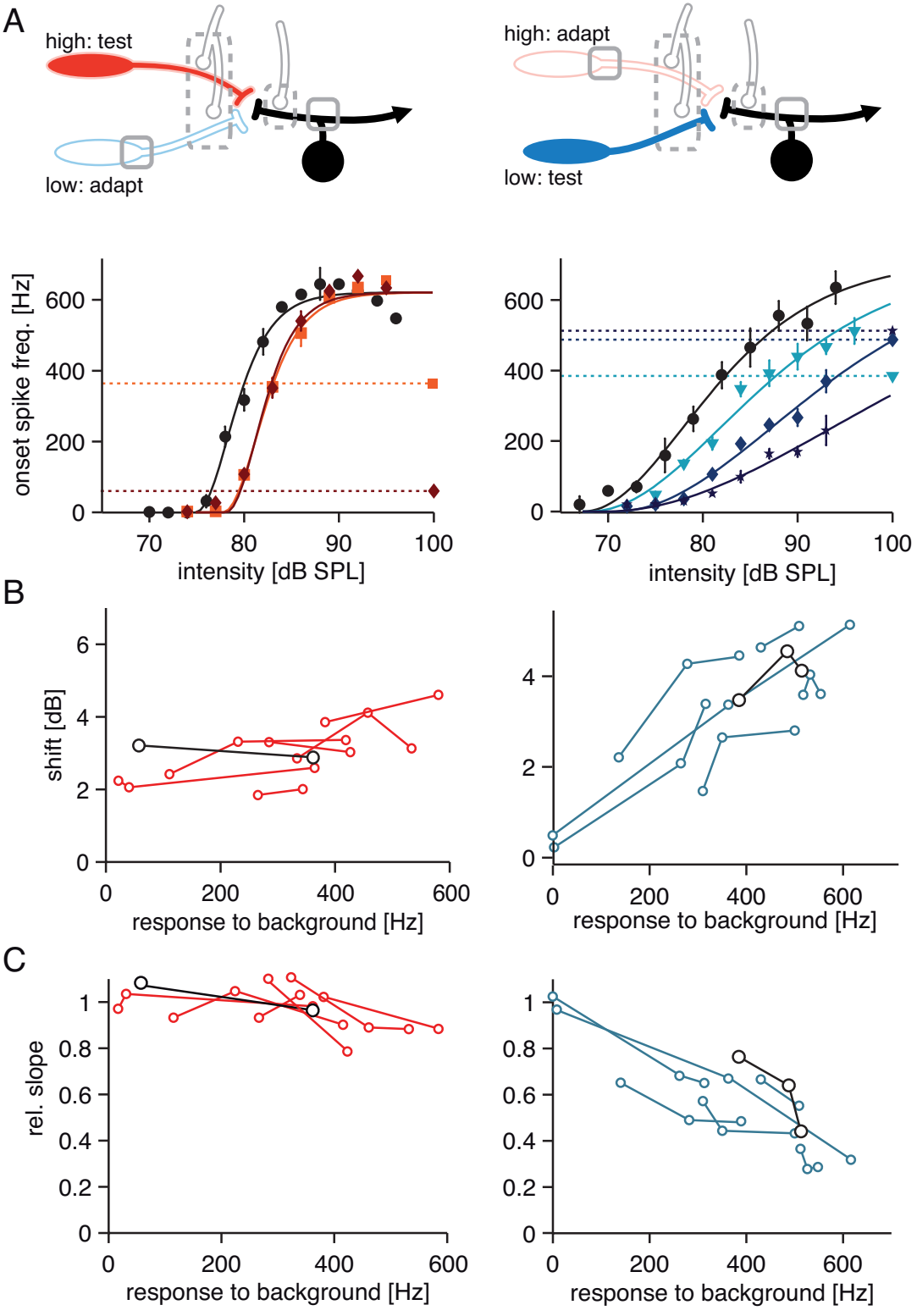
A
high: test
low: adapt
high: adapt
low: test
onset spike freq. [Hz]
intensity [dB SPL]
B
shift [dB]
response to background [Hz]
C
rel. slope
response to background [Hz]

Adaptation to high frequencies also mediated a moderate subtractive shift of low frequency response curves (Fig. 5.6C, right). This shift can well be attributed to intrinsic adaptation of AN2 as revealed by the current injection experiments (Fig. 5.5). Other than for adaptation to lower frequencies, the subtractive effect does not yield any indication of an additional inhibitory influence that would shift the response curves.

In summary, the subtractive component of adaptation is well explained by a combination of mechanisms within the receptors, by postsynaptic, frequency specific inhibition onto AN2, and intrinsic adaptation in AN2. However, the divisive part cannot be explained by these mechanisms.

5.3.4 Blocking of presynaptic inhibition

If the mechanism behind divisive adaptation is neither located in the receptors nor in the AN2 itself, adaptation could be caused by inhibitory input. There are two possible candidate sites: direct postsynaptic inhibition of the AN2, mainly mediated by the histaminergic omega neuron (Watson and Hardt, 1996) and presynaptic inhibitory GABAergic terminals at the receptor axons (Hardt and Watson, 1999).

Taking advantage of the different transmitters, presynaptic inhibition can be selectively blocked by applying picrotoxin. For these experiments, the adaptation protocol from the first experiment (Fig 5.3) using high frequency stimulation was repeated and adapted response curves before, during and after application of picrotoxin were measured (Fig. 5.7A). Picrotoxin did not alter the unadapted onset response curves, but had a profound effect on the adapted curves. Even at large background intensities the slope of the response curves did not change, if picrotoxin was present. The change in slope and the shift of the threshold level by parameterization of the response curves were quantified as before (Fig. 5.7B&C). For background intensities larger than 4 dB above threshold, a highly significant difference for the slope between either control condition and picrotoxin application was observed ($p < 0.001$, Fig. 5.7B). When presynaptic inhibition was blocked, no difference in slope between the different background adaptation levels could be observed, while the within-condition comparisons at different background intensities were all highly significant ($p < 0.001$). Thus, picrotoxin removed the divisive effect of adaptation entirely, providing strong evidence for presynaptic inhibition to mediate divisive gain control.

While the divisive part was removed by picrotoxin, blocking of presynaptic inhibition induced no or only weakly significant ($p < 0.05$) differences of the subtractive threshold shift (Fig. 5.7C). For those cases were the difference between picrotoxin and controls was significant, threshold shift was always larger when presynaptic inhibition was blocked. An explanation for this effect could be that without presynaptic inhibition, the AN2 receives a stronger adapting input itself. As intrinsic adaptation in AN2 is subtractive (Fig. 5.5), picrotoxin could indirectly enhance the subtractive part of adaptation. Thus, the weaker threshold shifts observed at the high frequency carrier (Fig. 5.4B) could be a direct consequence of presynaptic inhibition active during these stimuli.

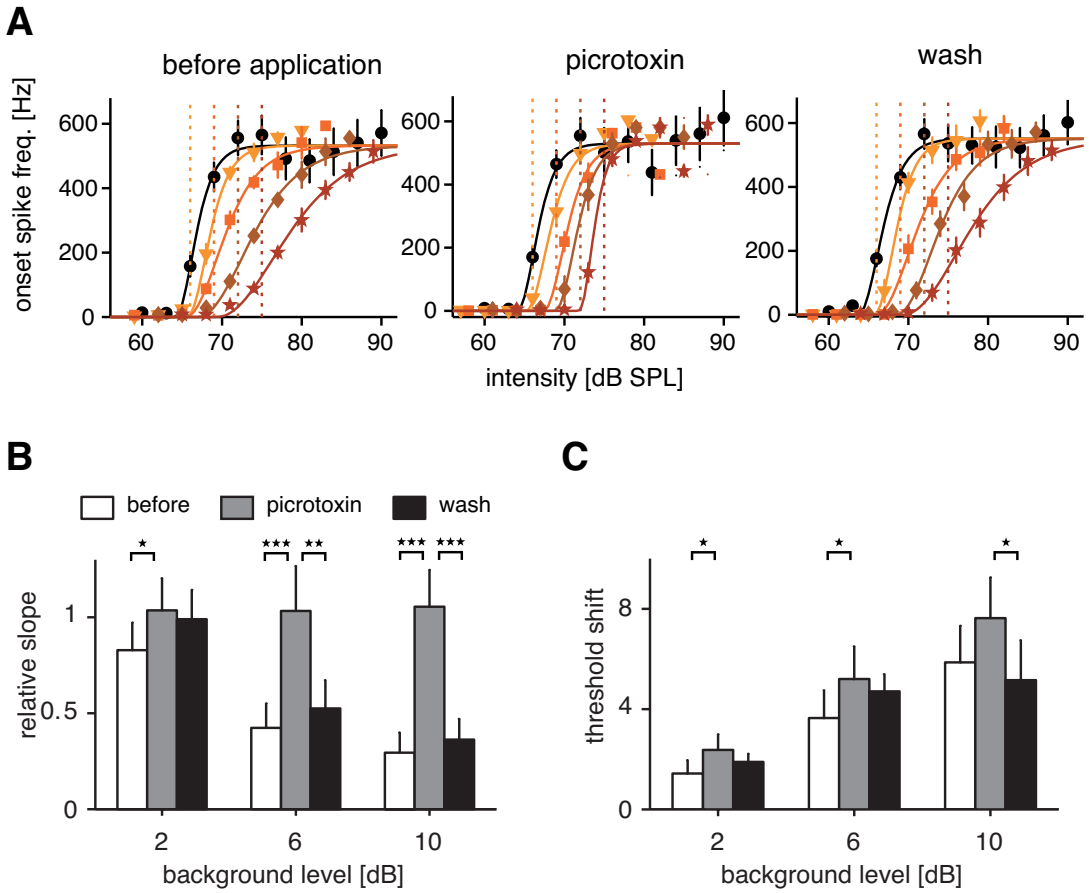

Figure 5.7: **Example of response curve changes due to adaptation before, during and after the application of pircrotoxin to block presynaptic inhibition.** In (A) adapted response curves of one cell at the high frequency stimulation are displayed for the different conditions (for details see Fig. 5.3). The histograms (C&D) show the values for the parametric fits in the different conditions for all recorded cells (n=6). The relative adaptation background level was pooled in three classes: 1–3 dB (2 dB label), 5–7 dB (6 dB) and 9–11 (10 dB label)). Error bars represent standard deviation between recordings. ($*p < 0.05; **p < 0.01; ***p < 0.001$).

5.4 Discussion

5.4.1 Summary

The auditory interneuron AN2 exhibited different forms of gain control in the two frequency channels constituted by direct synaptic input from two receptor populations (Hennig, 1988). In the lower frequency range, a subtractive effect of the background sound was observed, while high frequency backgrounds had a divisive effect on subsequent stimuli (Figs. 5.3 and 5.4). The origins of subtractive and divisive effects were disentangled using current injection as background (Fig. 5.5) and selective blocking of presynaptic inhibition (Fig. 5.7). Thereby, it was possible to show that presynaptic inhibition provides means for exact division of two subsequent signals along the input axis (Figs. 5.3 E and 5.4D).

5.4.2 Presynaptic inhibition and gain control

The term gain control is widely used in two different contexts. The first one applies mainly to control of motor patterns in invertebrates (Clarac and Cattaert, 1996) and vertebrates (Eccles et al., 1962; Rudomin, 2009) and focuses on the mechanism of presynaptic inhibition, allowing external control of synaptic efficacy. The second usage of the term is in its computational meaning as a divisive operation on the response function of a neuron (Abbott et al., 1997; Chance et al., 2002; Prescott and Koninck, 2003). To my knowledge there has been no attempt so far to unite these and thoroughly test the divisive character of the presynaptic inhibition.

Recently, presynaptic inhibition has been proposed to provide a mechanism for division of inputs (Olsen and Wilson, 2008; Root et al., 2008). GABAergic inputs to presynaptic terminals are omnipresent both in invertebrate (Clarac and Cattaert, 1996) and vertebrate (Rudomin, 2009) nervous systems. Presynaptic inhibition mediated by $GABA_A$ has been shown to open chloride channels, thereby increasing membrane conductance, which has a shunting effect on the afferent terminals (Cattaert and Manira, 1999). Shunting inhibition acts divisive on changes of the membrane potential (Carandini and Heeger, 1994; Nelson, 1994), and consequently on the amplitude of incoming action potentials. Thus, different levels of inhibition in response to the respective adapting background will divide the amplitude of action potentials invading the synaptic terminals (Fig. 5.8). This should lead to different numbers of vesicles released by the presynaptic cell and finally in EPSP amplitudes that are divided by a factor proportional to the inhibitory input. It has been shown that *postsynaptic* shunting inhibition alone is not effective as a gain control mechanism, because the shunting will influence both EPSP amplitude and spike generation, resulting in a net subtractive effect (Holt and Koch, 1997). This is different for presynaptic shunting inhibition, because only the conductance of the presynaptic membrane is altered and the divisively reduced EPSPs will translate to divisively reduced postsynaptic spike rates. Thus, presynaptic inhibition can now be added to the mechanisms mediating real divisive gain control, one of the central building blocks of neural computation from early sensory processing up to higher brain functions.

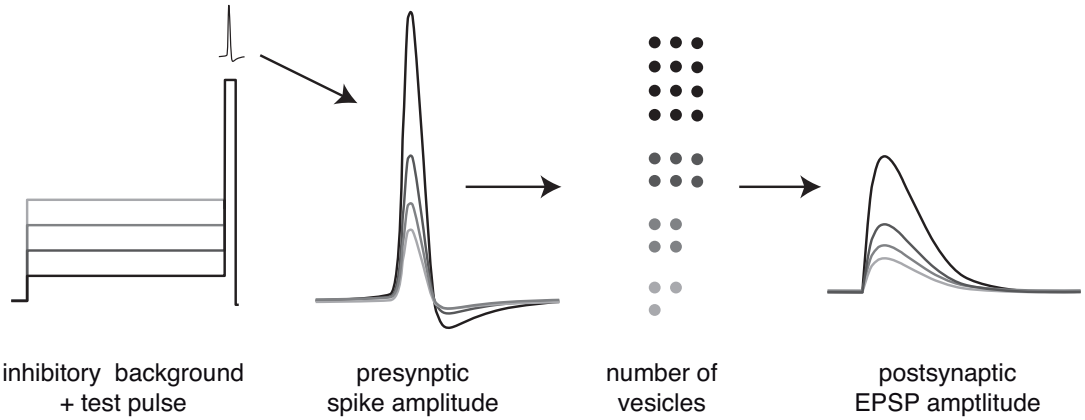

Figure 5.8: **Model of the emergence of divisive inhibition at presynaptic terminals.** A test pulse following different adaptation levels will elicit spikes (left panel), which have different amplitudes due to the shunting effect of presynaptic inhibition (centre-left). These divided spike amplitudes transfer to proportionate numbers of vesicles released to the synaptic cleft (centre-right) and subsequently to different levels of EPSPs postsynaptically.

5.4.3 Input gain-control vs. output gain-control

The present work shows an example of input gain-control since the divisive operation is performed on the input axis of the response curve (Ayaz and Chance, 2009). For a linear response curve, there is no difference between input and output gain-control, but the saturation of the sigmoidal nonlinearity restricts the dynamic range of the curve and *output* gain-control would reduce the maximal rate while keeping the dynamic range constant. In contrast, *input* gain-control will expand the dynamic range and therefore keep the capacity to code for intensity in the shallower response curves. The results presented here suggest that presynaptic inhibition mediates divisive gain control and thereby enlarges the dynamic range (Fig. 5.7A).

Since presynaptic inhibition does not act on receptor transduction or spike encoding, information about a wider intensity range must be present within the receptor population responses, although this is not reflected in the steep unadapted response curves of the AN2. Similar to the mammalian auditory system (Sachs and Abbas, 1974), the receptor sensitivities in crickets are stacked, resulting in a large dynamic range not of single receptors but in the entire population(Imaizumi and Pollack, 1999, 2001). Thus, in the unadapted state, the steep response curves of the AN2 reflects only the input of the receptor population with very low thresholds, because at higher intensities, the AN2 is already saturated. Where does the saturation come from? The simplest explanation is that it originates within AN2, after synaptic integration and cutting off input from receptors with higher threshold. Presynaptic inhibition would then change the gain at all synapses between single receptors and AN2, and the lower the gain, the more high-threshold receptors can contribute to the AN2 response curve without saturating it and would consequently enlarge its dynamical range.

5.4.4 What is the source of presynaptic inhibition?

GABAergic presynaptic terminals have been observed at cricket auditory receptor terminals (Hardt and Watson, 1999), but their origin remains elusive. One neuron that has been proposed to contribute to presynaptic inhibition is the corollary discharge interneuron (CDI), which receives direct input from the song pattern generator in the mesothoracic ganglion of crickets and inhibits the auditory system during singing (Poulet and Hedwig, 2002). However, there is no evidence for auditory input to the CDI (Poulet and Hedwig, 2003) and it is thus unlikely to mediate the gain control described here. Feedback from the brain can be discarded, because in all recordings the connectives between thorax and head were cut. The best-described inhibitory auditory interneuron in the prothorax of crickets is the omega neuron (Selverston et al., 1985; Pollack, 2005), but it is histaminergic (Watson and Hardt, 1996). In other cricket species, two tone experiments combining low and high frequency carriers revealed inhibition elicited by low frequency sound on high frequency stimuli (Nolen and Hoy, 1986, 1987; Libersat et al., 1994). The source of this inhibition is unknown, but its target is postsynaptic to AN2 and not presynaptic. Two tone suppression could, however, account for the relatively strong shifts observed at low background intensity for high frequency sounds in the cross-frequency experiments (Fig. 5.6C).

Presynaptic inhibition does not seem to be very fast, since blocking of it did not influence the onset responses (Fig. 5.7A), indicating a polysynaptic connection with a larger latency than direct excitation. A similar indirect afferent to afferent connection via local interneurons has been described for locust wing proprioceptors (Burrows and Matheson, 1994) and wind-sensitive afferents (Boyan, 1988).

Although the source of presynaptic inhibition as observed here remains unclear, one prediction about the properties of a potential input to the receptor terminals can be made. The divisive effect operated over an intensity range much larger than the dynamic range of the AN2 – any potential source of presynaptic inhibition would therefore be expected to have a shallow response curve. Also, it should not adapt its response curve in a similar manner as AN2 or the other ascending interneuron (AN1; Benda and Hennig, 2007) in order to reliably inhibit according to the absolute level of the 'background'. In general, for every mechanism that changes response curves relative to some absolute mean or overall variance of the stimulus statistics, these absolute values are saved in the state of the mechanism, i.e. the state of channels mediating adaptation currents or as in the present study, in the input driving presynaptic inhibition.

5.4.5 Biological relevance of gain control by presynaptic inhibition

The division of inputs is an operation that forms an important part of numerous neural computations (Salinas and Thier, 2000). In sensory processing it functions, among other roles, to achieve contrast or variance normalization (Brenner et al., 2000; Baccus and Meister, 2002; Dean et al., 2005) and to keep sensory neurons sensitive to broad distributions of stimuli (Olsen and Wilson, 2008). Gain modulation was present at higher frequencies, but at lower frequencies, only subtractive changes on the response curves were revealed (Fig. 5.4). For higher frequencies the most prominent role of the AN2 is for predator avoidance (Moiseff et al., 1978; Marsat and Pollack, 2006), but it could well play an important role in the assessment of higher harmonics of conspecific

sounds. While at low carrier frequencies, the relevant signals are highly stereotyped conspecific songs, the high frequency environment is more diverse and probably variance of relevant signals varies much more, possibly requiring a gain control mechanism as presented here. The subtractive shift observed at lower frequencies resembles what has been observed for the same frequency range in another auditory interneuron (Benda and Hennig, 2007), possible creating distance invariant representation of the stereotyped conspecific signals or separating the loudest of several singing males from its background, which requires a shift of the threshold and not a gain change (Chapter 6; Wimmer et al., 2008).

While the results of Chapters 3 & 4 revealed that the pattern of the placement of adaptation mechanism is relevant for the function of sensory coding, the results presented here uncovered the importance of the specifically recruited mechanism. But the result have implications for the placement of the mechanisms as well: in the convergent pathway present here, the mechanism for divisive gain control is placed *before* the combination of high and low frequency information, to allow for separate control of gain. Thus, it is not only important *where* adaptation takes place, but also *which mechanism* is recruited for adaptation to serve its computational role.

Part III. Why does adaptation act?

The function of adaptation: test of two competing hypotheses

6 Selective coding in the auditory pathway of crickets

6.1 Introduction

In the previous chapters, the architecture of adaptation was in the focus: *Where is adaptation placed?* And: *By which mechanism is it implemented?* Here, adaptation is examined from the perspective of its function: *Why is adaptation acting?* This question has been partly addressed in the theory chapter (4), but with an emphasis on the placement of the mechanisms. As in the previous chapter (5), the AN2 in the cricket auditory system will be examined, but at a larger time scale and for spike rates evaluated at larger time windows. In the context of separating time scales (see Chapter 4), the changes of the response curves reported here can be seen rather as a reaction to a slowly changing background while the divisive gain control described in Chapter 5 should be seen as an operation between subsequent signals. The work presented in this chapter is the result of a collaboration with Klaus Wimmer, who did large parts of the analysis presented here. It has been published in Wimmer et al. (2008).

Efficient encoding of natural signals is one of the major tasks sensory pathways have to accomplish. In order to do this, neural representation should be matched to the relevant part of incoming signals. Statistical properties of incoming signals are highly variable in a natural environment (e.g. the mean light level changes dramatically from a sunny region to a dark forest) but are mostly changing slowly over time (Nelken et al., 1999). Since the neural representation in sensory cells is limited to a certain range and resolution, the principle of efficient coding suggests that the nervous system should continually adapt its responses to changing statistical properties of the stimuli (Barlow, 1961). Firing rate adaptation changes the response curves of neurons in sensory pathways and has been shown to provide a mechanism for the adjustment of the encoding scheme in multiple systems (Baccus and Meister, 2002; Brenner et al., 2000; Dean et al., 2005; Fairhall et al., 2001; Maravall et al., 2007; Nagel and Doupe, 2006; Solomon et al., 2004). How the response curve is altered in response to a given stimulus should depend on what the relevant information is in the given context.

Here, the response properties of the AN2 at a time scale of seconds are explored. Two different principles that have been proposed to underlie adaptation of the response curve are tested: the principle of maximum information preservation (infomax) (Linsker, 1988) and that of background suppression by forward masking (Pollack, 1988; Sobel and Tank, 1994). The AN2 neuron provides an ideal model for studying the computational principles underlying adaptation, since (1) it receives direct input from auditory receptors and local interneurons at the first processing level (cf. Chapter 5, Fig. 5.5; Hennig, 1988), (2) on present evidence, it constitutes the only ascending representation of the auditory environment in the high frequency channel and thus a bottleneck for information transmission to higher centres (Horseman and Huber, 1994a,b; Wohlers and

Huber, 1982), and (3) it has a clear behavioural role because it is intimately involved in evasive behaviour in response to ultrasonic signals (Marsat and Pollack, 2006; Nolen and Hoy, 1984; Pollack and Martins, 2007). Several time constants of adaptation in the range from below 100 ms to several seconds are known for the receptor cells (Givois and Pollack, 2000), local interneurons (Pollack, 1988) and the ascending neurons (cf. Chapter 5, Benda and Hennig, 2007; Samson and Pollack, 2002) in this model system. Since auditory processing at the stage of the AN2 neuron is mainly feed-forward, adaptation is likely driven by the stimulus only rather than by task-dependent top-down processes.

The above mentioned principles lead to conflicting hypotheses about changes of the response curve when more than one 'signal' is present in an environment (Fig. 6.1). Following the infomax principle, the input-output transformation (the neuronal response curve) should maximize the information transmission between the neural representation and the stimulus. The optimal response curve depends on the statistical properties of the input signals, but internal noise and constraints on the possible changes limit the amount of information that can be conveyed.

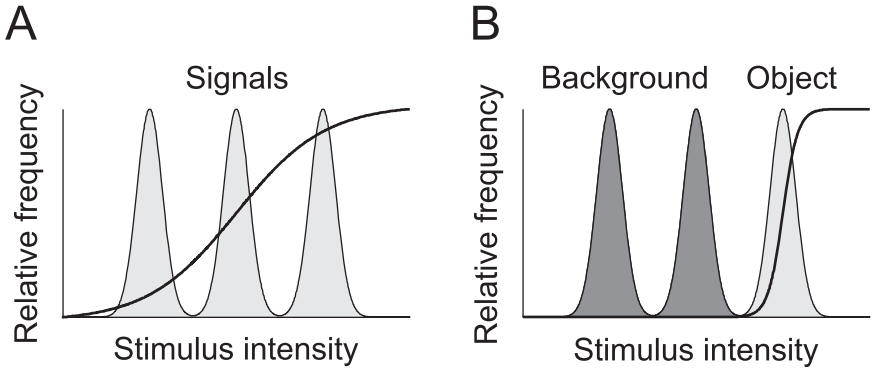

Figure 6.1: **Optimal sigmoidal stimulus response curves for a stimulus distribution consisting of three peaks** as predicted by two coding hypotheses. (A) Infomax: the dynamic range of the adapted response curve covers the whole range of input signals. Note that the optimal sigmoidal response curve is shown; generic optimal transmission would be attained by a response curve that has a derivative proportional to the local stimulus distribution. Such a response curve would be steep within peaks of the stimulus distribution and much flatter in between, thus it would be more staircase-like. (B) Background suppression: the response function optimally represents the most intense signal (light gray) whereas other signals (dark gray) are suppressed.

The infomax principle leads to the theoretical result that the derivative of the response curve should be proportional to the probability distribution of the stimuli, so that all available signals in a given environment are represented and every possible output rate occurs with equal probability. Laughlin (1981) tested this prediction and showed that contrast response curves in the fly visual system are matched to the statistics of natural images in order to maximize information transmission. Similar results have been reported for contrast response curves of retinal and LGN neurons in cat and monkey (Tadmor and Tolhurst, 2000). Information maximization can explain retinal coding in the spatial, temporal and chromatic domain (Atick, 1992).

A consequence of the infomax principle is that a change in the statistics of the sensory input must be compensated by a change in the response curve. Experimental evidence from the motion-sensitive H1 neuron in the fly supports this hypothesis: this neuron adapts its response curve to changing statistics of stimuli on several time scales (Brenner et al., 2000; Fairhall et al., 2001), in a way which is compatible with the infomax prediction. Experiments have also shown that adaptation enhances information transmission in visual cortex (Sharpee et al., 2006). Sharpee et al. estimated neural filters for the responses to natural inputs and to noise inputs matched for luminance and contrast, showing that neural filters adaptively changed with higher order statistics of input signals, so as to increase the mutual information between stimulus and neural response. Theoretical work also suggested that contrast adaptation in the mammalian visual system (Baccus and Meister, 2002; Carandini, 2000; Kohn and Movshon, 2003; Ohzawa et al., 1985; Solomon et al., 2004) could be understood as a consequence of the infomax principle (Adorján et al., 1999). However, it is difficult to quantify the role of adaptation in enhancing coding efficiency at higher stages in vertebrate sensory pathways since in these, coding is distributed among large populations of neurons and their responses are modulated by the activity of other neural populations or brain areas. Thus, simple sensory networks of invertebrates, whose representation are not heavily influenced by feedback signals, may provide a more suitable model to understand the principles lying behind sensory adaptation.

An alternative principle that may underlie adaptation is background suppression. Therefore, by forward masking (Sobel and Tank, 1994), a form of temporal inhibition, in which a continuous ('background') sound could modulate sensory sensitivity and suppresses the response to subsequent sounds. This form of forward masking in crickets could serve in a way that to segregate a single, most important signal is separated from other signals or background noise. It has been shown that an auditory interneuron (ON1) represents mainly the louder part of a stimulus with a bimodal intensity distribution (Pollack, 1988). Calcium aggregation in the omega neuron is a possible mechanism underlying this background suppression (Baden and Hedwig, 2007; Sobel and Tank, 1994). Similar findings have been made in bushcrickets: while multiple songs in choruses of singing males are present, only the most intense song was found to be represented in the auditory pathway (Römer and Krusch, 2000). These previous studies, however, address the phenomenon only qualitatively and not under the viewpoint of an encoding scheme and information transfer. Segregation of different auditory objects into different channels has also been studied in vertebrate hearing (Las et al., 2005; Nelken, 2004; Ulanovsky, 2003). In vertebrates, however, modulation of carrier frequency is assumed to play a crucial role in this stream segregation (Joris, 2004), complicating a detailed analysis. Information conveyed by carrier frequency modulation is very limited in crickets, as they possess only two broadly tuned frequency channels, one in the range around the carrier frequency of the calling songs (5 kHz) and another one mainly for frequencies above 15 kHz. Thus, crickets provide an ideal model system to study object-background segregation - in this simple auditory system, for a given frequency range, an auditory object can simply be seen as the loudest peak in the entire stimulus distribution.

The questions addressed in the study described here are: How does the neural response curve adapt to the statistics of the acoustic environment? Can this sensory system be characterized as a communication channel optimized for coding the inputs

such that as much information as possible is preserved (infomax principle)? Or does the system perform a preprocessing that leads to a high fidelity representation of only the loudest part of the stimuli (background suppression)?

To address these questions, the neural response curve of AN2 neurons were measured after adaptation to sound stimuli with either two or three peaks in their intensity distribution, depicted in Fig. 6.1. The two principles studied here predict conflicting changes of the form of the response curve when presenting a stimulus composed of more than one signal. Optimal background suppression should lead to a shift of the response curve in a way that only the peak with the highest intensity is represented (Fig. 6.1B). If infomax is the underlying principle, adaptation pursues the objective to maximize the information that the neuron's output conveys about its sensory input. Adaptation should thus change the response curve in a way that the whole stimulus range is encoded reliably (Fig. 6.1A).

Firing rate adaptation can change the stimulus-response curve basically in two ways (Benda and Herz, 2003): shifting the threshold to larger intensities and changing the slope of the curve. First the experimentally observed changes in the slope and the shift in response curves are compared to the optimal changes predicted by the two competing hypotheses. Differences between model prediction and data, however, do not necessarily imply that a particular hypothesis is unlikely to be true, because additional constraints may limit the potential of tuning curve changes. Therefore, in a second step, the mutual information between the sensory input and the neuronal response is calculated using the measured response curves. The infomax principle predicts that the mutual information between a particular stimulus distribution and the response should be highest for the response curve that is adapted to the stimulus distribution. The response curve adapted to the stimulus with three peaks should encode the three-peak stimulus better than the response curve adapted to the stimulus with two peaks. Background suppression, on the other hand, predicts that the mutual information should decrease for the 'background' signals and should increase for the most intense peak.

6.2 Methods

6.2.1 Stimulus protocols

The protocol used for characterizing the adaptation process in the ascending AN2 neuron is shown in Fig. 6.2. The different ensembles of auditory stimuli consisted of an adapting stimulus, a silent interval, and a test stimulus. The intensity of the adapting stimulus was adjusted at the beginning of the recording depending on the response strength of the neuron. Normally, the base line intensity of the adapting stimulus had a sound pressure level of 84 dB or 87 dB. The term relative intensity refers to the stimulus intensity relative to this base line intensity. Adapting stimuli are 16 kHz signals that were amplitude-modulated by bandpass-filtered Gaussian white noise with 100 Hz cut-off frequency. The Gaussian noise had a variance $\sigma^2 = 1.38\,\mathrm{dB}^2$ and a mean relative intensity $\mu = 0\,\mathrm{dB}$. Test stimuli were pure sinusoidal tones with a frequency of 16 kHz. To characterize adaptation, adapting stimuli with durations 75 ms, 150 ms, 300 ms, 600 ms, 1200 ms, 2400 ms and 4800 ms were used (Fig. 6.2A). For testing the recovery from adaptation, the stimuli had a 5 s adaptation phase followed by pauses of varying durations from 75 ms to 4800 ms (Fig. 6.2B).

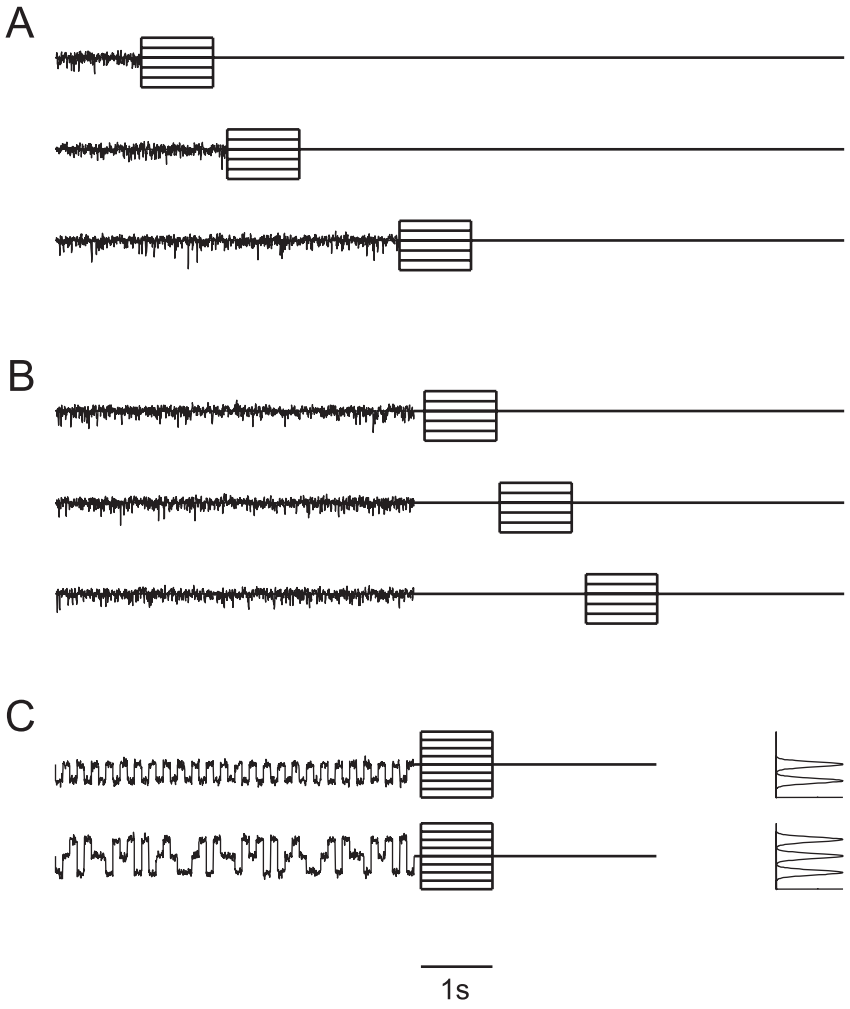

Figure 6.2: **Summary of the experimental protocols.** (A): Adaptation protocol. Amplitude-modulated noise signals (adapting stimuli with 0 dB average relative intensity) of variable duration (from 75 ms to 4800 ms) are followed by a test stimulus (16 kHz sinusoidal tone) with a duration of 1000 ms and a relative intensity ranging from -9 dB to +6 dB (several test stimuli are plotted on top of each other). (B): Recovery protocol. Amplitude-modulated noise signals (adapting stimuli) of 5 second duration are followed by a pause of variable length (from 75 ms to 4800 ms) and a test stimulus as in (A). (C): Adaptation protocol for amplitude-modulated noise stimuli drawn from a bimodal and a trimodal distribution (the corresponding amplitude distributions are shown in the right panel). Relative intensities of the test stimuli range from -6 dB to +6 dB.

Motivated by the competing coding hypotheses *infomax* and *background suppression*, the main goal was to examine the consequences of adaptation to different ensembles of auditory stimuli demanding different changes in the stimulus-response curve. In order to do this, multi-modal noise-like stimuli were designed, whose amplitude distribution had two or three modes, mimicking auditory scenes with multiple signals. The amplitude distribution of the bimodal stimulus is composed of two Gaussian distributions, with mean relative intensity $\mu_1 = -3\,\mathrm{dB}$, $\mu_2 = 0\,\mathrm{dB}$ and variance $\sigma^2 = 0.2\,\mathrm{dB}^2$. The trimodal stimulus has an additional peak modelled by a third Gaussian distribution with mean $\mu_3 = +3\,\mathrm{dB}$ and $\sigma^2 = 0.2\,\mathrm{dB}^2$. An example of these stimuli is shown in Fig. 6.2C, together with the respective amplitude distributions. The adaptation time was 5 s in these experiments and the silent interval before the test stimulus was 100 ms. In all experiments, the intensity response curves were determined by sinusoidal test stimuli with a frequency of 16 kHz and duration of 1 s, following the respective adaptation stimulus. The relative intensities of the test stimuli were $-9\,\mathrm{dB}$ to $+6\,\mathrm{dB}$. Each stimulus was presented at least five times.

6.2.2 Data analysis

Construction of intensity-response curves

Intensity-response curves were constructed in order to quantify the neural response, as shown in Figs. 6.3 and 6.4. Therefore, the spike count in a 200 ms time window was used, beginning 100 ms after test stimulus onset. The window was chosen such that the influence of the fast adaptation process is minimized (time constant of about 40 ms, similar to the one described for the AN1 neuron by Benda and Hennig, 2007). In AN2, this fast process is probably responsible for the gain change described in Chapter 5. Here, the coding of slower stimulus dynamics is considered, in order to separate the time scales. Hence, responses to unmodulated test stimuli within a 200 ms time window were measured.

In order to test for changes on the response curve, the response curves need to be parameterized. This is done by fitting a sigmoid response curve, relating stimulus intensity to spike rate as

$$r_i(x_i) = \frac{A}{1 + exp\left(-\frac{x_i - B_{50}}{C}\right)}, \tag{6.1}$$

where r_i is the underlying firing rate of the neuron, x_i is the stimulus intensity, A is maximum response of the cell, B_{50} is the stimulus intensity at 50% of maximum response, and C is a slope factor.

A common methodology to construct neuronal response curves is repeating a single experimental condition several times and then computing the mean of the observed spike counts and their variance. In a second step, a parametric model is fit to these data, typically using least-square approximation (cf. Chapter 5).

Here the changes of the response curve due to the two stimulus distributions are at the centre of interest. The two proposed coding principles provide exact predictions for the parameter changes. It is necessary to test for the significance of these parameter changes to distinguish the two hypotheses reliably. This, however, is difficult to

establish with traditional statistical methods.

Here, a Bayesian analysis (Gelman et al., 1995; MacKay, 2003) is used to account for the statistics of each trial to estimate the parameters accurately and to quantify the confidence limits of the parameter estimation. The method allows estimating the full probability distribution (posterior distribution) of the response curve parameters rather than only the mean value as with traditional methods. The work presented in Chapter 6 was established in a collaboration; the Bayesian analysis was developed and carried out by Klaus Wimmer. A detailed derivation of the joint posterior distributions of the parameters A, B_{50} and C of eq. 6.1 and the calculation of the calculation of the quantitative predictions for these values from the two coding hypotheses can be found in Appendix B. In the following, the procedure for the estimation of the parameters from the data is described as carried out by Klaus Wimmer.

Calculating the joint posterior distribution

Following (Gelman et al., 1995), the posterior was calculated for a range of A, B_{50} and C values using a grid of $200 \times 200 \times 200$ points and normalized across this grid. Initially a large parameter space was sampled (e.g. values for the parameter A in the range from 0 to three times the maximum observed firing rate of the neuron) that was narrowed to allow finer sampling in the region of non-zero posterior values. To simplify further analysis, 10000 random samples (A_i, $B_{50,i}$, C_i, with $i = 1 \ldots 10000$) were drawn independently from the joint posterior probability distribution. From these samples, the posterior distribution of any quantity of interest can be estimated, e.g., the posterior distribution of the response curve parameters 'location' B_{50} or of the 'slope' at half of the maximum response:

$$S_{50} = \frac{1}{4C}. \tag{6.2}$$

The slope S_{50} does not depend on the maximum response A, in order to be able to compare the response curve slopes from different neurons (i.e. for calculating the slope the neural responses are normalized to the interval between 0 and 1).

To summarize the results for all the recorded AN2 cells, the samples from the posterior distributions of individual cells were combined to obtain a 'combined posterior distribution' (assuming independence of individual experiments).

In the results section (Chapter 6 the mean of the corresponding posterior distributions is reported in order to characterize the expected values of the parameters (given the data). These expected parameter values were also used to illustrate the estimated sigmoid response curve. In most cases, the expected parameters and the parameters with the maximum posterior probability (i.e. the maximum a posteriori estimate) had very similar values.

Significance testing

Consider one of the parameters of interest, e.g. B_{50}, and its posterior distributions $P_1(B_{50}^1|y^1)$ and $P_2(B_{50}^2|y^2)$, for two stimulus conditions 1 and 2. Bayesian analysis provides us with samples from these distributions P_1 and P_2. To determine if B_{50}^1 is significantly different from B_{50}^2, the posterior distribution P_d of the difference $B_{50}^2 - B_{50}^1$ was calculated. This was done by repeatedly taking one sample $b1$ from the distribution

$P_1(B_{50}^1|y^1)$ and one sample b_2 from $P_2(B_{50}^2|y^2)$ and calculating the difference $b_2 - b_1$, giving one sample from the distribution P_d.

To determine a significant difference, the 95% posterior interval $[i_1, i_2]$ of P_d was calculated, defined as the range of values above, and below which lay 2.5 % of the samples. The values i_1 and i_2 can be directly estimated from the samples: i_1 corresponds to the 2.5th and i_2 to the 97.5th percentile. If the 95% posterior interval of P_d includes zero, the difference between and is not statistically significant. On the other hand, if the 95% posterior interval excludes zero the difference is regarded as significant. To test if an estimated parameter is significantly larger (smaller) than a certain value x, the right-tailed (left-tailed) posterior interval was calculated. If the right-tailed (left-tailed) posterior interval excludes the value x, i.e. less than 5% of the corresponding samples are smaller (larger) than x, the parameter is regarded as significantly larger (smaller) than x.

Time course of adaptation To characterize the time course of adaptation, a single exponential decay model was used:

$$y(t) = y_{min} + (y_{max} - y_{min}) \exp\left(\frac{-t}{\tau_a}\right), \tag{6.3}$$

where $y(t)$ is the neural response at time t, y_{min} and y_{max} are minimum and maximum response, and τ_a is the decay time constant. A similar single exponential model

$$y(t) = y_{min} + (y_{max} - y_{min}) \left[1 - \exp\left(\frac{-t}{\tau_a}\right)\right] \tag{6.4}$$

is used for describing the recovery from adaptation, where τ_r is the recovery time constant. Using the Bayesian approach, the posterior densities of the parameters of eqs. 6.3 and 6.4 were calculated in a similar manner as for the sigmoid response curve (eq. 6.1).

Numerical estimation of mutual information

The mutual information $I[\mathrm{Y}; X]$ between the sensory signal X and the neural response Y specifies how much information is conveyed on average about all possible signals. In order to compute the mutual information numerically, taking into account the influence of discrete, Poisson distributed spike counts, the joint probability distribution was calculated:

$$P(y, x) = P(y|x)P(x). \tag{6.5}$$

For each stimulus intensity x_i, the corresponding average of the firing rate r_i can be calculated using eq. 6.1. The distribution $P(y|x = x_i)$ is then given by a Poisson distribution with mean r_i (eq. B1). For all simulations, the stimulus X was discretized into bins of size 0.01 dB. At this resolution, the results did not depend on the bin size.

To measure the information that is associated with specific sensory signals, the stimulus specific information is defined by (Butts, 2003; Butts and Goldman, 2006):

$$i_{SSI}(x) = \sum_y P(y|x)(H[X] - H[X|\mathrm{Y} = y]), \tag{6.6}$$

where $H[X] = -\sum_x P(x) \log_2 P(x)$ is the entropy of the sensory signal X, and the conditional entropy of a particular response y is given by

$$H[X|\mathrm{Y} = y] = -\sum_x P(x|y) \log_2 P(x|y).$$

Stimulus-specific information can be interpreted as the average reduction of uncertainty about the sensory signal gained from one measurement given the stimulus x. Taking the weighted average over the stimulus-specific information for all possible signals, the mutual information between stimulus and response is obtained:

$$I[\mathrm{Y}; X] = \sum_x P(x) i_{SSI}(x). \tag{6.7}$$

Finally, the sum in eq. 6.7 from x_1 to x_2 was evaluated in order to determine the information associated with a certain stimulus range $[x_1, x_2]$.

6.3 Results

6.3.1 Time course of adaptation

In a first step, the effects of prolonged auditory stimulation in recordings of 6 AN2 neurons of *T. oceanicus* and 7 AN2 neurons of *T. leo* were studied. Previously, an adaptation process operating on a time scale of 40 ms had been characterized for the AN1 neuron (Benda and Hennig, 2007). Here, it is investigate whether adaptation also occurs on a slower time scale, better matched to changes in the acoustic environments.

Adaptation and recovery

The responses of AN2 neurons were recorded to test stimuli of different intensities, after adaptation to noise stimuli of varying duration (see Methods, Stimulus protocols). A typical example for the neural responses of an AN2 cell of *T. leo* is shown in Fig. 6.3. The spike rates after an adaptation period of 4800 ms are always lower than the corresponding responses after 600 ms and 75 ms adaptation time. Responses declined with prolonged stimulation during the test interval for the applied intensities that were higher than the intensities of the adapting stimuli (Fig. 6.3C-D), a phenomenon, which was observed in all the recorded cells. The rapid initial change, which is most pronounced for high intensities of the test stimulus (Fig. 6.3C-D) is caused by the fast firing-rate adaptation (similar to the adaptation in the AN1 neuron Benda and Hennig, 2007). To minimize an influence of the fast and the slow adaptation occurring during test, only spikes occurring between 100 ms and 300 ms after test stimulus onset were used for further analysis. Fig. 6.4A shows the stimulus response curves constructed from the spike counts within the interval mentioned above. Prolonged stimulation shifted the stimulus-response curves towards higher stimulus intensities. In the example shown, adapting for 4800 ms virtually eliminated the response to low relative intensities from -9 dB to -3 dB. Adaptation changes the range of relative intensities, over which the cell responds, but has little effect on the maximal firing rate. Fig. 6.4B shows data from the same cell when using stimuli for testing the recovery from adaptation. Adapting stimuli were always 5 s long, followed by a silent interval of varying

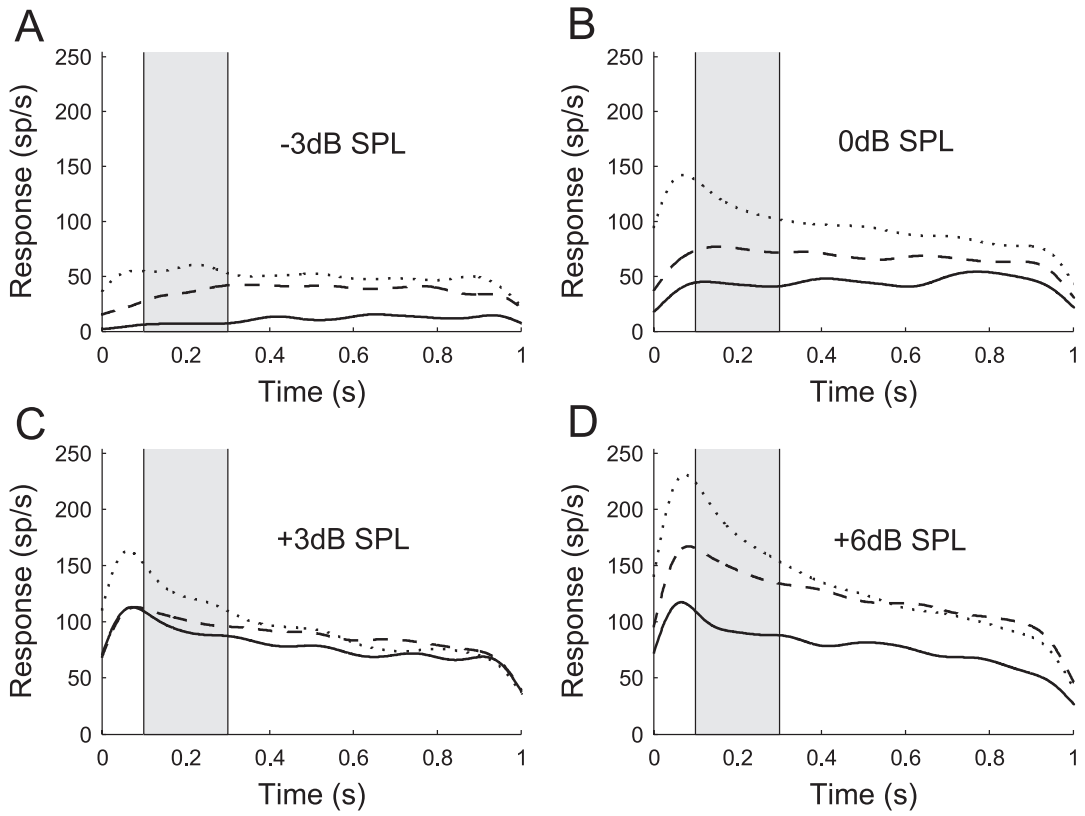

Figure 6.3: **Representative examples of the neural response after adaptation to noise stimuli** (AN2 neuron from a *T. leo*). Duration of the noise stimulus was 75 ms (dotted line), 600 ms (dashed line) and 4800 ms (solid line). (A)-(D): Responses (spike rates) during a test stimulus of 1 s duration (cf. protocol of Fig. 6.2A). Relative intensities of the test stimuli range from -3 dB (A) to +6 dB (D); the average relative intensity of the adapting stimulus was 0 dB. Each stimulus was presented 5 times and the recorded spike trains (1 ms resolution) were convolved with a Gaussian kernel ($\sigma = 50$ ms). The instantaneous spike rates were estimated by averaging over the 5 repetitions. The increase of the estimated rate during the first 50 ms is an artefact introduced by filtering the neural response with the Gaussian kernel. Note that the onset latency of the AN2 neuron is in the range of 15 to 18 ms. The spike counts during the sample period (shaded) from 100 ms to 300 ms are used to construct neural response curves.

duration and a test stimulus. After a recovery period of 4800 ms the neuron has almost recovered its state prior to adaptation. Hence, adaptation and recovery from adaptation operate on a similar time scale.

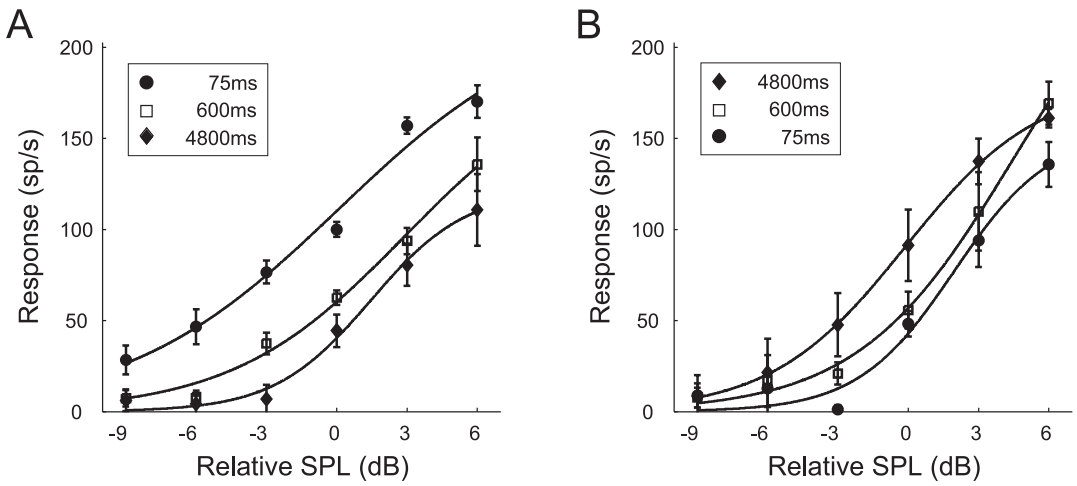

Figure 6.4: **Representative example of response curves for different adaptation (A) and recovery times (B)** (cf. protocols of Fig. 6.2A,B). The average relative intensity of the adapting stimulus was 0 dB. Symbols denote the average spike counts during the sample period (cf. Fig. 6.3) for different test intensities. Solid lines indicate the expected response curve, i.e. the response curve with the set of parameters with the mean value of the posterior distribution. Each stimulus protocol was repeated 5 times (the error bars indicate the standard deviation). The data shown was obtained from a *T. leo* (the same preparation as used in Fig. 6.3).

Time constants of adaptation

To quantify the time course of adaptation and recovery the neural responses to test stimuli that had the same relative intensity as the adapting stimuli (0 dB) was analysed. Additional cells were recorded with a reduced version of the stimulus protocol that only included these 0 dB test stimuli (the total number of cells available for each species and each stimulus protocol is stated in tab. 6.1). In order to determine the adaptation and recovery time constants τ_a and τ_r, an exponential decay model was fitted to the neural responses (see Methods for details). Fig. 6.5A,B show examples of recorded data and exponential fits for a *T. oceanicus* and a *T. leo* cell. Both time constants lie in the range of 1 second for both of these cells. This is considerably longer than the short-term firing rate adaptation, which operates on a time scale of 40 ms.

The values of the adaptation and recovery time constants are summarized in tab. 6.1 for both species. Comparing the time constants between *T. oceanicus* and *T. leo cells*, there were no significant differences. Furthermore, adaptation and recovery time constants have similar values.

Table 6.1: **Summary of the adaptation and recovery time constants.**

Species	Adaptation			Recovery from adaptation		
	τ_a	SD(ms)	n	τ_r(ms)	SD(ms)	n
T. oceanicus	1202	558	6	1947	1155	6
T. leo	1828	939	9	1674	582	11

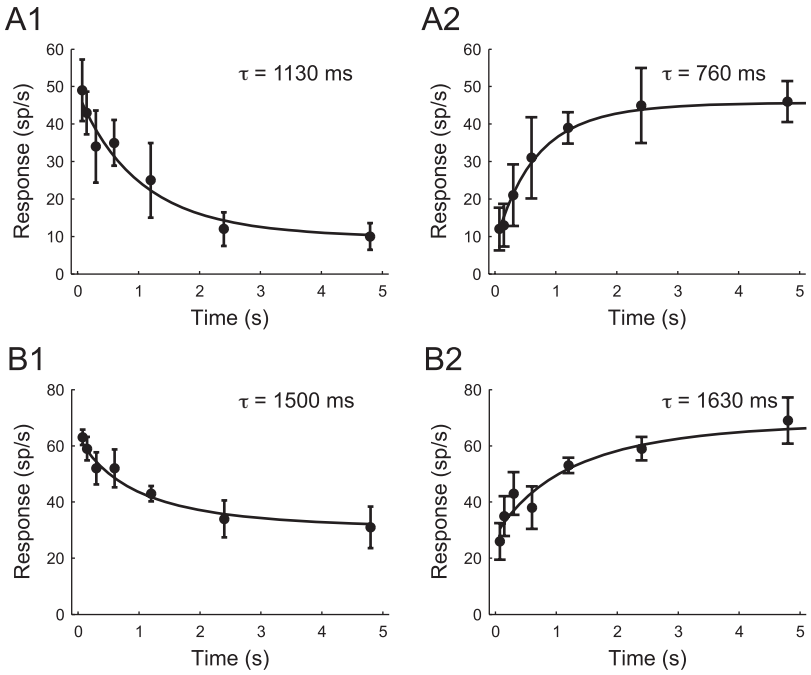

Figure 6.5: **Time course of adaptation and recovery** of a *T. leo* cell (A1& A2) and of a *T. oceanicus cell* (B1& B2). The response to the test stimulus is plotted against the duration of the adapting stimulus (A1& B1) and the delay between the adapting and the test stimulus (A2& B2). Displayed are the average spike counts in the 200 ms time window of the test stimulus (cf. Fig. 6.3). The intensity of the test stimulus was equal to the average intensity of the adapting stimulus (0 dB relative intensity). The error bars denote the standard deviation. Solid lines indicate the exponential function with the set of parameters with the highest value of the posterior distribution.

Summary time course of adaptation

In summary, the neuronal responsiveness of AN2 neurons is affected significantly by adaptation and this adaptation process operates on a time scale of seconds. The primary effect of adaptation is a change in the range of stimulus intensities over which the cell responds. This change will now be examined in more detail.

6.3.2 Adaptation to the statistics of the acoustic environment

The next step is to put to test the hypothesis that adaptation serves for adjusting the stimulus-response curve to the current acoustic environment. The infomax principle and the background suppression hypothesis both predict how the neural response curve should optimally change in response to a change in the statistics of the environment. In order to assess the response curve changes quantitatively, parameters of the optimal response curve under either hypothesis were computed (for detailed derivations of the optimal parameters see Appendix B).

Predictions for optimal response curves

Assuming the sigmoid transfer function of eq. 6.1 and the bimodal or trimodal stimulus distribution (see Methods, Stimulus protocols), optimal values for the response curve parameters for 'location' (B_{50}) and slope (S_{50}) can be obtained.

Infomax principle Fig. 6.6A shows the predicted response curves for the infomax principle for both stimulus distributions, under the assumption that the response curve parameters B_{50} and S_{50} can be optimally adjusted. The optimal value for B_{50} is $-1.50\,\mathrm{dB}$ for the bimodally distributed stimulus and $0.00\,\mathrm{dB}$ for the trimodally distributed stimulus, corresponding to a response curve shift of $+1.50\,\mathrm{dB}$. To cover the whole stimulus range, the slope should decrease for the trimodally distributed stimulus compared to the bimodally distributed stimulus by -35.3%, from $0.25\,\mathrm{dB}^{-1}$ to $0.16\mathrm{dB}^{-1}$. If it is assume that the neural system can only adjust B_{50} and the slope S_{50} is constant, the infomax principle would still predict a shift of the response curve of $1.50\,\mathrm{dB}$.

Background suppression Background suppression is a concept that is less well defined than the infomax principle, because it involves an assumption about the 'signal' vs. the 'background' part of a complex stimulus. In the following, it will be assumed, that the loudest signals of artificial environments, i.e. the 'loudest' Gaussian distributions of the multimodal stimulus distributions (see Fig. 6.6B) are encoded in an optimal way while the other ('background') signals are suppressed. Fig. 6.6B shows the predicted response curves when it is assumed that the loudest signal should be encoded reliably and other signals should be suppressed. The predicted difference between the response curve optimized for the bimodal and trimodal stimulus is a shift by $3.00\,\mathrm{dB}$ (from $B_{50} = 0.00\,\mathrm{dB}$ to $B_{50} = 3.00\,\mathrm{dB}$). The slope S_{50} does not change and remains at $0.98\,\mathrm{dB}^{-1}$. Predictions for both coding hypothesis is summarized in tab. 6.2.

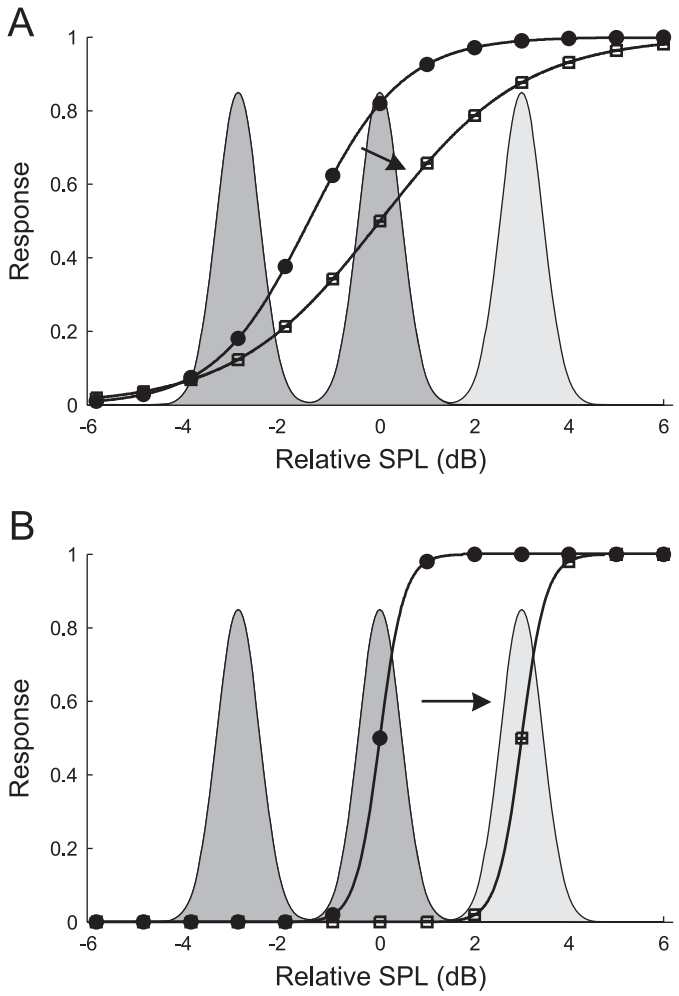

Figure 6.6: **Optimal response curves** for the bimodal (circles) and trimodal (squares) stimulus distribution predicted by the infomax principle (A) and the background suppression hypothesis (B). The figures show the predicted relationship between the response variable (spike rate) and the stimulus intensity. The Gaussian curves depict the probability distributions of stimulus intensity, where the dark shaded areas under the curve denote the bimodal stimulus distribution and the light shaded area under the curve the additional peak of the trimodal stimulus distribution (cf. Fig. 6.1).

Table 6.2: **Summary of predictions for the two coding hypothesis.** Values describe the change of the two response curve parameters between the tri- and bimodal stimulus distributions. The left column is for the case that slope and location of the response curve can change, the right column is for the assumption that adaptation cannot alter the slope.

	Shift and Change of slope		**Shift only**
	$\Delta B_{50}[dB]$	slope change [%]	ΔB_{50} $[dB]$
Infomax	1.5	-35.3	1.5
Background suppression	3	0	3

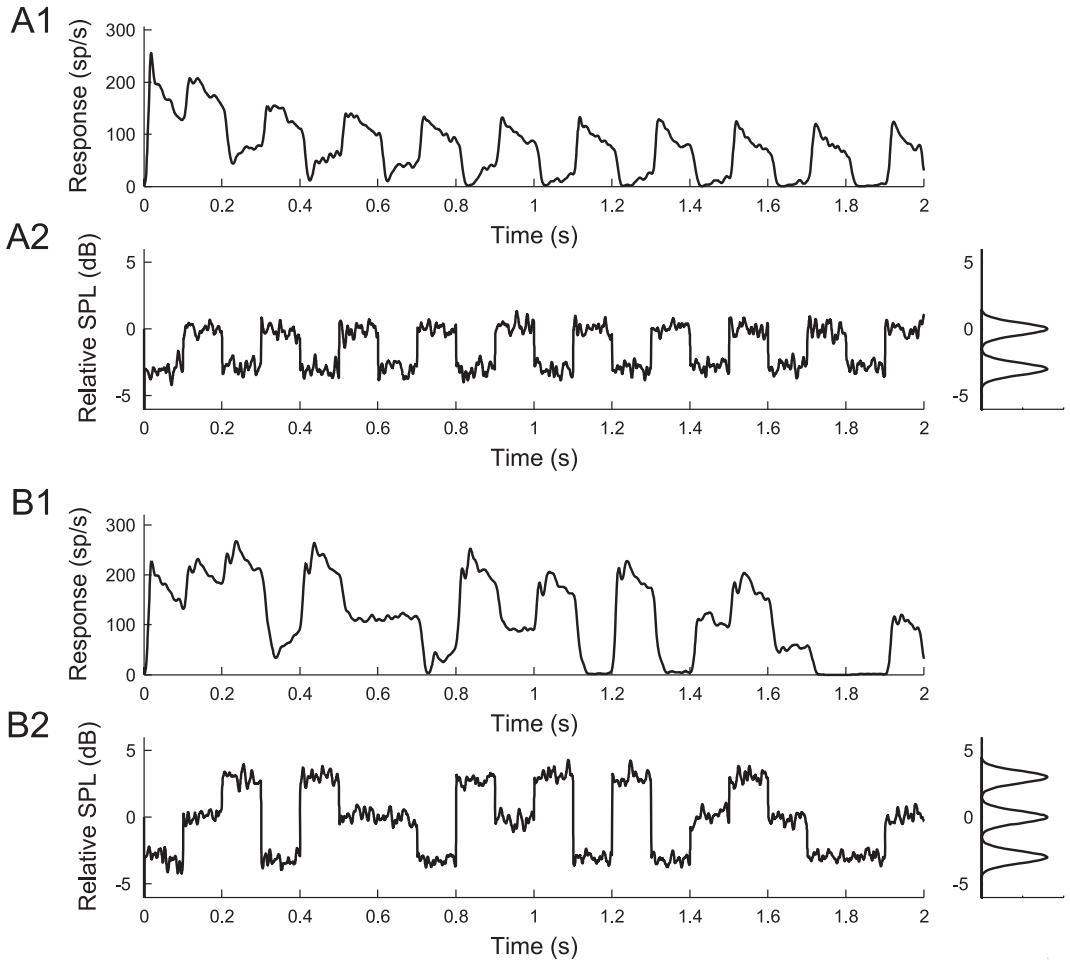

Figure 6.7: **Representative responses of an AN2 cell (*T. leo*) to the amplitude-modulated noise stimuli of Fig. 6.2C** . (A1& A2): Bimodal stimulus distribution. The envelope of an amplitude-modulated stimulus and the distribution of the stimulus amplitude are shown in (A2), the corresponding instantaneous spike rate is shown in (A1). (B1& B2): Trimodal stimulus distribution. The envelope of an amplitude-modulated stimulus and the distribution of the stimulus amplitude are shown in (B2), the corresponding spike rate is shown in (B1). The stimuli were presented 45 times and the recorded spike trains 1 ms resolution) were convolved with a Gaussian kernel ($\sigma = 5\,ms$). The instantaneous spike rates were estimated by averaging over the 45 repetitions.

Adaptation induced changes in the response curve parameters B_{50} and S_{50}

Responses from 25 AN2 cells were recorded for the two stimulus paradigms, 12 cells from *T. oceanicus* and 13 cells from *T. leo*. Since no significant differences in the adaptation and recovery time constants between the two species were found, data from both species was pooled for further analysis. Fig. 6.7 shows example traces and the amplitude distribution of the bimodal and trimodal sound stimuli together with the corresponding neural responses of a typical AN2 cell (instantaneous firing rate). Adaptation leads to a decrease of the neural responses to 0 dB peak signals (drawn from the high amplitude and intermediate amplitude peak for the bimodal and trimodal distribution) with time.

All response curves were quantified using sigmoid response functions (cf. Methods, eq. 6.1), and a Bayesian approach was used to determine the distribution of the corresponding parameters B_{50}, S_{50} and A (see Methods and Appendix B for details). A is the maximal rate at saturation. Some cells did not show response saturation in the trimodal stimulus condition within the tested range of stimulus intensities. In these cases, the uncertainty of the estimate of parameter A is high, and is reflected by a broad posterior distribution for this parameter. For most of the cells the test stimuli were strong enough to drive the cell to its maximum rate in both conditions. Although the response maximum occurs at higher stimulus intensities in the trimodal condition, no systematic change of the saturation response was observed. To fit the response curves, the response maximum A was assumed to have the same value for both stimulus conditions. Five cells were excluded from further analysis because the response curve corresponding to the expected parameter values (posterior means) did not provide a good fit to the data (the model accounted for less than 95% of the variability in the data; $R^2 < 0.95$). The further analysis is based on the remaining 20 cells.

Figure 6.8 *(following page):* **Typical examples of stimulus response curves after adaptation to the bimodal and to the trimodal stimulus distributions** (A1, B1, C1) and posterior densities of the corresponding response curve parameters (A2, B2, C2). (A1, A2; C1, C2): Results for AN2 cells of *T. leo*. (B1, B2): Results for an AN2 cell of a T. oceanicus. (A1, B1, C1) Circles and squares denote the mean spike counts in a 200 ms time window of the test stimulus after adaptation to the bimodal and trimodal distributions, measured for 9 different relative intensities of the test stimulus (cf. protocol of Fig. 6.2C). Error bars denote the standard deviation. Solid lines indicate the expected response curve, i.e. the response curve with the set of parameters with the mean value of the posterior distribution (see Methods and Appendix B for details). The shaded areas depict the intensity distribution of the stimuli (dark: bimodal stimulus distribution, light: additional peak of the trimodal stimulus distribution). (A2, B2, C2): Marginal posterior densities of the response curve parameters B_{50} (location) and S_{50} (slope). The posterior densities after adaptation to the bimodal solid lines) and trimodal dotted lines) stimulus distributions are shown in the top panels and the corresponding posterior densities of the changes ΔB_{50}, ΔS_{50}) between stimulus conditions in the bottom panels. Solid (dotted) lines on top of the figures depict the 95% posterior intervals. Significant changes between stimulus conditions are indicated by a star.

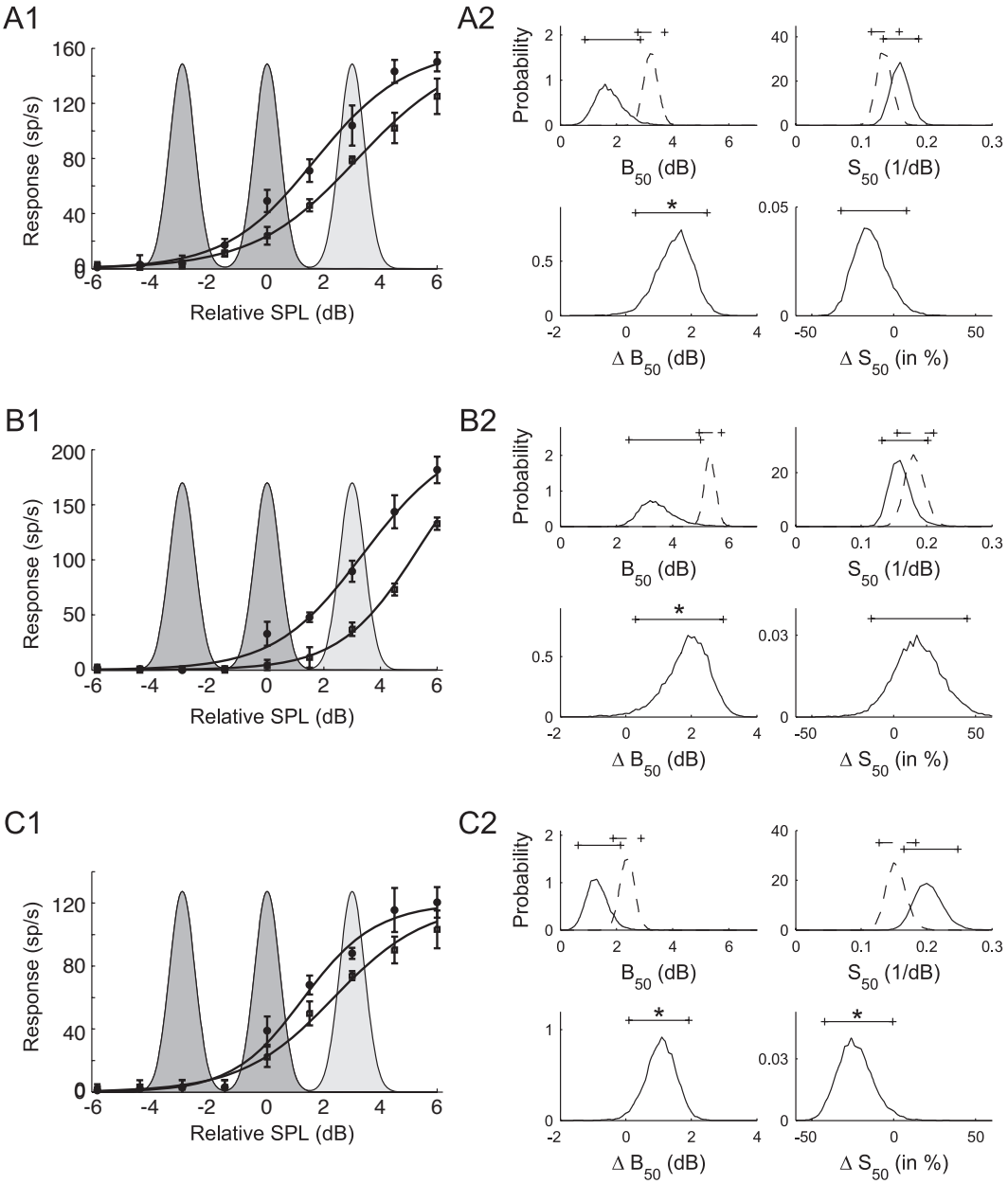
A1
A2
B1
B2
C1
C2
Response (sp/s)
Relative SPL (dB)
Probability
B50 (dB)
S50 (1/dB)
Δ B50 (dB)
Δ S50 (in %)
*

A representative example of adapted response curves of an AN2 neuron is shown in Fig. 6.8A1, where the response function is plotted for the parameters A, B_{50} and C, which correspond to the expected parameter values (posterior means). After adaptation to the bimodally distributed stimulus (filled symbols), the cell fired with 50% of its maximal rate (parameter B_{50}) at about 1.75 dB. Adaptation to the trimodally distributed stimulus (open symbols) shifted the response curve to higher stimulus intensities while the slope of the response curve changed only slightly. In fact, the results of the Bayesian parameter estimation, depicted in Fig. 6.8A2, revealed that the response curve parameter B_{50} significantly increased for the trimodal stimulus distribution. The mean of the posterior density changed from 1.74 dB to 3.23 dB (see Methods for the definition of statistical significance using Bayesian posterior intervals), while there was no significant change for the slope S_{50} (14% decrease from $0.160\,\mathrm{dB}^{-1}$). Fig. 6.8B shows data from a second cell. The mean value of the parameter B_{50} is 3.47 dB for the bimodally adapted response curve, and increased by 1.86 dB through adaptation to the trimodally distributed stimulus. The increase of B_{50} was again significant. The slope increased by 15% (from $0.161\,\mathrm{dB}^{-1}$ for adaptation to the bimodal stimulus) but Bayesian analysis revealed that the increase in slope was not significant. Fig. 6.8C shows data from a third cell. This cell showed a significant albeit less pronounced change in parameter B_{50} of $+1.06$ dB accompanied by a significant decrease in the slope S_{50} (decrease of the posterior mean by 23.5%).

Fig. 6.9 summarizes the mean values of the posterior densities of the B_{50} parameters for all 20 AN2 cells. Fig. 6.9A1 shows the values of parameter B_{50} after adaptation to the bimodal stimulus. The median value in the population is 2.34 dB (mean: 2.43 dB) and 2.02 dB (mean: 2.07 dB) for cells, in which adaptation to the trimodal stimulus led to individual statistically significant changes in parameter B_{50} compared to adaptation to the bimodal stimulus (black distribution). The optimal B_{50} value predicted by the infomax principle is -1.5 dB (star), while background suppression predicts a B_{50} value of 0 dB (circle). The combined posterior distribution of B_{50} is shown in Fig. 6.9A2 (mean: 2.43 dB). The measured B_{50} values are significantly larger than the values predicted by either hypotheses (infomax: -1.5 dB, background suppression: 0 dB). Fig. 6.9B1 shows the histogram of B_{50} values after adaptation to the trimodal stimulus (median: 3.92 dB, mean: 4.04 dB; individually significant cells: median: 3.57 dB, mean: 3.69 dB). These values are significantly larger than the infomax prediction, but similar to the background suppression prediction (Fig. 6.9B2). Fig. 6.9C1 quantifies the difference of the parameter B_{50} between the two adaptation conditions. The median of the distribution of differences is 1.53 dB (mean: 1.61 dB). The right-tailed posterior interval in Fig. 6.9C2 excludes the value 0 dB, indicating that adaptation to the trimodal stimulus significantly shifts the distribution of response curves towards higher signal intensities. Individual differences are statistically significant in 8 of 20 cells; the median of the changes in these cells is 1.46 dB (mean: 1.62 dB). The observed shifts are smaller than expected for optimal background suppression (predicted shift: 3 dB), but compatible with the infomax principle (predicted shift: 1.5 dB). Due to the high absolute values of the thresholds, however, the response curves do not allow for reliable encoding of the whole stimulus range.

Fig. 6.10 summarizes the mean estimates of the slope S_{50}, for all 20 AN2 cells. The slopes in the bimodal adaptation paradigm (shown in Fig. 6.10A1) have a median value of $0.16\,\mathrm{dB}^{-1}$ (mean: $0.17\,\mathrm{dB}^{-1}$), and are significantly smaller than the value of

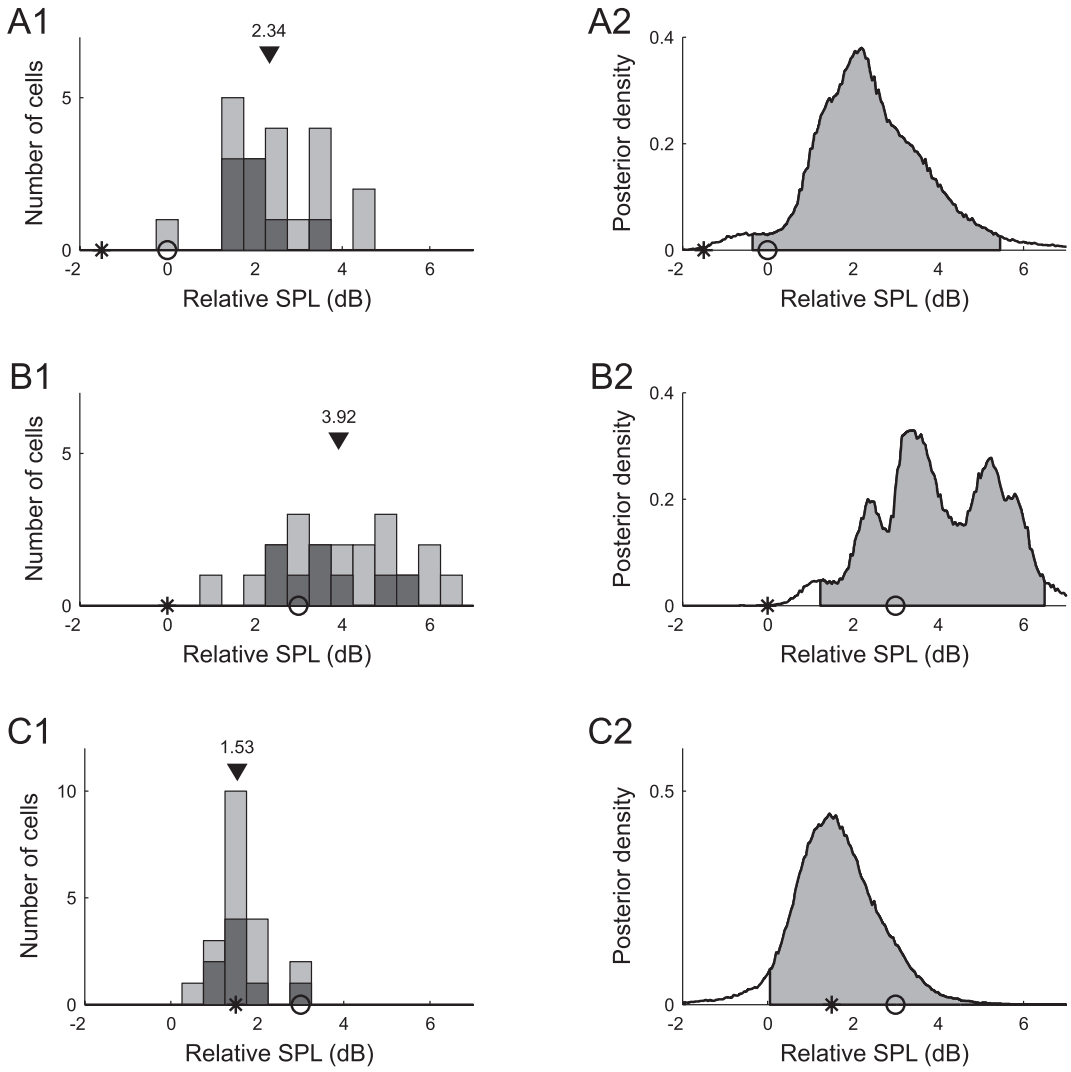

Figure 6.9: **Summary of adaptation induced changes of the response curve parameter B_{50} for all 20 AN2 cells.** Distribution of the mean values of the parameters B_{50} for individual cells (A1) and combined posterior density over all cells (A2) after adaptation to the bimodal stimulus distribution. (B1& B2): Distribution and combined posterior density of the parameter B_{50} after adaptation to the trimodal stimulus distribution. (C1& C2) Distribution and combined posterior density of the change of the parameter B_{50} between the two stimulus distributions. Symbols depict the values predicted by infomax (stars) and the background suppression hypothesis (circles). Triangles denote the median value. The distribution of cells that showed changes in B_{50} that were significant (Bayesian posterior intervals, see Methods) is marked black in (A1, B1, C1). Shaded areas depict the two-tailed 95% posterior intervals in (A2& B2) and the right-tailed 95% posterior interval in (C2).

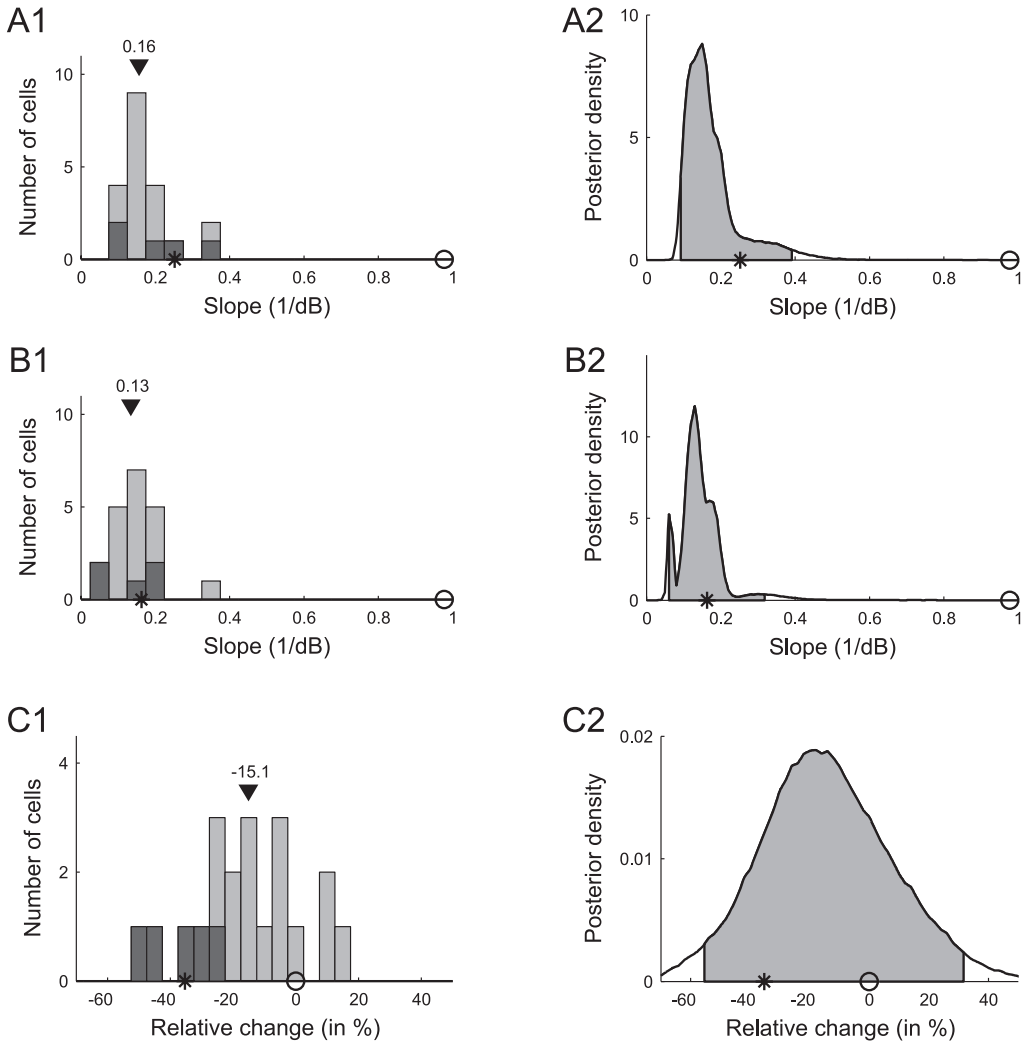

Figure 6.10: **Summary of adaptation induced changes of the slope S_{50} of the response curves.** Distribution of the mean values of the parameters S_{50} for individual cells (A1) and combined posterior density (see Methods) over all cells (A2) after adapting to the bimodal stimulus distribution. (B1& B2): Distribution and combined posterior density of the parameter S_{50} after adapting to the trimodal stimulus distribution. (C1& C2) Distribution and combined posterior density of the relative change of S_{50} between the two stimulus distributions. Symbols depict the values predicted by infomax (stars) and the background suppression hypothesis (circles). Triangles denote the median value. The distribution of cells that showed changes in S_{50} that were significant (Bayesian posterior intervals, sect. 7.3.2) is marked black in (A1, B1, C1). Shaded areas in (A2, B2, C2) depict the 95% posterior intervals.

$0.98\,\mathrm{dB}^{-1}$ predicted by the background suppression hypothesis (Fig. 6.10A2). The observed slopes S_{50} after adaptation to the trimodal stimulus are shown in Fig. 6.10B, and the relative change of the slope compared to the bimodal paradigm is quantified in Fig. 6.10C. The slope decreased for most cells (median: -15.1%, mean: -15.6%). Significant changes in S_{50} were found individually in 5 of 20 cells, and all of those cells showed decreases in slope. However, the changes are less pronounced than predicted by the infomax principle.

In summary, the main difference between the response curves adapted to the bimodal vs. the trimodal stimulus distribution is the shift towards higher stimulus intensities and a reduction in slope. This shift, however, is less pronounced than predicted by optimal background suppression, and the observed decrease in slopes is smaller than predicted by the infomax principle and larger than expected by background suppression. Together with the fact that the absolute thresholds are too high, these results seem not to favour either of the two coding hypotheses, if optimality is required.

Reliability of stimulus encoding

Adaptation in a biological system, which is constrained in multiple ways, may fall short of achieving the theoretical optimum, but may still lead to an improved representation according to the one or the other principle. In order to test for this, the mutual information between the stimulus and the neural response was calculated for the whole and for the high intensity part of the stimulus range. Therefore, 10000 samples were drawn from the joint posterior for the parameters A, B_{50}, S_{50}, for each cell and for each stimulus condition, and the corresponding response curves were calculated (see Methods, eq. 6.1). For each response curve, the joint distribution of stimulus and spike count was calculated assuming that spike counts are Poisson distributed with the underlying average spike count given by the response curve. Each of these joint distributions determines the mutual information (for details see Methods and Appendix B).

First, the whole stimulus range from $-4.5\,\mathrm{dB}$ to $4.5\,\mathrm{dB}$ is considered and calculate the mutual information between the stimulus (trimodal distribution) and the neural response, for the response curves obtained after adaptation to the bimodal and trimodal stimulus distributions. According to the infomax principle the purpose of adaptation is to reliably encode the whole stimulus range and thus, the mutual information between the trimodal stimulus and the neural response should increase for the trimodally compared to the bimodally adapted response curve (predicted increase between $0.12\,\mathrm{bit}$ and $0.25\,\mathrm{bit}$, depending on the maximum spike count; see Quantitative predictions in Appendix B).

For the example neurons in Fig. 6.8, however, a significant decrease in mutual information, could be observed, varying from a mean value of $-0.183\,\mathrm{bit}$ (Fig. 6.8A) to $-0.372\,\mathrm{bit}$ (Fig. 6.8B) and $-0.187\,\mathrm{bit}$ (Fig. 6.8C). This trend is confirmed by a full analysis of all 20 recorded AN2 cells (Fig. 6.11A), which shows that mutual information decreased for all cells. The median is $-0.21\,\mathrm{bit}$ (mean: $-0.21\,\mathrm{bit}$), and this decrease is significant (the left-tailed 95% posterior interval in Fig. 6.11A2 excludes the value $0\,\mathrm{dB}$). 15 of 20 cells showed an individually statistically significant decrease in mutual information (median $-0.24\,\mathrm{bit}$, mean -0.24 bit; black distribution in Fig. 6.11A1). These findings provide strong evidence against the infomax principle.

In order to test the background suppression hypothesis, the mutual information was calculated separately for the stimulus range from 1.5 dB to 4.5 dB (high-intensity peak, 'foreground') and from −4.5 dB to 1.5 dB (low-intensity peaks, 'background'). For the cells shown in Fig. 6.8, the mutual information decreased significantly by −0.184 bit (Fig. 6.8A), −0.335 bit (Fig. 6.8B) and −0.182 bit (Fig. 6.8C) for the stimulus range from −4.5 dB to 1.5 dB. While the mutual information for the peak of the distribution with the highest intensity increased slightly by +0.018 bit for the cell shown in Fig. 6.8A, in other cells, such as the ones shown in Fig. 6.8B,C, the mutual information decreased not only for the 'background' but also for the loudest signal (−0.038 bit vs. −0.005 bit). However, these changes in encoding of the loudest signal were not statistically significant. Fig. 6.11B summarizes the change in mutual information for the range from 4.5 dB to 1.5 dB for all 20 AN2 cells. Mutual information decreased significantly (the left-tailed 95% posterior interval in Fig. 6.11B2 excludes the value 0 dB; median −0.19 bit, mean −0.20 bit), and the decrease was individually significant for 16 of the 20 cells. The information transmitted about the 'loudest peak' (Fig. 6.11C), in the interval from 1.5 dB to 4.5 dB, remained constant (median 0.00 bit, mean −0.01 bit) and is not significantly different from zero (the 95% posterior interval in Fig. 6.11C2 includes the value 0 dB). In summary, these results are consistent with the background suppression hypothesis: the 'background' signals are suppressed compared to the loudest signal.

Figure 6.11 *(following page):* **Adaptation induced changes in the mutual information between the stimulus and the neural response.** (A1& A2): Distribution and combined posterior density of changes in the transmitted mutual information when considering the whole stimulus range (relative intensity from −4.5 dB to 4.5 dB) and the trimodal amplitude distribution. For each cell the change of the mutual information is calculated as the difference of the mutual information for the 'trimodal' (neural response adapted to the trimodal stimulus) and the 'bimodal' (neural response adapted to the bimodal stimulus) response curve. The distribution in (A1) is based on the mean values of changes in mutual information for individual cells. (B1& B2): Distribution and combined posterior density of changes in the transmitted mutual information when considering the stimulus range from −4.5 dB to 1.5 dB (including only the two low-intensity peaks of the trimodal stimulus distribution). (C1& C2): Distribution and combined posterior density of changes in the transmitted mutual information when considering the stimulus range from 1.5 dB to 4.5 dB (including only the high-intensity peak of the trimodal stimulus distribution). Triangles denote the median value. The distribution of cells that showed changes that were significant is marked black in (A1, B1, C1). Shaded areas depict the left-tailed 95% posterior intervals in (A2, B2) and the two-tailed 95% posterior interval in (C2).

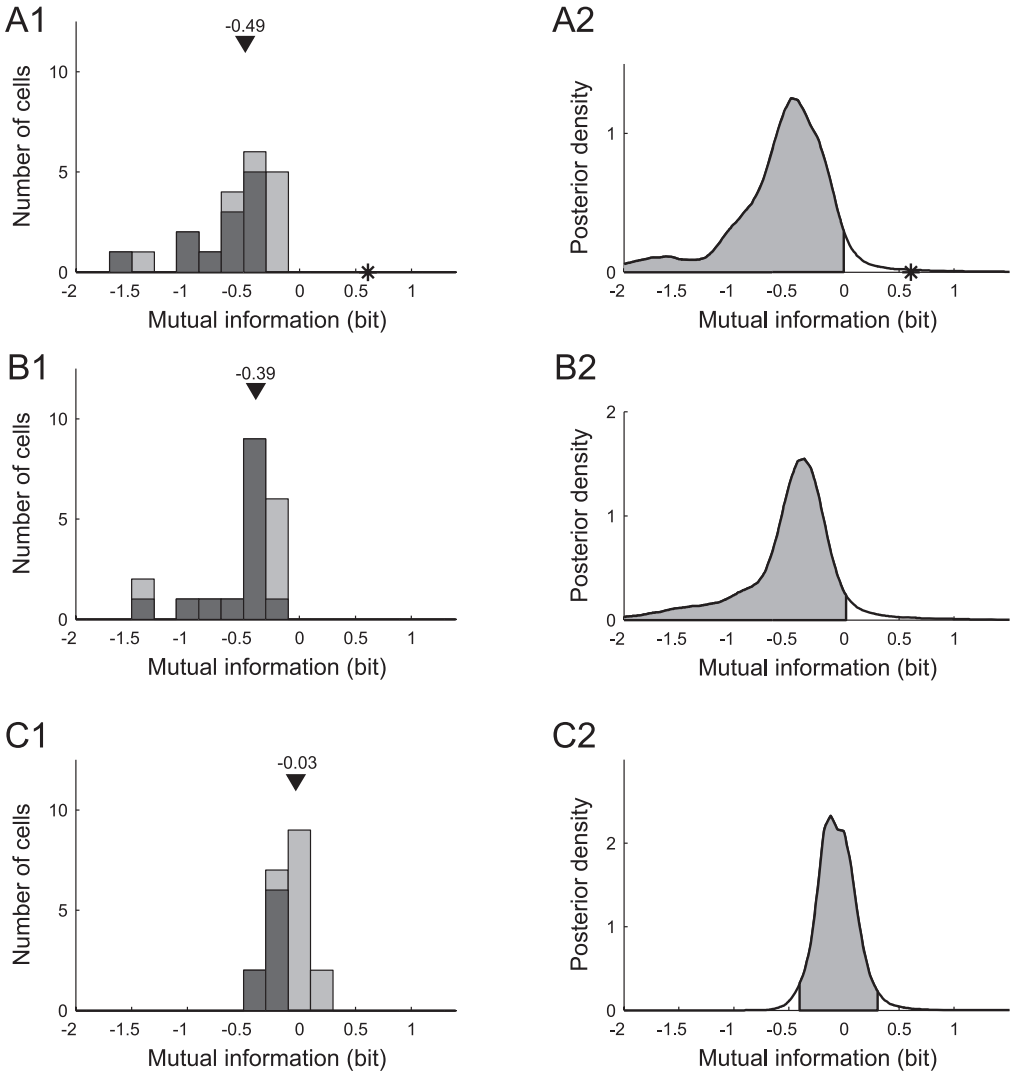
A1
-0.49
Number of cells
Mutual information (bit)
A2
Posterior density
Mutual information (bit)
B1
-0.39
Number of cells
Mutual information (bit)
B2
Posterior density
Mutual information (bit)
C1
-0.03
Number of cells
Mutual information (bit)
C2
Posterior density
Mutual information (bit)

Summary adaptation to stimulus statistics

In summary, the main difference between the response curves adapted to different stimulus distributions is a shift towards higher stimulus intensities and a small decrease in slope. This shift is less pronounced than predicted by optimal background suppression. The observed decrease in slope is smaller than predicted by the infomax principle and larger than expected by background suppression. Thus, if optimality is required, the results seem not to favour either of the two coding hypotheses. Calculations of mutual information on the other hand are consistent with background suppression but not with the infomax principle.

6.4 Discussion

6.4.1 Neurons in the auditory pathway of crickets adapt on several time scales

In the cricket auditory system, time scales of adaptation observed at first level interneurons range from short (below 100 ms, AN1: Benda and Hennig, 2007) over intermediate (ca. 300 ms; AN2: Samson and Pollack, 2002, receptors: Givois and Pollack, 2000) to long time constants (ca. 10 s; AN2: Samson and Pollack, 2002, receptors: Givois and Pollack, 2000). In the present study, firing rate adaptation with a time constant of about one second is described that was not reported before in the auditory ascending neuron AN2 of *T. oceanicus* and *T. leo* (Fig. 6.5, tab.6.1). At present the origin of adaptation in this small network is not known. There is likely a contribution to adaptation from the receptor neurons (Givois and Pollack, 2000). At the level of interneurons, both local cells (ON1, Pollack, 1988; Sobel and Tank, 1994) as well as the ascending interneuron AN2 (Samson and Pollack, 2002) exhibit long-lasting hyperpolarizations with intermediate time-constants (approx. 5 s) that may reflect adaptation processes at the level of the spike-generator in these cells. The primary task of the first stage of auditory processing in crickets is to maintain and possibly to condense relevant information for object localization and recognition for higher computational centres in the brain. In this context, it is remarkable to note that already at the first synapse several time scales of adaptation can be observed, similar to those reported from vertebrate systems (Ulanovsky, 2003) as well as other sensory modalities (Fairhall et al., 2001).

6.4.2 Infomax vs. background suppression

In the experiment described here, changes of the response curves of AN2 cells were measured, depending on different stimulus conditions (Fig. 6.8). The results revealed that the changes are compatible with background suppression (coding of the most intense signal part while suppressing the 'background') but not with infomax (optimal coding of the entire stimulus range). In general, the results presented here indicate a response threshold that is too high to allow for reliable encoding of the whole stimulus range (Fig. 6.8, 11). Most remarkably, adaptation reduced the amount of encoded information about the stimulus when considering the whole range of input signals (Fig. 6.11A). If only the mutual information between the loudest part of the signal and the neural response is taken into account, information rate stays nearly constant

(Fig. 6.11C) while at the same time, the neural output conveys less information about the first two peaks ('background') of the stimulus distribution (Fig. 6.11B). These results suggests that instead of coding the entire stimulus range, only a relevant part of the signal is reliable encoded, which likely results in a segregation of this part from the 'background'.

This is in contrast to other studies (fly visual system Fairhall et al., 2001; Laughlin, 1981; midbrain of guinea pigs Dean et al., 2005; inferior colliculus of cats Kvale and Schreiner, 2004; songbird auditory forebrain (Nagel and Doupe, 2006); rat barrel cortex Maravall et al., 2007) that reported that stimulus encoding is compatible with infomax. However, the infomax principle, which considers sensory systems as communication channels that are optimized for preserving all information from the sensory input, may fail to explain neural coding when considering stages where actual processing of information takes place (instead of mere transmission). Indeed, a recent study by Ringach and Malone (2007) has shown that neurons in the primary visual cortex of macaque maintain an operating point that does not maximize information transmission but is tuned to the detection of signals in background noise.

The findings presented here also stress the importance of 'relevant' information in the signal when talking about adjustment of coding strategies. Especially in sensory systems with very limited capacity, one can imagine that the pathway is tuned to perform a kind of preprocessing optimized for transmitting information only about behaviourally relevant signals. Other examples, in which optimal coding is not used to maximize the average information gained about the entire stimulus distribution, but only for the relevant part, include auditory receptors of locusts, which seem to maximize the information gained about specific, but less often occurring aspects of the stimuli (Machens et al., 2005) and stimulus specific adaptation in single neurons of auditory cortex that leads to an enhanced representation of low-probability sounds deviating from the distribution of the surrounding signal (Ulanovsky, 2003). Thus, maximizing the information conveyed about the entire current stimulus range is not always desirable, namely if the more important task is to filter out relevant signals, as is the case of stream segregation and novelty detection. In this context, it should be noted that the AN2 neuron in crickets may serve several functions. Under most stimulus conditions, relatively low firing rates will likely monitor slowly changing signals as observed in the present study (up to about 5 Hz). The AN2, however, can also operate in a burst mode with high intra-burst firing rates for the detection of bat calls (Marsat and Pollack, 2006), for which the analysis presented here is not appropriate. Nevertheless, low firing rates are likely to transmit relevant information since response curves built from spike counts similar to those in the present study are maintained at somewhat higher thresholds in wingless cricket morphs that are not at risk from bat predation (Pollack and Martins, 2007).

In addition to its relevance for slow signal features, the adaptation time course reported here is likely to adjust the operating point of the faster response dynamics (i.e., bursts). Therefore, the system could preserve a part of the dynamic range for even louder sounds in a way that it is able to detect brief, transient high-intensity signals (Ringach and Malone, 2007). Apart from possible physiological limitation, the non-optimal background suppression reported here could be the result of a trade-off between setting the operating regime for the bursting mode on the one hand and suppression of background noise on slower time scales on the other hand.

6.4.3 Optimality vs. improvement

While the results presented here are compatible with the background suppression hypothesis, the observed response curves do not represent an optimal solution if the task is indeed to filter out the most intense part of the stimulus. Generally, a neural system may achieve improved performance by means of different mechanisms as shown in a modelling study by (Schwabe and Obermayer, 2005). Depending on the specific physiological constraints, the resulting neural representation can be optimal or a trade-off between optimality and the flexibility of the neural circuit. Indeed, it was shown that, for example, the slope of the stimulus-response curve is not steep enough for optimal encoding of only the loudest peak of the bimodal or trimodal stimulus distribution, possibly because the neural gain can only increase to a limited value.

Here, a paradigm was proposed that allows quantifying the improvement in neural coding without requiring optimality: stimuli with two or three peaks in their amplitude distribution were used and the mutual information between parts of the stimulus range and the neural response was calculated. Infomax not only makes a very specific prediction of the optimal response curve parameters, but also predicts that encoding of the whole stimulus range should be improved through adaptation. Background suppression, on the other hand, predicts that only the encoding of the loudest signal part should improve while the 'background' is suppressed. Even if the measured response curves do not achieve optimality, one can still distinguish between background suppression and infomax by measuring the improvement of information transmission for parts of the stimulus range. This paradigm is rather general and should be applicable also to other sensory systems.

6.4.4 Stream segregations

The results of this study indicate that adaptation can help to discriminate auditory objects from background noise in an auditory system that is highly specialized for certain tasks. This raises the question whether this processing step is specific to simple auditory systems composed of only a few sensory neurons or if it could be a general design principle that also applies to the complex sensory network in vertebrates. A concept closely related to background suppression as discussed here is the separation of neural representations of discrete objects in multiple channels or 'streams' in higher auditory processing levels in vertebrates (Nelken, 2004). Neurons in the inferior colliculus of cats display the same firing pattern when a stimulus composed of a signal with or without background noise is presented, indicating a representation of the signal only (Chechik et al., 2006) and in auditory cortex, neurons show locking to the amplitude modulations of a low level sound but not to the noise it is embedded in (Las et al., 2005). The improvement in object-background-separation observed here is a very elementary form of stream segregation, separating only one relevant stream from the rest. This may be attributed to the specialization of the auditory system under study, but nonetheless yields insights into how one sensory channel is restricted to one auditory object. Notably, in crickets, this mechanism works on top of the segregation into different carrier frequency channels. Presently, it is not known whether this holds also for the second frequency channel in crickets, but background suppression has also been found for relevant communication signals in bushcrickets, separating sin-

gle males from background choruses (Römer and Krusch, 2000). In vertebrates, the use of carrier frequencies for stream segregation cannot be easily separated from effects of stimulus amplitude (Joris, 2004), complicating the analysis of underlying mechanisms. Insect model systems may thus be of great use to further explore a common design principle of vertebrate and invertebrate auditory systems: the representation of only the relevant information and the mechanism behind classification of auditory inputs.

7 Conclusion

The objective of this work was to reveal potential design principles that shape the organization of neural adaptation in sensory pathways. This was done along several examples from the auditory systems of crickets and grasshoppers. Adaptation was approached from different perspectives in order to include various aspects of adaptation. By the example of the auditory pathway of locusts it was shown that the exact pattern of distribution of adaptation mechanisms is governed by functionally motivated design principles with respect to directionality and pattern processing (Chapters 3 & 4). Thus, *where* adaptation takes place within a sensory pathway is an important aspect of neural adaptation. The second experimental study revealed divisive gain control in the AN2 of crickets mediated by a specific mechanism of adaptation – presynaptic inhibition (Chapter 5). Other mechanisms had a subtractive effect on the response curve of AN2. This study showed that *how* adaptation is realized is a second important aspect. The third part of this work examined the functional principles behind adaptation (Chapter 6). Although it was not possible to clearly distinguish what is the coding principle behind slow adaptation in AN2 of crickets, it became clear that the question *why* adaptation is beneficial for sensory processing needs to be considered thoroughly in studies on adaptation.

Even though adaptation was studied on different levels and under the different aspects described above, three themes on the functional design of adaptation and its arrangement emerge in all of the studies presented here: (1) the importance of the time scale adaptation works on, (2) competing functional demands on the effect of adaptation, and (3) the placement of adaptation mechanisms at specific sites within a sensory pathway. These three themes will now be discussed in more detail.

7.1 Time scales

In the theory of Chapter 4, a distinction of the static and dynamic examination of adaptation was made. Is this distinction valid? In order to understand the role of adaptation for sensory processing, stimuli dynamics have to be thoroughly defined. The stimuli relevant for adaptation that have been discussed throughout this work act on three different time scales: the background that changes slowly; behavioural relevant signals that occur at an intermediate time scale; and the rapidly changing fine structure of that signal.

Background The background has been discussed mainly in the context of the AN2 of crickets (Chapter 6), where the hypothesis was tested that adaptation serves to separate a behaviourally relevant signal from the background. The background usually changes slowly, on the time scale of several seconds to minutes (Nelken et al., 1999) and from the perspective of an auditory system dedicated to the recognition of specific signals, it

constitutes noise. The slow adaptation in the AN2 of crickets (time constants of 1-2 s) is fast relative to background dynamics, but it is slow relative to the occurrence of cricket songs (e.g. single chirp units in *T. leo* have a duration of 200-300 ms, intermittent with longer pauses). This means, the result of slow adaptation may be seen as temporary static change of the response curve of the AN2 of crickets if the response to conspecific songs is considered, but not from the perspective of the background dynamics. Slow adaptation possibly enables the system to reduce or eradicate the deterioration of the signal structure by background noise. It has to be noted that the stimuli used in Chapter 6 were not designed with the assumption of a separation of time scales, since the goal was to simulate several identical signals from different sources. In reality, background and relevant signal may be seperated by their time scales, providing a possible explanation for the unclear outcome.

Occurrence of the signal The second time scale that stimuli change with is that of the occurrence of the signal. The term 'occurrence' is used to separate it from the temporal fine structure that is important for recognition. The duration of signals of the insects discussed here typically falls in the range between 100 ms and 1 s (von Helversen et al., 2004; Otte and Cade, 1983). The parameters of the song that change on these time scales are mean intensity, due to the distance of the sender and directionality of the signal, while the amplitude of the signal changes an a much faster time scale. Adaptation in TN1 and BSN1 of the locust (Chapter 3) but also fast adaptation in the cricket auditory system (Benda and Hennig, 2007), is in the range between 20 ms to 50 ms, and can be seen as fast relative to the time scale of occurrence of the signal. Thus, if the signal as a whole is considered, adaptation results in a static change of the response curve. It removes the slow parameters mean intensity and directionality from the representation and thereby enables invariant representation of the temporal fine structure as was shown in the models of the grasshopper auditory pathway in Chapter 4 (for crickets, see Benda and Hennig, 2007).

During the theoretic considerations of directionality coding (Chapter 4), it was stated that adaptation in AN2 of locusts (Chapter 3) cannot be understood in terms of a static change of the response curve relative to a faster signal parameter, but rather as a dynamic mechanism to focus on the informative part of peripheral input. This statement depends critically on what is defined as the signal. From the perspective of the centrally located neuron, the relevant signal can also be defined as the difference between the responses of the peripheral neurons rather than of the real physical stimulus. The difference in the inputs from the periphery to the central neuron changes on two time scales. First, fast changes at the onset of the signal that originate in the physical stimulus and contain the correct directionality information. Second, the response difference changes slowly (and vanishes) because of peripheral adaptation. From the perspective of the central neuron, the only way to separate these two 'signal modulations' is by their time scales. Thus, intrinsic adaptation in the $\ominus$-neuron (or AN2 of locusts) may be seen as a separation of these two time scales, removing the slow changes due to peripheral adaptation in favour of the much faster onset of the signal.

Acoustic background noise, whose source is located at some angle relative to the animal, constitutes a second source of slow changes of peripheral input to the directionality coding neuron (Chapter 4: $\ominus$-neuron; Chapter 3: AN2 of locusts). In the mod-

els in Chapter 4 an environment without background noise was assumed. However, in the context of lateralized background noise, the excitation on both sides does not only reflect the locality of the signal, but also that of the background noise, which may lead to localization errors. Peripheral adaptation that is fast relative to the background may then be beneficial for directionality coding, because it will adjust the sensitivity at both sides separately and thereby remove the excitation difference that is caused by the background.

Amplitude modulations The third time scale concerns the amplitude modulation of the signals, ranging from few milliseconds in the fine structure within single pulses to the duration of the pulses (14-50 ms, von Helversen et al., 2004; Otte, 1992). The fast adaptation discussed here is slow relative to these changes and can approximately be seen as a static change of the response curve. Adaptation on the time scales observed here will, however, also shape the representation of the amplitude modulations dynamically and dynamic models are needed to evaluate the effect of adaptation (Torkkeli et al., 2001; Benda and Herz, 2003).

The distinct separation of time scales as discussed above is often not that clear, since different aspects of the sensory environment may change on similar time scales. Neural adaptation works on very different time scales as well, (Xu et al., 1996; Ulanovsky et al., 2004; Wark et al., 2009) and it has even been suggested to model them with power law dynamics (Drew and Abbott, 2006) instead of separating them in different time constants of exponential decays. However, even though the separation of time scales may seem somewhat artificial, it provides a tool to study adaptation in reaction to behaviourally relevant signals (Benda et al., 2005). The above examples reveal that adaptation can serve to separate different signals or different features of the same signal, if they change on distinct time scales. Such segregation of distinct objects into different streams is one of the main tasks of sensory pathways, especially in the auditory system, where temporal structure is an important quality of distinct objects (Las et al., 2005).

7.2 Competing demands

In the discussion of the different time scales of distinct signals, or of different aspects of the same signal, it has already emerged that sensory pathways often have to process more than one stream of information. In the following, the consequences of possibly competing demands that these streams make on adaptation are discussed.

Coding of the mean vs. coding of variance One example for such competing demands is the convergent coding of information from high and low frequency receptor populations in the AN2 of crickets discussed in the study on divisive gain control (Chapter 5). The two signal classes – conspecific for low frequency and predator signals for the high frequency – may demand different forms of adaptation, as reflected in the divisive gain control specific to the high frequency channel. As discussed above, time scales can separate sensory streams, but the different information could also be contained in distinct statistical properties of the stimulus: e.g. mean and variance. Although it was not explicitly tested in the study on divisive gain control in the AN2 of

crickets 5, gain modulation will change the representation of the variance of the signal, while shifts change coding of the mean of the signal. In a similar manner as adaptation can remove slow signal aspects in order to code for fast changes, the type of operation, by which adaptation affects the response curve could create invariance to mean intensity or invariance to signal variance, leaving the respective other unchanged. In the cricket pathway, adaptation operates differently on high and low frequency information, possibly because the two signal classes have different processing demands: (1) processing of a stereoptyped signal with little variation in the variance in the low frequency channel, and (2) coding of predator *and* conspecific signals that cover a large range of intensities in the high frequency channel.

Invariance or ambiguity? Two studies of the present work highlight that adaptation can help to separate different streams of information by removing other aspects. The slow adaptation in the AN2 of crickets may help to eliminate background noise (selective coding, Chapter 6). In the model of the pathway for temporal pattern processing (Chapter 4) adaptation removed the mean intensity and thereby enabled more reliable coding of fast amplitude modulations. These adaptation-aided separations are achieved by removing the nonrelevant information. The removal of one stimulus parameter in favour of the representation of another has been interpreted as a problem, because it generates ambiguity with respect to the removed information (Fairhall et al., 2001). However, if this removed information is irrelevant for the computational task performed, it constitutes noise. In this case, the ambiguity that results from adaptation is in fact invariance, which is just the desired effect.

Problems of ambiguity arise only if *both* features, the invariant parameter and the one it is invariant against are important for the system. This problem was encountered in directionality coding neuron ($\ominus$-neuron) in the models of Chapter 4, where adaptation peripherally removed the mean intensity at both sides, which constitutes the information that is central for coding of the stimulus direction. Adaptation to mean intensity is necessary, on the other hand, in order to impede saturation in the periphery. The models in Chapter 4 suggest divergent processing of directionality and temporal pattern in the periphery and shallow response curves to avoid this conflict, but it is not clear whether this is implemented in the real biological system.

Parallel processing The model suggestion is an example of a more general solution of the problem of different demands on adaptation for different aspects of the stimulus: parallel processing. The model in Chapter 4 suggests divergence of localization and pattern processing already in the periphery, *before* adaptation takes place. Then, in separate streams, invariance to the mean is realized in the pattern pathway, but not for localization. The same kind of anatomical separation of adaptation was observed in the auditory pathway of crickets (Chapter 5): high and low frequency signals are separated by the receptor populations already, and adaptation takes place *before* information converges, at the presynaptic terminals. A very similar principle of divergence and subsequent scaling has been proposed to underlie efficient information compression in binocular vision in vertebrates (Li, 1995).

Biological constraints However, often the separation of different signals may not be possible because of biological constraints or signal characteristics. For example, for directionality coding in the locust, shallow response curves in the periphery are beneficial, while steep curves may be needed for processing of the temporal pattern (Chapter 4). Shallow response curves may be difficult to obtain because of the physical constraint on the transduction process, and the only way to enlarge the dynamic range is by adaptation of the transducer. Also, divergent coding may be inefficient in terms of the number of cells needed and with respect to energy expenditure.

As a second example for biological constraint, the result of slow adaptation in the AN2 of crickets (selective coding, Chapter 6) could be an indication of the need for a compromise, when two conflicting demands have to be met in a single neuron. In the case of the AN2 of crickets, these competing demands are possibly the precise coding of the loudest out of several signals on the one hand and a representation of some aspects of the background on the other. Due to the lack of divergent pathways that transfer information about signal and background separately, both tasks cannot be realized in an optimal way.

7.3 Design principles for the placement of adaptation mechanisms in sensory pathways

The considerations about conflicting demands on adaptation for distinct signals or different parameters of the same signal have already led to one of the central principles for the organization of adaptation mechanisms: divergence and convergence. A second such principle that became apparent during the different chapters of this work is relative placement of nonlinearities and adaptation mechanism along sensory pathways. In the following, these two principles are discussed in more detail.

7.3.1 Divergence and convergence

Divergence in a sensory pathways means that the same information is transferred from one single part of the pathway to several different targets. If adaptation mechanisms are placed *after* such a divergence, they potentially alter the representation in these targets in very different ways. It would then be possible to match the conflicting demands of processing of different aspects separately.

But what about convergent pathways? Within this work, two examples of converging pathways have been discussed: the AN2 of crickets, where high and low frequency 'pathways' converge (divisive gain modulation, Chapter 5) and the two central neurons processing pattern and direction in the modelling section (Chapter 4). Any adaptation that is specific to one of the converging channels has to be achieved before convergence, like the divisive gain control in AN2 of crickets or the removal of mean intensity from the two sides in the inputs to the model $\oplus$-neuron. However, if the target of the converging pathways performs any type of comparison of its inputs, adaptation should not remove information about the parameter that is compared, like the intensity difference in the $\ominus$-neuron and AN2 of locusts (Chapters 3 & 4).

There is another aspect of convergence and adaptation (for a more detailed discussion see Chapter 3). Whenever a neuron is the target of many different presynaptic

cells and the overall activity of these varies slowly over a large range, the target neuron should adjust its own sensitivity in order to match its input-output relation to the current presynaptic activity. Thus, elements of sensory pathways with many inputs may have to adapt themselves (Solomon et al., 2004; Dunn et al., 2007). In this way, the target neuron could realize invariance with respect to the mean activity of its inputs. Perhaps, TN1 in the locust is an example for this design principle, as it probably sums up a large receptor population with stacked sensitivities: at high intensity levels, many of these will be active, while at low intensity levels, only few receptors with low threshold will provide input to TN1. Adaptation within TN1 could then help to adjust its own sensitivity to the number of receptors that are active. Whether adaptation is successful may critically depend on the nonlinearity of the transfer between receptors and spike output in TN1. The interaction of nonlinearities and adaptation mechanisms will be discussed in the next section.

7.3.2 The role of nonlinearities

Sensory adaptation is closely related to the nonlinearities of the pathway it occurs in. The response curves in this study are a way to measure these nonlinearities. In the studies of divisive gain change and selective coding in AN2 of crickets (Chapters 5 and 6) the change of these nonlinearities was used to quantify adaptation and to test predictions about its functional role. In the theory of Chapter 4 they were used to optimize information transfer. A classic model of sensory pathways is a serial combination of filters and static nonlinearities (Dayan and Abbott, 2001). As discussed above, if the stimulus changes quickly with respect to adaptation time constants, the effect of adaptation can be seen as static, resulting in different static nonlinearities. In this case, adaptation can be described by the changes of nonlinearities in the sensory pathway. One of the central results of this work is that adaptation usually acts on several distinct places along a sensory pathway. What is the effect of the serial combination of adaptation mechanism from the perspective of static nonlinearities?

The kind of change of a single nonlinearity that can be realized is limited by the underlying adaptation mechanism. The most common alterations caused by adaptation are additive shifts, for which the nonlinearity is shifted along the abscissa and a scaling, where the entire nonlinearity is multiplied by a factor, resulting in 'output gain-control' (cf. discussion of Chapter 5, sect. 5.4.3). By combining several nonlinearities in a serial manner, more complicated reshaping of the input-output relation of the entire pathway can be realized. An extensive consideration of this is beyond this discussion, but since it constitutes a central design principle behind the organization of adaptation mechanism, a short outlook about the combination of adaptation in two serial nonlinearities (Fig. 7.1) is given in the following.

If the first nonlinearity is shifted and not the second one (Fig. 7.2A1&A2), the result is a shift of the combined nonlinearity (Fig. 7.2A3). Examples for this scenario could be the AN2 of crickets (Chapter 5) at the low frequency carrier or the peripheral adaptation in the numerical simulations of Chapter 4. If the second nonlinearity shifts but the first one remains unchanged by adaptation, the net effect can be a combination of a

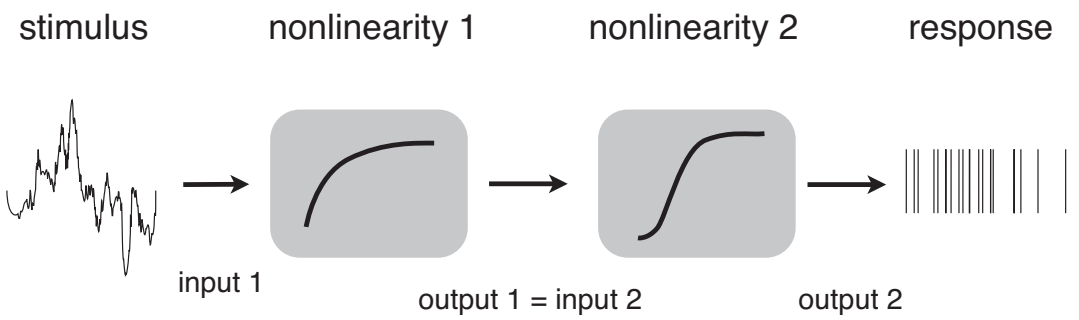

Figure 7.1: **Sensory pathway as a combination of serial nonlinearities.** The stimulus provides input to nonlinearity 1, whose output is the input of the next nonlinearity. The combined input-output function that describes the mapping of the sensory input to some measure of the final spike output (typically the spike frequency or the spike rate) is really a combination of several - adapting - nonlinearities along the pathway.

shift and a divisive scaling on the output of the combined nonlinearity (Fig. 7.2B1-B3). This is quite notable, because it suggests that the correct combination of nonlinearities that change subtraction due to adaptation can result in a divisive scaling. In the present work, no obvious example of such an interaction was observed, but the combination of subtractive effects of short term synaptic plasticity and an additional subtractive modulations of the input-output relation has recently been shown to generate divisive gain modulation (Rothman et al., 2009).

A third scenario, which has already been discussed in the context of gain modulation by presynaptic inhibition in Chapter 5, is the combination of a divisive operation and a second nonlinearity (Fig. 7.2C1-C3). Firstly, gain control is preserved when passing through the second nonlinearity. Notably, the output nonlinearity in Fig. 7.2C1 is transformed into an input nonlinearity Fig. 7.2C3, which was observed in the high frequency coding of AN2 in crickets (Chapter 5). If the first nonlinearity (Fig. 7.2C1) is characterized by very steep curves, the saturation of the second nonlinearity limits the response to high-intensity stimuli. If the first nonlinearity becomes shallower, due to adaptation, larger parts of it will be transferred by the second nonlinearity, resulting in a net input gain-control. This effect, even more than the ones shown in Fig. 7.2A&B depends on shape and relative position of the two nonlinearities. An extensive study could be of great interest, but goes beyond the scope of this work. The study of the combination of two nonlinearities affected by adaptation can be extended to longer serial chains of nonlinearities by summarizing the first two nonlinearities in the above way and then combining the resulting nonlinearity with the next one in the chain. For example the output gain-control as a result of the shift in the second nonlinearity (Fig. 7.2B3) could then be seen as the first, divisively affected nonlinearity in Fig. 7.2C1-C3 and it could be possible to generate input gain-control without a real divisively acting adaptation mechanism.

These consideration lead to an additional important design principle for adaptation mechanisms in a sensory pathway: adaptation, when it can be considered to be static

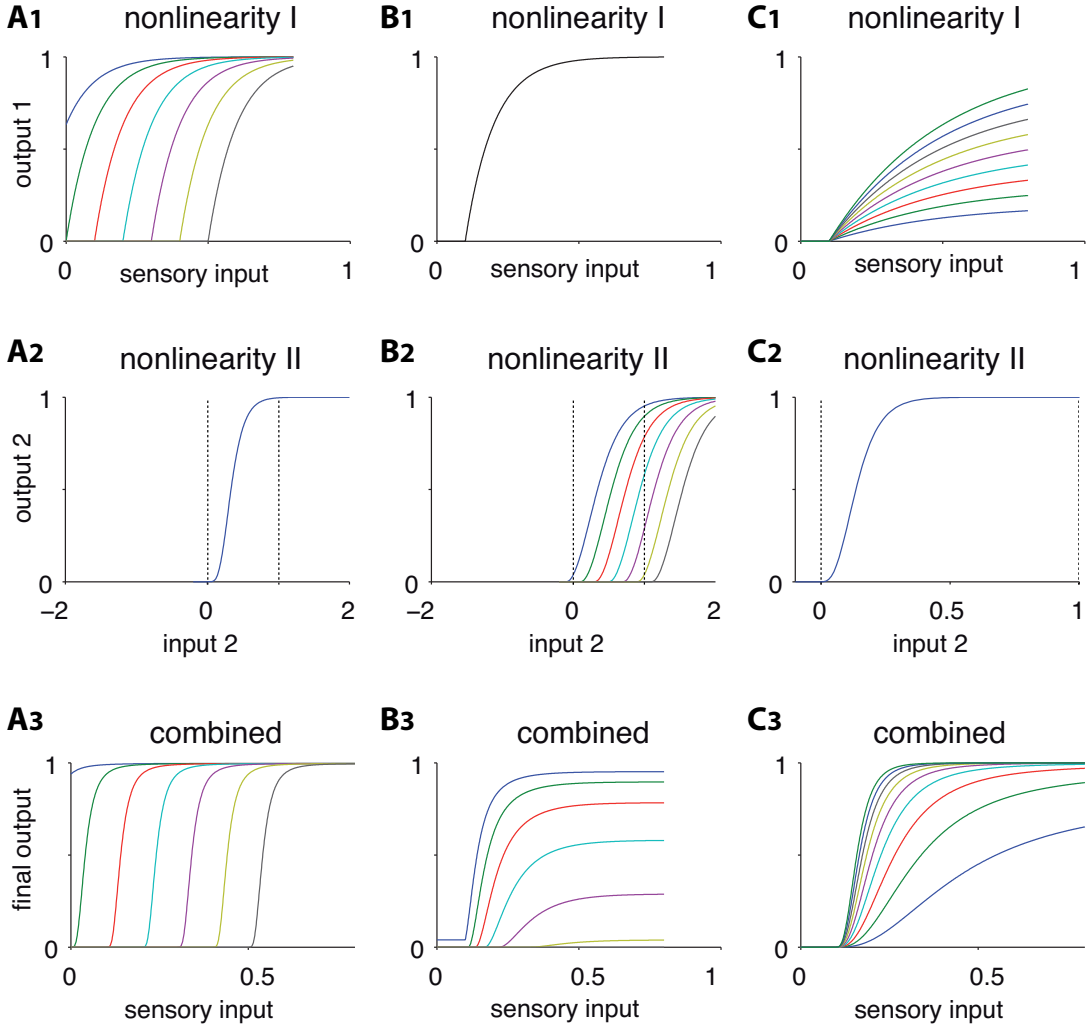

Figure 7.2: **Effect of adaptation in a pathway with two serial nonlinearities.** (A-C) show three different scenarios where and how adaptation affects the combined response curve of two serial nonlinearities. In (A1-A3), only the first nonlinearity is shifted by adaptation (A1, different colours correspond to different adaptation levels), while the second one remains unchanged (A2). The combined response curve is depicted in (A3). in (B1-B3), there is a shift in the second nonlinearity (B2) as a result of adaptation. In (C1-C3), adaptation acts divisive on the first nonlinearity (C1). In all cases, the first nonlinearity is modelled by a rectified exponential, the second is generated by a tangent hyperbolic. The dashed lines in (A2, B2 & C2) depict the input range [0-1] that results from the output of nonlinearity 1.

relative to the stimulus dynamics, acts primarily on the nonlinearities of the system and identification of these is an important aspect in the study of adaptation.

The goal of this thesis was to ask for general design principles that govern how adaptation mechanisms are organized in sensory pathways. In summary, it can be concluded that if one wants to understand the organization of adaptation in a sensory pathway, it is of central importance to understand (1) the time scale, on which adaptation acts *relative* to the relevant stimulus aspects, (2) the convergence and divergence of information, and finally (3) identify the nonlinearities, on which adaptation acts.

Above all, however, the oganization of adpaptation within a sensory pathway cannot be understood without the identification of the stimulus aspects that are relevant for the different parts of that pathway and whose processing is effected by adaptation.

Appendix A

A1 Numerical model of local neurons in Chapter 4

For the local neurons in Chapter 4, a modified version of the exponential integrate-and-fire neuron (Brette and Gerstner, 2005; Fourcaud-Trocmé et al., 2003) was used:

$$\tau_M \frac{dV}{dt} = IR_M + E_{leak} - V + \Delta_T \exp\left(\frac{V - V_T}{\Delta_T}\right). \tag{A1}$$

In eq. A1, τ_M is the membrane time constant, V the membrane potential and t the time. I denotes the input current, R_M the input resistance of the cell, Δ_T a slope factor and V_{thresh} the threshold current. At spike times ($V > 20\,\mathrm{mV}$), $V \rightarrow V_{reset}$.

Current input I is generated by passing the acoustic input s through a sigmoidal nonlinearity and adding a constant noise term σ_I:

$$I(s) = \frac{I_{max}}{1 + e^{-m(s - s_{mid})}} \pm \sigma_I. \tag{A2}$$

I_{max} is the maximal current driving the systems and therefore also limits spike frequency, m controls the slope and thus also determines the dynamic range of the response curve and s_{mid} denotes the midpoint of the nonlinearity: at $I(s_{mid}) = 0.5 I_{max}$.

Input-driven adaptation is introduced by the dependence of s_{mid} on the stimulus history:

$$s_{mid}(t) = \int_{-\infty}^{t} s_{rect}(\phi) \exp\left(\frac{(t - \phi)}{\tau_a}\right) d\phi + \frac{\log(k^{-1} - 1)}{m}, \tag{A3}$$

where τ_a is the time constant of adaptation. s_{rect} denotes the stimulus s passed through a halfway rectification with respect to the absolute threshold of the shift s_{thresh}:

$$s_{rect} = \begin{cases} s_{thresh} & \text{if } s \leq s_{thresh} \\ s & \text{else.} \end{cases} \tag{A4}$$

The parameter k appearing in the additional term of eq. A3 lies in the range $0 < k < 1$ and controls which point of the nonlinearity is shifted according to the stimulus history. This means, at $k = 0.5$, the midpoint of the nonlinearity is shifted to the weighted mean of the stimulus history, at lower values of k the adaptation resembles rather a threshold shift. For example, $k = 0.1$ means that the point where the nonlinearity reaches $0.1 I_{max}$ is shifted according to the stimulus history, rather than the midpoint. The values for the parameters used are given in tab. A1.

Table A1: Parameters used for the model of local neurons in Chapter 4.

Parameter	Meaning	Value
R_M	input resistance	20 MΩ
τ_M	membrane time constant	8 ms
E_{leak}	leak reversal potential	-60 mV
V_T	threshold voltage	-50 mV
V_{reset}	reset voltage	-70 mV
Δ_T	slope factor	2 ms
I_{max}	maximal input current	5.5 nA
σ_I	standard deviation of input current	0.35 nA
m	slope of input nonlinearity	0.15 dB^{-1}
τ_a	time constant of adaptation	40 ms
s_{thr}	absolute threshold of shift	40 dB
k	shift control constant)	0.38

A2 Numerical model of the ascending neuron (⊖) in Chapter 4

For the voltage course of ⊖-neuron-neuron in Chapter 4 the same model as for the local neurons was used and intrinsic adaptation was added to eq. A1:

$$\tau_M \frac{dV}{dt} = IR_M + E_{leak} - V + \Delta_T \exp\left(\frac{V - V_T}{\Delta_T}\right) - w \tag{A5}$$

$$\text{with the adaptation term} \qquad \tau_{adapt} \frac{dw}{dt} = w.$$

τ_{adapt} is the time constant of adaptation. At each spike time ($V > 20$ mV), a change of voltage Δ_a due to adaptation is added: $w \rightarrow w + \Delta_a$.

The synaptic input to the ⊖-neuron I is given by the sum of inhibitory and excitatory synaptic currents I_{inh} and I_{exc}, respectively. For both, each input spike at the time t_{ij} is replaced by an exponentially decaying postsynaptic potential. Subsequently, these potentials are summed over all input neurons i and spikes j. l and l denote the number of input cells (3 in all simulations presented here) and n_l the number of spikes generated by the ith cell:

$$I_{inh,exc}(t) = \frac{c_{inh,exc}}{l\tau_{inh,exc}} \sum_{i=1}^{l} \sum_{j=1}^{n_l} g_{inh,exc}(t - t_{ij}) \tag{A6}$$

$$\text{with} \qquad g_{inh,exc}(x) = \begin{cases} 0 & \text{if } x < 0 \\ exp\left(-\frac{x}{\tau_{inh,exc}}\right) & \text{else,} \end{cases}$$

where $c_{inh,exc}$ is a constant that scales the amplitude of single postsynaptic potentials.

Table A2: Parameters used for the model of ⊖-neuron in Chapter 4.

Parameter	Fast integration	Slow integration
τ_{inh} (IPSP decay)	1.5 ms	12.0 ms
τ_{exc} (EPSP decay)	4.8 ms	38.4 ms
c_{inh} (IPSP amplitude constant)	33.0 mV·ms	33.0 mV·ms
c_{exc} (EPSP amplitude constant)	24.9 mV·ms	24.9 mV·ms
a (adaptation magnitude)	2 mV	2 mV
τ_{adapt} (adaptation time constant	190 ms	190 ms

All relevant parameters that are not related to the input nonlinearity of the local neurons in tab. A1 also apply to the ⊖-neuron. Synaptic and adaptation parameters in eqs. A5 and A6 were fit to resemble the spike frequency time course of the AN2 in response to the 500 ms acoustic pulses described in Chapter 3. The parameters are listed in tab. A2. An example of how the model behaves without intrinsic adaptation can be seen in Fig. A1: in A, the ⊖-neuron is not adapting itself. Without intrinsic adaptation, the model fails to reproduces the burst-like behaviour of AN2. Instead, spike frequency decays exponentially.

In order to get a more realistic model and to examine the effect of intrinsic adaptation in the ⊖-neuron, intrinsic adaptation was fit to match the adaptation behaviour of the AN2 under current stimulation. If acoustic stimulation is applied to the resulting model, its response closely matches that of AN2 (Fig. A1).

A3 Design of artificial grasshopper songs in Chapter 4

For the time-resolved response to stimuli with amplitude modulations, an artificial grasshopper song was used, which was constructed as follows. The songs were composed of six syllables, separated by 17 ms pauses. Each syllable is constituted by six pulses, separated by 3 ms pauses. Pulses had 4 ms linear ramps at their on- and offset and lasted 10 ms overall, including the ramps.

A4 Analysis of the results of numerical modelling in Chapter 4

Calculation of mutual information

For the quantification of coding reliability, the mutual information between the spike count r and the intensity difference Δx was calculated in 50 ms time windows of the artificial grasshoppers song. The centre of the time window was moved over the 500 ms duration of the songs in 10 ms steps in order to quantify the time course of information transmission. The songs were presented to the model for 10 different mean intensity levels (54-72 dB in 2 dB steps), at 10 different interaural intensity levels each

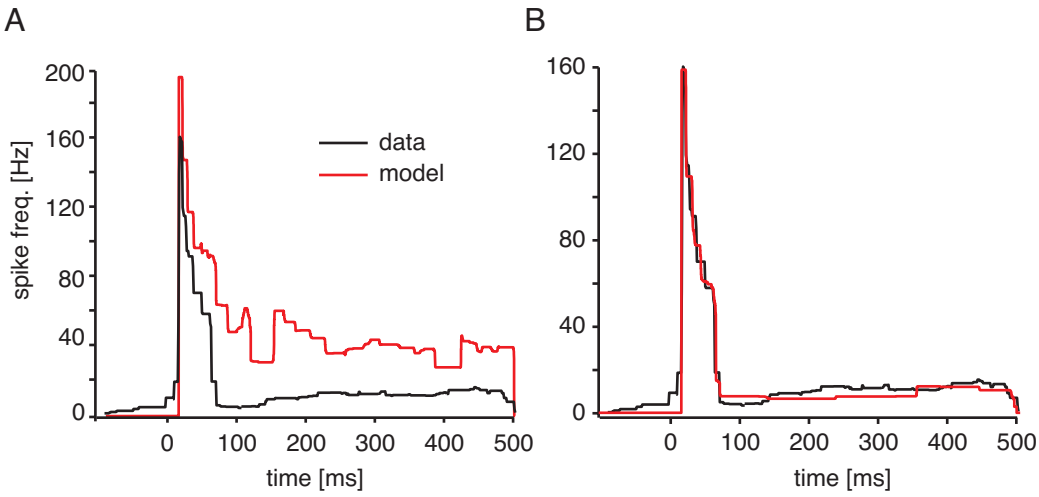

Figure A1: **Examples of $\ominus$-neuron model performance with and without intrinsic adaptation.** Spike frequency in response to a constant 500 ms acoustic stimulus starting at $t = 0$. The black lines show data from one of the AN2s presented in Chapter 3, the red lines the response of the modelled AN2 with input from each three excitatory and inhibitory local cells. In (A), no adaptation in the $\ominus$-neuron is implemented ($a = 0$). In (B), the model is run with the complete set of parameters of tab. A2, including strong, intrinsic adaptation ($a = 2$).

(0-9 dB). Each combination of mean level and intensity difference was repeated 1000 times, yielding 10000 repetitions for each intensity difference Δs. The mutual information in every time window was calculated by

$$I_{r\Delta x} = \sum_r \sum_{\Delta x} p_{r\Delta x}(r, \Delta s) \log_2 \left(\frac{p_{r\Delta x}(r, \Delta x)}{p_r(r) p_{\Delta x}(\Delta x)} \right), \tag{A7}$$

where $p_{r\Delta x}(r, \Delta x)$ is the joint probability of Δx and r; $p_{\Delta x}(\Delta x)$ and $p_r(r)$ are the marginal probabilities of Δx and r.

Classification of model responses

In order to test the invariance of directionality coding to mean levels, the responses of one ipsi- and one contralateral central neuron were compared over different time windows. In order to do this, the responses of the two neurons $r_{contra}(t)$ and $r_{ipsi}(t)$ were subtracted from each other and then the average of the respective time window was taken for each mean level and intensity difference: $\langle r_{ipsi} - r_{contra} \rangle_t$. In order to give a larger weighting to strong responses, responses were potentiated before subtraction and averaging: $\left\langle r^k_{ipsi} - r^k_{contra} \right\rangle_t$. Different values of k were tried out. For both model versions, with and without intrinsic adaptation, values of k between 2.5 and 3.5 yielded the best results of correct classification of intensity difference, but the adapting model was always better then the non-adapting version. Here, results for $k = 3$ are shown. Each combination of mean level and interaural intensity difference was repeated 100 times.

To quantify the classification success of the two model versions, confusion matrices were calculated. This was done by taking the average response for every interaural intensity difference, regardless of mean value. Since 33 mean levels (48-80 dB) were used, and each stimulation was repeated 100 times, 3300 trials were averaged for each intensity difference. Subsequently, the responses of all trials (3300 times 10 intensity difference $=$ 33000) were classified to the intensity difference, for which the absolute difference to the mean response was smallest. The mean classification result was calculated by evaluating the percentage of trials that were correctly classified for each intensity difference and then averaged over all intensity differences.

Appendix B

The study reported in Chapter 6 was carried out as a joint project with Klaus Wimmer, who did large parts of the analysis of the data. The derivation of the Baysian parameter estimation and the calculation of the quantitative predictions for the two coding hypotheses is given here as a reference for completeness. All of what is presented here was done by Klaus Wimmer.

B1 Bayesian data analysis: modelling input-response curves

Similar techniques as described here have been applied successfully to the analysis of intracellular membrane potential recordings (Gillespie et al., 2001). The analysis is based on the assumption that spikes are Poisson-distributed and that individual trials are independent of each other (i.e., their joint probability is equal to the product of their individual probabilities).

Let x_i denote the ith out of m stimulus intensities and n_i the number of times a stimulus with this intensity is presented. The corresponding number of spikes from an AN2 neuron is denoted by $y_{i,j}$, where j is the jth out of the n_i repetitions. If spikes are Poisson distributed, we obtain

$$P(y_{i,j}|r_i) = \frac{r_i^{y_{i,j}} e^{-r_i}}{y_{i,j}!}, \tag{B1}$$

where r_i is the rate average spike count underlying the neuron's response at the ith stimulus intensity. For a set $y_i = (y_{i,1}, \ldots, y_{i,ni})$ of spike counts of n_i independent and identically distributed observations, the likelihood $P(y_i|r_i)$ of r_i being the underlying rate average spike count becomes

$$P(y_{i,j}|r_i) = \prod_{j=1}^{n_i} \frac{1}{y_{i,j}!} r_i^{y_{i,j}} e^{-r_i} \tag{B2}$$

$$\propto r_i^{t(y_i)} e^{n_i r_i}, \tag{B3}$$

where the likelihood function is determined, up to a constant factor, by the sufficient statistic

$$t(y_i) = \sum_{j=1}^{n_i} y_{i,j}. \tag{B4}$$

We assume a sigmoid response curve, relating stimulus intensity to spike counts as

$$r_i = f(x_i) = \frac{A}{1 + exp\left(-\frac{x_i - B_{50}}{C}\right)}, \tag{B5}$$

where r_i is the underlying firing rate of the neuron, x_i is the stimulus intensity, A is maximum response of the cell, B_{50} is the stimulus intensity at 50% of maximum response, and C is a slope factor. Inserting this relationship into eq. B3 , we obtain the likelihood $P(y_i|r_i)$ in terms of the response curve parameters A, B_{50} and C:

$$P(y_i|A, B_{50}, C, x_i) \propto \left[\frac{A}{1 + exp\left(-\frac{x_i - B_{50}}{C}\right)}\right]^{t(y_i)} exp\left(-n_i\left[\frac{A}{1 + exp\left(-\frac{x_i - B_{50}}{C}\right)}\right]\right) \tag{B6}$$

Let $y = (y_1, \ldots, y_m)$ be the set of responses to stimuli with different intensities x_i, where $i = 1 \ldots m$. Applying Bayes' rule we obtain the joint posterior distribution

$$P(A, B_{50}, C|, y, x) \propto P(A, B_{50}, C)P(y|A, B_{50}, C, x) \tag{B7}$$

$$\propto P(A, B_{50}, C)\prod_{i=1}^{k} P(y_i|A, B_{50}, C, x_i) \tag{B8}$$

of the parameters A, B_{50} and C, given the observations, where $P(A, B_{50}, C)$ is the prior distribution of the response curve parameters A, B_{50}, C. In the following, we will use a non-informative, uniform prior distribution $P(A, B_{50}, C) = constant$.

B2 Quantitative predictions of the coding hypotheses in Chapter 6

Infomax principle

If infomax (Adorján et al., 1999; Atick, 1992; Linsker, 1988) is the underlying principle, adaptation pursues the objective to maximize the information that the neuron's output conveys about its sensory input. Formally, the goal is maximizing the mutual information $I[R; X]$ between the sensory sound signal X and the neuronal output firing rate R as a function of the response curve parameters. This is achieved by maximizing the output entropy $H[R]$ while minimizing the uncertainty $H[R|X]$ of the output once the input is fixed

$$I[R; X] = H[R] - H[R|X]. \tag{B9}$$

First, the optimal response curve parameters for a given signal distribution is computed and than, a sigmoid response function is calculated analytically, assuming additive noise. Next, the mutual information is estimated numerically in order to account for multiplicative (Poisson) noise. If only additive noise is assumed, with a probability distribution $P(n)$, the mutual information can be written as (Bell and Sejnowski, 1995; Nadal and Parga, 1994)

$$I[R; X] = H[R] - H[N]. \tag{B10}$$

Maximization of the mutual information is then equivalent to the maximization of the entropy of the output distribution, because the noise entropy $H[N]$ does not depend on the input-output-mapping, i.e. the neural response curve $r(x)$. Thus, one has to maximize

$$H[R] = -\sum_r P(r) \log_2 P(r), \tag{B11}$$

where the sum goes over all possible discrete response levels r (here, the spike counts in a 200 ms window; *cf. Bayesian data analysis). Formally, the response can be treated as a continuous variable (Atick, 1992), i.e. as firing rate, and using the relationship between differential and discrete entropy can be approximated the sum by an integral (Cover and Thomas, 1991):

$$\begin{aligned} H[R] = & -\sum_r P(r) \log_2 P(r) \rightarrow \\ & -\int P(r) \log_2 P(r) - log_2 \delta r, \quad \text{as } \Delta r \rightarrow 0 \end{aligned} \tag{B12}$$

Here, Δr is the limit on the resolution, with which the firing rate can be measured (the length of the bins of the discrete response levels). Note that in the limit $\Delta r \rightarrow 0$ the entropy $H[R]$ diverges (i.e., the information capacity of a continuous variable is unlimited). In the case $\Delta r \rightarrow 0$ and in the absence of noise the sensory signal X could be recovered perfectly from the firing rate R and thus any set of response curve parameters would be 'optimal'. However, if a finite maximum of the response curve is assumed the additive noise provides a resolution scale on the output and one can ask for an optimal response curve $f(x)$. In the low-noise limit one obtains (Nadal and Parga, 1994):

$$H[R] = -\int P(x) \log_2 \frac{P(x)}{\left| \frac{trmdf(x)}{\mathrm{d}x} \right|} \mathrm{d}x - \log_2 \Delta r \tag{B13}$$

$$= \int P(x) \log_2 \left| \frac{\mathrm{d}f(x)}{\mathrm{d}x} \right| \mathrm{d}x - \int P(x) \log_2 P(x) \mathrm{d}x - \log_2 \Delta r \tag{B13}$$

Since the second term of eq. B13 only depends on the signal distribution and the third term only depends on the resolution Δr, they are constant, and one has to maximize:

$$\int_{-\infty}^{\infty} P(x) \log_2 \left| \frac{\mathrm{d}f(x)}{\mathrm{d}x} \right| \mathrm{d}x \rightarrow \max. \tag{B14}$$

To compare how well a given sensory signal X with distribution $P(x)$ is encoded by response functions with different parameterizations (r_I and r_{II}), the difference in mutual information ΔI is computed. Under the assumption of small additive noise and for a fixed resolution Δr, this difference in mutual information is given by

$$\Delta I = \int_{-\infty}^{\infty} P(x) \log_2 \left| \frac{\mathrm{d}r_{II}(x)}{\mathrm{d}x} \right| \mathrm{d}x - \int_{-\infty}^{\infty} P(x) \log_2 \left| \frac{\mathrm{d}r_I(x)}{\mathrm{d}x} \right| \mathrm{d}x \tag{B15}$$

Assuming the sigmoid transfer function of eq. B5 and the bimodal or trimodal stimulus

distribution (*see Methods, Stimulus protocols), the optimal values for the response curve parameters A, B_{50} and C are obtained using eq. B14. Finally, the optimal value for the slope S_{50} is then computed using eq. 6.2.

Deutschsprachige Zusammenfassung

D1 Einleitung

Neuronale Adaptation dient dazu, eine Sinnesbahn kurzfristig an die aktuelle Umgebung des Tieres anzupassen. Ihr zeitlicher Verlauf lässt sich direkt beobachten, wenn man die Antwort einzelner Nervenzellen auf einen kontinuierlichen Reiz betrachte. Außerdem unterliegen der Adaptation eine Vielzahl verschiedener Mechanismen, die über die gesamte Sinnesbahn verteilt sein können. In der vorliegenden Arbeit wurde der Versuch unternommen, diese unterschiedlichen Betrachtungsebenen zusammenzuführen. Dazu wurden mehrere experimentelle und theoretische Studien durchgeführt, welche die Adaptation entlang dreier Fragestellung beleuchten sollen: (1) *Wo* findet Adaptation statt? (2) *Wie* wirkt Adaptation? (3) *Wozu* findet Adaptation statt?

Als Modellsystem für die hier betrachteten Fragestellungen diente die Hörbahn von Heuschrecken und Grillen. Bei beiden Tiergruppen ist einerseits die Verhaltensrelevanz der auditorischen Verarbeitung bekannt und andererseits sind die einzelnen Zellen der Hörbahn gut untersucht und elektrophysiologische Methoden etabliert.

Das Ziel der vorliegenden Arbeit war, mit Hilfe der einzelnen Studien herauszufinden, ob es allgemeine Konstruktionsprinzipien gibt, die das Auftreten von Adaptation in sensorischen Bahnen bestimmen, und wenn möglich, diese Konstruktionsprinzipien zu beschreiben.

D2 Der Ursprung von Adaptation in der Hörbahn der Heuschrecke

In Kapitel 3 werden die Ergebnisse einer experimentellen Studie vorgestellt, in der es darum ging, den Ursprung von Spikefrequenz-Adaptation in der Hörbahn der Heuschrecke zu untersuchen. Die Adaptation, die man bei der Untersuchung einer Zelle in der Hörbahn beobachtet, kann ihren Ursprung sowohl in Mechanismen innerhalb der Zelle selbst als auch präsynaptisch zu der beobachteten Zelle liegen.

Um den relativen Anteil intrinsischer und präsynaptischer Mechanismen an der Adaptation zu untersuchen, wurde während elektrophysiologischen Untersuchung verschiedener Zelltypen sowohl durch Strominjektion gereizt als auch durch akustisch Stimulation. Durch den Vergleich der jeweiligen Antworten auf die verschiedenen Reize konnten drei verschiedene Muster der Verteilung von Adaptationsmechansimen gefunden werden: (1) ein ausgeglichener Einfluss intrinsischer und präsynaptischer Adaptationsmechanismen in einem Interneuron, das über eine Population von Rezeptoren summiert (TN1), (2) das Vorherrschen von inhibitorischen Eingängen als Quelle von Spikefrequenz-Adaptation in einer Nervenzelle, die an der Weiterleitung von Information sowohl über Richtung als auch zeitliche Struktur von akustischen Signalen beteiligt ist (BSN1), (3) das Überwiegen von intrinsischen Adaptationsströmen, die

durch die Aktionspotentiale der Zelle selbst aktiviert werden, in einem Interneuron, das ausschließlich für die Signalrichtung kodiert (AN2).

Die wichtigste Schlussfolgerung aus den Ergebnissen dieses Kapitels ist, dass die Adaptationsmechanismen, die in verschiedenen Teilen der Hörbahn rekrutiert werden, sehr stark von Identität und Funktion der jeweils untersuchten Nervenzelle abhängen.

D3 Funktionelle Erwägungen zur Verteilung von Adaptation

In Kapitel 4 werden Modellierungen dargestellt, deren Fragestellungen von den Ergebnissen aus Kapitel 3 motiviert sind. Dabei geht es um die Frage, wo Adaptation in der Hörbahn wirken sollte, bezogen auf zwei verschieden Aufgaben: die Lokalisation eines Signals und die neuronal Abbildung dessen zeitlicher Struktur.

In der Hörbahn von Heuschrecken werden Informationen über die Richtung und die zeitlich Struktur eines Signals parallel verarbeitet. Dazu wird jeweils die neuronale Antwort der Rezeptoren auf den Reiz von den beiden Ohren zentral kombiniert: für die Richtungsbestimmung werden die Signale durch kontralaterale Inhibition voneinander abgezogen, für die Repräsentation des zeitlichen Musters werden die neuronalen Antworten zentral summiert. Das wirft die Frage auf, ob Adaptationsmechanismen in diesen beiden Informationskanälen eher in der Peripherie oder zentral angesiedelt sein sollten.

Dieser Fragestellung wird in Kapitel 4 auf zwei Weisen nachgegangen: (1) zuerst wurde eine analytische Modellierung durchgeführt, die ergab, dass für die Musterrepräsentation Adaptation in der Peripherie vorteilhaft ist, während diese für die Richtungskodierung sogar Nachteile bringt, weil sie die Richtungsinformation beseitigt. In einem zweiten Schritt (2) konnte dann mit Hilfe von Computersimulationen der Richtungsverarbeitung gezeigt werden, dass intrinsische Adaptation im zentralen, richtungsverarbeitenden Neuron eine Fokussierung der neuronalen Abbildung auf den Anfang des Stimulus ermöglicht. Damit wirkt die zentrale Adaptation dem Informationsverlust, der durch Adaptation in der Peripherie entsteht, entgegen. Auf diese Art und Weise konnten künstliche Heuschreckengesänge in der Simulation deutlich häufiger korrekt lokalisiert werden also ohne zentrale Adaptation.

D4 Präsynaptische Hemmung in der Hörbahn der Grille

In Kapitel 5 werden die Ergebnisse von elektrophysiolgischen Untersuchungen an einem Interneuron der Grille vorgestellt (AN2). Das AN2 der Grille ist sowohl im Frequenzbereich der arteigenen Gesänge als auch durch hochfrequenten Schall erregbar, wie er von Fledermäusen bei der Jagd abgegeben wird.

Durch intra- und extrazelluläre Ableitungen wurde untersucht ob (1) sich Adaptation unterschiedlich auf das Kodierungsschema in den beiden Frequenzkanälen auswirkt, und (2) welche Adaptationsmechanismen zu dieser Änderung jeweils beitragen. Die Veränderung des Kodierungsschemas wurde anhand von Kennlinien beschrieben.

Dabei konnte festgestellt werden, dass Adaptation im niedrigfrequenten Bereich einen subtraktiven Effekt auf die Kennlinien hat, also die Schwelle der Kennlinien verschiebt. Im hochfrequenten Bereich dagegen hatte Adaptation eine divisiven Effekt: bei den Kennlinien veränderte sich durch vorherige Adaptation auch die Steigung und

der dynamische Bereich. Eine solche divisive Kennlinienänderung kann die mathematische Operation der Division für das Nervensystem bereitstellen. Obwohl Division sehr wichtig für die neuronale Informationsverarbeitung ist, wurden bisher sehr wenig Mechanismen gefunden , die für einen divisiven Effekt (auch 'gain control' genannt) verantwortlich sein können. Deshalb wurde durch verschieden Kreuzadaptationsversuche und durch pharmakologische Eingriffe nach dem verantwortlichen Mechanismus gesucht. Es konnte gezeigt werden, dass präsynaptisch Hemmung für die divisive Operation verantwortlich ist. Durch Strominjektionen ausgelöste intrinsische Adaptation im AN2 selbst hatte dagegen einen rein subtraktiven Effekt.

D5 Selektive Informationskodierung in der Hörbahn der Grille

Das Kapitel 6 beschäftig sich nochmals mit dem AN2 der Grille. Auch hier werden die Ergebnisse elektrophysiologischer Untersuchungen beschrieben. Der Fokus bei diesen Experimenten lag dabei allerdings auf Adaptation auf einer längeren Zeitskala, die mit Zeitkonstanten im Bereich von 1-2 Sekunden beschrieben werden kann.

Die Experimente in Kapitel 6 stellen einerseits diese langsam verlaufende Adaptation dar und hatten andererseits das Ziel, die Frage zu beantworten, wozu diese 'langsame' Adaptation dient. Dabei wurden zwei alternative Hypothesen getestet: (1) die Adaptation verändert die Kennlinie so, dass möglichst die gesamte akustische Umgebung des Tieres abgebildet werden kann (*Infomax-Theorie*), (2) die Kennlinien werden durch Adaptation so verändert, dass nur das lauteste Signal von mehreren gleichzeitig vorhandenen dargestellt wird, wobei der 'Hintergrund' unterdrückt wird (*selektive Kodierung*).

Um diese beiden Hypothesen zu testen, wurde eine Umgebung mit mehreren gleichzeitig vorhandenen, akustischen Signalen simuliert. Die Hörbahn wurde jeweils für längere Zeit entsprechenden Stimuli ausgesetzt, um im Anschluss die durch Adaptation veränderten Kennlinien zu messen. Die beiden Hypothesen liefern dabei unterschiedliche Voraussagen. Weder die Vorhersagen für die Infomax-Theorie, noch diejenigen, die sich aus der selektiven Kodierung ergab, trafen genau zu. Eine anschließende Analyse der Transinformation ('mutual information') zeigte aber, dass Adaptation dazu führte, selektiv die Information über den Hintergrund zu unterdrücken, während die Information für das jeweils lauteste 'Signal' konstant blieb. Diese Analyse lieferte also Hinweise dafür, dass langsame Adaptation im AN2 der Grille selektive Kodierung des lautesten Signals ermöglicht.

D6 Schlussbetrachtung

In Kapitel 7 werden die Ergebnisse der einzelnen Studien zusammengefasst und unter dem Gesichtspunkt allgemeiner Konstruktionsprinzipien für Adaptation in sensorischen Bahnen betrachtet. Drei größere Themenkomplexe werden dabei in funktioneller Hinsicht diskutiert: (1) das Verhältnis des zeitlichen Verlaufes der Adaptation zu der Zeitskala, auf der sich relevante Aspekte des sensorischen Eingangs verändern, (2) wie sich widersprüchliche Ansprüche bei der Prozessierung von Signalen auf die Konstruktion der Adaptation auswirken, und (3) wo Adaptationsmechanismen innerhalb der sensorischen Bahn platziert sein sollten, unter besonderer Berücksichtigung von Divergenz, Konvergenz und von Nichtlinearitäten in der Sinnesbahn.

Zusammenfassend lässt sich sagen, dass sowohl die Adaptationsmechanismen, als auch deren genaue Platzierung innerhalb der sensorischen Bahn wesentlich für Sinnesleistungen sind. Ein umfassendes Verständnis neuronaler Adaptation ist nur unter Berücksichtigung dieser Konstruktionsprinzipien, sowie der für das Tier jeweils relevanten Signale möglich.

Bibliography

L. Abbott, J. Varela, K. Sen, and S. Nelson. Synaptic depression and cortical gain control. *Science*, 275(5297):221–224, 1997.

P. Adorján, C. Piepenbrock, and K. Obermayer. Contrast adaptation and infomax in visual cortical neurons. *Rev Neurosci*, 10(3-4):181–200, 1999.

J. T. Albert, B. Nadrowski, and M. C. Göpfert. Mechanical signatures of transducer gating in the drosophila ear. *Curr Biol*, 17(11):1000–6, 2007.

J. J. Atick. Could information theory provide an ecological theory of sensory processing? *Network-Comp Neural*, 3(2):231–251, 1992.

M. Avissar, A. Furman, J. Saunders, and T. Parsons. Adaptation reduces spike-count reliability, but not spike-timing precision, of auditory nerve responses. *J Neurosci*, 27 (24):6461–6472, 2007.

A. Ayaz and F. S. Chance. Gain modulation of neuronal responses by subtractive and divisive mechanisms of inhibition. *J Neurophysiol*, 101(2):958–68, 2009.

S. M. Baca, A. Marin-Burgin, D. A. Wagenaar, and W. B. Kristan. Widespread inhibition proportional to excitation controls the gain of a leech behavioral circuit. *Neuron*, 57 (2):276–89, 2008.

S. A. Baccus. From a whisper to a roar: adaptation to the mean and variance of naturalistic sounds. *Neuron*, 51(6):682–4, 2006.

S. A. Baccus and M. Meister. Fast and slow contrast adaptation in retinal circuitry. *Neuron*, 36(5):909–19, 2002.

S. A. Baccus and M. Meister. Retina versus cortex; contrast adaptation in parallel visual pathways. *Neuron*, 42(1):5–7, 2004.

T. Baden and B. Hedwig. Neurite-specific Ca^{2+} dynamics underlying sound processing in an auditory interneurone. *Dev Neurobiol*, 67(1):68–80, 2007.

F. Baldissera and B. Gustafsson. Firing behaviour of a neurone model based on the afterhyperpolarization conductance time course and algebraical summation. Adaptation and steady state firing. *Acta Physiol Scand*, 92(1):27–47, 1974.

F. Baldissera, B. Gustafsson, and F. Parmiggiani. Adaptation in a simple neurone model compared to that of spinal motoneurones. *Brain Res*, 52:382–4, 1973.

H. B. Barlow. Possible principles underlying the transformation of sensory messages. In *Sensory Communication*, pages 217—234. MIT Press, 1961.

H. B. Barlow and W. R. Levick. The mechanism of directionally selective units in rabbit's retina. *J Physiol (Lond)*, 178(3):477–504, 1965.

A. J. Bell and T. J. Sejnowski. An information-maximization approach to blind separation and blind deconvolution. *Neural Comput*, 7(6):1129–1159, 1995.

J. Benda. *Single Neuron Dynamics — Models Linking Theory and Experiment*. PhD thesis, Humboldt-Universität zu Berlin, 2002.

J. Benda and R. M. Hennig. Spike-frequency adaptation generates intensity invariance in a primary auditory interneuron. *J Comput Neurosci*, 2007.

J. Benda and A. V. M. Herz. A universal model for spike-frequency adaptation. *Neural Comput*, 15(11):2523–2564, 2003.

J. Benda, A. Longtin, and L. Maler. Spike-frequency adaptation separates transient communication signals from background oscillations. *J Neurosci*, 25(9):2312–21, 2005.

G. Boyan. Presynaptic inhibition of identified wind-sensitive afferents in the cercal system of the locust. *J Neurosci*, 8(8):2748, 1988.

G. S. Boyan. Common synaptic drive to segmentally homologous interneurons in the locust. *J Comp Neurol*, 321(4):544–554, 1992.

G. S. Boyan. Presynaptic contributions to response shape in an auditory neuron of the grasshopper. *J Comp Physiol A*, 184(3):279–294, 1999.

N. Brenner, W. Bialek, and R. de Ruyter van Steveninck. Adaptive rescaling maximizes information transmission. *Neuron*, 26(0896-6273):695–702, 2000.

R. Brette and W. Gerstner. Adaptive exponential integrate-and-fire model as an effective description of neuronal activity. *J Neurophysiol*, 94(5):3637, 2005.

D. A. Brown and P. R. Adams. Muscarinic suppression of a novel voltage-sensitive K^+ current in a vertebrate neurone. *Nature*, 283(5748):673–6, 1980.

M. Burrows and T. Matheson. A presynaptic gain control mechanism among sensory neurons of a locust leg proprioceptor. *J Neurosci*, 14(1):272–82, 1994.

D. A. Butts. How much information is associated with a particular stimulus? *Network*, 14:177–187, 2003.

D. A. Butts and M. S. Goldman. Tuning curves, neuronal variability, and sensory coding. *PLoS Biol*, 4(4):e92, 2006.

M. Carandini. Visual cortex: Fatigue and adaptation. *Curr Biol*, 10(16):R605–7, 2000.

M. Carandini and D. J. Heeger. Summation and division by neurons in primate visual cortex. *Science*, 264(5163):1333–6, 1994.

D. Cattaert and A. E. Manira. Shunting versus inactivation: Analysis of presynaptic inhibitory mechanisms in primary afferents of the crayfish. *J Neurosci*, 19(14):6079, 1999.

F. S. Chance, S. Nelson, and L. Abbott. Synaptic depression and the temporal response characteristics of V1 cells. *J Neurosci*, 18(12):4785–4799, 1998.

F. S. Chance, L. Abbott, and A. D. Reyes. Gain modulation from background synaptic input. *Neuron*, 35(4):773–82, 2002.

G. Chechik, M. Anderson, O. Baryosef, E. Young, N. Tishby, and I. Nelken. Reduction of information redundancy in the ascending auditory pathway. *Neuron*, 51(3):359–368, 2006.

F. Clarac and D. Cattaert. Invertebrate presynaptic inhibition and motor control. *Exp Brain Res*, 112(2):163–80, 1996.

T. M. Cover and J. A. Thomas. *Elements of Information Theory*. Wiley-Interscience, Hoboken, NJ, 1991.

P. Dayan and L. Abbott. *Theoretical Neuroscience: Computational and Mathematical Modeling of Neural Systems*. MIT Press, Cambridge, MA, 2001.

I. Dean, N. S. Harper, and D. McAlpine. Neural population coding of sound level adapts to stimulus statistics. *Nat Neurosci*, 8(12):1684–1689, 2005.

D. Derdikman, C. Yu, S. Haidarliu, K. Bagdasarian, A. Arieli, and E. Ahissar. Layer-specific touch-dependent facilitation and depression in the somatosensory cortex during active whisking. *J Neurosci*, 26(37):9538–47, 2006.

P. Drew and L. Abbott. Models and properties of power-law adaptation in neural systems. *J Neurophysiol*, 96(2):826–33, 2006.

F. A. Dunn, M. J. Lankheet, and F. Rieke. Light adaptation in cone vision involves switching between receptor and post-receptor sites. *Nature*, 449(7162):603–6, 2007.

J. Eccles, F. Magni, and W. Willis. Depolarization of central terminals of group I afferent fibres from muscle. *J Physiol (Lond)*, 1962.

A. L. Fairhall, G. Lewen, W. Bialek, and R. de Ruyter van Steveninck. Efficiency and ambiguity in an adaptive neural code. *Nature*, 412(6849):787–792, 2001.

P. Finlayson and D. Caspary. Synaptic potentials of chinchilla lateral superior olivary neurons. *Hear Res*, 38(3):221–228, 1989.

P. G. Finlayson and T. J. Adam. Excitatory and inhibitory response adaptation in the superior olive complex affects binaural acoustic processing. *Hear Res*, 103(1-2):1–18, 1997.

I. A. Fleidervish, A. Friedman, and M. J. Gutnick. Slow inactivation of Na^+ current and slow cumulative spike adaptation in mouse and guinea-pig neocortical neurones in slices. *J Physiol (Lond)*, 493 (Pt 1):83–97, 1996.

N. Fourcaud-Trocmé, D. Hansel, C. van Vreeswijk, and N. Brunel. How spike generation mechanisms determine the neuronal response to fluctuating inputs. *J Neurosci*, 23(37):11628–40, 2003.

F. Gabbiani and H. Krapp. Spike-frequency adaptation and intrinsic properties of an identified, looming-sensitive neuron. *J Neurophysiol*, 96(6):2951–2962, 2006.

F. Gabbiani, H. Krapp, C. Koch, and G. Laurent. Multiplicative computation in a visual neuron sensitive to looming. *Nature*, 420(6913):320–324, 2002.

A. Gelman, J. Carlin, H. Stern, and D. Rubin. *Bayesian Data Analysis*. Chapman & Hall/CRC, Boca Raton, FL, 1995.

H. C. Gerhardt and F. Huber. *Acoustic Communication in Insects and Anurans*. Chicago, IL. University Of Chicago Press, 2002.

D. C. Gillespie, I. Lampl, J. S. Anderson, and D. Ferster. Dynamics of the orientation-tuned membrane potential response in cat primary visual cortex. *Nat Neurosci*, 4(10): 1014–9, 2001.

V. Givois and G. S. Pollack. Sensory habituation of auditory receptor neurons: implications for sound localization. *J Exp Biol*, 203(17):2529–2537, 2000.

T. Gollisch and A. V. M. Herz. Input-driven components of spike-frequency adaptation can be unmasked in vivo. *J Neurosci*, 24(34):7435–44, 2004.

M. Hardt and A. Watson. Distribution of input and output synapses on the central branches of bushcricket and cricket auditory afferent neurones: Immunocytochemical evidence for GABA and glutamate in different populations of presynaptic boutons. *J Comp Neurol*, 403(3):281–294, 1999.

J. Heitwerth, R. Kern, J. van Hateren, and M. Egelhaaf. Motion adaptation leads to parsimonious encoding of natural optic flow by blowfly motion vision system. *J Neurophysiol*, 94(3):1761–1769, 2005.

R. M. Hennig. Ascending auditory interneurons in the the cricket *Teleogryllus commodus* (WALKER): comparative physiology and direct connections with afferents. *J Comp Physiol A*, 163:135–143, 1988.

R. M. Hennig and T. Weber. Filtering of parameters of the calling song by cricket females of two closely related species: a behavioural analysis. *J Comp Physiol A*, 180(6): 621–630, 1997.

R. M. Hennig, A. Franz, and A. Stumpner. Processing of auditory information in insects. *Microsc Res Tech*, 63:351–374, 2004.

K. J. Hildebrandt, J. Benda, and R. M. Hennig. The origin of adaptation in the auditory pathway of locusts is specific to cell type and function. *J Neurosci*, 29(8):2626, 2009.

G. R. Holt and C. Koch. Shunting inhibition does not have a divisive effect on firing rates. *Neural Comput*, 9(5):1001–13, 1997.

S. Hong, B. N. Lundstrom, and A. L. Fairhall. Intrinsic gain modulation and adaptive neural coding. *PLoS Comput Biol*, 4(7):e1000119, 2008.

G. Horseman and F. Huber. Sound localisation in crickets: I. Contralateral inhibition of an ascending auditory interneuron AN1 in the cricket *Gryllus bimaculatus*. *J Comp Physiol A*, 175:389–398, 1994a.

G. Horseman and F. Huber. Sound localisation in crickets: II. Modelling the role of a simple neuronal network in the prothoracic ganglion. *J Comp Physiol A*, 175:399–413, 1994b.

A. J. Hudspeth, Y. Choe, A. D. Mehta, and P. Martin. Putting ion channels to work: mechanoelectrical transduction, adaptation, and amplification by hair cells. *Proc Natl Acad Sci USA*, 97(22):11765–72, 2000.

K. Imaizumi and G. S. Pollack. Neural coding of sound frequency by cricket auditory receptors. *J Neurosci*, 19(4), 1999.

K. Imaizumi and G. S. Pollack. Neural representation of sound amplitude by functionally different auditory receptors in crickets. *J Acoust Soc Am*, 109 (3):1247–1260, 2001.

N. J. Ingham and D. McAlpine. Spike-frequency adaptation in the inferior colliculus. *J Neurophysiol*, 91(2):632–45, 2004.

N. J. Ingham and D. McAlpine. GABAergic inhibition controls neural gain in inferior colliculus neurons sensitive to interaural time differences. *J Neurosci*, 25(26):6187–98, 2005.

P. Joris. Neural processing of amplitude-modulated sounds. *Physiol Rev*, 84(2):541–77, 2004.

P. Kara, P. Reinagel, and R. C. Reid. Low response variability in simultaneously recorded retinal, thalamic, and cortical neurons. *Neuron*, 27(3):635–46, 2000.

Y. Katz, J. E. Heiss, and I. Lampl. Cross-whisker adaptation of neurons in the rat barrel cortex. *J Neurosci*, 26(51):13363–72, 2006.

A. Kohn and J. A. Movshon. Neuronal adaptation to visual motion in area mt of the macaque. *Neuron*, 39(4):681–91, 2003.

R. Krahe and B. Ronacher. Long rise times of sound pulses in grasshopper songs improve the directionality cues received by the CNS from the auditory receptors. *J Comp Physiol A*, 173(4):425–434, 1993.

M. N. Kvale and C. E. Schreiner. Short-term adaptation of auditory receptive fields to dynamic stimuli. *J Neurophysiol*, 91(2):604–12, 2004.

L. Las, E. A. Stern, and I. Nelken. Representation of tone in fluctuating maskers in the ascending auditory system. *J Neurosci*, 25(6):1503–13, 2005.

S. B. Laughlin. A simple coding procedure enhances a neuron's information capacity. *Z Naturforsch C*, 36(9-10):910–2, 1981.

S. B. Laughlin. The role of sensory adaptation in the retina. *J Exp Biol*, 146:39–62, 1989.

Z. Li. *Understanding ocular dominance from binocular dominance input statistics*, chapter 1, pages 397–402. Kluwer Academic Publishers, Norwell, MA, 1995.

F. Libersat, J. Murray, and R. R. Hoy. Frequency as a releaser in the courtship song of two crickets, *Gryllus bimaculatus* (DE GEER) and *Teleogryllus oceanicus*: a neuroethological analysis. *J Comp Physiol A*, 174:485–494, 1994.

R. Linsker. Self-organization in a perceptual network. *Computer*, 21:105–117, 1988.

H. Luksch, R. Khanbabaie, and R. Wessel. Synaptic dynamics mediate sensitivity to motion independent of stimulus details. *Nat Neurosci*, 7(4):380–388, 2004.

C. Ly and B. Doiron. Divisive gain modulation with dynamic stimuli in integrate-and-fire neurons. *PLoS Comput Biol*, 5(4):e1000365, 2009.

C. K. Machens, T. Gollisch, O. Kolesnikova, and A. Herz. Testing the efficiency of sensory coding with optimal stimulus ensembles. *Neuron*, 47(3):447–456, 2005.

D. J. C. MacKay. *Information Theory, Inference and Learning Algorithms*. Cambridge University Press, Cambridge, UK, 2003.

D. V. Madison and R. A. Nicoll. Control of the repetitive discharge of rat CA1 pyramidal neurones in vitro. *J Physiol (Lond)*, 354:319–31, 1984.

A. K. Magnusson, T. J. Park, M. Pecka, B. Grothe, and U. Koch. Retrograde GABA signaling adjusts sound localization by balancing excitation and inhibition in the brainstem. *Neuron*, 59(1):125–37, 2008.

M. Maravall, R. Petersen, A. L. Fairhall, E. Arabzadeh, and M. Diamond. Shifts in coding properties and maintenance of information transmission during adaptation in barrel cortex. *PLoS Biol*, 5(2):324–334, 2007.

V. Marquart. Local interneurons mediating excitation and inhibition onto ascending neurons in the auditory pathway of grasshoppers. *Naturwissenschaften*, 72(1):42–44, 1985.

G. Marsat and G. S. Pollack. Differential temporal coding of rhythmically diverse acoustic signals by a single interneuron. *J Neurophysiol*, 92(2):939–48, 2004.

G. Marsat and G. S. Pollack. A behavioral role for feature detection by sensory bursts. *J Neurosci*, 26(41):10542–10547, 2006.

D. McAlpine, D. Jiang, T. M. Shackleton, and A. R. Palmer. Responses of neurons in the inferior colliculus to dynamic interaural phase cues: evidence for a mechanism of binaural adaptation. *J Neurophysiol*, 83(3):1356–65, 2000.

M. D. McDonnell and N. G. Stocks. Maximally informative stimuli and tuning curves for sigmoidal rate-coding neurons and populations. *Phys Rev Lett*, 101(5):058103, 2008.

A. Moiseff, G. S. Pollack, and R. R. Hoy. Steering response of flying crickets to sound and ultrasound: mate attraction and predator avoidance. *Proc Natl Acad Sci USA*, 75 (8):4052–4056, 1978.

M. Moore and D. Caspary. Strychnine blocks binaural inhibition in lateral superior olivary neurons. *J Neurosci*, 3(1):237–242, 1983.

J. Nadal and N. Parga. Nonlinear neurons in the low-noise limit: a factorial code maximizes information transfer. *Network-Comp Neural*, 1994.

K. I. Nagel and A. J. Doupe. Temporal processing and adaptation in the songbird auditory forebrain. *Neuron*, 51(6):845–59, 2006.

M. Nawrot, C. Boucsein, V. R. Molina, A. Riehle, A. Aertsen, and S. Rotter. Measurement of variability dynamics in cortical spike trains. *J Neurosci Methods*, 169(2):374–390, 2008.

I. Nelken. Processing of complex stimuli and natural scenes in the auditory cortex. *Curr Opin Neurobiol*, 14(4):474–480, 2004.

I. Nelken, Y. Rotman, and O. Yosef. Responses of auditory-cortex neurons to structural features of natural sounds. *Nature*, 397(6715):154–157, 1999.

M. Nelson. A mechanism for neuronal gain control by descending pathways. *Neural Comput*, 6(2):242–254, 1994.

D. Neuhofer, S. Wohlgemuth, A. Stumpner, and B. Ronacher. Evolutionarily conserved coding properties of auditory neurons across grasshopper species. *Proc Roy Soc B-Biol Sci*, 275(1646):1965–74, 2008.

J. E. Niven, J. C. Anderson, and S. B. Laughlin. Fly photoreceptors demonstrate energy-information trade-offs in neural coding. *PLoS Biol*, 5(4):829–840, 2007.

T. Nolen and R. R. Hoy. Initiation of behavior by single neurons: the role of behavioral context. *Science*, 226(4677):992–4, 1984.

T. Nolen and R. R. Hoy. Phonotaxis in flying crickets. II. Physiological mechanisms of two-tone suppression of the high frequency avoidance steering behavior by the calling song. *J Comp Physiol A*, 159(4):441–56, 1986.

T. Nolen and R. R. Hoy. Postsynaptic inhibition mediates high-frequency selectivity in the cricket *Teleogryllus oceanicus*: implications for flight phonotaxis behavior. *J Neurosci*, 7(7):2081–2096, 1987.

W. Ocker and B. Hedwig. Interneurones involved in stridulatory pattern generation in the grasshopper *Chorthippus mollis* (CHARP.). *J Exp Biol*, 199(Pt 3):653–62, 1996.

I. Ohzawa, G. Sclar, and R. D. Freeman. Contrast gain control in the cat's visual system. *J Neurophysiol*, 54(3):651–667, 1985.

S. R. Olsen and R. I. Wilson. Lateral presynaptic inhibition mediates gain control in an olfactory circuit. *Nature*, 452(7190):956–960, 2008.

D. Otte. Evolution of cricket songs. *J Orthoptera Res*, 1:25–29, 1992.

D. Otte and W. Cade. African Crickets (*Gryllidea*). 1. *Teleogryllus* of Eastern and Southern Africa. *Proc Natl Acad Sci USA*, 135:102–127, 1983.

T. J. Park, A. Klug, M. Holinstat, and B. Grothe. Interaural level difference processing in the lateral superior olive and the inferior colliculus. *J Neurophysiol*, 92(1):289–301, 2004.

K. Pearson and R. Robertson. Interneurons co-activating hindleg flexor and extensor moto-neurons in the locust. *J Comp Physiol A*, 144:391–400, 1981.

J. L. Peña and M. Konishi. Auditory spatial receptive fields created by multiplication. *Science*, 292(5515):249–52, 2001.

G. S. Pollack. Selective attention in an insect auditory neuron. *J Neurosci*, 8(7):2635–2639, 1988.

G. S. Pollack. Who, what, where? Recognition and localization of acoustic signals by insects. *Curr Opin Neurobiol*, 10:763–767, 2000.

G. S. Pollack. Effect of the temporal pattern of contralateral inhibition on sound localization cues. *J Neurosci*, 25(26):6137–44, 2005.

G. S. Pollack and R. Martins. Flight and hearing: ultrasound sensitivity differs between flight-capable and flight-incapable morphs of a wing-dimorphic cricket species. *J Exp Biol*, 210:3160–3164, 2007.

J. F. A. Poulet and B. Hedwig. A corollary discharge maintains auditory sensitivity during sound production. *Nature*, 418(6900):872–876, 2002.

J. F. A. Poulet and B. Hedwig. A corollary discharge mechanism modulates central auditory processing in singing crickets. *J Neurophysiol*, 89(3):1528–1540, 2003.

S. A. Prescott and Y. D. Koninck. Gain control of firing rate by shunting inhibition: Roles of synaptic noise and dendritic saturation. *Proc Natl Acad Sci USA*, 100(4):2076, 2003.

P. Prinz and B. Ronacher. Temporal modulation transfer functions in auditory receptor fibres of the locust (*Locusta migratoria*). *J Comp Physiol A*, 188(7):577–587, 2002.

D. L. Ringach and B. J. Malone. The operating point of the cortex: neurons as large deviation detectors. *J Neurosci*, 27(29):7673–83, 2007.

H. Römer. Die lnformationsverarbeitung tympanaler Rezeptorelemente von *Locusta migratoria* (Acrididae, Orthoptera). *J Comp Physiol A*, 109:101–122, 1976.

H. Römer and M. Krusch. A gain-control mechanism for processing of chorus sounds in the afferent auditory pathway of the bushcricket *Tettigonia viridissima (Orthoptera; Tettigoniidae)*. *J Comp Physiol A*, 186(2):181–91, 2000.

H. Römer and V. Marquart. Morphology and physiology of auditory interneurons in the metathoracic ganglion of the locust. *J Comp Physiol A*, V155(2):249–262, 1984.

B. Ronacher and R. M. Hennig. Neuronal adaptation improves the recognition of temporal patterns in a grasshopper. *J Comp Physiol A*, 190(4):311–319, 2004.

B. Ronacher and R. Krahe. Song recognition in the grasshopper chorthippus biguttulus is not impaired by shortening song signals: implications for neuronal encoding. *J Comp Physiol A*, 183(6):729–735, 1998.

C. M. Root, K. Masuyama, D. S. Green, L. E. Enell, D. R. Nässel, C.-H. Lee, and J. W. Wang. A presynaptic gain control mechanism fine-tunes olfactory behavior. *Neuron*, 59(2):311, 2008.

J. Rothman, L. Cathala, V. Steuber, and R. Silver. Synaptic depression enables neuronal gain control. *Nature*, 457(7232):1015–1018, 2009.

P. Rudomin. In search of lost presynaptic inhibition. *Exp Brain Res*, 196(1):139–51, 2009.

M. B. Sachs and P. J. Abbas. Rate versus level functions for auditory-nerve fibers in cats: tone-burst stimuli. *J Acoust Soc Am*, 56(6):1835–47, 1974.

E. Salinas and P. Thier. Gain modulation: a major computational principle of the central nervous system. *Neuron*, 27(1):15–21, 2000.

A.-H. Samson and G. S. Pollack. Encoding of sound localization cues by an identified auditory interneuron: effects of stimulus temporal pattern. *J Neurophysiol*, 88(5): 2322–8, 2002.

M. V. Sanchez-Vives, L. G. Nowak, and D. A. McCormick. Cellular mechanisms of long-lasting adaptation in visual cortical neurons in vitro. *J Neurosci*, 20(11):4286–99, 2000a.

M. V. Sanchez-Vives, L. G. Nowak, and D. A. McCormick. Membrane mechanisms underlying contrast adaptation in cat area 17 in vivo. *J Neurosci*, 20(11):4267–85, 2000b.

J. Schul, M. Holderied, D. von Helversen, and O. von Helversen. Directional hearing in grasshoppers: neurophysiological testing of a bioacoustic model. *J Exp Biol*, 202 (Pt 2):121–33, 1999.

L. Schwabe and K. Obermayer. Adaptivity of tuning functions in a generic recurrent network model of a cortical hypercolumn. *J Neurosci*, 25(13):3323–32, 2005.

A. Selverston, H.-U. Kleindienst, and F. Huber. Synaptic connectivity between cricket auditory interneurons as studied by selective photoinactivation. *J Neurosci*, 5(5): 1283–1292, 1985.

T. O. Sharpee, H. Sugihara, A. V. Kurgansky, S. P. Rebrik, M. P. Stryker, and K. D. Miller. Adaptive filtering enhances information transmission in visual cortex. *Nature*, 439 (7079):936–942, 2006.

E. Sobel and D. Tank. In vivo Ca^{2+} dynamics in a cricket auditory neuron: an example of chemical computation. *Science*, 263:863–826, 1994.

S. G. Solomon, J. W. Peirce, N. T. Dhruv, and P. Lennie. Profound contrast adaptation early in the visual pathway. *Neuron*, 42(1):155–62, 2004.

A. Stumpner and B. Ronacher. Auditory interneurones in the metathoracic ganglion of the grasshopper *Chorthippus biguttulus*: I. Morphological and physiological characterization. *J Exp Biol*, 158(1):391–410, 1991.

A. Stumpner and B. Ronacher. Neurophysiological aspects of song pattern recognition and sound localization in grasshoppers. *Am Zool*, 34(6):696–705, 1994.

C. Sutherland, B. Doiron, and A. Longtin. Feedback-induced gain control in stochastic spiking networks. *Biol Cybern*, 100(6):475–89, 2009.

Y. Tadmor and D. J. Tolhurst. Calculating the contrasts that retinal ganglion cells and lgn neurones encounter in natural scenes. *Vision Res*, 40(22):3145–3157, 2000.

B. Todd. The identification of peaks in physiological signals. *Comput Biomed Res*, 32(4): 322–35, 1999.

P. Torkkeli, S.-I. Sekizawa, and A. French. Inactivation of Voltage-Activated Na^+ Currents Contributes to Different Adaptation Properties of Paired Mechanosensory Neurons. *J Neurophysiol*, 85(4):1595–1602, 2001.

N. Ulanovsky. Processing of low-probability sounds by cortical neurons. *Nat Neurosci*, 6(4):391–8, 2003.

N. Ulanovsky, L. Las, D. Farkas, and I. Nelken. Multiple time scales of adaptation in auditory cortex neurons. *J Neurosci*, 24(46):10440–10453, 2004.

A. Vogel and B. Ronacher. Neural correlations increase between consecutive processing levels in the auditory system of locusts. *J Neurophysiol*, 97(5):3376–3385, 2007.

A. Vogel, R. M. Hennig, and B. Ronacher. Increase of neuronal response variability at higher processing levels as revealed by simultaneous recordings. *J Neurophysiol*, 93 (6):3548–3559, 2005.

D. von Helversen and J. Rheinlaender. Interaural intensity and time discrimination in an unrestraint grasshopper – a tentative behavioral-approach. *J Comp Physiol A*, 162 (3):333–340, 1988.

D. von Helversen and O. von Helversen. Acoustic pattern recognition and orientation in orthopteran insects: parrallel or serial processing. *J Comp Physiol A*, 177:767–774, 1995.

D. von Helversen, R. Balakrishnan, and O. von Helversen. Acoustic communication in a duetting grasshopper: receiver response variability, male strategies and signal design. *Anim Behav*, 68:131–144, 2004.

B. Wark, A. L. Fairhall, and F. Rieke. Timescales of inference in visual adaptation. *Neuron*, 61(5):750–761, 2009.

A. H. Watson and M. Hardt. Distribution of synapses on two local auditory interneurones, ON1 and ON2, in the prothoracic ganglion of the cricket: relationships with GABA-immunoreactive neurones. *Cell Tissue Res*, 283(2):231–46, 1996.

G. Wendler. Pattern recognition and localization in cricket phonotaxis. In *Advances in Life Science: Sensory Systems and Communication in Arthropods*, pages 387–394. Birkhäuser Verlag, Basel, 1990.

G. Weschke and B. Ronacher. Influence of sound pressure level on the processing of amplitude modulations by auditory neurons of the locust. *J Comp Physiol A*, 194(3): 255–265, 2008.

L. Westerman and R. Smith. Rapid and short-term adaptation in auditory-nerve responses. *Hear Res*, 15(3):249–260, 1984.

K. Wimmer, K. J. Hildebrandt, R. M. Hennig, and K. Obermayer. Adaptation and selective information transmission in the cricket auditory neuron AN2. *PLoS Comput Biol*, 4(9):e1000182, 2008.

D. Wohlers and F. Huber. Processing of sound singals by six types of neurons in the prothoracic ganglion of the cricket, *Gryllus campestris* L. *J Comp Physiol A*, 146:161–173, 1982.

Z. Xu, J. Payne, and M. Nelson. Logarithmic time course of sensory adaptation in electrosensory afferent nerve fibers in a weakly electric fish. *J Neurophysiol*, 76(3): 2020–2032, 1996.

G. Yates, D. Robertson, and B. Johnstone. Very rapid adaptation in the guinea-pig auditory-nerve. *Hear Res*, 17(1):1–12, 1985.

U. Ziehm, K. J. Hildebrandt, and J. Benda. Adaptive coding in a feed forward network. In *Proceedings of the 8th Meeting of the German Neuroscience Society*, 2009.

Selbständigkeitserklärung

Ich erkläre, dass ich die vorliegende Arbeit selbständig und nur unter Verwendung der angegebenen Literatur und Hilfsmittel angefertigt habe.

Berlin, den 23.02.2010 Kai Jannis Hildebrandt

Publikationen

Artikel in wissenschaftlichen Zeitschriften

- Hildebrandt KJ, Benda J, Hennig RM (2009) The Origin of Adaptation in the Auditory Pathway of Locusts is Specific to Cell Type and Function. *J Neurosci* 29:2626-2636
- Wimmer K*, Hildebrandt KJ*, Hennig RM, Obermayer K (2008) Adaptation and Selective Information Transmission in the Cricket Auditory Neuron AN2. *PLoS Comput Biol* 4(9): e1000182. doi:10.1371/journal.pcbi.1000182

  * equal contribution

Artikel in Vorbereitung

- Hildebrandt KJ, Benda J, Hennig RM (2010) Presynaptic inhibition mediates divisive gain control in the cricket auditory pathway. *Neuron*, in prep.

Konferenzbeiträge

- Hildebrandt KJ, Benda J, Hennig RM (2009) Two different modes of gain control in a single cricket auditory interneuron (AN2). Proceedings of the 8th Meeting of the German Neuroscience Society, Göttingen, Germany
- Ziehm U, Hildebrandt KJ, Benda J (2009) Adaptive Coding in a feed forward network. Proceedings of the 8th Meeting of the German Neuroscience Society, Göttingen, Germany
- Hildebrandt KJ, Benda J, Hennig RM (2008) Context dependent adaptation in cricket auditory interneurons. Society for Neuroscience Abstracts 34
- Wimmer K, Hildebrandt KJ, Hennig RM, Obermayer K (2007) Adaptation and efficient sensory processing in the cricket auditory system. Society for Neuroscience Abstracts 33
- Hildebrandt KJ, Benda J, Hennig RM (2007) Spike frequency adaptation in an insect auditory pathway. Proceedings of the 7th Meeting of the German Neuroscience Society, Göttingen, Germany.
- Hildebrandt KJ, Wimmer K, Hennig RM, Obermayer K (2006) Firing rate adaptation in a cricket auditory interneuron as adjustment to local stimulus statistics. Invertebrate Sound and Vibration (ISV), University of Toronto, Canada.

- Hildebrandt KJ and Hennig RM (2005) Neural Representation and Filtering of Simple Temporal Patterns in the Lower Auditory Pathway of Crickets. Proceedings of the 6th Meeting of the German Neuroscience Society, Göttingen, Germany.
- Hildebrandt KJ, Zander JF, Loschen S, Hennig RM (2004) Temporal processing in the lower auditory pathway of crickets: comparing neurons and species. Proceedings of the 7th International Congress for Neuroethology, Nyborg, Denmark

Danksagung/Acknowledgments

An allererster Stelle gilt mein Dank Matthias Hennig, der mich nicht nur an allen erdenklichen Fronten und mit unendlicher Energie bei der Erstellung dieser Arbeit unterstützt hat, sondern mir im Laufe der Jahre so viel über wissenschaftliches Denken und Schreiben beigebracht hat. Er war immer für mich da, wenn es hakte – ohne seine Bereitschaft, sich voll in die Probleme zu stützen, bei deren Lösung ich gerade im Leerlauf trat, ist die vorliegende Arbeit undenkbar. Ich nehme aus den Jahren dieser Zusammenarbeit einen großen Schatz mit.

Auch bei Jan Benda möchte ich mich für seine sehr engagierte Betreuung bedanken, seine unbedingte Unterstützung für mich, die wertvollen Diskussionen und seinen ansteckenden Enthusiasmus. Jan hat mir gezeigt, dass Begeisterung für „klassische" Biologie und Theorie kein Widerspruch sein müssen, sondern die Kombination aus beiden Gebieten der interessanteste Weg ist, um Nervensysteme zu verstehen.

Bernd Ronacher hat mich unterstützt, wo er konnte. Ich danke ihm für sein Interesse an meiner Arbeit, für die vielen fruchtbaren Diskussionen und Ratschläge, und für alles, was ich im Laufe der Jahre in seiner Arbeitsgruppe gelernt habe.

Ich weiß kaum, wie ich der gesamten Arbeitsgruppe Verhaltensphysiologie danken soll. Ihr habt mir gezeigt, dass Arbeit in der Wissenschaft so viel mehr bedeutet, als das rein Inhaltliche: sondern die Bereitschaft, sich jederzeit mit den Problemen der Anderen zu beschäftigen (und ohne Murren auch die tausendste Kennlinie, die ich an die Tafel male, zu betrachten), die anderen zu trösten und in den harten Zeiten experimentellen Misserfolgs wiederaufzubauen und auch mal die Wissenschaft Wissenschaft sein zu lassen. Ohne Euch wäre meine Entscheidung, weiter wissenschaftlich zu Arbeiten, vielleicht anders ausgefallen. Obwohl ich glaube, dass es unmöglich sein wird, eine vergleichbare Truppe zu finden. Die Latte hängt zu hoch.

Jan möchte ich für viele Diskussionen und Tipps danken, für die sofortige Beschäftigung mit kleineren oder größeren Fragen zu Informationstheorie, Matlabfunktio-nen und anderen theoretischen Problemen, die ich gerne – wann immer sie mir durch den Kopf geschossen sind – an ihn gerichtet habe. Es war eine sehr schöne Zimmergemeinschaft. Auch seiner „Vorgängerin" Sandra danke ich für die tolle Gemeinschaft und alle Diskussionen, die wir geführt haben. Florian wünsche ich das Beste für seine Arbeit an den Grillen: halte die Fahne hoch!

Daniela war eine tolle Vorkämpferin und Mitstreiterin and der Front des intrazellulären Ableitens. Deine Beharrlichkeit hat mir Mut gemacht. Auch Daniela möchte ich für alle kritischen Fragen und Diskussionen danken. Nic gebührt Dank für ihre ständige Hilfsbereitschaft, egal ob es um das Aufnehmen von Grillengesängen, um Fragen zu statistischen Tests oder die Bedienung von Pipetten ging. Olaf danke ich für seine Hilfe bei allen Problemen, die LabView und der Versuchssteuerung betrafen, für viele Diskussionen um Richtungshören, Adapation, vorlaufende Inhibition, Fussball, aber vor allem dafür, dass er soviel dazu begetragen hat, dass die Verhaltensphysiolo-

gie immmer mehr WG als sprödes Labor war. Außerdem gilt Regina Lübke Dank für die Pflege und das sorgfältige Sortieren der Grillen und alle andere Hilfe.

Die Arbeit an der Funktion der langsamen Adaptation in der Grille ist in einer engen und sehr inspirierenden Zusammenarbeit mit Klaus Wimmer entstanden. Für seine engagierte Arbeit an diesen Problemen, unsere Diskussionen und seine Einblicke in Bayes'sche Verfahren und Informationsverarbeitung im visuellen System gilt ihm großer Dank. In diesem Zusammenhang möchte ich mich auch bei Lars Schwabe, der einen großen Anteil an der Entwicklung der Versuche hatte, und bei Klaus Obermayer für sein Engagement für dieses Projekt bedanken.

Die Arbeit von Ulrike Ziehm, ihre Modelle zur Entstehen der Invarianz im Nervensystem der Grille, und die Diskussionen mit ihr haben mir nicht nur viel Freude bereitet, sondern auch mein Denken über Adaptation verändert und vertieft.

The theory chapter is unthinkable without many people at the *Advanced course on computational neuroscience* in Freiburg. Zhaoping Li has taken much time to discuss my problems and to apply her work on binocular vision to them. My tutor Hermann Cuntz has helped me with the implementation of the numerical models. Israel Nelken showed great interest in my work and the discussions with him spurred my interest for auditory processing in the cortex. I also would like to thank Asli Ayaz for our discussions on input and output gain-control and the insights I got from these, I enjoyed them very much.

Wisschenschaft ist viel mehr als das, was am Ende auf dem Blatt steht. Wie alle Arbeit, an die man mit persönlichem Interesse herangeht, reicht sie weit in das Privatleben hinein und umgekehrt. Ich möchte die Gelegenheit nutzen, auch denjenigen zu danken, die diese Arbeit genauso prägen, weil sie mich geprägt haben.

Ich danke Ansgar Siemer und Jan Ohlberger für unseren gemeinsamen Weg in die Wissenschaft und die vielen Gedanken, Zweifel und Ermutigungen über viele Jahre hinweg. Dank gilt auch meinen Mitbewohnern und Mitbewohnerinnen, ohne die gerade die experimentellen Phasen meiner Arbeit kaum zu ertragen gewesen wären, und die mich ertragen haben, wenn ich zerschlagen nach gescheiterten Experimenten nach Hause kam. Daniel, Jan, Anne, Hanna, Krischi: ihr ward meine Familie in dieser Zeit.

Mein größter Dank gilt Merle, die in der ganzen Zeit alles auf einmal war: Motivatorin, Trösterin, Kritikerin, Ratgeberin und die am meisten von meinen Tiefs (und gelegentlichen Hochs) erlitten hat. Ich weiß nicht, was ich ohne Dich gemacht hätte. Vielen Dank, dass Du da bist.